ABSTRACT

DOSHI, VISHWARAJ DILESH. Dynamics of Interacting Stochastic Systems on Networks. (Under the direction of Dr. Do Young Eun).

Interaction based stochastic dynamics are powerful tools for obtaining non trivial theoretical results, and for explaining various real world scenarios such as the competitive dynamics of opinions, products, or epidemics on networks. However, they are under utilized and often overlooked when it comes to the development of useful algorithms and analytical tools for graphs.

In this research, we first develop a framework in which we construct a stochastic process comprising interacting random walks on a graph and show that a suitably scaled version of our stochastic process converges to the *Fiedler vector* of graph Laplacian matrices, for a sufficiently large number of walks. The Fiedler vector of a graph, namely the eigenvector corresponding to the second smallest eigenvalue of a graph Laplacian matrix, plays an important role in spectral graph theory with applications in problems such as graph bi-partitioning and envelope reduction. Our random walk based framework does not require a priori knowledge of the entire graph, while deterministic algorithms designed to estimate this quantity do - a major problem when the graph in question is at least partially unexplored. Importantly, unlike any existing random walk based methods such as Markov Chain Monte Carlo (MCMC) methods where the focus is on the *first* eigenvector, our framework with interacting random walks converges to the *second* eigenvector of any reversible Markov chain kernel in general, opening up the door to higher order eigenvector approximation via purely random walk methods.

We also study *self-repellent* random walks on graphs, which interact with their own past history and tend to prioritize transitions to less visited nodes. While similar mechanisms have been studied in the past, existing works tend to focus on special graph topologies, such as complete graphs and grids. Motivated by potential applications such as graph sampling and revision protocols seen in evolutionary game theory, we show how self-repellent walks can be designed such that their occupational measures converge to any target probability distribution. We do so by providing almost sure convergence and a central limit theorem results for the same, and also show that our self-repellent mechanism can achieve smaller asymptotic covariance than the well known simple random walk.

In addition to random walk based algorithms, we answer key open questions in the

literature of *Susceptible-Infected-Susceptible* (SIS) models of epidemic spread. The single virus SIS model is well analyzed in literature, with precise conditions existing for global convergence to the *dichotomy* of outcomes: a virus-free network, or a pandemic state. However, when it comes to the competition between two such epidemics over a network, a situation more likely to arise in the real world and captured by the so called *bi-virus* or *bi-SIS* models of epidemic spread, existing works have been unsuccessful in characterizing convergence properties for a large subset of the model parameter space. This includes the set of all parameters for which the competitiveness of the bi-virus system could be significant enough to attain coexistence of the epidemics. We solve this open problem and completely characterize the model parameter space; giving precise necessary and sufficient conditions that lead to global convergence of the system to a *trichotomy* of possible outcomes: a virus-free state, a single-virus state, and to a coexistence state – the first such result.

For bi-SIS epidemic models, we also prove monotonicity of the coexistence equilibria (CE) with respect to effective infection rates of the two viruses, and provide the first quantitative analysis of such equilibria in the form of upper bounds involving spectral radii of the underlying graphs, as well as positive equilibria of related single-virus systems. Our results provide deeper insight into how the long term infection probabilities are affected by system parameters.

Dynamics of Interacting Stochastic Systems on Networks

by
Vishwaraj Dilesh Doshi

A dissertation submitted to the Graduate Faculty of
North Carolina State University
in partial fulfillment of the
requirements for the Degree of
Doctor of Philosophy

Operations Research

Raleigh, North Carolina
2022

APPROVED BY:

Dr. Arvind Saibaba	Dr. Yunan Liu
Dr. Michael Kay	Dr. Do Young Eun Chair of Advisory Committee

DEDICATION

This dissertation is dedicated to my mother, Deepa Doshi, my father, Dilesh Doshi, and to my lovely wife and pillar of support, Savni.

BIOGRAPHY

Vishwaraj Doshi was born on 24'th January, 1994, in Mumbai (then Bombay), India. He spent twenty-one years of his life there, the final four of which went into successfully pursuing his Bachelor's of Mechanical Engineering from the University of Mumbai from 2011 to 2015. Upon completing his Bachelor's he moved to the United States, where in 2017, he completed his Master's in Operations Research from North Carolina State University, Raleigh, NC (NCSU). Since 2017, Vishwaraj has been pursuing his Ph.D. in Operations Research at NCSU.

ACKNOWLEDGEMENTS

This dissertation, five years in the making, has directly or indirectly been a product of multiple people who have played a constant role in my academic journey as mentors, teachers, colleagues and friends.

My biggest thanks and deepest gratitude goes to my Ph.D. advisor, Dr. Do Young Eun, who, through his invaluable comments and constructive criticisms, has taught me to conduct original, meaningful scientific research. Over countless hours of discussions, he has imbibed in me a deep appreciation for the value of setting high standards for one's work, and being unbiased and meticulous in one's approach - a trait which will have a great impact on my future career. Without his constant motivation and support, this dissertation would not have been possible.

My sincere thanks also go to Dr. Michael Kay, Dr. Arvind Saibaba, and Dr. Yunan Liu for being part of my research committee. Dr. Michael Kay has been a constant mentor throughout his tenure as director of the Operations Research graduate program, and I would like to thank him for always being there and patiently helping me with my numerous queries over the years. Dr. Arvind Saibaba, and Dr. Yunan Liu, through rigorous classes on matrix analysis and stochastic processes, have taught me the tools which have been vital to my research efforts, and will continue to be invaluable in my future career. They have been the greatest teachers to me, and I am grateful to them.

It has also been a great pleasure working with my lab-mates over the years, especially Jie Hu, from whom I have learnt a lot over the countless brainstorming sessions that we have had while co-authoring our papers. Last but far from being the least, my special acknowledgements go to Jessica Mele and Marwen Zrida for being the greatest of friends.

TABLE OF CONTENTS

LIST OF TABLES

LIST OF FIGURES

Chapter 1

Introduction and Overview

With the explosion in technological growth over the past few decades and the prevalence of messaging services, social networks, internet of things, and the world wide web in general, the influence of network dynamics on our daily activities can be felt now more than ever. Observations made on the propagation of social network phenomena such as memes, fake news, and other trends, brings forth the well established argument that human societies and organizations can be modelled as large networks or graphs, upon which ideas, rumours, opinions, vices, diseases, and other phenomena spread via edges representing interactions between individual communities. The modern push towards a data driven world and the increase in large scale data mining capabilities as a result is helping uncover more and more of such hidden networks that have a significant influence on our lives. The development of models and algorithms to help understand, learn from, and manipulate these networks and related dynamics is therefore becoming an increasingly important field of research.

Networking dynamics are often stochastic in nature. In this research, we take a closer look at two of the most prominent ones:

Random walk based estimation algorithms on graphs: Random walk based algorithms have proven to be robust methods for the task of estimating various network statistics. The graphs in question are often very large and at least partially unexplored. In such cases, storing the topological information of the entire network is often infeasible, rendering deterministic tools such as iterative, power-method based techniques inapplicable. Random walk based methods, on the other hand, provide a way to deal with the above challenges by performing *in-situ* computations as they explore the graph on-the-fly. As exhibited time and again in the field of Markov Chain Monte Carlo (MCMC) [55, 84, 101], they can be used

robustly to estimate target quantities on graphs without really feeling the repercussions of scale, lack of knowledge of the state space or the effect of dynamically changing graph topology.

Models of epidemic, opinion spread on networks: Graph based epidemic models are widely employed to analyze the spread of real-world phenomena such as communicable diseases [74, 56], computer viruses, malware [49, 137, 66], product adoption [8, 104, 107], opinions and rumors [128, 142, 82]. The propagation of such phenomenon (which we cumulatively refer to as *epidemics* or *viruses*) usually takes place via processes such as human contact, word-of-mouth, exchange of emails or even in social media platforms. Graph based techniques, with edge based mechanisms to model information spread, have therefore proven to be effective in capturing such epidemic dynamics [11, 48, 43].

Both, random walk based algorithms and graph based epidemic models have enjoyed considerable attention throughout the second half of the past century and up till recent times. However, since the seminal, pioneering works such as the development of the Metropolis Hastings random walk [55] for sampling on general undirected graphs from any given probability distribution, and the analysis of an epidemic model for the spread of Gonorrhea [74] that set up the benchmark in terms of analysis and qualitative results in the epidemic model literature, the general scope of possible results in these fields remain largely un-extended. We elaborate on this, and discuss how one possible way of breaking through these existing theoretical barriers is by introducing *interactions* into the study of such techniques.

1.1 A need for interaction based dynamics

1.1.1 Interaction based random walk algorithms

We describe the following in the context of Markov Chain Monte Carlo (MCMC) methods since they are among the most commonly employed methods for sampling on graphs an estimating various network statistics.

Overview and limitations of existing methods:

MCMC methods for sampling from large graphs essentially employ random walks that are Markovian and ergodic in nature, meaning that the underlying (stochastic) transition

kernels have nice properties such as, aperiodicity, positive recurrence and irreducibility. The ergodic theorem for such Markov chains ensures that the empirical distribution $\bar{\mathbf{x}}(t) = [x_i(t)]$ of the stochastic process $X(t)$, given by $x_i(t) = (1/t)\sum_{k=1}^{t} \mathbb{1}_{\{X(k)=i\}}$ for all nodes i of the graph, converges to the stationary distribution $\boldsymbol{\pi}$ of the Markov chain, that is $x_i(t) \to \pi_i$ for all i. This stationary distribution $\boldsymbol{\pi}$ is the solution to $\boldsymbol{\pi}^T\mathbf{P} = \boldsymbol{\pi}^T$, such that $\boldsymbol{\pi}^T\mathbf{1} = 1$ and $\boldsymbol{\pi} > \mathbf{0}$, and is the eigenvector corresponding to the largest eigenvalue of $\mathbf{P}$, also referred to as the first/leading/principal eigenvector of the Markov chain kernel. Sampling each node visited by the random walk is then equivalent to sampling from $\boldsymbol{\pi}$ in the long run, and the problem is then the design of a Markov chain whose stationary distribution coincides with the desired sampling distribution, given up front. Techniques to do this have been well established, such as the acceptance-rejection framework which forms part of the famous Metropolis Hastings algorithm, and importance-reweighting schemes which allow the use of simple random walks for sampling [101].

While the convenient properties of the underlying linear Markovian kernels of such estimators have allowed the extensive application of classical probability and linear algebra techniques, with useful theoretical results on mixing times and asymptotic variance of the estimates [1], application settings have largely been restricted to those accommodated for by the initial works in the field. This is because of a reliance on the ergodic theorem of Markov chains [26], which only guarantees convergence of the estimates to the leading eigenvector of the kernel, severely restricting the family of algorithms to only the estimation of positive vectors that are either probability distributions or various centrality measures such as PageRank. However, there are important network quantities other than leading eigenvectors, such as *higher order* eigenvectors of graph Laplacian matrices, for which no random walk based approximation algorithms exist. The field of spectral graph theory [32] is dedicated to analysing the properties of these matrices, and it so happens that higher order eigenvectors of these graph Laplacian matrices are key to performing tasks such as spectral clustering [114, 135]. We make the crucial observation that the *combinatorial* Laplacian $\mathbf{L}$ can be used to generate a continuous time Markov chain (CTMC) with transition rate matrix (or kernel) $\mathbf{Q} = -\mathbf{L}$. Thus an eigenvector vector $\mathbf{v}_k$ of $\mathbf{L}$ can be interpreted as the an eigenvector of $\mathbf{Q}$ corresponding to the smallest positive eigenvalue $\lambda_2(\mathbf{L})$, which opens up the possibility of using random walks to approximate it. This relationship between graph Laplacian matrices and reversible Markov chains on discrete, finite state spaces is bijective, implying that there exists a (weighted) directed graph for every reversible Markov chain kernel as well. Therefore any interactive random walk based method to extract information

on the eigenvectors of a graph Laplacian matrix can also be used to extract information on the eigenvectors of a reversible Markov chain kernel as well. Considering this important connection, the lack of any such methods towards the approximation of higher order eigenvectors of Markovian kernels, given their importance, is concerning.

Expanding theoretical boundaries by employing interactons

Interaction based stochastic processes is a major branch of probability theory. These include systems of stochastic processes that interact with each other according to their location on the state space [87], as well as processes which interact with their own empirical distributions [19], or both. Interaction mechanisms can be thought of as intuitive ways of introducing non-linearities to the stochastic process, with analysis of limiting behavior usually performed through the study of a closely related deterministic system rather than depending on the ergodic theorem.

An example is the self-interacting, non-Markovian process originally described in [2], with further analysis and extensions in [19, 25], whose empirical distribution converges to the *quasi-stationary* distribution QSD) of a sub-stochastic (transient) Markov chain kernel. The QSD by definition is the long run distribution of a transient Markov chain conditioned on the event that it never gets absorbed by the absorbing states, and very recently the interacting mechanisms in [19] were leveraged to develop a non-Markovian Monte Carlo algorithm for sampling on a *directed* graph from any given probability distribution [76]. This was the first such extension of the original setting in the Metropolis Hastings, and even though the QSD is still a leading eigenvector (of a sub-stochastic matrix), this is a good example of how simple interactive terms can be employed to expand the theoretical boundaries. Considering the fact that this first true extension of use cases of Random walk samplers took nearly fifty years, it is clear that little attention has been given to leveraging these interaction mechanisms for more algorithmic purposes.

1.1.2 Competitive interactions in models of epidemic spread

Classical models of epidemic spread focus on the qualitative description of the propagation of a single disease/virus strain/epidemic over a population. By qualitative, we mean that they focus on being able to capture and explain fundamental characteristics, such as the epidemic eventually infecting everyone in models like the *Susceptible-Infected* (SI) model if recovery from the infection is not possible; or the epidemic being strong enough to

go pandemic and having a constant long run presence in models like the *Susceptible-Infected-Susceptible* (SIS) model where recovery and reinfection of individuals are both allowed. In recent years, the development of models which capture the competition of two or more of such epidemics has seen a surge of interest. In particular, models capturing the behavior of *two competing* epidemics of the *Susceptible-Infected-Susceptible* (SIS) types, also known as the *bi-virus* or *bi-SIS* models, have garnered significant attention over the years [104, 108, 109, 138, 83].

Epidemic models take the form of ordinary differential equations (ODEs) and their analysis involves the identification of fixed points of the system, their uniqueness properties, and ultimately showing the convergence of the solution trajectories to those fixed points. The technique via Lyapunov functions has historically been a popular method to prove convergence to fixed points and was also used in epidemiology literature to derive the convergence properties of the SIS epidemic model. The SIS model was originally introduced in [74] to capture the spread of Gonorrhea due to contact between individuals in a population, and was further developed in [95, 130, 50, 81, 136, 51]. The central result for SIS epidemics, originally proved using Lyapunov functions in [74], is a *dichotomy* arising from the relation between model parameter ($\tau > 0$) representing the effective infection rate or strength of the virus,[1] and a threshold value ($\tau^* > 0$). When $\tau \leq \tau^*$, the virus spread is not strong enough and the system converges to a 'virus-free' state. When $\tau > \tau^*$, it converges to a state where the virus infects a non-zero portion of the population. Attempts have also been made to perform similar convergence analysis for the bi-virus epidemic model [104, 109, 138, 83]. The key questions posed in such literature are: Can both competing epidemics coexist over the network? If not, which one prevails? Or do both die out? This *trichotomy* of possible results is what the recent literature has been trying to characterize.

While the original SIS model introduced in [74] had the aggregate infection and recovery rates of a node as *linear* functions of the number of infected neighbors, there has been a push towards studying more generalized models where these rates are made heterogeneous (across nodes) and *non-linear* [12, 64, 68, 13]. Realistic assumptions such as infection rates tending to saturation with continual increase in neighborhood infection [85] have become more commonplaces, implying that the models employing strictly linear spreading dynamics often provide overestimates to the real world infection rates [138]. In some special cases, non-linear recovery rates also have an interpretation linking them to reliability theory

[1] $\tau = \beta/\delta$, where $\beta > 0$ stands for the infection rate of the virus and $\delta > 0$ the recovery rate from the virus. Section 4.1 provides a detailed explanation.

in the form infection duration with increasing failure rates (*failure* here being the recovery of an infected node). Allowing for non-linear infection and recovery rates leads to a more general version of the bi-virus model on overlaid graphs, albeit much more complicated, and the complete convergence criterion is yet to be fully established [109, 138].

Surprisingly, convergence properties of competing models are not as well established as those of their single-virus counterparts. In bi-virus models for instance, most recent attempts to establish convergence to various possible equilibria of the system, and the corresponding conditions on the virus strength, have not really gone beyond resorting to use the original Lyapunov functional in [74] and convergence results therein. However, we observe that models with such competition based interactions end up satisfying certain monotonicity properties with respect to a specially designed cone-based partial ordering of the state space. From basic real analysis, we know that monotone sequences in closed and bounded subsets of $\mathbb{R}^n$ converge [140]. Using this as the starting point, we believe that the complete qualitative analysis of competition based epidemic models is indeed possible.

1.2 Research focus

For the rest of this report, we build on the intuition provided in Section 1.1. The research work in this report focuses on:

• **Designing interactive random walks to approximate the *second* eigenvector, or Fiedler vector of reversible Markov chains:** By the second eigenvector, we are referring to the eigenvector corresponding to the second largest eigenvalue of reversible CTMC kernels, or the second smallest eigenvalue of graph Laplacian matrices; usually referred to as the Fiedler vector. Originally introduced by Miroslav Fiedler in his works on algebraic connectivity [45, 46], the Fiedler vector has found applications in areas such as graph partitioning and clustering [102, 103, 39, 94, 114, 141, 38, 96, 4], graph drawing [70], graph colouring [9], envelope reduction [14] and the analysis of proteins [73, 111]. It plays an important role in spectral graph theory [34, 32], providing powerful heuristics by solving relaxations of NP-hard, integer problems on graph bi-partitioning [135, 112, 52]. While MCMC techniques, by employing various versions of random walks and via the ergodic theorem, are successful in estimating π (or sampling according to π) - the first/leading/principal eigenvector of the Markov chain kernel $\mathbf{Q}$, no similar techniques have provided extensions to the second eigenvector. We take a step forward and provide a framework based on interacting random

walks, a suitably scaled version of which achieves the *second eigenvector* of the class of reversible Markov chain transition matrices, for sufficiently large number of walks. To the best of our knowledge, our framework is the first one to do so, and opens up possibilities of estimating higher order eigenvectors by using such interacting random walk based techniques.

• **Designing Self-Repelling Markov Chains to speed up convergence of MCMC estimators:** Random walks on graphs can suffer from slow diffusion, depending on the topology. When using them to drive Markov chain Monte Carlo algorithms, samples obtained can often be highly correlated - an undesirable side effect that can increase estimator variance [cite]. We design a *self-repellent random walk* (SRRW) which is less likely to transition to nodes that were highly visited in the past, and more likely to transition to seldom visited nodes. This form of interaction with its own past history puts the random walk in the class of *self-interacting Markov chains* (SIMC) - generally described as a technique to simulate nonlinear Markovian kernels. We prove convergence of the SRRWs on general graphs by providing a Strong Law of large Numbers (SLLN) result and a Central Limit Theorem (CLT) for its occupational/empirical measure. We show that the SRRW achieves a smaller asymptotic covariance than the well known simple random walk (SRW) in the sense of Loewner ordering of covariance matrices, thereby exploring its potential as a (nonlinear) MCMC estimator.

• **Providing complete characterization of the trichotomy of outcomes for the competing, bi-SIS epidemic model:** We analyze the bi-virus model with *non-linear* infection and recovery rates (or the *non-linear bi-virus model* in short) and provide the complete characterization of the trichotomy of the outcomes with necessary and sufficient conditions under which the system globally converges to one of the three possible points: (i) a 'virus-free' state, (ii) a 'single-virus' equilibrium, or (iii) an equilibrium where both viruses coexist over the network. While the result for convergence to the virus-free state of the bi-SIS model is not new for non-linear infection and linear recovery rates, our proof for the same is the most general form known to date, covering the case with both infection *and* recovery rates being non-linear. The proof of convergence to the virus-free state of the *bi-virus* model is straightforward, and directly follows from the convergence criterion for the *single-virus* SIS model with non-linear rates. However, the convergence results for fixed points where only one of the two viruses survives, or to the equilibrium where both viruses coexist, are not as straightforward to establish, rendering the typical Lyapunov

based approach largely inapplicable.

In proving these results, we first show, using a specially constructed cone based partial ordering, that the bi-virus epidemic model possesses some inherent monotonicity properties. We then use novel techniques from the theory of *monotone dynamical systems* (MDS) [119] to prove our main results - the *global* stability of the system for any possible combination of the model parameters, starting from any initial point in the state space.

• **Quantifying the coexistence equilibria of bi-SIS epidemic models:** To complement out qualitative study on global convergence of bi-SIS models on multi-layered graphs, we also provide quantitative results characterizing the behaviour of coexistence equilibria (CE) of the bi-SIS model on general graphs with respect to effective infection rates τ_1, τ_2 of the two competing viruses. Building upon crucial observations obtained via fixed point analysis of the bi-virus system in the MDS framework, we provide new results on the relationship between the long run probability of being infected by Virus 1 versus that of Virus 2, with regards to change in system parameters τ_1, τ_2. These results are sharper than those emerging out of mere convergence analysis, and enable us to further quantify the connection between the CE and the positive equilibrium of corresponding single-SIS models, as well as the spectral radius of the underlying graphs in the form of various upper bounds. We also briefly show via numerical results that the upper bounds are successful in capturing the trend in which the CE fixed points change with the system parameters. Our results provide a deeper understanding of how the increase (decrease) in strength of one virus affects the presence of its competitor over the network, showing that the expected decrease (increase) can be more drastic than one would expect.

1.3 Current Status Quo

We briefly look at existing techniques for approximating the Fielder vector, and current status quo when it comes to analysing the bi-SIS epidemic model.

• **Existing Fiedler vector approximation techniques:** Since no random walk based techniques exist, ours is the first attempt to the approximation of the Fielder vector using random walk methods. Hence, we just have a brief look at the deterministic methods often employed for approximating the Fiedler vector. We will not provide a comparison of these

works with ours, since they assume that the entire graph in question is given up front, which is not the same as our problem setting which requires no such assumption.

The most notable of these deterministic algorithms are techniques based on graph sparsification [122, 123, 124], and multi-level/multi-grid techniques [14, 15, 29, 44]. Both of these focus on pruning edges of the graph to obtain a 'sparser' or 'coarser' subgraph. Fiedler vector computation is then performed on these subgraphs to obtain approximations to the Fiedler vector of the original graph. While the pruning can be done via innovative probabilistic rules based on measures such as effective resistance [122], or using greedy, deterministic rules [15], the core computation of the Fiedler vector is still carried out by various kinds of power methods. The Fiedler vector is also directly related to the mixing time[80, 1, 26] via the corresponding second eigenvalue $\lambda_2(\mathbf{Q})$, also known as the spectral gap, and algorithms to approximate this quantity [33, 53, 67] are fundamentally different from those estimating the Fiedler vector. Other techniques include [24], which approximates the Fiedler vector in a distributed fashion over ad-hoc networks, where 'ad-hoc' refers to the nodes having the ability to process information locally and exchange information with neighbors in a synchronous fashion, and 'distributed' refers to each node estimating it's own component of the Fiedler vector using a local version of power iterations; and [125], which uses techniques such as matrix deflation to develop another power method to numerically compute the Fiedler vector using the dominant eigenvector of a slightly smaller matrix.

- **Study of random walks employing self-avoidance/repelling mechanisms:** Theoretical studies on random walks on countable state spaces employing self-repelling mechanisms, where the repulsion is 'soft' in the sense that past visited nodes are never completely avoided with probability one, have mainly been conducted on state spaces such as the 1 or d-dimensional lattices [127, 3, 131]. While many of these studies take into account not just the vertex visit count but the also number of times edges are traversed, the theoretical results, while still intriguing, are often not suitable to the design of real world algorithms on finite networks. Some works do consider finite topologies such as complete graphs [31, 105], although interactions in this case are not with the random walker's own empirical measure, and are instead with that of an opposing particle. Although the analytical approach therein using stochastic approximation and the ODE method is more aligned with the techniques in Chapter 3, there is little control over the dynamics and the knowledge of its stationary distribution. In summary, the study of self-repelling random walkers on general graphs that can be designed in a way that it allows for a degree of control over their occupational

measures, has remained a largely unexplored territory.

• **Status quo on analysis of the bi-virus epidemic model:** Of all the recent works concerning the spread of SIS type bi-virus epidemics on overlaid networks, [138] and [109] provide conditions under which the system globally converges to the state where one virus survives while the other dies out. [138] approaches the problem of showing global convergence by employing the classic technique via Lyapunov functions. However, finding appropriate Lyapunov functions is a highly non-trivial task, and as mentioned in [109], is even more difficult due to the coupled nature of the bi-virus ODE system. This can be seen in the condition they derive in [138] for the case where, say, Virus 1 dies out and Virus 2 survives. When τ_1 and τ_2 represent the effective strengths of Virus 1 and Virus 2, respectively, their condition translates to $\tau_1 \leq \tau_1^*$ where τ_1^* is the threshold corresponding to the single-virus case, meaning that Virus 1 would not have survived even if it was the only epidemic present on the network. More importantly, [138] is unable to characterize convergence properties for $\tau_1 > \tau_1^*$ and $\tau_2 > \tau_2^*$.

The authors in [109] take a different approach and tackle this problem by applying their 'qualitative analysis' technique, which uses results from other dynamical systems that bound the solutions of the bi-virus ODE; and provide conditions under which the system globally converges to single-virus equilibria. As we show later in Section 4.4.2, however, their conditions not only characterize just a *subset* of the actual space of parameters that lead to global convergence to the single-virus equilibria (which they themselves pointed out), but the size of this subset is highly sensitive to the graph topology, often much smaller than what it should be in general. In other words, a complete characterization of the *entire* space of model parameters, on which the system globally converges to one of the trichotomic states, has still been recognized as an open problem in the bi-virus literature [138, 109, 83].

• **Existing quantitative results for bi-SIS systems:** Threshold conditions for the single-virus SIS model have been repeatedly, independently rediscovered [30, 90], with follow-up works [130, 129] being successful in establishing quantitative bounds on the long run infection probabilities/market share/influence in the case when the virus/product/opinion persists, even showing convexity of the average infection probabilities in $1/\tau$ in some cases [90]. However when it comes to bi-SIS epidemics, apart from a few results which are simply by-products of the techniques utilized for the convergence proofs in [41, 139], there is a lack of quantitative bounds on coexistence equilibria, and little understanding of their

monotonicity properties with respect to the system parameters.

1.4 Organization

The rest of the report is organized as follows. In Chapter 2, we detail the construction of our interactive random walk based stochastic process and provide a complete analysis of the same to formally prove the convergence of a suitably scaled version of the process to the Fiedler vector for any time reversible Markov chain kernel, along with simulations to support the same. In Chapter 3 once again employ self-interactions as a source of nonlinearity in state transitions to design the self-repellent random walk, showing its improvement over the classical simple random walk, via analysis of the covariance matrix arising out of second order convergence results. In Chapter 4, we work on the analysis of the bi-virus epidemic model and give precise conditions under which the system globally converges to the trichotomy of possible outcomes. We then take a closer look at the co-existence equilibria of bi-virus models, providing quantitative analysis in Chapter 5. We then provide our concluding remarks in Chapter 6

Chapter 2

Fiedler Vector Approximation via Interacting Random Walks

In this chapter, we begin by giving the basic notations and an introduction to the Fiedler vector via its application in graph partitioning in Section 2.1. The main theoretical results are distributed among Sections 2.2, 2.3 and 2.4. In Section 2.2, we detail the construction of our stochastic process and via Theorem 2.2.4 we relate it to a system of ordinary differential equations (ODEs) as its fluid limit. We show that over a finite time horizon, the stochastic process rarely deviates from the solution of the ODE when the number of walkers is sufficiently large. Section 2.3 is devoted to the stability analysis of the resulting deterministic ODE system, where we show using a Lyapunov function that the Fiedler vector is the only asymptotically stable fixed point of a suitably scaled version of the system, while all others being unstable. In Section 2.4 we bring together our results from Sections 2.2 and 2.4 to formally show that for sufficiently large number of walkers, our stochastic process spends most of its time in the long run around the asymptotically stable Fiedler vector, while never getting stuck around an unstable fixed point. In Section 2.5, we provide numerical results to support our theoretical findings and also simulations over time varying dynamic graphs to show the robustness of our framework in that setting. In Section 2.6, we extend all our results to include various graph Laplacians and time reversible Markov chain kernels. Section 4.7 provides our concluding remarks.

2.1 Preliminaries

2.1.1 Basic notations

Let $\mathcal{G}(\mathcal{N},\mathcal{E})$ denote a general, undirected, connected graph, with $\mathcal{N}$ being the set of nodes and $\mathcal{E}$ being the set of edges, represented by pairs (i,j) for $i,j\in\mathcal{N}$. Let the cardinality of $\mathcal{N}$ be given by a natural number N (i.e. $|\mathcal{N}|=N$). The mathematical quantities best capturing all the information of $\mathcal{G}(\mathcal{N},\mathcal{E})$ are the 'adjacency matrix' $\mathbf{A}$[1] defined as $\mathbf{A}_{ij}\triangleq 1$, if $(i,j)\in\mathcal{E}$ and 0, otherwise $\forall i,j\in\mathcal{N}$, and the diagonal 'degree matrix' $\mathbf{D}$ of the graph defined as $\mathbf{D}_{ii}\triangleq\sum_{j\in\mathcal{N}}A_{ij}\ \ \forall i\in\mathcal{N}$. We call $\mathbf{D}_{ii}$ the 'degree' of node $i\in\mathcal{N}$, and alternatively represent it as $d(i)\triangleq\mathbf{D}_{ii}$.

Since vectors and matrices will be used throughout the chapter, we standardize their notation. Lower case, bold faced letters will be used to represent vectors (e.g. $\mathbf{v}\in\mathbb{R}^N$), while upper case, bold faced letters will be used to represent matrices (e.g. $\mathbf{M}\in\mathbb{R}^{N\times N}$), unless clarified otherwise. The i^{th} (ij^{th}) entry of vector $\mathbf{v}$ (matrix $\mathbf{M}$) will be denoted by v_i or $[\mathbf{v}]_i$ (M_{ij} or $[\mathbf{M}]_{ij}$), depending on the situation. We let $\mathbf{D}_{\mathbf{v}}:=\text{diag}(\mathbf{v})$ represent the diagonal matrix with $[\mathbf{D}_{\mathbf{v}}]_{ii}=v_i$. Also denote by $\mathbf{1}=[1,1,\cdots,1]^T$ and $\mathbf{0}=[0,0,\cdots,0]^T$, the N-dimensional vectors of all ones and zeros respectively, and $\mathbf{e}_k$ for all $k\in\{1,\cdots,N\}$ represent the canonical basis vectors in R^N, which take value 1 at their k^{th} entry, 0 at every other entry.

The use of '$\mathbf{Q}$' will be reserved exclusively for representing transition rate matrices of continuous time Markov chains (CTMCs). '$\mathbf{P}(\cdot)$' will be used to denote the probability measure, while simple '$\mathbf{P}$' will be used exclusively for transition probability matrices of discrete time Markov chains (DTMCs). Note that throughout the chapter, we shall often refer to these matrices using the umbrella term *kernel* of Markov chains. Vectors such as $\mathbf{x}(t)$ and $\mathbf{y}(t)$, with t being time, will be used to denote (deterministic) solutions to systems of ordinary differential equations (ODEs). However, if indexed by a parameter, for example $\mathbf{x}^n(t)$ and $\mathbf{y}^n(t)$, they will be used to denote stochastic processes (also parameterized by n). This distinction between notations of similar deterministic and stochastic quantities shall be reiterated when we define such quantities later on.

Finally, we let $\|\cdot\|$ denote the Euclidean norm for any Euclidean space (i.e. with the

[1] In the case of a weighted graph, we replace $\mathbf{A}$ by the weighted adjacency matrix $\mathbf{W}$, where the ij^{th} entries represent the weights assigned to each edge. All other equations remain the same. However, we will safely exclude any further, separate mention of weighted graphs because the scope of our results is broad enough to cover not just weighted graphs, but also similar quantities such as kernels of time reversible Markov chains, as we shall observe later in Section 2.6.

appropriate dimensions implicitly understood), and use $\tilde{\cdot}$ to denote normalized versions of vectors, or sets containing normalized vectors.

2.1.2 Graph Laplacians

Consider an undirected, connected graph $\mathcal{G}(\mathcal{N},\mathcal{E})$. The quantity of interest throughout the chapter will be the *Combinatorial Laplacian*, which is defined as

$$\mathbf{L} \triangleq \mathbf{D} - \mathbf{A}.$$

$\mathbf{L}$ is a symmetric (due to the graph being undirected), positive-semidefinite matrix with non negative eigenvalues. Since the graph is connected, $\mathbf{A}$, and as a result $\mathbf{L}$, are irreducible matrices. Thus, the Perron Frobenius (PF) [65, 88] theorem applies and the smallest eigenvalue 0 (with eigenvector being $\mathbf{1}$) has multiplicity 1. We denote by $0 = \lambda_1 < \lambda_2 \leq \cdots \leq \lambda_N$, the spectrum of $\mathbf{L}$, with $\mathbf{1} = \mathbf{v}_1, \mathbf{v}_2, \cdots, \mathbf{v}_N$ being the corresponding eigenvectors.

Closely related to the combinatorial Laplacian is the *normalized or symmetric Laplacian*, which goes by

$$\mathscr{L} \triangleq \mathbf{D}^{-1/2}\mathbf{L}\mathbf{D}^{-1/2} = \mathbf{I} - \mathbf{D}^{-1/2}\mathbf{A}\mathbf{D}^{-1/2}.$$

Also a symmetric positive semi-definite matrix, it's smallest eigenvalue is 0 (with corresponding eigenvalue being $\mathbf{D}^{1/2}\mathbf{1}$). Denote by $0 = \bar{\lambda}_1 < \bar{\lambda}_2 \leq \cdots \leq \bar{\lambda}_N$, the spectrum of $\mathbf{L}$, with $\mathbf{D}^{1/2}\mathbf{1} = \bar{\mathbf{v}}_1, \bar{\mathbf{v}}_2, \cdots, \bar{\mathbf{v}}_N$ being the corresponding eigenvectors.

The third graph Laplacian we introduce is the *random walk Laplacian*, denoted by $\mathbf{L}^{rw}$. We shall define it using the combinatorial and symmetric Laplacians as

$$\mathbf{L}^{rw} \triangleq \mathbf{D}^{-1}\mathbf{L} = \mathbf{D}^{-1/2}\mathscr{L}\mathbf{D}^{1/2} = \mathbf{I} - \mathbf{D}^{-1}\mathbf{A}.$$

It gets its name because $\mathbf{P} = \mathbf{D}^{-1}A$ is a stochastic matrix (all the rows add up to one) which defines a simple random walk in discrete time on the graph. $\mathbf{L}^{rw}$ is not a symmetric matrix. However, note that due to the similarity transformation (second equality), it shares the same spectrum as $\mathscr{L}$ with its left eigenvectors given by $\mathbf{v}_i^{rw} = \mathbf{D}^{1/2}\bar{\mathbf{v}}_i$ where $\bar{\mathbf{v}}_i$ is an eigenvector of $\mathscr{L}$. The PF eigenvector of $\mathbf{L}^{rw}$ is therefore given by $\mathbf{v}_1^{rw} = \mathbf{D}\mathbf{1}$, the vector with its entries being the degree of the respective node.

2.1.3 Graph bi-partitioning and Fiedler vector

The second eigenvalue of $\mathbf{L}$, i.e. λ_2, is known as the algebraic connectivity of a graph, and the corresponding eigenvector is commonly referred to as the *Fiedler vector*. We shall however use the term *Fiedler vector* to refer to second eigenvectors of any graph Laplacian matrix. To convey the relevance of the Fiedler vector, we look at the problem of bi-partitioning a graph, whose objective is to partition a connected graph into two connected subgraphs in the most 'natural' way possible. This is often interpreted as partitioning the graph into two subgraphs S and S^c with the fewest number of edges interlinking them, but also not having meaningless solutions such as partitioning the graph at leaf nodes. This train of thought has evolved into the study of problems such as the *Ratio-cut* problem (*RCut*) [135, 52] and the *Normalized-cut* problem (*NCut*) [135, 112], among others. Define $\text{Cut}(S) \triangleq (1/2)\sum_{i\in S}\sum_{j\in S^c} A_{ij}$, for any $S \subset \mathcal{N}$. The *RCut* problem for graph bi-partitioning is given by

$$\text{RCut}(\mathcal{G}) = \min_{S\subset\mathcal{N}} \text{RCut}(S) = \min_{S\subset\mathcal{N}} \Big(\frac{\text{Cut}(S)}{|S|} + \frac{\text{Cut}(S^c)}{|S^c|} \Big), \tag{2.1}$$

Unfortunately, minimizing the *RCut* over all subsets of $\mathcal{N}$ is an NP hard problem. [52] showed that by enlarging the integer valued domain into the real valued domain, approximate solutions can be found efficiently. For the *RCut* problem, this real valued relaxation is given by

$$\text{RCut}(\mathcal{G}) \approx \min_{\mathbf{f}\perp\mathbf{1},\ \mathbf{f}\neq 0} \frac{\mathbf{f}^T\mathbf{L}\mathbf{f}}{\mathbf{f}^T\mathbf{f}},$$

the solution to which is well known, and is the Fiedler vector $\mathbf{v}_2$ of $\mathbf{L}$. Likewise, a relaxation of the similar *NCut*[2] problem is solved by $\bar{\mathbf{v}}_2$, the Fiedler vector of the normalized Laplacian $\mathscr{L}$ (or equivalently, the Fiedler vector of $\mathbf{L}^{rw}$, since they share the same signs for the entries, leading to the same partition). Partitioning according to the signed entries of these second eigenvectors therefore solves natural relaxations to well-defined but difficult to solve bi-partitioning problems, and these observations have paved the way for spectral clustering[34, 32, 94, 40, 141, 38, 52, 112, 102, 113] as a powerful data analysis tool.

[2]The *NCut* problem is similar to the *RCut* problem with the terms $|S|$ and $|S^c|$ in the denominator replaced by $\text{Vol}(S)$ and $\text{Vol}(S^c)$, where $\text{Vol}(S) \triangleq \sum_{i\in S} d(i)$.

2.2 A multi-walk, interacting stochastic process with a deterministic limit

We aim to construct a random walk based process which, in the long run, can approximate the Fiedler vector (second eigenvector of $\mathbf{L} = \mathbf{D} - \mathbf{A}$). Our process consists of multiple random walks interacting with each other in a prescribed manner. This can also be written as a density dependent process (with parameter 'n' proportional to the number of random walks) that has a deterministic fluid limit. In this section we provide construction of our stochastic process, and the result on its convergence to a deterministic process (its fluid limit).

2.2.1 The interacting stochastic process

Let $\mathcal{G}(\mathcal{N}, \mathcal{E})$ be any undirected, connected graph, with $N = |\mathcal{N}|$ as before. For any $n \in \mathbb{N}$, consider $2n$-many random walkers traversing $\mathcal{G}(\mathcal{N}, \mathcal{E})$ according to a CTMC generated by the kernel $\mathbf{Q} = -\mathbf{L} = \mathbf{A} - \mathbf{D}$. These $2n$ walkers are split into two groups, of n walkers each, by labeling them as either 'type-x' or 'type-y'. Define the stochastic process $\big(X(t), Y(t)\big)_{t\geq 0}$, where $X(t) \in \mathbb{N}_0^N$ ($Y(t) \in \mathbb{N}_0^N$) is a vector such that $X(t)_i$ ($Y(t)_i$) indicates the number of type-x (type-y) walkers present at node $i \in \mathcal{N}$ at time $t \geq 0$. Since there are n walkers of each type, we have $\sum_{i\in\mathcal{N}} X(t)_i = \sum_{i\in\mathcal{N}} Y(t)_i = n$ for all $t \geq 0$. The state space is given by

$$\Gamma_n \triangleq \left\{ (X, Y) \in \mathbb{N}_0^N \times \mathbb{N}_0^N \;\middle|\; \sum_{i\in\mathcal{N}} X_i = \sum_{i\in\mathcal{N}} Y_i = n \right\}. \tag{2.2}$$

Ever so often, a type-x walker traversing the graph may find itself at a node with type-y walkers present. Such an event is what we call an 'interaction'. When an interaction occurs, every type-y walker present 'kills' each type-x walker present with rate κ/n, for some scalar $\kappa \in (0, +\infty)$. In return, every type-x walker present 'kills' each type-y walker present with rate κ/n. Another way to describe this interaction is in a pairwise manner. Given any possible 'pair' of one type-x and one type-y walker present at node j, they both kill each other with rate κ/n. At every node $j \in \mathcal{N}$ there are $X(t)_j Y(t)_j$ such pairs at any time $t \geq 0$. Thus, overall, type-x or type-y walkers die with rate $\frac{\kappa}{n} X(t)_j Y(t)_j$. Upon being killed, the 'dead' walker relocates to the position of another randomly selected walker of the same type. At time $t > 0$, this is equivalent to saying that a killed type-x walker will redistribute to

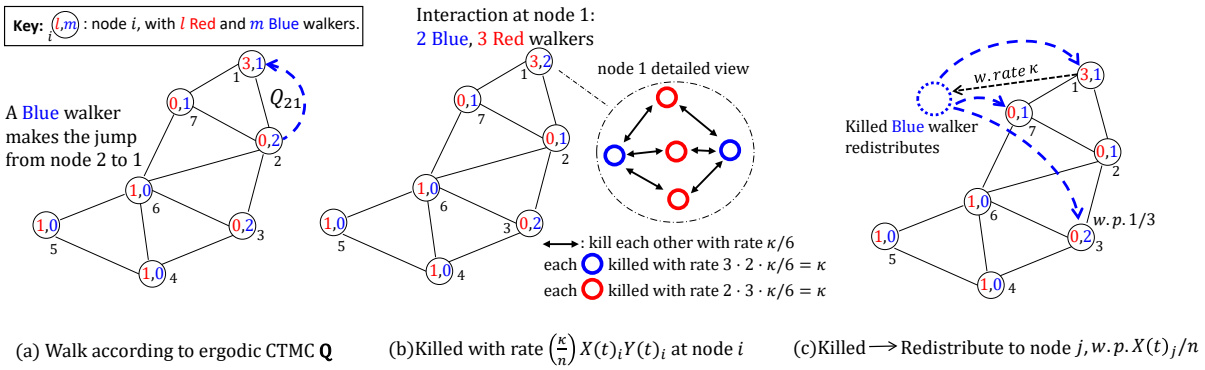

Figure 2.1 The interaction and redistribution mechanism.

some node $i \in \mathcal{N}$ with probability $X^n(t)_i/n$, which is proportional to the number of type-x walkers present at node i. Similarly, a killed type-y walker will redistribute to node $i \in \mathcal{N}$ with probability $Y^n(t)_i/n$.

Consider Figure 2.1 as an example of an interaction event. We consider $n = 6$. The colour blue is used for type-x walkers, while red is used for type-y walkers. At each node, the number of *blue* and *red* walkers present is given by the respectively coloured numeric entry. Figure 2.1(a) shows a *blue* walker moving from its initial position at node 2, to node 1, with rate Q_{21}. Figure 2.1(b) shows a snapshot of the system at a time right after the event in Figure 2.1(a). Node 1 is now the site of interactions between 2 *blue* and 3 *red* walkers. A detailed view of the interactions at node 1 is shown, where an arrow represents a pair of walkers killing each other with rate κ/n. Let $r \in \mathbb{N}$ count the number of arrows connected to any particular walker. Then, that walker is killed by the group of the other type walkers with the total rate $\frac{\kappa}{n} \cdot r$. Following this logic, each *blue* walker in Figure 2.1(b) is killed with rate $\frac{\kappa}{6} \cdot 3 = \kappa/2$. Since there are two *blue* walkers present, one of them is killed with rate $\frac{\kappa}{2} \cdot 2 = \kappa$. Similarly, each *red* walker is killed individually with rate $\kappa/3$, and since there are three *red* walkers, one of them is killed with rate κ. Therefore the rate with which a *blue* walker dies is the same at which a *red* walker dies at node 1. Finally, Figure 2.1(c) shows an event in which a *blue* walker is killed at node 1. Upon death, it instantaneously relocates to the position of another *blue* walker chosen uniformly at random. That is, it randomly redistributes to node i with probability $X(t)_j/n$. A similar redistribution would occur if a *red* walker was to die instead of a *blue* walker, in which case it would redistribute to node j with probability $Y(t)_j/n$.

Events of the process $\big(X(t), Y(t)\big)_{t\geq 0}$ involve type-x or type-y walkers going from a node j to another node i. This corresponds to jumps of size $(\mathbf{e}_i - \mathbf{e}_j, 0)$ for type-x and $(0, \mathbf{e}_i - \mathbf{e}_j)$

for type-y walkers. At any state $(X, Y) \in \Gamma_n$, jumps can be caused by walking from $j \to i$ according to the base CTMC kernel $\mathbf{Q}$, which happens with rate $Q_{ji}X_j$ for type-x walkers and $Q_{ji}Y_j$ for type-y walkers. The jumps can also occur as a result of being killed at node j and redistributed to node i. As mentioned earlier, one of the type-x walkers at node j is killed with rate $\frac{\kappa}{n}X(t)_j Y(t)_j$, upon which it redistributes to i with probability $\frac{X_i}{n}$. Therefore, the jump $j \to i$ occurs with the overall rate $\frac{\kappa}{n}X(t)_j Y(t)_j \frac{X_i}{n}$ for type-x walkers. Similarly, type-y are killed at j and redistributed to i with overall rate $\frac{\kappa}{n}X(t)_j Y(t)_j \frac{Y_i}{n}$.

Hereafter, for any state $(X, Y) \in \Gamma_n$, we use $\mathbf{x} \in \mathbb{R}^N$ to denote the density distribution of type-x walkers over the graph, with $x_i \triangleq \frac{X_i}{N}$. Similarly we use $\mathbf{y} \in \mathbb{R}^N$ to denote the density distribution of type-y walkers over the graph, with $y_i \triangleq \frac{Y_i}{N}$. Let $\bar{\mathbf{Q}}^n_{x:j\to i}(X, Y)$ denote the total rate with which jumps of type $(\mathbf{e}_i - \mathbf{e}_j, 0)$ occur, and similarly let $\bar{\mathbf{Q}}^n_{y:j\to i}(X, Y)$ denote the total rate with which jumps of size $(0, \mathbf{e}_i - \mathbf{e}_j)$ occur. From all of the above, these two quantities can be written as

$$\bar{Q}^n_{x:j\to i}(X, Y) = Q_{ji}X_j + (\frac{\kappa}{n}Y_jX_j)x_i = n\big(Q_{ji}x_j + (\kappa y_j x_j)x_i\big) \tag{2.3}$$

$$\bar{Q}^n_{y:j\to i}(X, Y) = Q_{ji}Y_j + (\frac{\kappa}{n}X_jY_j)y_i = n\big(Q_{ji}y_j + (\kappa x_j y_j)y_i\big). \tag{2.4}$$

We can think of $\bar{Q}^n_{x:j\to i}$ and $\bar{Q}^n_{y:j\to i}$ for all $i, j \in \mathcal{N}, i \neq j$ as the off-diagonal entries of a $2N \times 2N$ dimensional matrix $\bar{\mathbf{Q}}(X, Y)$. This matrix is then the transition rate matrix of the CTMC $\big(X(t), Y(t)\big)_{t\geq 0}$ on a finite state space Γ_n as in (2.2), and we have now fully characterized our stochastic process.

2.2.2 A closely related deterministic system

Define the density dependent version of the stochastic process $(X(t), Y(t))_{t\geq 0}$ as $(\mathbf{x}^n(t), \mathbf{y}^n(t))_{t\geq 0} \triangleq (X(t)/n, Y(t)/n)_{t\geq 0}$. Its state space Θ_n is a version of Γ_n where each entry is scaled by $\frac{1}{n}$, or more precisely,

$$\Theta_n = \Sigma_n \times \Sigma_n, \tag{2.5}$$

where $\Sigma_n = \Sigma \cap \{\frac{1}{n}\mathbf{u} \mid \mathbf{u} \in \mathbb{Z}^N\}$, with $\Sigma \triangleq \{\mathbf{u} \in \mathbb{R}^N \mid \mathbf{u}^T\mathbf{1} = 1, \mathbf{u} \geq 0\}$ and $\mathbb{Z}^N$ being the N-dimensional grid. Jumps of size $\frac{1}{n}(\mathbf{e}_i - \mathbf{e}_j, 0)$ and $\frac{1}{n}(0, \mathbf{e}_i - \mathbf{e}_j)$ for the process $\big(\mathbf{x}^n(t), \mathbf{y}^n(t)\big)_{t\geq 0}$ occur with rates (2.3),(2.4). Using this information, we can define a vector field $F : \Theta_n \to \mathbb{R}^{2N}$. For any $(\mathbf{x}, \mathbf{y}) \in \Theta_n$, $F(\mathbf{x}, \mathbf{y})$ captures the average change in $(\mathbf{x}, \mathbf{y}) \in \Theta_n$ per unit time, and is

written as

$$F(\mathbf{x},\mathbf{y}) = \big(F_x(\mathbf{x},\mathbf{y}), F_y(\mathbf{x},\mathbf{y})\big), \tag{2.6}$$

where

$$F_x(\mathbf{x},\mathbf{y}) \triangleq \sum_{i\in\mathcal{N}} \sum_{j\in\mathcal{N}, j\neq i} \frac{(\mathbf{e}_i - \mathbf{e}_j)}{n} \bar{Q}^n_{x:j,i}(\mathbf{x},\mathbf{y}) \tag{2.7}$$

$$F_y(\mathbf{x},\mathbf{y}) \triangleq \sum_{i\in\mathcal{N}} \sum_{j\in\mathcal{N}, j\neq i} \frac{(\mathbf{e}_i - \mathbf{e}_j)}{n} \bar{Q}^n_{y:j,i}(\mathbf{x},\mathbf{y}). \tag{2.8}$$

The following result helps us write the above two equations in a more compact form.

Proposition 2.2.1. *(Proof in Appendix A.1.1.) For any* $(\mathbf{x},\mathbf{y}) \in \Theta_n$*, we have*

$$F_x(\mathbf{x},\mathbf{y}) = \mathbf{Q}^T\mathbf{x} + [\kappa \mathbf{x}^T\mathbf{y}]\mathbf{x} - \kappa \mathbf{D}_\mathbf{y}\mathbf{x} \tag{2.9}$$

$$F_y(\mathbf{x},\mathbf{y}) = \mathbf{Q}^T\mathbf{y} + [\kappa \mathbf{x}^T\mathbf{y}]\mathbf{y} - \kappa \mathbf{D}_\mathbf{x}\mathbf{y} \tag{2.10}$$

Proposition 2.2.1 allows us to consider the following system of ordinary differential equations:

$$\begin{aligned} \frac{d}{dt}\mathbf{x}(t) &= F_x\big(\mathbf{x}(t),\mathbf{y}(t)\big) \\ \frac{d}{dt}\mathbf{y}(t) &= F_y\big(\mathbf{x}(t),\mathbf{y}(t)\big) \\ \mathbf{x}(0)^T\mathbf{1} &= \mathbf{y}(0)^T\mathbf{1} = 1, \end{aligned} \tag{2.11}$$

where we let $\big(\mathbf{x}(t),\mathbf{y}(t)\big)_{t\geq 0}$ denote solutions to (2.11) for $t \geq 0$ (this is sometimes referred to as the semi-flow of F). Note the distinction between the notations $\big(\mathbf{x}^n(t),\mathbf{y}^n(t)\big)$ and $\big(\mathbf{x}(t),\mathbf{y}(t)\big)$, where the former is a stochastic process (parameterized by n), while the latter is the deterministic solution to an ODE system. For the next result, let $\|\cdot\|$ denote the Euclidean norm in $\mathbb{R}^{2N}$, and S be the subset of $\mathbb{R}^{2N}$ given by

$$S \triangleq \{(\mathbf{x},\mathbf{y}) \in \mathbb{R}^{2N} \mid \mathbf{x}^T\mathbf{1} = \mathbf{y}^T\mathbf{1} = 1\}. \tag{2.12}$$

Proposition 2.2.2. *(Proof in Appendix A.1.2.)* $F : S \to \mathbb{R}^{2N}$ *is Lipschitz continuous with Lipschitz constant* $M < \infty$*, and for every initial point* $\big(\mathbf{x}(0),\mathbf{y}(0)\big) \in S$*, there exists a unique*

solution to the system (2.11).

The set S is an invariant set for the ODE system (2.11). Indeed, observe that for any $(\mathbf{x},\mathbf{y}\in S)$ we have $d(\mathbf{1}^T\mathbf{x})/dt = \mathbf{1}^T F(\mathbf{x},\mathbf{y}) = \mathbf{1}^T\mathbf{Q}^T\mathbf{x}+\kappa\mathbf{x}^T\mathbf{y}-\kappa\mathbf{y}^T\mathbf{x}=0$ since $\mathbf{Q1}=0$. Similarly, $d(\mathbf{1}^T\mathbf{y})/dt=0$, and any solution starting in S stays in S. We will only consider such solutions in our analysis of the ODE. To ensure that this is the case, we rewrite (2.11) as an equivalent system given by

$$\begin{aligned}\frac{d}{dt}\mathbf{x}(t) &= \mathbf{Q}^T\mathbf{x}(t)+\Lambda_x(t)\mathbf{x}(t)-\kappa\mathbf{D}_{\mathbf{y}(t)}\mathbf{x}(t)\\ \frac{d}{dt}\mathbf{y}(t) &= \mathbf{Q}^T\mathbf{y}(t)+\Lambda_y(t)\mathbf{y}(t)-\kappa\mathbf{D}_{\mathbf{x}(t)}\mathbf{y}(t)\\ \mathbf{x}(t)^T\mathbf{1} &= \mathbf{y}(t)^T\mathbf{1}=1\ \big(\forall\, t\geq 0\big),\end{aligned} \tag{2.13}$$

where $\Lambda_x(t)$ and $\Lambda_y(t)$ are real valued scalars. By summing up all the entries of $\frac{d}{dt}\mathbf{x}(t)$ and $\frac{d}{dt}\mathbf{x}(t)$ and substituting $\mathbf{x}(t)^T\mathbf{1}=\mathbf{y}(t)^T\mathbf{1}=1$, it can be easily seen that $\Lambda_x(t)=\Lambda_y(t)=\kappa\mathbf{x}(t)^T\mathbf{y}(t)$. Thus, we retrieve the original system and hence the equivalence. Moving forwards, we will use $\Lambda(t)\triangleq\Lambda_x(t)=\Lambda_y(t)=\kappa\mathbf{x}(t)^T\mathbf{y}(t)$ in our equations. Before proceeding with our first important result, we make an observation about fixed points $(\mathbf{x}^*,\mathbf{y}^*)$ of (2.13).

Remark 2.2.3. *Any fixed point* $(\mathbf{x}^*,\mathbf{y}^*)\in S$ *of* (2.13) *has all strictly positive entries. In other words, there exists no* $i\in\mathcal{N}$ *such that* $x_i^*=0$ *or* $y_i^*=0$.

Proof. (Remark 2.2.3) Consider $(\mathbf{x}^*,\mathbf{y}^*)\in S$ to be fixed points of (2.13). Then, the i^{th} entry of $\mathbf{x}^*$ satisfies the equation

$$0=\sum_{j\in\mathcal{N}}Q_{ji}x_j^*+[\kappa\mathbf{x}^{*T}\mathbf{y}^*]x_i-\kappa x_i^*y_i^*.$$

Suppose $x_i^*=0$. Then the above equation becomes $0=\sum_{j\in\mathcal{N},\ j\neq i}Q_{ji}x_j^*$. This means that for any $j\in\mathcal{N}$ such that $Q_{ji}>0$ (implying that node j is a neighbor of node i), the corresponding entry $x_j^*=0$. This in turn leads to $x_k^*=0$, for all neighbors k of node j. Since our graph is connected, there is always a path connecting node i to any other node of the graph, implying $\mathbf{x}=\mathbf{0}$. Similarly, if $y_i^*=0$, following the same steps as before gives us $\mathbf{y}^*=\mathbf{0}$. This is in violation of the third equation in (2.13), giving us a contradiction. This completes the proof. □

We are now ready to state the main result connecting the stochastic process from Section 2.2.1 and the deterministic ODE system from Section 2.2.2.

2.2.3 From stochastic to deterministic dynamics

In this section we show that the stochastic process from Section 2.2.1, indexed by n, almost surely converges to the deterministic ODE system from Section 2.2.2. Before we state the theorem, we make the following assumption.

A1: For any $n \in \mathbb{N}$, $\big(\mathbf{x}(0), \mathbf{y}(0)\big) = \big(\mathbf{x}^n(0), \mathbf{y}^n(0)\big)$.

Theorem 2.2.4. *(Proof in Appendix A.1.3.) Consider the family of stochastic processes (indexed by n)* $\big\{\big(\mathbf{x}^n(t), \mathbf{y}^n(t)\big)_{t\geq 0}\big\}_{n\in\mathbb{N}}$, *with kernels* $\big(\bar{\mathbf{Q}}^n\big)_{n\in\mathbb{N}}$ *defined as in* (2.3) *and* (2.4). *Let* $\big(\mathbf{x}(t), \mathbf{y}(t)\big)$ *be solutions to the ODE system* (2.11) *that satisfy (A1). Then, for all* $T \in (0, \infty)$, *we have*

$$\lim_{n\to\infty} \sup_{0\leq t\leq T} \|\big(\mathbf{x}^n(t), \mathbf{y}^n(t)\big) - \big(\mathbf{x}(t), \mathbf{y}(t)\big)\| = 0 \quad a.s. \tag{2.14}$$

More precisely, for any $\epsilon > 0$ *and* $T \in (0, \infty)$, *we have*

$$\begin{aligned} &\mathbf{P}\Big(\sup_{0\leq t\leq T} \big\|\big(\mathbf{x}^n(t), \mathbf{y}^n(t)\big) - \big(\mathbf{x}(t), \mathbf{y}(t)\big)\big\| \geq \epsilon \Big) \\ &\quad \leq 4N(N-1)\exp\left(-n(1+\kappa)T \cdot h\Big(\frac{\epsilon e^{-MT}}{\sqrt{2}N(N-1)(1+\kappa)T} \Big) \right), \end{aligned} \tag{2.15}$$

where $h(x) \triangleq (1+x)\log(1+x) - x$, M *is the Lipschitz constant from Proposition 2.2.2, and* $N = |\mathcal{N}|$ *is the size of the graph.*

(2.15) gives an upper bound on the probability that, uniformly over a finite time horizon $[0, T]$, the stochastic process indexed by $n \in \mathbb{N}$ deviates from the solution to the deterministic process by at least $\epsilon > 0$, provided they start at the same initial point. A discussion on the effect of parameters n, κ and N on the bound (2.15) and the long run behavior (as $T \to \infty$) is deferred to the end of Section 2.4.

2.3 Analysis of the deterministic flow and convergence to FV

From Theorem 2.2.4, the solutions $\big(\mathbf{x}(t), \mathbf{y}(t)\big)_{t\geq 0}$ of the ODE system (2.13) serve as a deterministic approximation for the CTMC $\big(\mathbf{x}^n(t), \mathbf{y}^n(t)\big)_{t\geq 0}$ for larger values of $n \in \mathbb{N}$. Then, it makes sense to analyze the trajectories of the ODE system for its convergence prop-

erties and the nature of its fixed points. For the rest of the chapter, we use the notation $\Lambda(t) = \Lambda_x(t) = \Lambda_y(t)$ mentioned earlier.

2.3.1 Fixed points of the system

We first state a consequence of the Courant-Fischer min-max theorem [65, 88] (specific to our case), which we shall refer to later in this Section.

Lemma 2.3.1. *Let* $\tilde{S} \triangleq \{\mathbf{w} \in \mathbb{R}^N \mid \mathbf{w}^T\mathbf{1} = 0, \|\mathbf{w}\| = 1\}$. *Given a CTMC kernel* $\mathbf{Q} = -\mathbf{L}$, *where* $\mathbf{L}$ *is a Laplacian matrix with eigenvalues ordered as* $0 = \lambda_1 < \lambda_2 \leq \cdots \leq \lambda_N$, *we have*

$$\lambda_2 = \min_{\mathbf{u} \in \tilde{S}} \mathbf{u}^T[-\mathbf{Q}]^T\mathbf{u}, \tag{2.16}$$

with $\tilde{\mathbf{v}}_2 = \mathbf{v}_2/\|\mathbf{v}_2\|$ *being the minimizer, and*

$$\lambda_k = \max_{\mathbf{u} \in \tilde{S},\ \mathbf{u} \perp \{\mathbf{v}_{k+1}, \cdots, \mathbf{v}_N\}} \mathbf{u}^T[-\mathbf{Q}]^T\mathbf{u}, \tag{2.17}$$

with $\tilde{\mathbf{v}}_k = \mathbf{v}_k/\|\mathbf{v}_k\|$ *being the maximizer.*

Let $\mathbf{z}(t) \triangleq \mathbf{x}(t) - \mathbf{y}(t)$ for all $t \geq 0$, and consider an (implicit) system of equations obtained by subtracting the second equation of (2.13) from the first one, which then reads as

$$\begin{aligned} \frac{d}{dt}\mathbf{z}(t) &= \mathbf{Q}^T\mathbf{z}(t) + \Lambda(t)\mathbf{z}(t) \\ \mathbf{z}(t)^T\mathbf{1} &= 0 \ \big(\forall\, t \geq 0\big). \end{aligned} \tag{2.18}$$

Let Ω denote the set of fixed points of (2.18). Any fixed point $\mathbf{z}^* \in \Omega$ satisfies

$$-\mathbf{Q}^T\mathbf{z}^* = \mathbf{L}^T\mathbf{z}^* = \Lambda^*\mathbf{z}^* \tag{2.19}$$

$$\mathbf{z}^{*T}\mathbf{1} = 0 \tag{2.20}$$

for some $\Lambda^* \in (0, \infty)$, and could therefore be a (left) eigenvector of $\mathbf{L}$ (up to a scalar multiple), or the *zero* vector (which we shall often refer to as the *origin*). Since, for any $t \geq 0$, $\mathbf{z}(t) = \mathbf{0}$ if and only if $\mathbf{x}(t) = \mathbf{y}(t)$, the fixed point $\mathbf{0} \in \Omega$ of (2.18) corresponds to the invariant set S_0 of (2.13), defined as

$$S_0 \triangleq \{(\mathbf{x}, \mathbf{y}) \in S \mid \mathbf{x} = \mathbf{y},\ \mathbf{x}^T\mathbf{1} = \mathbf{y}^T\mathbf{1} = 1\}. \tag{2.21}$$

To exclude, from our analysis, the case where trajectories of (2.18) might hit *zero* after some finite time, or equivalently trajectories of (2.13) might enter set S_0 and stay there for all future times, we show the following result.

Proposition 2.3.2. *For all sufficiently large κ, the invariant set S_0 defined in* (2.21) *is an unstable set for the system* (2.13).

Proof. Recall the form of the Jacobian of $F : \mathbb{R}^{2N} \to \mathbb{R}^{2N}$ from Appendix A.2. When evaluated at $\mathbf{x} = \mathbf{y}$ (which we shall use here in place of $\mathbf{x}^*$ and $\mathbf{y}^*$ to denote fixed points), we can write it as

$$\mathbf{J}_F(\mathbf{x},\mathbf{x}) = \begin{bmatrix} \mathbf{Q} & 0 \\ 0 & \mathbf{Q} \end{bmatrix} + \kappa \begin{bmatrix} \mathbf{x}\mathbf{x}^T + \mathbf{D}_\mathbf{x}\mathbf{D}_\mathbf{x} - \mathbf{D}_\mathbf{x} & \mathbf{x}\mathbf{x}^T - \mathbf{D}_\mathbf{x} \\ \mathbf{x}\mathbf{x}^T - \mathbf{D}_\mathbf{x} & \mathbf{x}\mathbf{x}^T + \mathbf{D}_\mathbf{x}\mathbf{D}_\mathbf{x} - \mathbf{D}_\mathbf{x} \end{bmatrix}$$

$$= \begin{bmatrix} \mathbf{Q}^T & 0 \\ 0 & \mathbf{Q}^T \end{bmatrix} + \kappa \begin{bmatrix} \mathbf{D}_\mathbf{x}^2 & 0 \\ 0 & \mathbf{D}_\mathbf{x}^2 \end{bmatrix} + \kappa \begin{bmatrix} 1 & 1 \\ 1 & 1 \end{bmatrix} \otimes \left[\mathbf{x}\mathbf{x}^T - \mathbf{D}_\mathbf{x}\right],$$

Here, $\mathbf{D} \otimes \mathbf{E}$ denotes the Kronecker product of two square matrices $\mathbf{D}$ and $\mathbf{E}$. To simplify further analysis, we write down the above matrix as $\mathbf{J}_F(\mathbf{x},\mathbf{x}) = \mathbf{A} + \mathbf{B} + \mathbf{C}$, where

$$\mathbf{A} = \begin{bmatrix} \mathbf{Q}^T & 0 \\ 0 & \mathbf{Q}^T \end{bmatrix}, \quad \mathbf{B} = \kappa \begin{bmatrix} \mathbf{D}_\mathbf{x}^2 & 0 \\ 0 & \mathbf{D}_\mathbf{x}^2 \end{bmatrix}$$

$$\mathbf{C} = \kappa \begin{bmatrix} 1 & 1 \\ 1 & 1 \end{bmatrix} \otimes \left[\mathbf{x}\mathbf{x}^T - \mathbf{D}_\mathbf{x}\right]$$

For any symmetric matrix $\mathbf{M} \in \mathbb{R}^{N\times N}$, let $\lambda_1(\mathbf{M}) \le \lambda_2(\mathbf{M}) \le \cdots \le \lambda_N(\mathbf{M})$ denote the ordering of its eigenvalues. Observe that the eigenvalues of $\mathbf{A}$ are the same as those of $\mathbf{Q}$ with double the multiplicity, implying $\lambda_{2N}(\mathbf{A}) = 0$, and $\lambda_{2k}(\mathbf{A}) = \lambda_k(\mathbf{Q})$ for all $k \in \{1, \cdots, N\}$. The eigenvalues of $\mathbf{B}$ are the diagonal elements. Thus, $\lambda_1(B) = \kappa \min_{i\in\mathcal{N}} x_i^2$ and $\lambda_{2N}(B) = \kappa \max_{i\in\mathcal{N}} x_i^2$.

For matrix $\mathbf{C}$, observe that $\mathbf{x}\mathbf{x}^T - \mathbf{D}_\mathbf{x}$ has a *zero* row sum, with negative diagonal entries and non-negative off-diagonal entries. It therefore defines a CTMC transition rate matrix, and we have $\lambda_{2N}(\mathbf{x}\mathbf{x}^T - \mathbf{D}_\mathbf{x}) = 0$, with the other eigenvalues being strictly negative. It can also be checked that the matrix of all ones on the left of the Kronecker product has the spectrum $\{2, 0\}$. The eigenvalues of the Kronecker product are equal to eigenvalues of the two involved matrices cross multiplied. We therefore obtain $2N$ eigenvalues of $\mathbf{C}$, with $\lambda_{2N}(\mathbf{C}) = \cdots = \lambda_{N-1}(\mathbf{C}) = 0$, and the others being strictly negative.

The Weyl's inequality[65, 88] for real symmetric matrices $\mathbf{D}, \mathbf{E} \in \mathbb{R}^{N\times N}$ is given, for any

$k \in \{1, \cdots, N\}$, as

$$\lambda_1(\mathbf{D}) + \lambda_k(\mathbf{E}) \leq \lambda_k(\mathbf{D}+\mathbf{E}) \leq \lambda_N(\mathbf{D}) + \lambda_k(\mathbf{E})$$

Applying the lower bound of Weyl's inequality on $\lambda_{N-1}(\mathbf{A}+\mathbf{B}+\mathbf{C})$, we get

$$\lambda_1(\mathbf{A}) + \lambda_{N-1}(\mathbf{B}+\mathbf{C}) \leq \lambda_{N-1}(\mathbf{A}+\mathbf{B}+\mathbf{C}).$$

Applying the lower bound of Weyl's inequality once again, this time on $\lambda_{N-1}(\mathbf{B}+\mathbf{C})$, we get

$$\lambda_1(\mathbf{A}) + \lambda_1(\mathbf{B}) + \lambda_{N-1}(\mathbf{C}) \leq \lambda_{N-1}(\mathbf{A}+\mathbf{B}+\mathbf{C}).$$

Now since $\lambda_1(\mathbf{A}) = \lambda_1(\mathbf{Q}) = -\lambda_N(\mathbf{L})$, $\lambda_{N-1}(\mathbf{C}) = 0$ and $\lambda_1(\mathbf{B}) = \kappa \min_{i \in \mathcal{N}} x_i^2$, we get

$$-\lambda_N(\mathbf{L}) + \kappa \min_{i \in \mathcal{N}} x_i^2 \leq \lambda_{N-1}(\mathbf{J}_F(\mathbf{x}, \mathbf{x})).$$

As a consequence of Remark 2.2.3 in Section 2.2.1, $x_i > 0$ for every $i \in \mathcal{N}$. This means the $N+1$ largest eigenvalues of the Jacobian become positive for all sufficiently large $\kappa > 0$, and each fixed point in S_0 has an unstable space[3] of minimum dimension $N+1$ associated with the linearized system at the point [100]. Therefore the set S_0 is linearly unstable in S. This concludes the proof. □

The above result is equivalent to saying that the fixed point $\mathbf{0} \in \Omega$ of (2.18) is unstable. This allows us to consider trajectories starting from $\big(\mathbf{x}(0), \mathbf{y}(0)\big) \in S \setminus S_0$, or equivalently, from $\mathbf{z}(0) \neq 0$, which will be useful in Section 2.3.2.

2.3.2 Convergence to the Fiedler vector

From Section 2.3.1, we know that the set Ω of fixed points of (2.18) contains any scalar multiples $c\,\mathbf{v}_k$ of the (left) eigenvectors $\mathbf{v}_k$ of $\mathbf{L}$ for $k \geq 2$. This includes $\mathbf{0}$, which we showed to be an unstable fixed point in Proposition 2.3.2. The next question is about the convergence properties of the ODE system, and we have the following.

[3] An unstable space of a point is the set where trajectories move away from the point. For individual fixed points, it is usually enough to show that this unstable space is at least 1-dimensional to guarantee instability. This can be done by showing that one of the eigenvalues of the Jacobian evaluated at the point is positive (for linear instability)[100]. However when showing instability of all points associated to an invariant, k-dimensional set given by K, we need to show that the unstable space of these points is of dimension at least $k+1$, in order to rule out the unstable spaces made of vectors pointing simply inside set K. Showing the existence of an unstable space of dimension $k+1$ hence shows instability of the set K itself.

Theorem 2.3.3. *Trajectories of the system* (2.18) *always converge to a fixed point. Furthermore, the Fiedler vector* $\mathbf{v}_2$ *is an asymptotically stable fixed point of the ODE system (2.18), with all others being unstable.*

The rest of this section is devoted to the proof of Theorem 2.3.3. First, we provide a 'Lyapunov function' $V : \mathbb{R}^N \to [0,+\infty)$ with strictly negative slope along trajectories of (2.13), at any point which is not in Ω (i.e. not a fixed point). This will subsequently be shown in Proposition 2.3.4. We then put together our proof of Theorem 2.3.3, where we show convergence to a fixed point using the LaSalle invariance principle (Theorem A.2.2 in Appendix A.2). This will prove the first statement of Theorem 2.3.3. To prove the second statement, we use the Lyapunov stability theory to show that all the fixed points of type $c\mathbf{v}_k$ ($k \geq 3, c \neq 0$) are unstable, and the only possible candidate left for convergence, i.e., $c\mathbf{v}_2$, is asymptotically stable. For the sake of completeness, we provide relevant definitions and results from the theory surrounding LaSalle invariance principle and Lyapunov stability in Appendix A.2.

Recall that the set S_0 is unstable and we only consider trajectories starting from $S \setminus S_0$. For such trajectories, since $\mathbf{z}(t) \neq \mathbf{0}$ in $S \setminus S_0$, we can construct another (implicit) system whose solutions are

$$\tilde{\mathbf{z}}(t) \triangleq \frac{\mathbf{z}(t)}{\|\mathbf{z}(t)\|} \text{ for all } t \geq 0. \tag{2.22}$$

Trajectories of (2.22) are always contained in the set $\tilde{S} = \{\mathbf{w} \in \mathbb{R}^N \mid \mathbf{w}^T \mathbf{1} = 0, \|\mathbf{w}\| = 1\}$. Non-zero fixed points of (2.18) will also be fixed points of this new system. However, this time, they are normalized, and isolated in space, unique up to only a sign. This will make it easier to apply the LaSalle principle later to show convergence. Since we are now working in the normalized space, we let $\{\tilde{\mathbf{v}}_2, \cdots, \tilde{\mathbf{v}}_N\}$ denote the normalized eigenvectors of $\mathbf{L}$, and denote the set of fixed points as $\tilde{\Omega} = \{\tilde{\mathbf{v}}_2, \cdots, \tilde{\mathbf{v}}_N\}$.[4]

Define the Lyapunov function $V : \mathbb{R}^N \to [0, \infty)$ as

$$V(\mathbf{u}) = \frac{1}{2}\mathbf{u}^T[-\mathbf{Q}]^T\mathbf{u} = \frac{1}{2}\mathbf{u}^T\mathbf{L}\mathbf{u}, \quad \text{for any } \mathbf{u} \in \mathbb{R}^N. \tag{2.23}$$

We shall now analyze the function $V(\mathbf{u})$ over trajectories $\tilde{\mathbf{z}}(t)$ as defined in (2.22).

Proposition 2.3.4. *For trajectories of (2.13) starting from any* $(\mathbf{x}(0), \mathbf{y}(0)) \in S \setminus S_0$*, we have* $\frac{d}{dt}V(\tilde{\mathbf{z}}(t)) \leq 0$*, with equality only at the fixed points* $\tilde{\Omega}$ *that are left eigenvectors of* $\mathbf{L}$*.*

[4] Technically, it should be $\tilde{\Omega} = \{\pm\tilde{\mathbf{v}}_2, \cdots, \pm\tilde{\mathbf{v}}_N\}$, but we use $\tilde{\mathbf{v}}_k$ to refer to $\pm\tilde{\mathbf{v}}_k$ irrespective of the sign.

Proof. For the rest of this section, we suppress the '(t)' notation and assume it implicitly. We also use $\dot{f}$ to mean $\frac{d}{dt}f$ whenever convenient. Observe that

$$V(\tilde{\mathbf{z}}(t)) = \frac{1}{2}\tilde{\mathbf{z}}^T[-\mathbf{Q}]^T\tilde{\mathbf{z}} = \frac{1}{2}\frac{\mathbf{z}^T[-\mathbf{Q}]^T\mathbf{z}}{\mathbf{z}^T\mathbf{z}}.$$

Differentiating V along the trajectories of (2.18) gives

$$\frac{d}{dt}V(\tilde{\mathbf{z}}(t)) = \frac{1}{2(\mathbf{z}^T\mathbf{z})^2}\Big([\mathbf{z}^T\mathbf{Q}^T\mathbf{z}]\big[\frac{d}{dt}\mathbf{z}^T\mathbf{z}\big] - [\mathbf{z}^T\mathbf{z}]\big[\frac{d}{dt}\mathbf{z}^T\mathbf{Q}^T\mathbf{z}\big]\Big). \tag{2.24}$$

First, we have

$$\frac{d}{dt}\Big(\mathbf{z}^T\mathbf{z}\Big) = 2\mathbf{z}^T\dot{\mathbf{z}}(t) = 2\Big(\mathbf{z}^T\mathbf{Q}^T\mathbf{z} + \Lambda(t)\mathbf{z}^T\mathbf{z}\Big), \tag{2.25}$$

and similarly we have

$$\frac{d}{dt}\Big(\mathbf{z}^T[-\mathbf{L}]\mathbf{z}\Big) = \dot{\mathbf{z}}^T\mathbf{Q}^T\mathbf{z} + \mathbf{z}^T\mathbf{Q}^T\dot{\mathbf{z}} = 2\Big(\Lambda(t)\mathbf{z}^T\mathbf{Q}^T\mathbf{z} + \mathbf{z}^T[\mathbf{Q}^2]^T\mathbf{z}\Big). \tag{2.26}$$

By substituting (2.25) and (2.26) into (2.24), we get

$$\frac{d}{dt}V(\tilde{\mathbf{z}}(t)) = \frac{\big(\mathbf{z}\mathbf{Q}^T\mathbf{z}\big)^2 - \big(\mathbf{z}^T[\mathbf{Q}^2]^T\mathbf{z}\big)(\mathbf{z}^T\mathbf{z})}{(\mathbf{z}^T\mathbf{z})^2} \tag{2.27}$$

To show (2.27) is non-positive, we leverage the property of $\mathbf{Q} = -\mathbf{L}$ being a symmetric matrix whose eigenvectors $\{\tilde{\mathbf{v}}_1, \tilde{\mathbf{v}}_2, \cdots \tilde{\mathbf{v}}_N\}$ form an orthonormal basis for $\mathbb{R}^N$. Thus, any vector $\mathbf{z} \in \mathbb{R}^N$ can be written as a linear combination of these orthonormal eigenvectors. Since the trajectory $\mathbf{z}$ always satisfies $\mathbf{z}^T\mathbf{v}_1 = \mathbf{z}^T\mathbf{1} = 0$, we can write $\mathbf{z} = \sum_{k=2}^N c_k\tilde{\mathbf{v}}_k$, where $c_k = \mathbf{z}^T\tilde{\mathbf{v}}_k$ and similarly,

$$\mathbf{z}^T\mathbf{z} = \sum_{k=2}^N c_k^2, \;\; \mathbf{z}^T[-\mathbf{Q}^T]\mathbf{z} = \sum_{k=2}^N \lambda_k c_k^2, \;\; \mathbf{z}^T[\mathbf{Q}^2]^T\mathbf{z} = \sum_{k=2}^N \lambda_k^2 c_k^2. \tag{2.28}$$

Substituting these into (2.27) yields

$$\frac{d}{dt}V(\tilde{\mathbf{z}}(t)) = \left[\sum_{k=2}^N \lambda_k \frac{c_k(t)^2}{\Big(\sum_{k=2}^N c_k(t)^2\Big)}\right]^2 - \left[\sum_{k=2}^N \lambda_k^2 \frac{c_k(t)^2}{\Big(\sum_{k=2}^N c_k(t)^2\Big)}\right]. \tag{2.29}$$

Now, for each $t > 0$, define a discrete random variable $R(t)$ which takes values λ_k with

probability $\frac{c_k(t)^2}{\sum_{k=2}^{N} c_k(t)^2}$ for $k \in \{2,3,\cdots,N\}$. We can then rewrite (2.29) as

$$\frac{d}{dt} V(\tilde{\mathbf{z}}(t)) = E[R(t)]^2 - E[R(t)^2] = -\text{Var}[R(t)] \leq 0, \tag{2.30}$$

where the equality $\frac{d}{dt} V(\mathbf{z}(t)) = 0$ holds when the random variable $R(t)$ is constant, i.e., when only one of the $c_k(t)$'s is non-zero. In other words, we have zero derivative only when $\tilde{\mathbf{z}}(t)$ hits an eigenvector $\tilde{\mathbf{v}}_k$ for some $k = 2,3,\cdots,N$. This completes the proof. □

Using the above results and Theorem A.2.4 from Appendix A.2, which is regarding the stability of fixed points, we are now ready to prove Theorem 2.3.3.

Proof. (Theorem 2.3.3) First, we use the LaSalle invariance principle (Theorem A.2.2) to prove convergence to *a* fixed point. Note that any trajectory originating from $\tilde{S} = \{\mathbf{w} \in \mathbb{R}^N \,\big|\, \mathbf{w}^T \mathbf{1} = 0, \|\mathbf{w}\| = 1\}$ (and as a result never leaving $\tilde{S}$) is relatively compact. This is because $\tilde{S}$ is a closed and bounded subset of a finite dimensional Euclidean space $\mathbb{R}^N$, and hence compact. Also, the fixed points $\{\tilde{\mathbf{v}}_2, \tilde{\mathbf{v}}_3, \cdots, \tilde{\mathbf{v}}_N\}$ of $\left(\tilde{\mathbf{z}}(t)\right)_{t\geq 0}$ are isolated in $\tilde{S}$. Then, Theorem A.2.2 implies that the solutions given by (2.22) have all their trajectories starting from $\tilde{\mathbf{z}}(0) \in \tilde{S}$ converge to *a* fixed point (i.e. no limit cycles exist and convergence to a point is guaranteed).

Now, we use Proposition A.2.4(i) to show that the Fiedler vector $\tilde{\mathbf{v}}_2$ is an asymptotically stable fixed point. We already know from (2.16) in Lemma 2.3.1 that $\tilde{\mathbf{v}}_2$ is the global minimizer of the Lyapunov function V, and by Proposition A.2.4(i), it is asymptotically stable.

To see why the eigenvectors $\tilde{\mathbf{v}}_k \in \tilde{\Omega} \setminus \{\tilde{\mathbf{v}}_2\}$ are unstable, we show that they can never be local minima. Indeed, for any $\alpha \in (0,1)$ and $k > 2$, let $\mathbf{p} = \tilde{\mathbf{v}}_k + \alpha(\tilde{\mathbf{v}}_2 - \tilde{\mathbf{v}}_k) = (1-\alpha)\tilde{\mathbf{v}}_k + \alpha\tilde{\mathbf{v}}_2$. Then, we have again as a consequence of (2.17) in Lemma 2.3.1 that $V(\mathbf{p}) < V(\tilde{\mathbf{v}}_k)$. Moreover, if $\tilde{\mathbf{z}}(0) = \mathbf{p}$ we have $\dot{V}(\tilde{z}(0)) < 0$ by Proposition 2.3.4. Therefore, for $k > 2$, $\tilde{\mathbf{v}}_k$ is definitely not a local minimizer, and is thus unstable in view of Proposition A.2.4(ii).

In summary, we have shown that the Fiedler vector is the only asymptotically stable fixed point of (2.18), with all other fixed points (eigenvectors) being unstable. This completes the proof. □

2.4 From deterministic back to stochastic dynamics

In this section, we take the opportunity to reflect upon the results in Sections 2.2 and 2.3, and their influence on the long run behaviour of the stochastic process constructed in Section 2.2.1. Theorem 2.2.4 made the first connection between stochastic processes $(\mathbf{x}^n(t), \mathbf{y}^n(t))$ for $n \in \mathbb{N}$, and the solution $(\mathbf{x}(t), \mathbf{y}(t))$ of the deterministic ODE system (2.11) (or, consequently, between $\mathbf{z}^n(t) \triangleq \mathbf{x}^n(t) - \mathbf{y}^n(t)$ and $\mathbf{z}(t)$ in (2.18)) by showing that uniformly over a finite time horizon (and sufficiently large n) the stochastic process rarely deviates from the solution of the ODE system. This prompted us to analyze system (2.18) and in Theorem 2.3.3, we gave stability results on all the fixed points of (2.18). The Fiedler vector $\mathbf{v}_2$ (up to a constant multiple) turned out to be an asymptotically stable fixed point, with all the higher eigenvectors $\mathbf{v}_k$, $k \geq 3$ (up to constant multiples) being unstable. This gives us reason to believe that a working algorithm simulating the interacting stochastic process $(\mathbf{x}^n(t), \mathbf{y}^n(t))$ should have $\mathbf{z}^n(t)$ converge to $c\mathbf{v}_2$ in some sense, provided it never gets stuck around other, unstable fixed points forever. In this section, we make this intuition precise by resorting to results in [22], Sections 2.2.2 and 2.2.3.

For any set $B \subset \mathbb{R}^N$ and given $\mathbf{z}^n(0) \in B$ (stochastic process starts in B), let

$$T^n(B) = \inf\{t \geq 0 \mid \mathbf{z}^n(t) \notin B\}$$

define the *exit time* from set B. Similarly, let

$$H^n(B, T) = \frac{1}{T} \int_0^T \mathbb{1}_{\{\mathbf{z}^n(s) \in B\}} ds$$

denote the (random) fraction of time the stochastic process $\mathbf{z}^n(t)$ spends inside set B in the interval $[0, T]$. Note that $\mathbf{z}^n(t)$ takes values on the N-dimensional grid $(\mathbb{Z}^N)$ scaled by the factor $1/n$. Denote this scaled grid by $\frac{1}{n}\mathbb{Z}^N$. Then, $\mathbf{z}^n(t) \in B$ for some $B \in R^N$ and $t \geq 0$ is possible only if $B \cap \frac{1}{n}\mathbb{Z}^N \neq \emptyset$. Using this, define for every $k \geq 2$ the set $B(\mathbf{v}_k, m)$ as the smallest open ball containing $c\mathbf{v}_k$, but not the *origin*, such that $B(\mathbf{v}_k, m) \cap \frac{1}{m}\mathbb{Z}^N \neq \emptyset$. Note that as m increases, $B(\mathbf{v}_k, m)$ gets smaller and smaller for each $k \geq 0$ (since resolution of the grid $\frac{1}{m}\mathbb{Z}^N$ gets finer), until the sets do not intersect anymore, and $\lim_{m\to\infty} B(\mathbf{v}_k, m) = \{c\mathbf{v}_k, c \in \mathbb{R}\}$[5].

[5]The above can also be done for the normalized version $\tilde{\mathbf{z}}(t)$, in which case the fixed points are $\tilde{\mathbf{v}}_k$ and truly isolated in space, making construction of the isolating simple. However, we construct $B(\mathbf{v}_k, m)$ the way we do to emphasize that for larger n, $B(\mathbf{v}_k, m)$ can be taken to be tighter around $c\mathbf{v}_k$ for larger m.

Therefore for large values of m, the sets $B(\mathbf{v}_k, m)$ for $k \geq 2$ are disjoint and never contain two or more different eigenvectors as fixed points, thereby isolating them. Also, for any set $B \subset \mathbb{R}^N$ containing $\mathbf{v}_k$, $k \geq 3$, let $\bar{B}$ represent all points in B such that starting from those points, the ODE trajectories $\mathbf{z}(t)$ leave B in finite time (i.e. subset of the unstable space of $\mathbf{v}_k$ which is contained in B). Then, we can prove the following by adapting Propositions 3 and 4 in [22] to our system.

Proposition 2.4.1. *Consider m sufficiently large such that $B(\mathbf{v}_k, m)$ for all $k \geq 2$ are disjoint. Then,*

(i) for any $k \geq 3$ and sufficiently large n, the stochastic process originating from $\mathbf{z}^n(0) \in \bar{B}(\mathbf{v}_k, m)$ leaves the neighborhood $B(\mathbf{v}_k, m)$ of $\mathbf{v}_k$ in finite time with high probability. More precisely,

$$\mathbf{P}\left(\limsup_{n\to\infty} T^n(B(\mathbf{v}_k, m)) < +\infty\right) = 1.$$

(ii) for n sufficiently large and any $B(\mathbf{v}_2, m)$ where $m \leq n$, with high probability the process $\mathbf{z}^n(t)$ spends almost all its time, in the long run, in the neighborhood $B(\mathbf{v}_2, m)$. More precisely, for every $m \in \mathbb{N}$,we have

$$\lim_{n\to\infty} [\liminf_{T\to\infty} H^n(B(\mathbf{v}_2, m), T)] = 1 \quad a.s.$$

The above result states that for all sufficiently large n, the stochastic process spends only finite time in a neighborhood of the unstable fixed points $\mathbf{v}_k$, $k \geq 3$. It then proceeds to spend almost all its time, in the long run, in a neighborhood of the asymptotically stable fixed point $\mathbf{v}_2$. The second statement of Proposition 2.4.1 is especially helpful to us. Since it implies that for all sufficiently large n, the stochastic process spends most of its time in a small neighborhood of $\mathbf{v}_2$ with high probability, we expect to observe that $\frac{1}{T}\int_0^T \mathbf{z}^n(s)ds \approx \mathbf{v}_2$ via simulations, for large time horizon T. In the next section, we provide numerical results to show that this is indeed the case for interacting random walks over different values of n.

Lastly, recall the bound (2.15) in Theorem 2.2.4. (2.15) only gives information on how closely the stochastic process follows the solution to the ODE system, and is not by any means a measure of how quickly $\mathbf{z}^n(t)$ might converge to $\mathbf{v}_2$. That being said, the bound in (2.15) increases with κ and N, but decreases in n. Therefore, theoretically, increases in κ and N need to be compensated by increasing n if we want (2.15) to ensure that the stochastic

process $\left(\mathbf{x}^n(t),\mathbf{y}^n(t)\right)_{t\geq 0}$ closely follows the solution $\left(\mathbf{x}(t),\mathbf{y}(t)\right)_{t\geq 0}$ of the ODE system (2.11). However in practice our framework turns out to be forgiving and requires only moderately large n to work well with a wide range of N and κ, as we shall observe in the next section.

2.5 Numerical results

We begin by providing our simulation setup in Section 2.5.1. In Section 2.5.2 we present simulation results over a range of parameters and different graphs in order to confirm our main theoretical results from Sections 2.2, 2.3 and 2.4. In Section 2.5.3 we consider the setting of dynamic graphs, and present numerical results that show the robustness of the performance of framework over a dynamic topology.

2.5.1 Simulation setup

We source two real world datasets, one is about a social network of dolphins (62 nodes, 159 edges) [86] and the other is about the Facebook social network (4039 nodes, 88234 edges) from the SNAP repository [79]. They are undirected, connected graphs, each having its own combinatorial Laplacian matrix $\mathbf{L}$. Walking according to $\mathbf{Q}=-\mathbf{L}$ on any graph is very natural, since it requires only local information.[6] For a specifically chosen n, we keep track of the quantities $\hat{\mathbf{x}}^n(t)\triangleq\frac{1}{t}\int_0^t\mathbf{x}^n(s)ds$ and $\hat{\mathbf{y}}^n(t)\triangleq\frac{1}{t}\int_0^t\mathbf{y}^n(s)ds$, the empirical density distributions of type-x and type-y walkers; and our Fiedler vector estimator $\hat{\mathbf{z}}^n(t)\triangleq\hat{\mathbf{x}}^n(t)-\hat{\mathbf{y}}^n(t)$ for all $t\geq 0$.

To show how our framework approximates the Fiedler vector and leads to a natural bi-partition of the graph, we illustrate in Figure 2.2 the progression of a single simulation run over the *Dolphins* graph, with $n=15$ walkers in each group and $\kappa=1000$ kept constant throughout the run. Figures 2.2(a), (b) and are 'snapshots' taken at times $t=0$ (initial configuration), 10 and 50 respectively. The color of a node represents which group of walkers hold majority at that node, and its intensity depends on the corresponding (normalized) value of $\hat{\mathbf{z}}^n(t)$. Figure 2.2(d) is an illustration of what the spectral bi-partitioning using the true value (computed offline) of $\mathbf{v}_2$ would be. As the simulation progresses, we can observe the bi-partition taking shape and Figure 2.2(c) and (d) end up closely resembling each

[6] A walker at node i, will stay there for a random exponential time with rate $d(i)$, after which it will move to a neighbor of i chosen uniformly at random. Hence, the walker uses only local information to walk according to CTMC $\mathbf{Q}=-\mathbf{L}$.

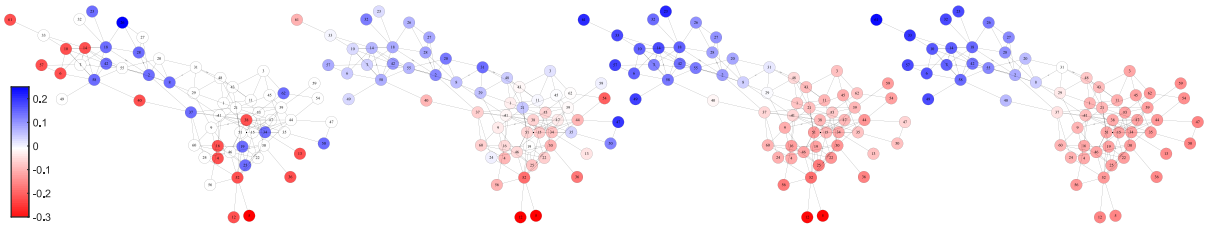

(a) Normalized $\hat{\mathbf{z}}^n(t)$; $n = 15, t = 0$ (b) $\hat{\mathbf{z}}^n(t)$; $n = 15, t = 10$ (c) $\hat{\mathbf{z}}^n(t)$; $n = 15, t = 50$ (d) Normalized FV ($\tilde{\mathbf{v}}_2$)

Figure 2.2 Colormap showing progression of the algorithm over a short time. Red and blue colors denote which group of walkers has majority at the corresponding node, while intensity of the color depends on the value of the corresponding FV estimate. (d) shows partition obtained using entries of the actual Fiedler vector.

other.

We wish to make these observations from Figure 2.2 more concrete, and show quantitatively that the quantity $\hat{\mathbf{z}}^n(t)$ converges to the Fiedler vector $\mathbf{v}_2$ over time. For this purpose we use two metrics to help visualize the convergence, namely the Rayleigh quotient (RQ) and the cosine similarity (CS), which are given respectively by

$$RQ(\hat{\mathbf{z}}^n(t)) \triangleq \frac{\hat{\mathbf{z}}^n(t)^T \mathbf{L} \hat{\mathbf{z}}^n(t)}{\|\hat{\mathbf{z}}^n(t)\|^2}, \qquad CS(\hat{\mathbf{z}}^n(t)) \triangleq \frac{|\hat{\mathbf{z}}^n(t)^T \mathbf{v}_2|}{\|\hat{\mathbf{z}}^n(t)\| \cdot \|\mathbf{v}_2\|}.$$

From Lemma 2.3.1, $RQ(\cdot)$ achieves its minimum, λ_2 at the Fiedler vector $\mathbf{v}_2$. Therefore $RQ(\hat{\mathbf{z}}^n(t))$ approaching λ_2 signifies that $\hat{\mathbf{z}}^n(t)$ approaches $\mathbf{v}_2$. The cosine similarity $CS(\hat{\mathbf{z}}^n(t))$ tracks the angle between $\mathbf{v}_2$ and $\hat{\mathbf{z}}^n(t)$. $CS(\hat{\mathbf{z}}^n(t)) = 1$ if $\hat{\mathbf{z}}^n(t)$ aligns with $\mathbf{v}_2$, implying its convergence, and $CS(\hat{\mathbf{z}}^n(t)) = 0$ if it is orthogonal to $\mathbf{v}_2$. $CS(\hat{\mathbf{z}}^n(t)$ does not just track the convergence, but also tests Proposition 2.4.1(i), i.e. whether $\hat{\mathbf{z}}^n(t)$ ever gets stuck near one of the unstable fixed points, $\mathbf{v}_k$ for $k \geq 3$. Such a case would cause $CS(\hat{\mathbf{z}}^n(t)) = 0$, and will be fairly visible in our results if it is a common occurrence. For each simulation run, every random walker starts at an initial position on the graph selected uniformly at random. We use 100 different runs for each simulation setup and display results as averaged over the 100 runs. To test these simulations, we pre-compute values of λ_2 and $\mathbf{v}_2$ for our datasets and use them to compare with RQ and to obtain values of CS respectively. It should be noted that this is purely for comparison purposes, and our framework never requires such computations to be carried out.

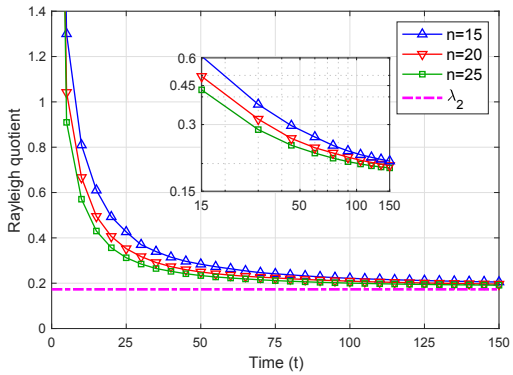

(a) RQ vs t over different n; $\kappa = 1000$ (inset plotted on log-log scale)

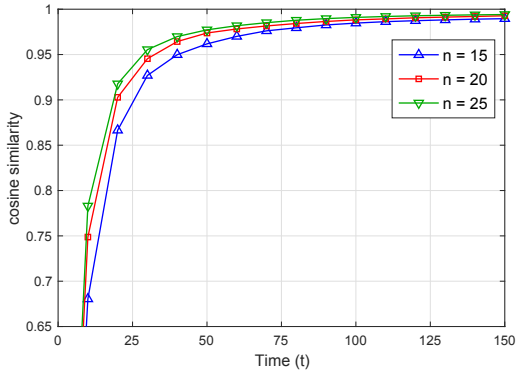

(b) CS vs t over different$n$; $\kappa = 1000$

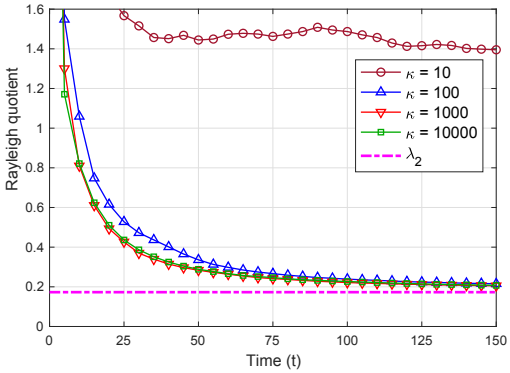

(c) RQ vs t over different κ; $n = 15$

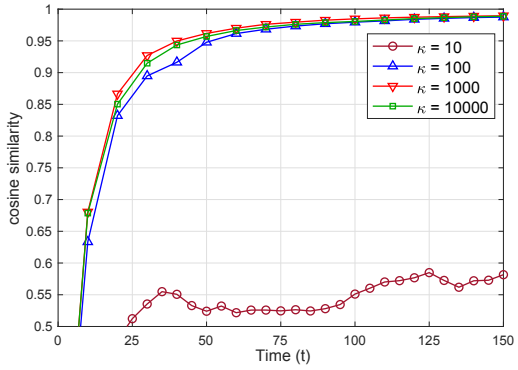

(d) CS vs t over different κ; $n = 15$

Figure 2.3 Simulations for the *Dolphins* graph.

2.5.2 Simulation results over a range of parameters

We first present simulation results for the *Dolphins* graph. Figures 2.3(a) and (b) show the results for values of $n = 15, 20$ and 25 for each type of walker, with κ set at 1000. For each n, simulation shows the Rayleigh quotient RQ approaching λ_2 of the Laplacian of the graph. This hints convergence to $\mathbf{v}_2$, which is also confirmed by the cosine similarity CS approaching *one*. The inset in Figure 2.3(a) plots the data on the log-log scale, and shows that RQ decays roughly polynomially fast to λ_2 for each n. As would be expected, $\mathbf{z}^n(t)$ for $n = 25$ outperforms the other two choices of n early on in the simulation, but its early advantage in performance is less pronounced as the simulation progresses.

Figures 2.3(c) and (d) show convergence results under different values of $\kappa = 10, 100, 1000$

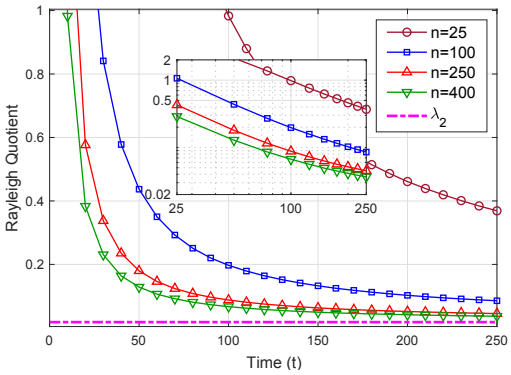

(a) RQ vs t over different n; $\kappa = 10000$ (inset plotted on log-log scale)

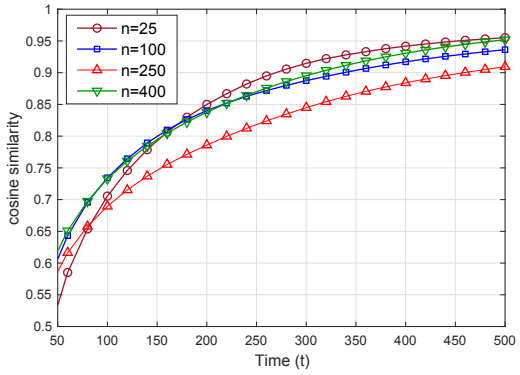

(b) CS vs t over different n; $\kappa = 10000$

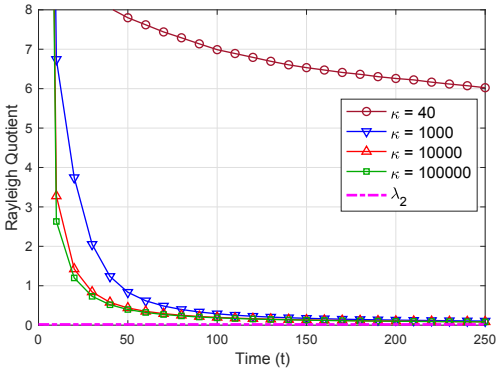

(c) RQ vs t over different κ; $n = 100$

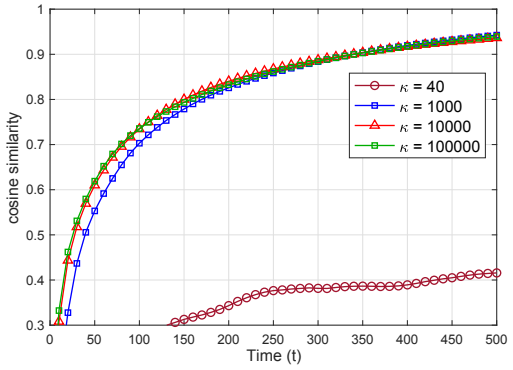

(d) CS vs t over different κ; $n = 100$

Figure 2.4 Simulations for the *ego-Facebook* graph.

and 10000, while keeping $n = 15$ for each run. Observe that the simulation results for $\kappa = 10$ do not show any convergence to the Fiedler vector. This can be attributed to the failure of $\kappa = 10$ in satisfying Proposition 2.3.2 by not being sufficiently large. For larger values of κ, we observe robust convergence over a wide range of values with no visible trend in κ. We now present simulation results for the *ego-Facebook* graph, where we perform similar simulations as before. it is interesting to see how well our interacting random walk based method scales to a larger graph. Figures 2.4(a) and (b) show simulation results for $n = 25, 100, 250$ and 400, for a fixed $\kappa = 10000$. As can be seen in Figure 2.4(a), the Rayleigh quotient for all four simulation sets converges towards λ_2. The inset in Figure 2.4(a) shows that similar to results for the *Dolphins* graph, RQ decays roughly polynomially to λ_2. The simulation for $n = 25$ seems to perform worst, at least early on, and $n = 400$ performs best

early on. An increase in n clearly shows faster convergence of RQ, but the big improvement from $n = 25$ to $n = 100$ is nowhere to be seen between $n = 250$ and $n = 400$. This appears to be because the probability of the stochastic process of deviating from the deterministic ODE decays exponentially fast in n, as theorized in Theorem 2.2.4. This is also the reason why even though *ego-Facebook* is a much larger graph than *Dolphins*, even values of n that are less that 3% of the graph size can provide good approximations, compared to about 50% needed for the much smaller *Dolphins* graph. In the longer run, $\hat{\mathbf{z}}^n(t)$ for all the simulations seems to align well enough with $\mathbf{v}_2$, as can be seen in Figure 2.4(b). Even for small number of walkers ($n = 25$), the CS eventually catches up with the rest and shows the expected close alignment with $\mathbf{v}_2$. This suggests that if high precision approximation is not needed, lower values of n can provide quick, yet reasonably accurate approximations of the Fiedler vector. This is useful for applications such as graph partitioning, where only the signs of the entries of the Fiedler vector matter, not the numerical entries themselves.

We also present simulations over *ego-Facebook* to test the effect of κ. Figures 2.4 (c) and (d) show the results for $\kappa = 40, 1000, 10000$ and 100000, keeping $n = 100$ constant over all the run[7]. We can observe that $\kappa = 40$ fails to be sufficiently large to satisfy Proposition 2.3.2 and does not show convergence to $\mathbf{v}_2$. As observed before for the *Dolphins* graph, there is no visible trend when it comes to κ influencing the performance of the simulation, with similar performance for a wide range of higher values of κ. Overall from simulation results of both the *Dolphins* and *ego-Facebook* graphs, it appears that as long as κ is large enough to satisfy Proposition 2.3.2 (which it seems to satisfy as long as κ is atleast of order $o(N)$) its value does not affect the performance of our framework, with convergence being robust for any choice of large κ.

It should be noted that in no simulated case did large N or large κ affect the ability of our stochastic process $\left(\mathbf{x}^n(t), \mathbf{y}^n(t)\right)_{t\geq 0}$ to closely follow the solutions $\left(\mathbf{x}(t), \mathbf{y}(t)\right)_{t\geq 0}$ of our ODE system (2.11), even though they possibly could have caused the bound in (2.15) from Theorem 2.2.4 to grow large[8]. This is because (2.15) is just an upper bound and in reality, the $\left(\mathbf{x}^n(t), \mathbf{y}^n(t)\right)$ could closely follow $\left(\mathbf{x}(t), \mathbf{y}(t)\right)$ over a much larger range of parameters. Moreover, it is an upper bound for the largest deviation over a finite time horizon $[0, T]$ and not for each time $t > 0$, meaning that it provides a worst case bound and efforts taken to make it smaller can be overkill.

[7]We plot these on a different scale compared to Figures 2.4(a) and (b) to accommodate all the results in a single frame.

[8]Failure to converge for smaller values of κ in Figures 2.3(c) and (d), and Figures 2.4(c) and (d) is attributed

2.5.3 Simulations on dynamic graphs

Our random walk based framework is also expected to perform well in the setting of dynamic graphs. In this section we provide simulation results to support that statement. We modify the *Dolphins* and *ego-Facebook* graphs by removing sets of nodes at certain time points during the course of each simulation run. When a node is removed, we also delete all the edges associated with it. While the instances at which these changes occur are selected for convenience of presentation, the sets of nodes to be removed are randomly generated before the simulation begins, with the condition that their removal does not affect the connectivity of the original graph. To differentiate the dynamic graphs from the original one, we rename our dynamic version of the graphs with node removal as *Dolphins-dyn* and *ego-Facebook-dyn*, respectively. We change the graphs three times in total by deleting a different set of nodes and all related edges at each of those instances. Overall, we delete around 21.0% of nodes from the original *Dolphins* graph and 12.4% of nodes from the original *ego-Facebook* graph, maintaining their connectivity as we do so. Table 2.1 gives details about the times at which nodes are removed and the number of nodes removed.

Table 2.1 Statistics of the dynamic changes made

	(t_1, # removed)	(t_2, # removed)	(t_3, # removed)
Dolphins-dyn	(25, 4 nodes)	(75, 3 nodes)	(100, 6 nodes)
ego-Facebook-dyn	(50, 196 nodes)	(100, 150 nodes)	(125, 154 nodes)

During the three pre-selected times $t_1, t_2, t_3 > 0$ when all the nodes from the corresponding sets are removed, any random walker currently located at the removed node is redistributed to the position of another randomly selected walker (of the same group) present at an unremoved node of the graph[9]. While plotting the Rayleigh quotient for the dynamic graphs, we represent by the black dotted lines the values of $\lambda_2(\mathcal{G})$, the algebraic connectivity of $\mathcal{G}$, updated to reflect the changes in graph topology.

Figures 2.5(a) to (d) show our simulation results under the dynamic graph setting over

to failure to satisfy Proposition 2.3.2, and is an intrinsic trait of the ODE system (2.11) itself and not the stochastic process.

[9]We did this only for convenience of the simulation, and the redistribution need not follow a prescribed rule since our theory allows for convergence starting from any arbitrary initial condition.

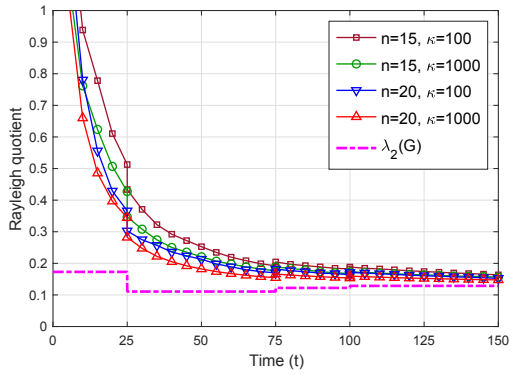

(a) RQ vs t for *Dolphins*-dyn

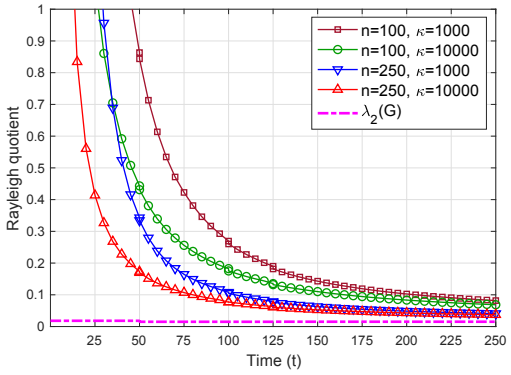

(b) RQ vs t for *ego-Facebook*-dyn

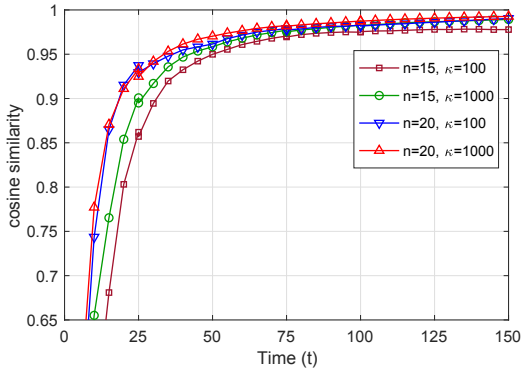

(c) CS vs t for *Dolphins*-dyn

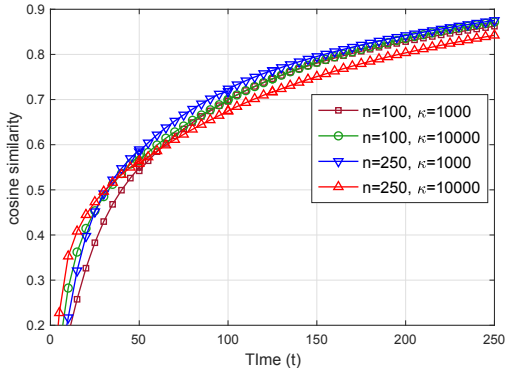

(d) CS vs t for *ego-Facebook*-dyn

Figure 2.5 Simulations for *Dolphins* and *ego-Facebook* graphs subject to node removals.

a range of parameters. Figures 2.5(a) and (b) show results concerning Rayleigh quotient RQ for the *Dolphins-dyn* and *ego-Facebook-dyn* graphs. We represent by the black dotted lines, the values of λ_2 updated to reflect the modification in graph topology. As expected, we observe small jumps in RQ at the times when nodes are deleted. Better visible in Figure 2.5(a) than in Figure 2.5(b), these jumps are similar in size to the jumps in $\lambda_2(\mathcal{G})$, and apart from these, the Rayleigh quotient values monotonically decrease with time without any unexpected fluctuations. From this, we can safely conclude that even after nodes are deleted, trajectories of the simulation do not diverge from their intended paths and keep converging to the Fiedler vector (of the updated/modified graphs). While they do not diverge, the trajectories do face minor changes in terms of a small loss in progress, as can be observed across all the values of n and κ in Figure 2.5(c) at time $t = 25$, where the

cosine similarity CS for *Dolphins-dyn* drops due to deletion of nodes. On the other hand, these changes can also be minor improvements/gains in progress as can be seen more clearly for $n = 250, \kappa = 1000$ in Figure 2.5(d) at time $t = 50$, where CS for *ego-Facebook-dyn* actually increases due to deletion of nodes. Therefore changes in topology can randomly be either beneficial, or disadvantageous depending on the random state the simulation is in. However, these random effects seem too minor to be a cause of concern, and there is no observable improvement or reduction in performance.

Thus, we can conclude that the framework behaves as would be expected and is robust to dynamical changes in topology, as long as the graph remains connected. It should be noted that even if the graph gets disconnected from time to time, the framework will still, by its design, converge to the Fiedler vector as long as connectivity is eventually restored again[10].

2.6 Extensions to reversible Markov Chains

In Section 2.2 the CTMC used as the basis for constructing our stochastic process was given by $\mathbf{Q} = -\mathbf{L}$, the negative of the combinatorial Laplacian. We then went on the show convergence of a suitably scaled version of this process to the Fiedler vector $\mathbf{v}_2$ of $\mathbf{L}$ in Section 2.3 and discussed the long run behavior of our stochastic process in Section 2.4. In this section, we generalize our results by extending them to not just the combinatorial Laplacian $\mathbf{L}$, but also any time reversible CTMC kernel which, is an important part of our contribution.

Consider the kernel $\mathbf{Q} \in \mathbb{R}^{N\times N}$ of an ergodic time reversible CTMC on a finite state space $\mathcal{N}$ (where $|\mathcal{N}| = N$), not necessarily symmetric. We denote by $\pi \in \mathbb{R}^N$, its stationary distribution ($\pi^T \mathbf{Q} = 0$). The vector π is also the first left eigenvector of $\mathbf{Q}$. If we now define our stochastic process in Section 2.2.1 and all the consequent systems with respect to time reversible $\mathbf{Q}$, we still have $\mathbf{z}^n(t)^T \mathbf{1} = 0$ (and $\mathbf{z}(t)^T \mathbf{1} = 0$) by construction. Earlier in Section 2.2 when $\mathbf{Q}$ was a symmetric matrix, its eigenvectors formed an orthogonal basis of the N-dimensional Euclidean space. This meant that being orthogonal to $\mathbf{1}$ automatically guaranteed being in a set where $\mathbf{v}_2$ minimized the Lyapunov function V. This, however, is not the case for any general non-symmetric, time reversible CTMC kernel $\mathbf{Q}$. We will extend

[10] For a disconnected graph, the Fiedler vector is not well defined, since the second eigenvalue is also *zero*, and no longer strictly positive. Therefore talking about the Fiedler vector of the whole graph makes sense only when it is connected.

our results to time reversible Markov chain kernels by introducing a specially constructed inner product which ensures orthogonality to the first left eigenvector of $\mathbf{Q}$, π.

For these purposes, we first formally define time reversible Markov chains.

Definition 2.6.1. *A Markov chain with* $\mathbf{Q}$ *is called 'time reversible' if and only if there exists a unique* π *such that for all* $i, j \in \mathcal{N}$, $i \neq j$, *the pair* $(\pi, \mathbf{Q})$ *satisfies the 'detailed balance equation'* $\pi_i Q_{ij} = \pi_j Q_{ji}$.

For a given pair $(\pi, \mathbf{Q})$, define an N-dimensional vector space $\mathscr{H}_{\frac{1}{\pi}}$ endowed with an inner product $\langle \cdot, \cdot \rangle_{\frac{1}{\pi}}$, defined as

$$\langle \mathbf{x}, \mathbf{y} \rangle_{\frac{1}{\pi}} = \mathbf{x}^T \Pi^{-1} \mathbf{y}, \quad \text{for any } \mathbf{x}, \mathbf{y} \in \mathbb{R}^N$$

where $\Pi = \mathbf{D}_\pi$.

Lemma 2.6.2. *[26] The pair* $(\pi, \mathbf{Q})$ *is reversible if and only if* $\mathbf{Q}^T$, *acting as a linear operator from* $\mathscr{H}_{\frac{1}{\pi}}$ *onto itself, satisfies* $\langle \mathbf{Q}^T \mathbf{u}, \mathbf{v} \rangle_{\frac{1}{\pi}} = \langle \mathbf{y}, \mathbf{Q}^T \mathbf{v} \rangle_{\frac{1}{\pi}}$.

Such operators are called self-adjoint or Hermitian and always have real eigenvalues. Thus, we can define the ordering of eigenvalues of $-\mathbf{Q}$ as $0 = \lambda_1 < \lambda_2 \leq \lambda_3 \leq \cdots \leq \lambda_N$, just like we did for $\mathbf{L}$. The eigenvectors of self-adjoint operators are orthogonal with respect to the related inner product. Hence, for any two left eigenvectors $\mathbf{v}_i$ and $\mathbf{v}_k$ of $\mathbf{Q}$, $i \neq k$, we have $\langle \mathbf{v}_i, \mathbf{v}_k \rangle_{\frac{1}{\pi}} = 0$. Picking $i = 1$, and substituting $\mathbf{v}_1 = \pi$, we obtain

$$\langle \pi, \mathbf{v}_k \rangle_{\frac{1}{\pi}} = \pi^T \Pi^{-1} \mathbf{v}_k = \mathbf{1}^T \mathbf{v}_k = 0.$$

Therefore, the Euclidean subspace that is orthogonal to $\mathbf{1}$, is also a subspace of $\mathscr{H}_{\frac{1}{\pi}}$ orthogonal to π in terms of our new inner product, $\langle \cdot, \cdot \rangle_{\frac{1}{\pi}}$. Also, $\mathbf{z}^n(t)^T \mathbf{1} = 0 \iff \langle \mathbf{z}^n(t), \pi \rangle_{\frac{1}{\pi}} = 0$, giving us the desired orthogonality with π. This allows us to recover results from Section 2.3 by a redefinition of the Lyapunov function V in terms of $\langle \cdot, \cdot \rangle_{\frac{1}{\pi}}$, i.e.

$$V(\mathbf{u}) = \frac{1}{2} \langle \mathbf{u}, -\mathbf{Q}^T \mathbf{u} \rangle_{\frac{1}{\pi}} \text{ for all } \mathbf{u} \in \mathscr{H},$$

and appropriately using the new inner product (i.e. $\langle \mathbf{u}, \mathbf{w} \rangle_{\frac{1}{\pi}}$ instead of $\mathbf{u}^T \mathbf{w}$, for any two vectors $\mathbf{u}$ and $\mathbf{w}$) wherever necessary. The results from Section 2.4 never required a specific form of $\mathbf{Q}$ to work as long the results from Sections 2.2 and 2.3 held, and now therefore hold true for any choice of time reversible $\mathbf{Q}$.

From the above, we have extended our main results to be applicable to any time reversible CTMC kernel $\mathbf{Q}$. It is important to note that our extension is purely based on an update in the inner product used for the analysis purposes in Section 2.3, and requires no modification to the way our stochastic process is constructed in Section 2.2, making $\mathbf{Q}$ simply a *plug-and-play* term in our framework.

We now show the applicability of this extension to any ergodic, time reversible DTMC kernel $\mathbf{P}$ as well. The Fiedler vector for such matrices is now the eigenvector corresponding to the second largest eigenvalue of $\mathbf{P}$, also known as the spectral gap [80, 1, 26]. We start by defining a CTMC kernel $\mathbf{Q}_p$ based on the time reversible $\mathbf{P}$ as $\mathbf{Q}_p \triangleq \mathbf{P}-\mathbf{I}$[11]. Suppose π is the unique stationary distribution of $\mathbf{P}$, such that the pair $(\pi,\mathbf{P})$ satisfies the *detailed balance equation* (DBE) from Definition 2.6.1. Then, the pair $(\pi,\mathbf{Q}_p)$ also satisfies the DBE and $\mathbf{Q}_p$ is a time reversible CTMC. This means that all our theoretical results stand for $\mathbf{Q}_p$ if we use it as the basis for generating our stochastic process in Section 2.2.1. Therefore, $\mathbf{z}^n(t)$ for a system of random walkers, which walk according to the CTMC $\mathbf{Q}_p = \mathbf{P}-\mathbf{I}$ and interact in the same manner as in the previous sections, will approximate $\mathbf{v}_2$ of the DTMC $\mathbf{P}$[12] in the long run.

We can also apply this extension to the random walk Laplacian $L^{rw} = \mathbf{I}-\mathbf{D}^{-1}\mathbf{A}$, and the normalized Laplacian $\mathscr{L} = \mathbf{I}-\mathbf{D}^{-1/2}\mathbf{A}\mathbf{D}^{-1/2}$, introduced earlier in Section 2.1.2. We can do this by first observing that $\mathbf{D}^{-1}\mathbf{A}$ is a DTMC kernel with the degree distribution vector $\frac{1}{\mathbf{d}^T\mathbf{1}}\mathbf{d}$ serving as its stationary distribution. The pair $\left(\frac{1}{\mathbf{d}^T\mathbf{1}}\mathbf{d},\mathbf{D}^{-1}\mathbf{A}\right)$ is also time reversible [1, 26] and satisfies the DBE. Thus, setting $\mathbf{Q}_{rw} \triangleq \mathbf{D}^{-1}\mathbf{A}-\mathbf{I} = -\mathbf{L}^{rw}$ as our CTMC kernel extends all the results of the chapter to the random walk Laplacian and allows us to obtain approximations for $\mathbf{v}_2^{rw}$, the Fiedler vector of the random walk Laplacian. Given a component $[\mathbf{v}_2^{rw}]_i$, the corresponding component of the Fiedler vector $\bar{\mathbf{v}}_2$ of the normalized Laplacian $\mathscr{L}$ can be obtained by setting $[\bar{\mathbf{v}}_2]_i = [\mathbf{v}_2^{rw}]_i/\sqrt{d(i)}$, due to the similarity relationship between the two matrices as shown in Section 2.1.2. Therefore, once $[\mathbf{v}_2^{rw}]_i$ is approximated, a simple localized computation involving only the degree of the concerned node allows us to obtain $[\bar{\mathbf{v}}_2]_i$ as well. With this, we can now use our framework to approximate (on-the-fly) the Fiedler vectors of all the three important graph Laplacians as special cases of our extended theoretical results.

[11] See that $\mathbf{Q}_p\mathbf{1} = (\mathbf{P}-\mathbf{I})\mathbf{1} = 0$, and $\mathbf{Q}_p$ has non-negative off-diagonal entries and negative diagonal entries. It is therefore a well defined CTMC kernel

[12] Since eigenvectors of $\mathbf{Q}_p$ and $\mathbf{P}$ are the same.

2.7 Concluding remarks

In this chapter, given any time reversible Markov Chain kernel, we have detailed the construction of a stochastic process based on interacting random walkers. Random walk algorithms usually relate to the leading/principal eigenvectors of their respective kernels. In fact, the field of Markov chain Monte Carlo (MCMC) is dedicated to the problem of using a random walk to sample according to a given probability distribution. Famous examples include the Metropolis Hastings Random walk and the Gibbs sampler [55, 84, 101, 77], which construct Markov chains and leverage the ergodic theorem to sample according to its first eigenvector. While usually these are restricted to sampling on undirected graphs, [76] samples from a directed graph using a novel method which involves *mapping* a target distribution to the quasi-stationary distribution (QSD) of a sub-stochastic Markov chain. However, this technique also essentially leverages properties of a leading eigenvector, which is the QSD in this case. No such random walk type technique has been applied towards approximating the second eigenvector. By relating our stochastic process to a deterministic ODE system we show convergence to the second eigenvector, making our random walk based method a first in literature.

Chapter 3

Self Repellent Random Walks on General Graphs

We begin this chapter by providing basic notations, and introduce the topic of nonlinear Markov chains, specifically self-interacting Markov chains on finite state spaces, and also introduce the simple random walk (SRW) on a general graph. With these preliminaries in place, we introduce our self-repellent random walk (SRRW) algorithm in Section 3.3, giving the precise form of the transition kernel and introducing a closely related deterministic system whose analysis will be crucial to obtaining our main results. In Section 3.4 we establish the global convergence result for the deterministic system using the aid of a Lyapunov function. We use this in Section 3.5 to provide first order and second order convergence results for a slightly modified SRRW process with random truncations; showing that the SRRW improves over the well-studied simple random walk (SRW) in the sense of a Loewner ordering of co-variance matrices. In Section 3.6, we provide numerical results that support our theoretical results, and end this chapter with our conclusion in Section 3.7.

3.1 Preliminaries

3.1.1 Basic Notation

Since vectors and matrix will be recurring mathematical quantities throughout the chapter, we standardize their notations. Lower case, bold faced letters will be used to represent

vectors[1] (e.g. $\mathbf{v} \triangleq [v_i]_{i\in\mathcal{N}} \in \mathbb{R}^N$), and upper case, bold faced letters are reserved for matrices (e.g. $\mathbf{M} \triangleq [M_{ij}]_{i,j\in\mathcal{N}} \in \mathbb{R}^{N\times N}$, unless clarified otherwise. For any vector $\mathbf{v}$, the term diag($\mathbf{v}$) denotes a diagonal matrix with v_i as the i'th diagonal entry. Also, denote by $\mathbf{1} \triangleq [1,\cdots,1]^T$ and $\mathbf{0} \triangleq [0,\cdots,0]^T$ the vector of all ones and zeros respectively. Eigenvalues will always be indexed such that subscripts $N,\cdots,1$ are assigned from the largest to smallest eigenvalues (in modulus). We denote by $\leq_L$ ($<_L$) Loewner ordering of matrices, such that $\mathbf{A} \leq_L \mathbf{B}$ ($\mathbf{A} <_L \mathbf{B}$) means $\mathbf{x}^T(\mathbf{A}-\mathbf{B})\mathbf{x} \leq 0$ (< 0) for any $\mathbf{x} \in \mathbb{R}^N$. Throughout the chapter, we will use $\Sigma \triangleq \{\mathbf{x} \in \mathbb{R}^N \mid \mathbf{1}^T\mathbf{x} = 0,\ x_i \in [0,1]\}$ to denote the probability simplex, and Int(Σ) to denote its interior.

We use $\mathcal{G}(\mathcal{N},\mathcal{E})$ denote a general, undirected, possibly weighted, connected graph, with $\mathcal{N} \triangleq \{1,\cdots,N\}$ being the set of nodes, and $\mathcal{E}$ being the set of edges where $(i,j) \in \mathbb{E}$ denotes an edge for $i,j \in \mathcal{N}$. Denote by $\mathbf{A} = [a_{ij}]_{i,j\in\mathcal{N}}$, the 'adjacency matrix' of $\mathcal{G}(\mathcal{N},\mathcal{E})$, where $a_{ij} = 0$ if $(i,j) \notin \mathcal{E}$, and $a_{ij} > 0$ otherwise.[2] The use $\deg(i) \triangleq \sum_{j\in\mathcal{N}} a_{ij}$ to denote the 'degree' of each node $i \in \mathcal{N}$, with the 'degree matrix' $\mathbf{D}$ of the graph being a diagonal matrix with deg(i) as the i'th diagonal entry.

The use of matrices $\mathbf{K}$ and $\mathbf{P}$ (in various forms such as involving superscripts) will be reserved for transition probability matrices of discrete time Makrov chains (DTMC's). Note that throughout the chapter, we shall often refer to these matrices using the umbrella term *kernel* of Markov chains. Vectors such as $\mathbf{x}(t)$, with $t \in \mathbb{R}_+$ being time, will be used to denote (deterministic) solutions to systems of ordinary differential equations (ODEs), while those of the form $\mathbf{x}_n$, with $n \in \mathbb{N}_0$ being a discrete time step, will be reserved for stochastic sequences. For any vector valued function $F : \mathbb{R}^N \to \mathbb{R}^N$ with $f_i : \mathbb{R}^N \to \mathbb{R}$ being its i'th component, we denote by $\mathbf{J}_F(\mathbf{u})$, the Jacobian matrix of $F(\cdot)$ evaluated at $\mathbf{u} \in \mathbb{R}^N$, where $\mathbf{J}_F(\mathbf{x})_{ij} \triangleq \frac{\partial f_i(\mathbf{x})}{\partial x_j}\Big|_{\mathbf{x}=\mathbf{u}}$

3.1.2 Simple Random Walk on General Graphs

We review the simple random walk on an undirected, connected graph $\mathcal{G}(\mathcal{N},\mathcal{E})$, with $\mathbf{A} = [a_{ij}]_{i,j\in\mathcal{N}}$ being its adjacency matrix. Denote by $\{Y_n\}_{n\geq 0}$ a simple random walker (SRW) over the node set $\mathcal{N}$ of the graph. At any time, the SRW transitions from its current node to a neighbouring node uniformly at random. In other words if $Y_n = i \in \mathcal{N}$ at time $n \in \mathbb{N}_0$, then $Y_{n+1} = j$ w.p. $1/\deg(i)$ if $(i,j) \in \mathcal{E}$. The *linear* Markov kernel for SRW is then given by

[1] All vectors are assumed to be column vectors.

[2] In case of unweighted graphs, $a_i j = 1$ when $(i,j) \in \mathcal{E}$.

$\mathbf{K}^{\text{srw}} = [K_{ij}^{\text{srw}}]_{i,j\in\mathscr{N}}$, where

$$K_{ij}^{\text{srw}} = \frac{a_{ij}}{\deg(i)}; \tag{3.1}$$

or equivalently, $\mathbf{K}^{\text{srw}} = \mathbf{D}^{-1}\mathbf{A}$, where $\mathbf{D}$ is a diagonal matrix with its i'th diagonal entry being the degree $\deg(i)$ of the corresponding node. Since the underlying graph is connected, $\{Y_n\}_{n\geq 0}$ is an ergodic MC, and there exists a unique invariant distribution which solves the detailed balance equation. For SRW, the stationary distribution is simply the *degree proportional distribution* denoted by $\mathbf{d} = [d_i]_{i\in\mathscr{N}}$, where $d_i \triangleq \deg(i)\big/\sum_k \deg(k)$ for all $i \in \mathscr{N}$.

We now mention some results regarding the spectrum of $\mathbf{K}^{\text{srw}}$. Let $(\lambda_i, \mathbf{u}_i)$ (similarly $(\lambda_i, \mathbf{v}_i)$) be left (right) eigenvalue-eigenvector pairs of $\mathbf{K}^{\text{srw}}$, where the normalization is such that $\mathbf{u}_i^T\mathbf{v}_i = 1$. Following similar steps to those in Chapter 2 Section 2.1.2 for the *random walk Laplacian* therein, we can deduce that λ_i's are real. They are ordered as $1 = \lambda_N > \lambda_{N-1} \geq \cdots \geq \lambda_1 > -1$, and we have $\mathbf{u}_N = \mathbf{d}$ and $\mathbf{v}_N = \mathbf{1}$. Moreover, we know (from reversibility of $\mathbf{K}^{srw}$) that $\mathbf{u}_i = \text{diag}(\mathbf{d})\mathbf{v}_i$ and $\mathbf{u}_i^T\mathbf{v}_j = 0$ for all $i, j \in \mathscr{N}$. These facts will be used in the later sections when analyzing the performance the self-repellent random walk.

3.2 Self-Interacting Markov Chains - Literature Review

We now provide a general introduction to the topic of stochastic processes driven by nonlinear Markov kernels, specifically self interacting Markov chains, to put our subsequent sections in context with the wider literature on this topic. Consider a discrete time stochastic process $\{X_n\}_{n\in\mathbb{N}_0}$ over a finite state space $\mathscr{N} \triangleq \{1, \cdots, N\}$, where state transition probabilities from $i \to j$ are given by mappings $K : \mathscr{N} \times \mathscr{N} \times \Sigma \to [0,1]$, that is

$$K_{ij}[\mathbf{x}] \triangleq \mathbb{P}(X_{n+1} = j \mid X_n = i,\, \mathbf{x}), \quad \forall\, i, j \in \mathscr{N}, \tag{3.2}$$

where $\mathbf{x} \in \Sigma$ is the nonlinearity inducing probability vector. The transition probability matrix $\mathbf{K}[\mathbf{x}] \triangleq \big[K[\mathbf{x}]_{ij}\big]_{i,j\in\mathscr{N}}$ is a called a (discrete time) nonlinear Markov kernel. For each $\mathbf{x} \in \Sigma$, ergodicity assumptions on $K[\mathbf{x}]$ ensure the existence and uniqueness of invariant measures $\pi(\mathbf{x}) \in \Sigma$ satisfying the balance equation $\pi(\mathbf{x})^T\mathbf{K}[\mathbf{x}] = \pi(\mathbf{x})^T$. A problem of interest requiring further analysis is the root finding problem - determining the existence, possible uniqueness, and convergence of the stochastic process in some sense to a $\mathbf{x}^* \in \Sigma$ which satisfies $\pi(\mathbf{x}^*) = \mathbf{x}^*$. The freedom in choice of $\mathbf{K}[\cdot]$ and the nature of its argument $\mathbf{x}$ can lead to the design of stochastic processes driven by nonlinear Markov kernels to perform

tasks such as higher order eigenvector estimation [42](also see Chapter 2), and sampling from directed graphs [76], although this connection with nonlinear Markov chains was not explicitly mentioned in those works. However, despite recent progress on the topics [69, 93], there is still no unifying framework which we can directly utilize for the analysis of algorithms driven by nonlinear kernels..

The process $\{X_n\}_{n\geq 0}$ is termed as *self-interacting* when the nonlinear Markov kernel takes as argument the occupational measure $\mathbf{x}_n \in \Sigma$, given by

$$\mathbf{x}_n \triangleq \frac{1}{n+1}\sum_{k=0}^{n} \boldsymbol{\delta}_{X_k}, \tag{3.3}$$

that is, the $n+1$'th transition is driven by the kernel $\mathbf{K}[\mathbf{x}_n]$ for all $n \in \mathbb{N}$.[3] The term self-interacting Markov chains (SIMC) was initially introduced in [36, 35] where they were described as heuristic procedures for solving the root finding problem $\boldsymbol{\pi}(\mathbf{x}^*) = \mathbf{x}^*$. Later works [5, 6] employed them for Monte carlo tasks and analyzed *genetic*-SIMC kernels - where the nonlinearity is primarily in the form of random restarts of the Markov Chain via jumps to a previously visited state, sampled from some distribution which is a function of the empirical measure $\mathbf{x}_n$. Closely related are the so-called *iteracting* Markov chain Monte Carlo (i-MCMC) algorithms [92, 28], which also inlucde the equi-energy sampler [71, 110] as a special case, utilize $n-$many parallel random walks running at n different levels - the nonlinear jump for the random walk at level $k \leq n$ depending on interactions with the occupational measures of random walks running at the 1'st to $k-1$'th levels. With a large augmentation of the original state space (to the power of N), the i-MCMC is still an example of SIMC, and it was shown that these i-MCMC algorithms can be designed to sample from N different probability distributions in parallel. The nonlinearities in both genetic-SIMC and i-MCMC algorithms come from the random jumps caused by self-interactions, the Markovian component involved in the local diffusion of the process itself being a linear kernel. This is different from the nonlinear MC studied in this chapter which assumes no such special structure, and our results are not a special case of the aforementioned literature.

Weak convergence results were obtained in [36] under certain assumptions on the

[3] Self-interactions or interactions with a random walker's own occupational measures are different from the interaction based mechanism defined in Chapter 2 Section 2.2. Although the underlying kernel therein is also a (continuous time) nonlinear Markov kernel, the interactions are with the *density* distribution many different random walkers over the graph, as opposed to interacting with history as in SIMC.

nonlinear Markov kernel which imply (in a weak sense) contraction of $\boldsymbol{\pi}(\mathbf{x})$ with respect to a total-variation norm, which still remains the most general convergence result for SIMCs. However, it is not always possible to show contractions with respect to standard L^p norms, especially when the nonlinear kernel is not uniformly Lipschitz as is the case for the SRRW introduced in the following section. In this case, we will still show a contraction property as part of our first order convergence proof, albeit with respect to the Hilbert's projective metric [78]. Convergence proofs in [6] and [36] involve analyzing the solutions of the Poisson equation [cite] and its regularity, which also forms a vital part in proving the convergence of stochastic approximation (SA) algorithms via the so-called ODE method [54, 17].

Indeed, SIMCs have been studied as stochastic approximations as well, mainly in the form of vertex reinforced random walks (VRRWs) [97, 16, 21, 105, 75, 20]. In its most basic form, the VRRW on a graph $\mathcal{G}(\mathcal{N},\mathcal{E})$ with adjacency matrix $\mathbf{A}$, is driven by a nonlinear Markov kernel with transition probabilities of the form

$$K[\mathbf{x}]_{ij} = \frac{a_{ij}g(x_j)}{\sum_k a_{ij}g(x_j)},$$

where $g : [0,1] \to \mathbb{R}_+$ is an increasing function. The self-interacting implementation is thus biased towards visiting the more frequently visited nodes. The VRRW was originally introduced in [97], later analyzed for various types of graphs [99, 133, 134, 126, 21], and have often been interpreted as sampling algorithms for revision protocols in the field evolutionary game theory [98, 18]. This type of SIMC is the closest to the one we study in this chapter, the key difference being that our self-repellent mechanism is a form of negative-reinforcement, as opposed to the positive-reinforcement process of VRRWs.

3.3 Self Repellent Random Walk

Let $\mathcal{G}(\mathcal{N},\mathcal{E})$ be an undirected, connected, possibly weighted graph with adjacency matrix $\mathbf{A}$. We aim to design a nonlinear Markov chain which, at stationarity, samples from the degree proportional probability distribution $\mathbf{d} \in \mathrm{Int}(\Sigma)$. We assume that the visit count for each node is set to one at the start of the process, that is $\mathbf{x}_0 = \mathbf{1}/N$ where $\mathbf{x}_n$ is the historical empirical distribution/occupational measure as defined in (3.3). Suppose that at any time $n \in \mathbb{N}_0$, the random walker's current location is node $i \in \mathcal{N}$, that is $X_n = i$. At time $n+1$, the walker moves to a neighbor j of i with probability inversely proportional to the ratio of the

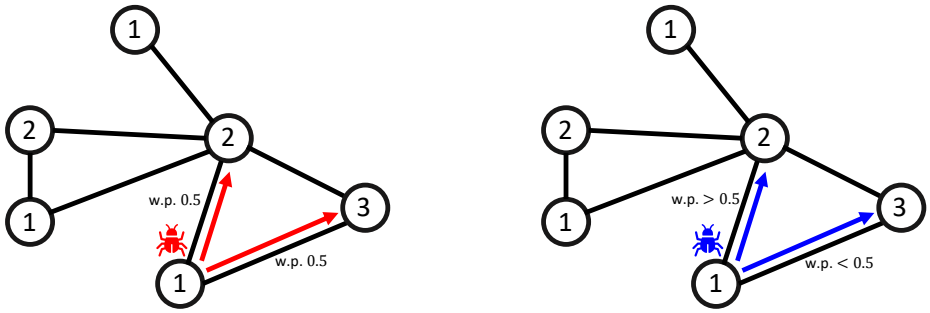

(a) Simple random walk (b) Self-repellent walk with $\alpha = 0.4$

Figure 3.1 SRW vs SRRW dynamics. The probability of moving to the node with 3 past visit counts is 0.37 for SRRW, while it is 0.5 for SRW.

visit count to node j and its degree; that is

$$\mathbb{P}(X_{n+1} = j \mid X_n = i, X_{n-1}, \cdots, X_0) \propto \left(\frac{1 + \sum_{k=0}^{n} \mathbb{1}_{\{X_k = j\}}}{\deg(j)} \right)^{-\alpha} = \left(\frac{x_i}{d_i} \right)^{-\alpha},$$

where $\alpha \geq 0$ is a parameter which controls the sensitivity of the transition probabilities to differences in visit counts between nodes. Since $\mathbf{x}_t$ captures the visit counts from time steps 0 to $n-1$, the conditioning on $\{X_{n-1}, \cdots, X_0\}$ can be replaced by conditioning on $\mathbf{x}_n$. This allows us to write the nonlinear transition probability kernel $\mathbf{K}[\mathbf{x}] \triangleq \left[K[\mathbf{x}]_{ij} \right]$, as defined in (3.2), as

$$K[\mathbf{x}]_{ij} = \frac{a_{ij} \left(\frac{x_j}{d_j} \right)^{-\alpha}}{\sum_k a_{ik} \left(\frac{x_k}{d_k} \right)^{-\alpha}}, \tag{3.4}$$

for each $\mathbf{x} \in \text{Int}(\Sigma)$, where the denominator serves as a normalizing term. With this description of the SRRW in mind, we can write the sequence of occupational measures $\{\mathbf{x}_n\}_{n \in \mathbb{N}_0}$ as a recursion, given by

$$\mathbf{x}_{n+1} = \mathbf{x}_n + \frac{1}{n+2} \left(\boldsymbol{\delta}_{X_{n+1}} - \mathbf{x}_n \right), \tag{3.5}$$

for any $n \in \mathbb{N}$, where $X_{n+1} = j$ with probability $K[\mathbf{x}_n]_{X_n, j}$ as given in (3.4), 'step-size' has $n+2$ in the denominator instead of $n+1$ to account for the initial choice of $\mathbf{x}_0$.

Remark 3.3.1. *Setting $\alpha = 0$ in (3.1) coincides with the SRW case, where the random walker visits any of the neighbors of the currently occupied node with equal probability as seen in Figure 3.1(a). On the other hand, as seen in Figure 3.1, SRRW prioritizes the neighbor with a smaller ratio of visit count to degree. All the results presented in this chapter allow for $\alpha = 0$, and will thus trivially apply to the SRW case as well. This will neatly set the stage for*

comparing, in some sense, the performance of two types of random walks.

Note that $\mathbf{K}[\mathbf{x}]$ is only well defined for $\mathbf{x} \in \text{Int}(\Sigma)$, and not on the boundary of Σ, the probability simplex.[4] This will not be major of concern due to the initial choice of $\mathbf{x}_0$ and, in some sense, the invariance of the sequence $\{\mathbf{x}_n\}_{n\in\mathbb{N}_0}$ in $\text{Int}(\Sigma)$, as shall be seen in later sections. The following result shows the existence and uniqueness of an invariant distribution associated with $\mathbf{K}[\mathbf{x}]$ for every $\mathbf{x} \in \text{Int}(\Sigma)$, and will allow us to further decompose the update rule in (3.5).

Proposition 3.3.2. *For any $\mathbf{x} \in Int(\Sigma)$ there exists a unique probability distribution $\pi(\mathbf{x}) = [\pi_i(\mathbf{x})]_{i\in\mathcal{N}} \in Int(\Sigma)$ which solves $\pi(\mathbf{x})^T \mathbf{K}[\mathbf{x}] = \pi(\mathbf{x})^T$, and is given by*

$$\pi_i(\mathbf{x}) = \frac{\sum_{j\in\mathcal{N}} a_{ij}\left(\frac{x_i}{d_i}\right)^{-\alpha}\left(\frac{x_j}{d_j}\right)^{-\alpha}}{\sum_{k\in\mathcal{N}}\sum_{l\in\mathcal{N}} a_{kl}\left(\frac{x_k}{d_k}\right)^{-\alpha}\left(\frac{x_l}{d_l}\right)^{-\alpha}}, \tag{3.6}$$

for all $i \in \mathcal{N}$. Furthermore, the pair $(\pi(\mathbf{x}), \mathbf{K}[\mathbf{x}])$ is reversible for all $\mathbf{x} \in Int(\Sigma)$, that is, it solves $\pi_i(\mathbf{x})K[\mathbf{x}]_{ij} = \pi_j(\mathbf{x})K[\mathbf{x}]_{ji}$ for all $i, j \in \mathcal{N}$.

Proof in Appendix B.1. □

The uniqueness of $\pi(\mathbf{x})$ allows us to rewrite the update rule (3.5) in the form

$$\mathbf{x}_{n+1} = \mathbf{x}_n + \frac{1}{n+2}\left(F(\mathbf{x}_n) + \epsilon(X_{n+1}, \mathbf{x}_n)\right), \tag{3.7}$$

where $F(\mathbf{x}_n) \triangleq \pi(\mathbf{x}_n) - \mathbf{x}_n$, and $\epsilon(X_{n+1}, \mathbf{x}_n) \triangleq \boldsymbol{\delta}_{X_{n+1}} - \pi(\mathbf{x}_n)$ for all $n \in \mathbb{N}_0$. The sequence $\{\mathbf{x}_n\}_{n\geq 0}$ is then an example of a *stochastic approximation* (SA) algorithm with *state-dependent* noise $\epsilon : \mathcal{N} \times \text{Int}(\Sigma) \to \mathbb{R}^N$, and *mean-field* $F : \text{Int}(\Sigma) \to \mathbb{R}^N$ (see, for instance, Chapter 6 in [54]). Its limiting behaviour can be deduced by analyzing the convergence properties of trajectories $\{\mathbf{x}(t)\}_{t\geq 0}$ of the ODE system given by

$$\frac{d}{dt}\mathbf{x}(t) = F(\mathbf{x}(t)) = \pi(\mathbf{x}(t)) - \mathbf{x}(t), \tag{3.8}$$

[4] The boundary includes all $\mathbf{x} \in \Sigma$ such that $x_i = 0$ for some $i \in \mathcal{N}$.

which can be written for all $i \in \mathcal{N}$ as

$$\frac{d}{dt} x_i(t) = f_i(\mathbf{x}(t)) = \frac{\sum\limits_{j \in \mathcal{N}} a_{ij} \left(\frac{x_i}{d_i}\right)^{-\alpha} \left(\frac{x_j}{d_j}\right)^{-\alpha}}{\sum\limits_{k \in \mathcal{N}} \sum\limits_{l \in \mathcal{N}} a_{kl} \left(\frac{x_k}{d_k}\right)^{-\alpha} \left(\frac{x_l}{d_l}\right)^{-\alpha}} - x_i(t). \tag{3.9}$$

We conclude this section by giving the following remark, which widens the scope of our results in this chapter.

Remark 3.3.3 (SRRW for a given target distribution)**.** *Let* $\mathbf{P}$ *be a time-reversible*[5] *Markov kernel with stationary measure* $\boldsymbol{\eta} \in Int(\Sigma)$*. Then, by setting* $\mathbf{A} = diag(\boldsymbol{\eta})\mathbf{P}$*, or equivalently* $a_{ij} = \eta_i P_{ij}$ *gives us* $\mathbf{d} = \boldsymbol{\eta}$*, since* $d_i = \sum_j a_{ij} \big/ \sum_k \sum_l a_{ij} = \eta_i \sum_j P_{ij} \big/ \sum_k \eta_k \sum_l P_{kl} = \eta_i$ *for all* $i \in \mathcal{N}$*. Moreover,* $a_{ij} = \eta_i P_{ij} = \eta_j P_{ji} = a_{ji}$*, the new matrix* $\mathbf{A}$ *is also symmetric, and can therefore be considered to be the adjacency matrix of an undirected, weighted, connected graph with the same edge set* $\mathcal{E}$ *(with possible addition of self-loops). With this observation, we can construct a SRRW for any given target distribution* $\boldsymbol{\eta}$*, where* $\mathbf{P}$ *can then be a Metropolis Hastings algorithm; and all the results in this chapter will still hold. It is worth noting that one only needs to know* η_i*'s up to a constant multiple, and* P_{ij}*'s up to a constant multiple for each* $i \in \mathcal{N}$*, in order to deduce state transition probabilities.*

3.4 Analysis of the ODE - Global convergence

Before formalizing the relationship between the sequence of occupational measures $\{\mathbf{x}_n\}_{n \in \mathbb{N}_0}$ satisfying the SA update rule (3.5), and the trajectories $\{\mathbf{x}(t)\}_{t \geq 0}$ of the ODE system (3.8) in Section 3.5, we first analyze the latter and characterize its convergence properties. As the first step towards establishing global convergence properties, we establish sufficient conditions that guarantee uniqueness of the fixed points (3.8). Global convergence is then obtained by introducing a Lyapunov function and applying LaSalle's invariance principle (Definition A.2.1 and Theorem A.2.2 respectively).

First, we observe that for any $\alpha \geq 0$, the degree proportional vector $\mathbf{d} \in \text{Int}(\Sigma)$ solves the fixed point equation $F(\mathbf{d}) = \boldsymbol{\pi}(\mathbf{d}) - \mathbf{d} = \mathbf{0}$, and is therefore a fixed point of the ODE system

[5] Check Definition 2.6.1 in Chapter 2 for a formal definition of time-reversible Markov chains.

(3.8). Indeed, observe that for each $i \in \mathcal{N}, \alpha \geq 0$, setting $x_i(t) = d_i$ in (3.9) gives us

$$f_i(\mathbf{d}) = \frac{\sum\limits_{j\in\mathcal{N}} a_{ij}}{\sum\limits_{k\in\mathcal{N}}\sum\limits_{l\in\mathcal{N}} a_{kl}} - d_i = \frac{\deg(i)}{\sum\limits_{k\in\mathcal{N}} \deg(k)} - d_i = 0.$$

The following result provides sufficient conditions to ensure the *uniqueness* of $\mathbf{d}$ as the fixed point of (3.8).

Lemma 3.4.1. *For all $\alpha \in [0, 1/2)$, the degree proportional probability vector $\mathbf{d} \in Int(\Sigma)$ is the unique fixed point of* (3.9).

Proof in Appendix B.2. □

The proof of Lemma 3.4.1 first involves showing that $\pi : \text{Int}(\Sigma) \to \text{Int}(\Sigma)$ is a contraction mapping with respect to Hilbert's projective metric[6] $d_H(\cdot,\cdot)$, that is by showing that $d_H(\pi(\mathbf{x}), \pi(\mathbf{x})) < d_H(\mathbf{x}, \mathbf{y})$ for any $\mathbf{x}, \mathbf{y} \in \text{Int}(\Sigma)$ and $0 \leq \alpha < 1/2$.

Let $V : \text{Int}(\Sigma) \to \mathbb{R}$ be given by

$$V(\mathbf{x}) = \sum_i \sum_j a_{ij} \left(\frac{x_i}{d_i}\right)^{-\alpha} \left(\frac{x_j}{d_j}\right)^{-\alpha}, \tag{3.10}$$

We will now show that the mapping $V(\cdot)$ is a *strict* Lyapunov function for (3.8).

Lemma 3.4.2. *Derivatives of $V(\cdot)$ along trajectories of the ODE system* (3.8) *evaluated at any $\mathbf{x} \in Int(\Sigma)$ is non-positive, that is $\frac{d}{dt}V(\mathbf{x}) \leq 0$, with equality if and only if $\mathbf{x} = \mathbf{d}$, the unique fixed point of* (3.8).

Proof in Appendix B.2. □

The uniqueness of $\mathbf{d}$ as the fixed point of (3.8) is critical, since it guarantees that $V(\mathbf{x}) > V(\mathbf{d})$ for all $\mathbf{x} \in \text{Int}(\Sigma) \setminus \{\mathbf{d}\}$; a fact not obvious from directly examining (3.10). The derivative being non-positive also ensures that $\{\mathbf{x}(t)\}_{t\geq 0} \subset \text{Int}(\Sigma)$ for any initial point $\mathbf{x}(0) \in \text{Int}(\Sigma)$, implying that solutions of the ODE system leave $\text{Int}(\Sigma)$ positively invariant. The global convergence result now follows from a straightforward application of LaSalle's invariance principle.

[6] Hilbert's projective metric, as in Definition B.2.1 in Appendix B, has been effectively applied in proving convergence of nonlinear positive (with respect to some partial ordering) operators, in what is now known as nonlinear Perron Frobenius theory [78].

Theorem 3.4.3. *For all initial points* $\mathbf{x}(0) \in Int(\Sigma)$*, the trajectories* $\{\mathbf{x}(t)\}_{t\geq 0}$ *converge to the unique fixed point* $\mathbf{d}$*, that is,* $\mathbf{x}(t) \xrightarrow{t\to\infty} \mathbf{d}$.

Proof in Appendix B.2. □

Before moving on to the next section where we provide first and second order convergence results for the sequence of occupational measures $\{\mathbf{x}_n\}_{n\geq 0}$, we give the following result for the Jacobian matrix $\mathbf{J}_F(\mathbf{x})$ of $F(\mathbf{x})$, when evaluated at $\mathbf{x} = \mathbf{d}$. To capture its dependence on the parameter $\alpha \geq 0$, we use the notation $\mathbf{J}(\alpha) \triangleq \mathbf{J}_F(\mathbf{d})$. In the following result, λ_i's, $\mathbf{u}_i$'s and $\mathbf{v}_i$'s, as originally defined in Section 3.1.2, are the eigenvalues, and corresponding left and right eigenvectors of the SRW kernel $\mathbf{K}^{\text{srw}} = \mathbf{D}^{-1}\mathbf{A}$ respectively,

Proposition 3.4.4. *For any* $\alpha \geq 0$*, we have*

$$\mathbf{J}(\alpha) = 2\alpha \mathbf{d}\mathbf{1}^T - \alpha \mathbf{A}\mathbf{D}^{-1} - (\alpha+1)\mathbf{I}. \tag{3.11}$$

Furthermore, let μ_i *denote the i'th eigenvalue of* $\mathbf{J}(\alpha)$*. Then, we have*

$$\mu_N = -1 \quad > \quad \mu_{N-1} = \alpha(-1-\lambda_{N-1}) - 1 \quad \geq \cdots \geq \quad \mu_1 = \alpha(-1-\lambda_1) - 1, \tag{3.12}$$

with $\mathbf{u}_i$ *(*$\mathbf{v}_i$*) being the right (left) eigenvectors corresponding to* μ_i *for all* $i \in \mathcal{N}$.

Proof in Appendix B.2. □

3.5 Convergence and asymptotic performance of SRRW

As mentioned briefly in Section 3.3, the nonlinear Markovian kernal $\mathbf{K}[\mathbf{x}]$ that drives the sequence $\{X_n, \mathbf{x}_n\}_{n\in\mathbb{N}_0}$ via the update rule (3.5) is only well defined in Int(Σ) and not over the entire probability simplex Σ. This also means that $\boldsymbol{\pi}(\mathbf{x})$ is not Lipchitz in Int(Σ), and as a result neither is $F(\mathbf{x})$. Unfortunately, most of the classical SA theorems [cite] require $F(\mathbf{x})$ to be Lipschitz to ensure that SA iterates remain bounded, by ensuring in some sense, the regularity of the state dependent noise terms $\epsilon(X_n, \mathbf{x}_n)$ in (3.7). While the boundedness of the iterate sequence $\{\mathbf{x}_n\}_{n\in\mathbb{N}_0}$ is not a concern in our setting, since $\mathbf{x}_n \geq \mathbf{0}$ and $\mathbf{1}^T\mathbf{x}_n = 1$ for all $n \in \mathbb{N}_0$, the classical proof techniques (see Chapter 6 in [54]) still depend on $F(\mathbf{x})$ to be Lipchitz.

In this section, we look at a modification of the SRRW update rule (3.5) involving randomly occurring truncations at the boundaries of a sequences of expanding sets, following

which, the algorithm restarts in the interior of a suitable, compact subset of Int(Σ). For this modified SRRW update rule, we apply the results from [7] and [47] (or alternative [37]) to obtain almost sure convergence of the sequence of occupational measures $\{\mathbf{x}_n\}_{n\in\mathbb{N}_0}$ to the degree proportional distribution $\mathbf{d}$, and also provide a central limit theorem for the same.

3.5.1 SRRW with random truncations

Define a sequence of compact subsets $\{\mathscr{K}_n\}_{n\in\mathbb{N}_0}$ of Int(Σ), where for each $n\in\mathbb{N}_0$, we have $\mathscr{K}_n \triangleq \left\{\mathbf{x}\in\Sigma \mid x_i \in \left[\frac{1}{n+M}, 1-\frac{1}{n+M}\right]\right\}$, for some (possibly large) positive integer M. We have

$$\mathscr{K}_n \subset \mathscr{K}_{n+1} \quad \forall n\in\mathbb{N}_0, \quad \text{and } \cup_{n\in\mathbb{N}_0}\mathscr{K}_n = \text{Int}(\Sigma). \tag{3.13}$$

Consider the following stochastic approximation update rule, with $\mathbf{x}_0\in\mathscr{K}_0$, $X_0\in\mathscr{N}$, $\varsigma_0=0$, $\kappa_0=0$ and $\nu_0=0$, such that for all $n\in\mathbb{N}$, we have:

$$\begin{aligned}
&\text{set} \qquad \mathbf{x}_{n+\frac{1}{2}} = \mathbf{x}_n + \frac{1}{\varsigma_n+2}\left(\boldsymbol{\delta}_{X_{n+1}} - \mathbf{x}_n\right)\\
&\text{update} \;\; (\mathbf{x}_{n+1},\, \varsigma_{n+1},\, \kappa_{n+1},\, \nu_{n+1}) = \begin{cases} (\mathbf{x}_{n+\frac{1}{2}},\, \varsigma_n+1,\, \kappa_n,\, \nu_n+1), & \text{if } \mathbf{x}_{n+\frac{1}{2}}\in\mathscr{K}_{\kappa_n} \\ (\mathbf{x}_0,\, \varsigma_n+1-\nu_n,\, \kappa_n+1,\, 0), & \text{otherwise} \end{cases},
\end{aligned} \tag{3.14}$$

where X_{n+1} is drawn from $\mathbf{K}[\mathbf{x}_n]_{X_n,\cdot}$ for all $n\in\mathbb{N}$.

In the above, $\mathbf{x}_{n+\frac{1}{2}}$ can be thought of as 'proposal' obtained via the regular update as in (3.5). The integers ς_n, κ_n and ν_n are *counters* which keep track the current step-size index, the index of the truncation set $\mathscr{K}_{\kappa_n}$ at iteration n, and number of steps since the last truncation/restart of the algorithm. If the proposal $\mathbf{x}_{n+\frac{1}{2}}$ lies within the current truncation set $\mathscr{K}_{\kappa_n}$, it is 'accepted' by setting $\mathbf{x}_{n+1}=\mathbf{x}_{n+\frac{1}{2}}$ and the algorithm moves forward by incrementing ς_n and ν_n by one, while keeping κ_n and as a result the current truncation set $\mathscr{K}_{\kappa_n}$ the same for the next iteration. Otherwise, the algorithm is effectively restarted from the initial position by setting $\mathbf{x}_{n+1}=\mathbf{x}_0$ and resetting the step-size index ς_n back to the index at the previous truncation event. In this case, the truncation set is also enlarged by incrementing κ_n by one.

Remark 3.5.1. *The original update rule* (3.5) *is simple to implement since it does not require the size of the underlying graph $\mathscr{G}(\mathscr{N},\mathscr{E})$ to be known a priori. In comparison, there is no straightforward way to implement* (3.14) *without knowing the graph size, since* $\mathbf{x}_{n+\frac{1}{2}}\in\mathscr{K}_{\kappa_n}$

(or $\notin \mathscr{K}_{\kappa_n}$) needs to be checked at every iteration; and it can also prove to be computationally expensive for large graph sizes. However, we will show in Section 3.6 that numerical results from simulating the update rule (3.5) *(without truncations) also align with the theoretical results derived in this section for* (3.14)*. Therefore, the introduction of the truncation based mechanism is mostly just for mathematical rigour, and the search for more general proof techniques not requiring random restarts of the algorithm is still an ongoing work.*

3.5.2 Main results

We are now prepared to state the main results of the chapter. The first theorem below provides a first-order, almost sure convergence result (SLLN) for the sequence of occupational measures $\{\mathbf{x}_n\}_{n\geq 0}$ satisfying update rule (3.14), and also provides a second order (CLT) result.

Theorem 3.5.2. *Let $\{\mathbf{x}_n\}_{n\geq 0}$ be the iterates of* (3.14)*. For any initial $(\mathbf{x}_0, X_0) \in Int(\Sigma)\times\mathscr{N}$, and large enough M such that $\mathbf{x}_0 \in \mathscr{K}_0$, we have*

$$\mathbf{x}_n \xrightarrow[n\to\infty]{a.s.} \mathbf{d} \quad \textit{and,} \quad \sqrt{n}(\mathbf{x}_n - \mathbf{d}) \xrightarrow[n\to\infty]{dist.} N(\,\mathbf{0}, \mathbf{V}(\alpha)\,), \tag{3.15}$$

where $\mathbf{V}(\alpha)$ is the covariance matrix, which is given for all $\alpha \in [0, 1/2)$ by

$$\mathbf{V}(\alpha) = \int_0^\infty e^{t(\mathbf{J}(\alpha)+\mathbf{I}/2)}\mathbf{U}e^{t(\mathbf{J}(\alpha)+\mathbf{I}/2)^T}\,dt, \tag{3.16}$$

with

$$\mathbf{U} = \sum_{k=1}^{N-1} \frac{1+\lambda_k}{1-\lambda_k}\mathbf{u}_k\mathbf{u}_k^T. \tag{3.17}$$

Proof in Appendix B.3. □

The first-order result in the above is in departure from the more classical analysis of SA algorithms, which first prove that a continuous time version[7] of the stochastic sequence $\{\mathbf{x}_n\}_{n\geq 0}$, is indistinguishable in the long run from deterministic trajectories $\{\mathbf{x}_n\}_{n\geq 0}$, when compared over any compact time interval.[8] The almost sure convergence then follows by establishing the convergence properties of the mean field ODE system, which may not

[7] Constructed via a suitable interpolation in the time parameter.

[8] We say that the continuous time interpolation is an *asymptotic pseudo-trajectory* of the flow generated by the mean field ODE system [17].

necessarily be via Lyapunov function techniques. Instead, for Theorem 3.5.2, we apply Theorem 5.5 in [7], which ensures a more direct form of convergence without first establishing an asymptotic pseudo-trajectory property for the stochastic system. However, as a critical component of the proof, it requires the existence of a Lyapunov function such as the one we constructed for Lemma (3.4.2). The proof techniques therein ensure that the number of restarts of (3.14) are finitely many almost surely, with the tail probability of the number of restarts decreasing super-exponentially (Theorem 5.4 in [7]).

The spectral form of matrix $\mathbf{U}$ as shown in (3.17) is entirely in terms of eigenvalues and (left) eigenvectors of the SRW kernel $\mathbf{K}^{\text{srw}}$ introduced in Section 3.1.2. Recall from Proposition 3.4.4 that the entire spectrum and eigenspace of $\mathbf{J}(\alpha)$, and also that of $e^{t(\mathbf{J}(\alpha)+\mathbf{I}/2)}$ as a result, can also be written in terms of the eigenvalues and vectors of $\mathbf{K}^{\text{srw}}$ and $\alpha \geq 0$. This encourages further analysis of the covariance matrix $\mathbf{V}(\alpha)$ given by (3.16), leading to the following important result.

Theorem 3.5.3. *For any $\alpha_1 > \alpha_2 > 0$, we have*

$$\mathbf{V}(\alpha_1) <_L \mathbf{V}(\alpha_2) <_L \mathbf{V}(0).^9 \tag{3.18}$$

Proof in Appendix B.3. □

The above Loewner ordering result tells us that processes with larger α, and therefore a higher degree of self-repellence, achieve a smaller variance in the estimation of $\mathbf{d}$ along any principal axis. While this is only useful for $\alpha \in [0, 1/2)$, this condition on α is utilized only as a sufficient condition in Lemma 3.4.1 to ensure the uniqueness of $\mathbf{d}$ as the fixed point of (3.8). Therefore, larger degrees of self interaction in terms of larger α could lead to a improved SRRW under more general results guaranteeing uniqueness of $\mathbf{d}$. Via numerical results in the next section, we will see that the uniqueness indeed holds for larger α, with the monotone ordering predicted by Theorem 3.5.3 also observed for $\alpha \geq 1/2$.

3.6 Simulation results

In this section, we simulate the SRRW on a few real world graphs, walking according to the update rule without truncations (3.5). We compare the convergence of the occupational measures of multiple SRRWs over a wide range of $\alpha \geq 0$, with that of the SRW ($\alpha = 0$), and the non-backtracking random walk (NBRW) [77]. The NBRW is a modification of SRW, where at

every time step, the random walker avoids the node visited at the previous time step with probability one. This was shown to be an improvement over SRW in sense of achieving a smaller asymptotic variance [77].

We source our real world, undirected graphs from the SNAP repository [79] - the subgraph of a social network (Facebook) with 4,039 nodes and 88,234 edges, and an Autonomous Systems graph (AS-733) with 6,047 nodes and 13,233 edges. We run SRW, NBRW, and eight different SRRWs with $\alpha \in \{0.1, 0.2, 0.3, 0.4, 0.5, 1.0, 2.0, 10.0\}$, and for each random walker, we calculate the total variation distance TVD($\mathbf{x}_n, \mathbf{d}$) between its occupational measure $\mathbf{x}_n$ at time $n \geq 0$ and the degree distribution vector $\mathbf{d}$, given by

$$\text{TVD}(\mathbf{x}_n, \mathbf{d}) \triangleq \frac{1}{2}\|\mathbf{x}_n - \mathbf{d}\|_1, \tag{3.19}$$

where $\|\cdot\|_1$ denotes the 1-norm, given by $\|\mathbf{u}\| = \sum_{i \in \mathcal{N}} |u_i|$ for any $\mathbf{u} \in \mathbb{R}^N$. For all simulation runs, the starting position $X_0 \in \mathcal{N}$ of the random walkers is chosen uniformly at random, with $\mathbf{x}_0 = \mathbf{1}/N$, consistent with the description in Section 3.3. In total, we average our TDV plots over 500 simulation runs for each type of random walker.

Our simulation results are shown in Figures 3.2 (Faceboook graph) and 3.3 (AS-733 graph). For all different random walkers, we can observe convergence to the target distribution $\mathbf{d}$ in Figures 3.2(a) and 3.3(a), which are plotted over the semi-log scale. This suggests a geometric rate of convergence, even for SRRW with $\alpha \geq 0.5$. Recall that our convergence results in Theorem 3.5.2 were only shown for $\alpha \in [0, 0.5)$, which was the sufficient condition to guarantee uniqueness of $\mathbf{d}$ as the fixed point of (3.8). The observed convergence of SRRW for $\alpha \geq 0.5$ in our simulation points to a potential relaxation of the uniqueness condition to cover a much wider range of $\alpha \geq 0$. In the asymptotic regime, that is TDV vs n plotted in Figures 3.2(b) and 3.3(b), we can observe the eventual ordering of TDV($\mathbf{x}_n, \mathbf{d}$) in α, in line with the performance ordering predicted for covariance matrices in Theorem 3.5.3, with larger values of α achieving smaller TDV. While SRRW performing better than SRW for all $\alpha > 0$ is as predicted by Theorem 3.5.3, we also observe that in cases of both the graphs, SRRW achieves a smaller TDV than even NBRW. While there is no theory supporting this observation, the comparison between self-repellent and non-backtracking mechanisms is nevertheless interesting, and can be a topic of future research.

Even though Theorems 3.5.2 and 3.5.3 were shown for the truncation based update rule (3.14), the simulation results in this section which do no employ any truncations or random restarts, still algin with the theoretical expectation. Thus, it is likely that the first

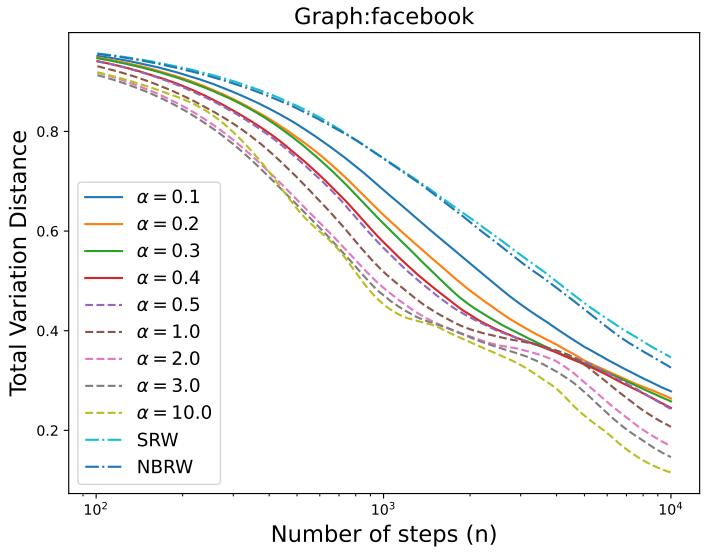

(a) TDV($\mathbf{x}_n, \mathbf{d}$) vs n, semi-log scale

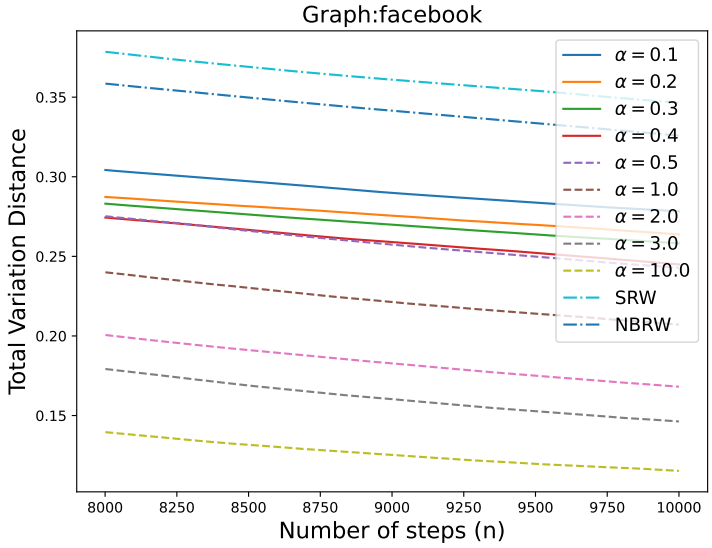

(b) TDV($\mathbf{x}_n, \mathbf{d}$) vs n, linear scale; asymptotic regime

Figure 3.2 Simulation results for Facebook graph

order convergence and CLT result in Theorem 3.5.2 also holds for occupational measures satisfying the original update rule (3.5), as previously mentioned in Remark 3.5.1.

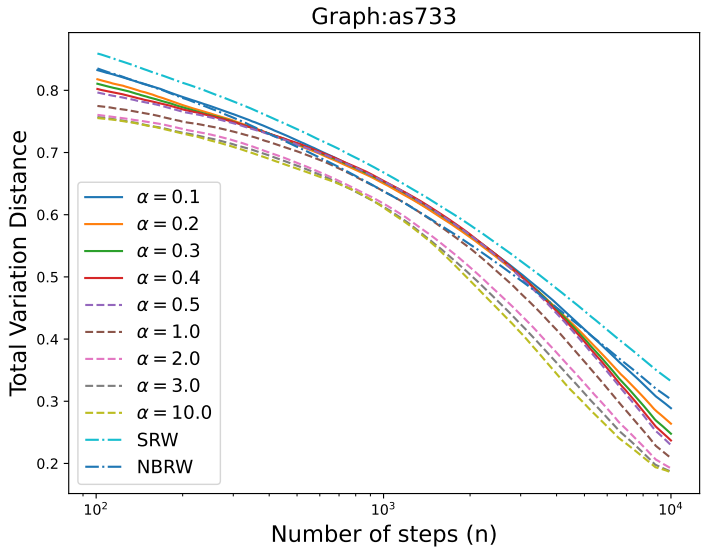

(a) TDV($\mathbf{x}_n, \mathbf{d}$) vs n, semi-log scale

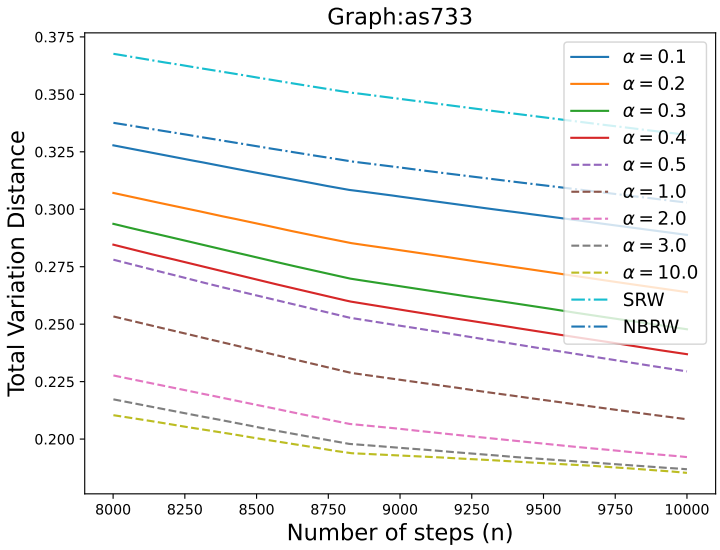

(b) TDV($\mathbf{x}_n, \mathbf{d}$) vs n, linear scale; asymptotic regime

Figure 3.3 Simulation results for AS-733 graph

3.7 Conclusion

In this chapter, we introduced a *self-repellent random walk* which can be designed to achieve any target distribution $\boldsymbol{\eta} \in \mathrm{Int}(\Sigma)$ via nonlinear interacting with its own occupational measure. We provide convergence results for the sequence of occupational measures by first analyzing a closely related deterministic process whose convergence is proved with the aid of a Lyapunov function, and then utilizing results from stochastic approximation theory to establish first and second order convergence results for a modified update rule with random restarts or truncations. Our results are still restricted to the case where $\alpha \in [0, 1/2)$, although numerical results point to possibilities of relaxing on this condition, as well as proving the necessary convergence results without the need of random restarts. In light of these possible improvements on the results shown in this chapter, our theory of self-repellent random walks is still a work in development.

Chapter 4

Competitive Epidemics on Graphs - Global Convergence and Coexistence

In Section 4.1, we first introduce the basic notation used throughout the chapter, along with the classical (single-virus) SIS model and the bi-virus model. We then provide the generalization to non-linear infection and recovery rates in Section 4.2 with some key assumptions on the infection and recovery rate functions, complimented by a discussion in Appendix C.3 regarding a special class of recovery rates. In Section 4.3, we provide a primer to the MDS theory, and establish monotonicity results for the single-virus SIS model, proving the convergence result for the single-virus model with non-linear infection and recovery rates whose proofs are deferred to Appendix C.5. We then go on to show in Section 4.4.1 that the non-linear bi-virus model is also a monotone dynamical system with respect to a specially constructed cone-based partial ordering, and include the main convergence results in Section 4.4.2. In Section 4.5 we take the opportunity to provide a more intuitive version of our results by considering the special case of linear infection and recovery rates, along with brief comparisons with the existing literature. In Section 4.6, we provide numerical results which confirm our theoretical findings. We then conclude in Section 4.7.

For better readability of the chapter, all technical proofs of the main results are deferred to Appendices C.5 and C.6. The appendices also include some selected definitions and results from matrix theory (Appendix C.1), ODE theory (Appendix C.2), and from MDS theory (Appendix C.4), which we use as part of our proofs of the Theorems in Section 4.4.2.

4.1 Preliminaries

4.1.1 Basic Notations

We standardize the notations of vectors and matrices by using lower case, bold-faced letters to denote vectors ($\mathbf{v}\in\mathbb{R}^N$), and upper case, bold-faced letters to denote matrices ($\mathbf{M}\in\mathbb{R}^{N\times N}$). We denote by $\lambda(\mathbf{M})$ the largest *real part*[1] of all eigenvalues of a square matrix $\mathbf{M}$. We use $\text{diag}(\mathbf{v})$ or $\mathbf{D}_\mathbf{v}$ to denote the $N\times N$ diagonal matrix with entries of vector $\mathbf{v}\in\mathbb{R}^N$ on the diagonal. Also, we denote $\mathbf{1}\triangleq[1,\cdots,1]^T$ and $\mathbf{0}\triangleq[0,\cdots,0]^T$, the N-dimensional vector of all ones and zeros, respectively. For vectors, we write $\mathbf{x}\leq\mathbf{y}$ to indicate that $x_i\leq y_i$ for all i; $\mathbf{x}<\mathbf{y}$ if $\mathbf{x}\leq\mathbf{y}$ and $\mathbf{x}\neq\mathbf{y}$; $\mathbf{x}\ll\mathbf{y}$ when all entries satisfy $x_i<y_i$. We use $\mathcal{G}(\mathcal{N},\mathcal{E})$ to represent a general, undirected, connected graph with $\mathcal{N}\triangleq\{1,2,\cdots,N\}$ being the set of nodes and $\mathcal{E}$ being the set of edges. When we refer to a matrix $\mathbf{A}=[a_{ij}]$ as the adjacency matrix of some graph $\mathcal{G}(\mathcal{N},\mathcal{E})$, it satisfies $a_{ij}\triangleq\mathbb{1}_{\{(i,j)\in\mathcal{E}\}}$ for any $i,j\in\mathcal{N}$; we use $d_{min}(\mathbf{A})$ and $d_{max}(\mathbf{A})$ to denote the minimum and maximum degrees of the nodes of the corresponding graph. Since we only consider connected graphs, all the adjacency matrices in this chapter are automatically considered to be irreducible (see Definition C.1.1 in Appendix C.1).

4.1.2 SIS Model with Linear rates

Consider the graph $\mathcal{G}(\mathcal{N},\mathcal{E})$, and assume that at any given time $t\geq 0$, each node $i\in\mathcal{N}$ of the graph is either in an *infected (I)*, or in a *susceptible (S)* state. An infected node can infect each of its susceptible neighbors with rate $\beta>0$.[2] It can also, with rate $\delta>0$, be cured from its infection and revert to being susceptible again. We write $\mathbf{x}(t)=[x_i(t)]\in\mathbb{R}^N$, where $x_i(t)$ represents the probability that node $i\in\mathcal{N}$ is infected at any given time $t\geq 0$. Then, the dynamics of the SIS model can be captured via the system of ODEs given by

$$\frac{dx_i(t)}{dt}\triangleq\beta(1-x_i(t))\sum_{j\in\mathcal{N}}a_{ij}x_j(t)-\delta x_i(t) \tag{4.1}$$

[1] We use the λ notation instead of something like λ_{Re}, since it will mostly be used in cases where the largest eigenvalue is real, for which λ itself is the largest real eigenvalue. For example, $\lambda(\mathbf{A})$ becomes the spectral radius for any non-negative matrix $\mathbf{A}$ [89].

[2] We say an event occurs with some *rate* $\alpha>0$ if it occurs after a random amount of time, exponentially distributed with parameter $\alpha>0$.

for all $i \in \mathcal{N}$ and $t \geq 0$. In a matrix-vector form, this can be written as

$$\frac{d\mathbf{x}}{dt} \triangleq \beta \operatorname{diag}(\mathbf{1}-\mathbf{x})\mathbf{A}\mathbf{x} - \delta\mathbf{x} \tag{4.2}$$

where we suppress the (t) notation for brevity. The system (4.2) is positively invariant in the set $[0,1]^N$, and has $\mathbf{0}$ as one of its fixed points (the virus-free equilibrium). The following result is well known from [74], which we will generalize in Section 4.3.2.

Theorem 4.1.1 (Theorem 3.1 in [74]). *Let $\tau \triangleq \beta/\delta$. Then,*

(i) either $\tau \leq 1/\lambda(\mathbf{A})$, and $\mathbf{x}^* = \mathbf{0}$ is a globally asymptotically stable fixed point of (4.2)*;*

(ii) or $\tau > 1/\lambda(\mathbf{A})$, and there exists a unique, strictly positive fixed point $\mathbf{x}^* \in (0,1)^N$ such that $\mathbf{x}^*$ is globally asymptotically stable in $[0,1]^N \setminus \{\mathbf{0}\}$.

4.1.3 Bi-Virus Model with Linear rates

Consider two graphs $\mathcal{G}_1(\mathcal{N}, \mathcal{E}_1)$ and $\mathcal{G}_2(\mathcal{N}, \mathcal{E}_2)$, on the same set of nodes $\mathcal{N}$ but with different edge sets $\mathcal{E}_1$ and $\mathcal{E}_2$. At any given time $t \geq 0$, a node $i \in \mathcal{N}$ is either *infected by Virus 1*, *infected by Virus 2*, or is *susceptible*. A node infected by Virus 1 infects each of its susceptible neighbors with rate $\beta_1 > 0$, just like in the SIS model, but does so only to nodes which are its neighbors with respect to the graph $\mathcal{G}_1(\mathcal{N}, \mathcal{E}_1)$. Nodes infected by Virus 1 also recover with rate $\delta_1 > 0$, after which they enter the susceptible state. Similarly, nodes infected by Virus 2 infect their susceptible neighbors, this time with respect to the graph $\mathcal{G}_2(\mathcal{N}, \mathcal{E}_2)$, with rate $\beta_2 > 0$, while recovering with rate $\delta_2 > 0$. This competing bi-virus model of epidemic spread, also referred to as the SI_1I_2S model, can be represented by the following ODE system:

$$\begin{aligned} \frac{dx_i}{dt} &\triangleq \beta_1\big(1-x_i-y_i\big)\sum_{j\in\mathcal{N}} a_{ij}x_j - \delta_1 x_i \\ \frac{dy_i}{dt} &\triangleq \beta_2\big(1-x_i-y_i\big)\sum_{j\in\mathcal{N}} b_{ij}y_j - \delta_2 y_i \end{aligned} \tag{4.3}$$

for all $i \in \mathcal{N}$ and $t \geq 0$. In matrix-vector form, (4.3) becomes:

$$\begin{aligned} \frac{d\mathbf{x}}{dt} &\triangleq \beta_1 \operatorname{diag}(\mathbf{1}-\mathbf{x}-\mathbf{y})\mathbf{A}\mathbf{x} - \delta_1\mathbf{x} \\ \frac{d\mathbf{y}}{dt} &\triangleq \beta_2 \operatorname{diag}(\mathbf{1}-\mathbf{x}-\mathbf{y})\mathbf{B}\mathbf{y} - \delta_2\mathbf{y}, \end{aligned} \tag{4.4}$$

where $\mathbf{A} = [a_{ij}]$ and $\mathbf{B} = [b_{ij}]$ are the adjacency matrices of graphs $\mathcal{G}_1(\mathcal{N}, \mathcal{E}_1)$ and $\mathcal{G}_2(\mathcal{N}, \mathcal{E}_2)$, respectively.

4.2 Epidemic Models with Non-linear Infection and Recovery rates

In this section, we introduce the single-virus and bi-virus SIS models with nonlinear infection and recovery rates. Non-linearities can be attributed to the spread and recovery from the virus being related to the susceptibility of the disease (or its prevalence in the population) in a more complicated manner. This is more general than simply exponential random variables with constant rates used to model the spreading and recovery processes, which in aggregate scale linearly with the infection probabilities.[3] This is shown to be limiting in accurately modelling the trajectories of an infection spread; the linear scaling of the infection and recovery rates shown to being an overestimate to what is observed in reality [138, 68]. Many works thus argue for the modelling of these spreading processes with non-linear functions [13, 12, 64, 85]. We first present the more general single-virus SIS model with a set of intuitive assumptions (A1)–(A5) for the non-linear infection and recovery rates.

4.2.1 SIS Model with Non-linear rates

In (4.1) the term $\sum_{j\in\mathcal{N}} a_{ij}x_j(t)$ denotes the overall rate at which a susceptible node $i \in \mathcal{N}$ gets infected by its neighbors. In what follows, we replace this by a generic function $f_i(\mathbf{x}(t))$, thereby allowing the overall infection rate for each node to be any non-linear function of $x_j(t)$ for all neighbors j of i. Similarly, we replace the term $\delta x_i(t)$, denoting the overall recovery rate for any node $i \in \mathcal{N}$, by a non-linear function $q_i(\mathbf{x}(t))$. This generic version of the SIS model, allowing for non-linear infection and recovery rates, is given by the ODE

$$\frac{dx_i(t)}{dt} = \bar{f}_i(\mathbf{x}(t)) \triangleq (1-x_i(t))f_i(\mathbf{x}(t)) - q_i(\mathbf{x}(t)) \tag{4.5}$$

[3] 'Aggregate' here refers to the mean field approximation which is one way to derive SIS-type ODEs. Another way is the large population mean field *limit* of a stochastic process, where the connection to the corresponding ODE system is formed via the Kurtz's theorem [**?**]. In this case, linearity is induced by the uniform or homogeneous mixing assumption which is also a subject of criticism in epidemiology literature [12, 64, 68, 13].

for all $i \in \mathcal{N}$ and $t \geq 0$. In a matrix-vector form, this can be written as

$$\frac{d\mathbf{x}}{dt} = \bar{F}(\mathbf{x}) \triangleq \text{diag}(\mathbf{1} - \mathbf{x})F(\mathbf{x}) - Q(\mathbf{x}) \tag{4.6}$$

where $F(\mathbf{x}) = [f_i(\mathbf{x})] \in \mathbb{R}^N$, and $Q(\mathbf{x}) = [q_i(\mathbf{x})] \in \mathbb{R}^N$ are the vectors of non-linear infection and recovery rate functions, respectively. We assume that they are continuous and twice differentiable in $[0,1]^N$, with $\mathbf{J}_F(\mathbf{x})$ and $\mathbf{J}_Q(\mathbf{x})$ denoting the Jacobians of F and Q respectively, evaluated at any point $\mathbf{x} \in [0,1]^N$. We now make the following key assumptions:

(A1) $F(\mathbf{0}) = \mathbf{0}$ and $Q(\mathbf{0}) = \mathbf{0}$;

(A2) $[\mathbf{J}_F(\mathbf{x})]_{ij} = \frac{\partial f_i(\mathbf{x})}{\partial x_j} > 0$ for all $i \neq j$ with $a_{ij} > 0$, otherwise $[\mathbf{J}_F(\mathbf{x})]_{ij} = 0$;

(A3) $\left[\mathbf{J}_Q(\mathbf{x})\right]_{ii} = \frac{\partial q_i(\mathbf{x})}{\partial x_i} > 0$, and $\left[\mathbf{J}_Q(\mathbf{x})\right]_{ij} = \frac{\partial q_i(\mathbf{x})}{\partial x_j} \leq 0$ for all $i \neq j$, $\mathbf{x} \in [0,1]^N$. Moreover, $\sum_{j \neq i} \left[\mathbf{J}_Q(\mathbf{x})\right]_{ij} < \left[\mathbf{J}_Q(\mathbf{x})\right]_{ii}$;

(A4) $f_i(\mathbf{x})$ is concave in $[0,1]^N$, that is, $\frac{\partial^2 f_i}{\partial x_j \partial x_k} \leq 0$ for all $i, j, k \in \mathcal{N}$;

(A5) $q_i(\mathbf{x})$ is convex function of $x_i \in [0,1]^N$, and a concave function of x_j for all $j \neq i$. That is, $\frac{\partial^2 q_i}{\partial^2 x_i} \geq 0$ and $\frac{\partial^2 q_i}{\partial x_j \partial x_k} \leq 0$ for all $i \in \mathcal{N}$, and $j, k \in \mathcal{N} \setminus \{i\}$.

Assumption (A1) ensures that the virus-free state is a fixed point of (4.6), while (A2) is a proximity assumption that models infection spread only through edges of the underlying graph. Assumption (A3) concerns with the recovery rate, allowing it to be reduced by infected neighbors while still being no-negative. (A4) and (A5) assume concavity properties of the functions $f_i(\mathbf{x})$ and $q_i(\mathbf{x})$ in x_j for any neighbor j of i. This allows the effect of neighborhood infection x_j to *saturate*[4] as x_j increases. Assumption (A5) also assumes convexity of $q_i(\mathbf{x})$ in *local* infection x_i, which means that increase in recovery rate caused by x_i can be larger as x_i increases.

Examples for non-linear infection rates satisfying (A1)–(A5) include logarithmic functions $f_i(\mathbf{x}) = \sum_j a_{ij} \ln(1 + x_j)$, similar to those in [138]. Examples of non-linear recovery rates include polynomial functions such as $q_i(\mathbf{x}) = (1 + x_i)^k - 1$ for any $k \geq 1$. A special class of the permissible non-linear recovery rates, where the infection duration is dependent

[4] As x_j increases for any neighbor j of node i, the magnitude of the *resulting change* in both infection rate $f_i(\mathbf{x})$ and recovery rate $q_i(\mathbf{x})$ decreases. This is similar to the case of diminishing returns.

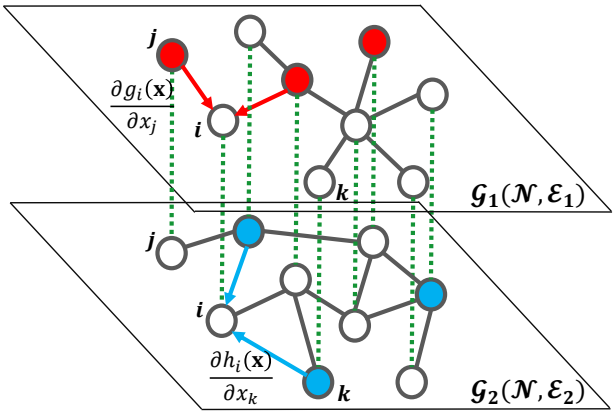

Figure 4.1 Bi-Virus epidemic spread across overlaid graphs sharing the same set of nodes. Red and Blue arrows denote the spread of Virus 1 and 2, respectively from infected nodes j and k (coloured Red and Blue) to the susceptible node i (uncoloured) with the instantaneous rates as shown. The infected Red and Blue nodes also recover with a total rate of $r_i(\mathbf{x})$ and $s_i(\mathbf{y})$ for any node $i \in \mathcal{N}$, respectively.

solely on local infection x_i, is related to processes that have *decreasing failure rates* (DFR)[5]. This special class of recovery processes that are DFR also includes the case of linear recovery rates. Note that our assumptions allow $f_i(\mathbf{x})$ and $q_i(\mathbf{x})$ to be *heterogeneous* across all nodes $i \in \mathcal{N}$, and the case with linear rates in (4.2) readily satisfies (A1)–(A5). This also extends to the linear bi-virus model (4.4) being a special case of the non-linear bi-virus model introduced in the next subsection, with infection and recovery rate functions therein satisfying the same assumptions (A1)–(A5).

4.2.2 Bi-Virus Model with Non-linear rates

The Bi-Virus model with non-linear infection and recovery rates is given by the following coupled system of ODEs:

$$\begin{aligned} \frac{d\,x_i}{d\,t} &= \bar{g}_i(\mathbf{x},\mathbf{y}) \triangleq \big(1-x_i-y_i\big)\,g_i(\mathbf{x}) - r_i(\mathbf{x}) \\ \frac{d\,y_i}{d\,t} &= \bar{h}_i(\mathbf{x},\mathbf{y}) \triangleq \big(1-x_i-y_i\big)\,h_i(\mathbf{y}) - s_i(\mathbf{y}) \end{aligned} \tag{4.7}$$

[5] *Failure rate* for a non-negative random variable is defined as the ratio between its probability density function (PDF) and its complimentary cumulative distribution function (CCDF). In the context of infection duration, *decreasing failure rate* means that nodes recover at a decreased rate the longer they stay continuously infected. A more detailed discussion regarding the connection to SIS recovery rates can be found in Appendix C.3.

for all $i \in \mathcal{N}$ and $t \geq 0$. In a matrix-vector form, (4.7) becomes:

$$\begin{aligned} \frac{d\mathbf{x}}{dt} &= \bar{G}(\mathbf{x},\mathbf{y}) \triangleq \operatorname{diag}(\mathbf{1}-\mathbf{x}-\mathbf{y})\, G(\mathbf{x}) - R(\mathbf{x}) \\ \frac{d\mathbf{y}}{dt} &= \bar{H}(\mathbf{x},\mathbf{y}) \triangleq \operatorname{diag}(\mathbf{1}-\mathbf{x}-\mathbf{y})\, H(\mathbf{y}) - S(\mathbf{y}), \end{aligned} \tag{4.8}$$

Where $G(\mathbf{x}) = [g_i(\mathbf{x})]$, $R(\mathbf{x}) = [r_i(\mathbf{x})]$, and $H(\mathbf{y}) = [h_i(\mathbf{y})]$, $S(\mathbf{y}) = [s_i(\mathbf{y})]$ are the non-linear infection and recovery rate functions for viruses 1 and 2, respectively. The pairs (G, R) and (H, S) each satisfy the assumptions (A1)–(A5); where G and H specifically satisfy (A2) with respect to their corresponding graphs with adjacency matrices $\mathbf{A}$ and $\mathbf{B}$, respectively. Figure 4.1 illustrates of how these competing epidemics spread over the corresponding overlaid graphs.

Assumptions (A1)–(A5) are also more general (weaker) than those assumed in [109, 138], where the recovery rates are restricted to being linear functions and are thus a special case of our model. We emphasize that while the set off assumptions for non-linear rates are mostly similar to (slightly more general than) those in literature, the characterization of all convergence scenarios for their respective bi-virus models is incomplete, as we shall discuss later in Section 4.5.

4.3 Monotone Dynamical Systems and the Single Virus Epidemic

In this section, we provide a succinct introduction to monotone dynamical systems (MDS) and some important definitions therein. We go on to show that the SIS model (4.6) is a monotone dynamical system (specifically a cooperative system) and briefly apply these MDS techniques to epidemic models by deriving the exact convergence result of the non-linear SIS model. We also observe that Theorem 4.1.1 is a special case for when the infection and recovery rates are linear.

4.3.1 Monotone Dynamical Systems - A Primer

A well known result from real analysis is that monotone sequences in compact (closed and bounded) subsets of $\mathbb{R}^n$ converge in $\mathbb{R}^n$ [140]. This simple, yet powerful result has been fully integrated with the theory of dynamical systems in a series of works [57, 58, 59, 61,

60, 116, 120, 121, 63, 118], which cumulatively form the theory of *monotone dynamical systems* (MDS). The foundations of MDS were laid down in [57, 58, 59, 61, 60] which study ordinary differential equations, specifically *cooperative* ODE systems. We here provide a brief, informal introduction to such ODE systems, with more details in Appendix C.4.

A central tool in the theory of MDS is the notion of *generalized cone-orderings*, which extends the concept of monotonicity in vector spaces.

Definition 4.3.1. *Given a convex cone $K \subset X$ for any vector space X, the cone-ordering $\leq_K$ ($<_K, \ll_K$) generated by K is an order relation that satisfies*

(i) $\mathbf{x} \leq_K \mathbf{y} \iff (\mathbf{y}-\mathbf{x}) \in K$;

(ii) $\mathbf{x} <_K \mathbf{y} \iff \mathbf{x} \leq_K \mathbf{y}$ *and* $\mathbf{x} \neq \mathbf{y}$; *and*

(iii) $\mathbf{x} \ll_K \mathbf{y} \iff (\mathbf{y}-\mathbf{x}) \in int(K)$, *for any* $\mathbf{x}, \mathbf{y} \in X$.

Note that, '$\ll_K$' implies '$<_K$' and is a stronger relation. Cone-orderings generated by the positive orthant $K = \mathbb{R}^n_+$ are simply denoted by $\leq$ ($<, \ll$), that is, without the 'K' notation.

Let $\phi_t(\mathbf{x})$ denote the solution of a dynamical system at some time $t > 0$ starting from an initial point $\phi_0(\mathbf{x}) = \mathbf{x} \in \mathbb{R}^n$.

Definition 4.3.2. *Given a cone-ordering $\leq_K$ ($<_K, \ll_K$), the dynamical system is said to be monotone if for every $\mathbf{x}, \mathbf{y} \in \mathbb{R}^n$ such that $\mathbf{x} \leq_K \mathbf{y}$, we have $\phi_t(\mathbf{x}) \leq_K \phi_t(\mathbf{y})$ for all $t > 0$. The system is called strongly monotone if for all $\mathbf{x}, \mathbf{y} \in \mathbb{R}^n$ such that $\mathbf{x} <_K \mathbf{y}$, we have $\phi_t(\mathbf{x}) \ll_K \phi_t(\mathbf{y})$ for all $t > 0$.*

The main result from MDS theory says that (almost) every solution trajectory of a *strongly monotone* system always converges to some equilibrium point of the system [58, 121, 63, 119]. If the system has only one stable fixed point, then this in itself is enough to prove global convergence. Monotonicity properties of a dynamical system can therefore be leveraged as an alternative to constructing Lyapunov functions, which is often intractable.

Consider the following autonomous ODE system

$$\dot{\mathbf{x}} = \bar{F}(\mathbf{x}), \tag{4.9}$$

where $\bar{F}(\mathbf{x}) = [\bar{f}_i(\mathbf{x})] \in \mathbb{R}^n$ is the vector field. If $\phi_t(\mathbf{x})$ is the solution of this ODE system, we say the system is *co-operative* if it is monotone. There are ways to find out whether an ODE

system is co-operative or not. In particular, one can answer this by observing the Jacobian of the vector field [117]. The so-called *Kamke condition* [118] says that (4.9) is co-operative with respect to the cone-ordering generated by the positive orthant $K = \mathbb{R}^n_+$ if and only if

$$\frac{\partial \bar{f}_i}{\partial x_i} \geq 0, \qquad \text{for all } i \neq j. \tag{4.10}$$

While it is not straightforward to obtain such a clean condition for any general convex cone K, one can still deduce the co-operative property of the ODE with respect to any one of the other orthants of $\mathbb{R}^n$ by observing the signed entries of the Jacobian. We will show how this is done for the bi-virus system (4.4) later in Section 4.4.1.

If the Jacobian of an ODE system is an irreducible matrix in a subset D of the state space, we say that the ODE system is *irreducible in* D (Definition C.4.2 in Appendix C.4). If the ODE system is co-operative in D as well as irreducible in D, then it is strongly monotone in D (Theorem C.4.4 in Appendix C.4). To prove convergence properties, we should ideally be able to show that our system is strongly monotone in the entirety of the state space it is contained in, for which we can directly apply the main MDS convergence result. However, this is often not the case, and one needs additional results from MDS literature to prove convergence. These details are deferred to Appendix C.4.

4.3.2 Monotonicity and convergence of SIS epidemic models

The following proposition establishes the monotonicity of the single-virus SIS model with non-linear infection and recovery rates with respect to the regular ordering relationship (cone-ordering generated by R^N_+).

Proposition 4.3.3. *The ODE system* (4.6) *is cooperative in* $[0,1]^N$ *and irreducible in* $(0,1)^N$ *with respect to the cone-ordering generated by the positive orthant* $\mathbb{R}^N_+$.

We now state the convergence criterion for the non-linear single-virus SIS model.

Theorem 4.3.4. *Let* $\mathbf{J}_F(\mathbf{x})$ *and* $\mathbf{J}_Q(\mathbf{x})$ *denote the Jacobian matrices of the vector valued infection and recovery rate functions* $F(\mathbf{x})$ *and* $Q(\mathbf{x})$ *from* (4.6)*, respectively. Then,*

(i) either $\lambda(\mathbf{J}_F(\mathbf{0}) - \mathbf{J}_Q(\mathbf{0})) \leq 0$*, and* $\mathbf{x}^* = 0$ *is the globally asymptotically stable fixed point of* (4.6)*;*

(ii) or $\lambda(\mathbf{J}_F(\mathbf{0})-\mathbf{J}_Q(\mathbf{0}))>0$*, and there exists a unique, strictly positive fixed point* $\mathbf{x}^*\gg 0$ *such that* $\mathbf{x}^*$ *is globally asymptotically stable in* $[0,1]^N\setminus\{\mathbf{0}\}$.

The proof for Theorem 4.3.4 utilizes a result from the monotone dynamical systems literature, provided as Theorem C.5.1 in Appendix C.5. It was originally proved and applied to linear SIS epidemics in [72] as an alternate proof of the convergence properties of the model for Gonorrhea spread in [74], which is a special case of our non-linear model (4.6). We can also see this in the following remark.

Remark 4.3.5. *For the single-virus SIS model with linear infection and recovery rates* (4.2)*, the conditions derived in Theorem 4.3.4 reduce to those in Theorem 4.1.1.*

Proof. By substituting $F(\mathbf{x})=\beta\mathbf{A}\mathbf{x}$ and $Q(\mathbf{x})=\delta\mathbf{x}$ in (C.7) (Jacobian of the single-virus system (4.6), mentioned in the proof of Theorem 4.3.4) and evaluating at $\mathbf{x}=\mathbf{0}$, we get $\mathbf{J}_{\bar{F}}(\mathbf{0})=\mathbf{J}_F(\mathbf{0})-\mathbf{J}_Q(\mathbf{0})=\beta\mathbf{A}-\delta\mathbf{I}$. The condition $\lambda(\mathbf{J}_F(\mathbf{0})-\mathbf{J}_Q(\mathbf{0}))=\lambda(\beta\mathbf{A}-\delta\mathbf{I})>0$ (≤ 0) can be rewritten as $\tau>1/\lambda(\mathbf{A})$ ($\leq 1/\lambda(\mathbf{A})$) where $\tau=\beta/\delta$, which as the same as in Theorem 4.1.1. □

While Theorem 4.3.4 can likely also be shown using the steps in [74], which were recreated again in [138], it requires first the application of two different Lyapunov functions and also requires proving the uniqueness of the positive fixed point. Using Theorem C.5.1 is a simpler way to derive the same results, and the details of the proof are deferred to Appendix C.5.

4.4 Main results for the nonlinear Bi-Virus model

We provide the necessary and sufficient results on the non-linear infection and recovery rates of the bi-virus system (4.8) for convergence to each of the three different kinds of equilibria: the virus-free, the single-virus equilibrium, and the co-existence equilibrium. However, before stating the main convergence results (proofs deferred to Appendix C.6), we establish the monotonicity of the non-linear bi-virus model.

4.4.1 Monotonicity of the Bi-Virus epidemic models

We first revisit the Kamke condition from Section 4.3.1, in this instance given for a the *southeast cone-ordering* as stated below.

Southeast cone-ordering and the Kamke condition

Consider the cone-ordering generated by the convex cone $K = \{\mathbb{R}^N_+ \times \mathbb{R}^N_-\} \subset \mathbb{R}^{2N}$. This cone is one of the orthants of $\mathbb{R}^{2N}$, and for $N = 1$, it would correspond to the *southeast* orthant of $\mathbb{R}^2$ $\left(K = \{\mathbb{R}_+ \times \mathbb{R}_-\} \subset \mathbb{R}^2\right)$. For any two points $(\mathbf{x}, \mathbf{y}), (\bar{\mathbf{x}}, \bar{\mathbf{y}}) \in \mathbb{R}^{2N}$, it satisfies the following:

(i) $(\mathbf{x}, \mathbf{y}) \leq_K (\bar{\mathbf{x}}, \bar{\mathbf{y}}) \iff x_i \leq \bar{x}_i$ and $y_i \geq \bar{y}_i$ for all $i \in \mathcal{N}$;

(ii) $(\mathbf{x}, \mathbf{y}) <_K (\bar{\mathbf{x}}, \bar{\mathbf{y}}) \iff (\mathbf{x}, \mathbf{y}) \leq_K (\bar{\mathbf{x}}, \bar{\mathbf{y}})$ and $(\mathbf{x}, \mathbf{y}) \neq (\bar{\mathbf{x}}, \bar{\mathbf{y}})$;

(iii) $(\mathbf{x}, \mathbf{y}) \ll_K (\bar{\mathbf{x}}, \bar{\mathbf{y}}) \iff x_i < \bar{x}_i$ and $y_i > \bar{y}_i$ for all $i \in \mathcal{N}$.

This type of cone-ordering is often referred to as the *southeast cone-ordering*, and the corresponding cone K is the *southeast orthant* of $\mathbb{R}^{2N}$. As shown in [117], the Kamke condition for determining whether an ODE system is cooperative or not with respect to the positive orthant $\mathbb{R}^{2N}_+$ can be generalised for cone-orderings generated by any orthant of $\mathbb{R}^{2N}$, including the southeast orthant. Once again, this is done by observing the Jacobian of the respective ODE system. Consider the $2N$ dimensional system given by

$$\dot{\mathbf{x}} = \bar{G}(\mathbf{x}, \mathbf{y}) \text{ and } \dot{\mathbf{y}} = \bar{H}(\mathbf{x}, \mathbf{y}),$$

where $\bar{G}(\mathbf{x}, \mathbf{y}) = [\bar{g}_i(\mathbf{x}, \mathbf{y})]$ and $\bar{H}(\mathbf{x}, \mathbf{y}) = [\bar{h}_i(\mathbf{x}, \mathbf{y})]$ are vector-valued functions in $\mathbb{R}^N$. The Kamke condition for this system with respect to the southeast cone-ordering [117] is

$$\frac{\partial \bar{g}_i}{\partial x_j} \geq 0, \ \frac{\partial \bar{h}_i}{\partial y_j} \geq 0, \ \forall i \neq j, \quad \text{and} \quad \frac{\partial \bar{g}_i}{\partial y_j} \leq 0, \ \frac{\partial \bar{h}_i}{\partial x_j} \leq 0, \ \forall i, j.$$

Roughly speaking, the Jacobian $\mathbf{J}_{\bar{G}\bar{H}}(\mathbf{x}, \mathbf{y})$ of the system, evaluated at all points in the state space, should be in the following block matrix form (where the signs are not strict):

$$\mathbf{J}_{\bar{G}\bar{H}} = \begin{bmatrix} * & + & + & - & - & - \\ + & * & + & - & - & - \\ + & + & * & - & - & - \\ - & - & - & * & + & + \\ - & - & - & + & * & + \\ - & - & - & + & + & * \end{bmatrix} \tag{4.11}$$

Note that the state space of the ODE system (4.4) is given by $D \triangleq \left\{(\mathbf{x}, \mathbf{y}) \in [0,1]^{2N} \mid \mathbf{x} + \mathbf{y} \leq \mathbf{1}\right\}$.

Proposition 4.4.1. *The ODE system* (4.8) *(the nonlinear bi-virus model) is cooperative in D with respect to the southeast cone-ordering. It is also irreducible in Int(D).*

Proof. For all $(\mathbf{x},\mathbf{y}) \in D$ and $i \neq j \in \mathcal{N}$, we have

$$\frac{\partial \bar{g}_i(\mathbf{x},\mathbf{y})}{\partial x_j} = (1-x_i-y_i)\frac{\partial g_i(\mathbf{x})}{\partial x_j} - \frac{\partial r_i(\mathbf{x})}{\partial x_j} \geq 0$$

and

$$\frac{\partial \bar{h}_i(\mathbf{x},\mathbf{y})}{\partial y_j} = (1-x_i-y_i)\frac{\partial h_i(\mathbf{y})}{\partial y_j} - \frac{\partial s_i(\mathbf{x})}{\partial y_j} \geq 0$$

since $\frac{\partial g_i(\mathbf{x})}{\partial x_j} \geq 0$, $\frac{\partial r_i(\mathbf{x})}{\partial x_j} \leq 0$ and $\frac{\partial h_i(\mathbf{y})}{\partial y_j} \geq 0$, $\frac{\partial s_i(\mathbf{y})}{\partial y_j} \leq 0$ from assumptions (A2) and (A3), and $(1-x_i-y_i) \geq 0$. Moreover for all $i \in \mathcal{N}$,

$$\frac{\partial \bar{g}_i}{\partial y_i} = -g_i(\mathbf{x}) \leq 0 \text{ and } \frac{\partial \bar{h}_i}{\partial x_i} = -h_i(\mathbf{y}) \leq 0,$$

with $\partial \bar{g}_i/\partial y_j = \partial \bar{h}_i/\partial x_j = 0$. Thus, the Kamke conditions are satisfied and the system is cooperative in D.

The Jacobian $\mathbf{J}_{\bar{G}\bar{H}}(\mathbf{x},\mathbf{y})$ of system (4.4) is written as

$$\mathbf{J}_{\bar{G}\bar{H}}(\mathbf{x},\mathbf{y}) = \begin{bmatrix} \mathbf{S}_{\mathbf{xy}}\mathbf{J}_G(\mathbf{x}) - \mathbf{D}_{G(\mathbf{x})} - \mathbf{J}_R(\mathbf{x}) & -\mathbf{D}_{G(\mathbf{x})} \\ -\mathbf{D}_{H(\mathbf{y})} & \mathbf{S}_{\mathbf{xy}}\mathbf{J}_H(\mathbf{y}) - \mathbf{D}_{H(\mathbf{y})} - \mathbf{J}_S(\mathbf{y}) \end{bmatrix}, \tag{4.12}$$

where $\mathbf{S}_{\mathbf{x},\mathbf{y}} \triangleq \text{diag}(\mathbf{1}-\mathbf{x}-\mathbf{y})$, $\mathbf{D}_{G(\mathbf{x})} \triangleq \text{diag}(G(\mathbf{x}))$ and $\mathbf{D}_{H(\mathbf{y})} \triangleq \text{diag}(H(\mathbf{y}))$. Since the infection rate functions satisfy assumption (A2) for their corresponding underlying graphs, $\mathbf{J}_G(\mathbf{x})$ and $\mathbf{J}_H(\mathbf{y})$ follow the sign structure of $\mathbf{A}$ and $\mathbf{B}$ respectively and are irreducible. The off-diagonal blocks of $\mathbf{J}_{\bar{G}\bar{H}}(\mathbf{x},\mathbf{y})$ are diagonal matrices with non-zero diagonal entries for $(\mathbf{x},\mathbf{y}) \in \text{Int}(D)$, and there does not exist a permutation matrix that would transform this into a block upper triangular matrix. Hence, by Definition C.4.2, the system is irreducible in Int(D), and this completes the proof. □

From Proposition 4.4.1, we deduce that the non-linear bi-virus system of ODEs (4.8) is co-operative in D, and thus strongly monotone in Int(D) in view of Theorem C.4.4 in Appendix C.4. This property also extends to the linear bi-virus system (4.4) which is a special case of (4.8).

4.4.2 Convergence and Coexistence properties of the Bi-Virus model

We are now ready to establish results on convergence properties of the bi-virus model and provide conditions for coexistence of two viruses in the non-linear bi-virus model as in (4.8).

Let $\mathbf{x}^*$ and $\mathbf{y}^*$ be the globally attractive fixed points of the single-virus SIS models that system (4.8) would reduce to when Virus 2 and 1, respectively, are not present over the network. These systems are given by

$$\dot{\mathbf{x}} = F^x(\mathbf{x}) \triangleq \bar{G}(\mathbf{x},\mathbf{0}) = \text{diag}(\mathbf{1}-\mathbf{x})G(\mathbf{x}) - R(\mathbf{x}), \tag{4.13}$$

$$\dot{\mathbf{y}} = F^y(\mathbf{y}) \triangleq \bar{H}(\mathbf{0},\mathbf{y}) = \text{diag}(\mathbf{1}-\mathbf{y})H(\mathbf{y}) - S(\mathbf{y}); \tag{4.14}$$

and by Theorem 4.3.4, $\mathbf{x}^* = \mathbf{0}$ ($\mathbf{y}^* = \mathbf{0}$) if $\lambda(\mathbf{J}_G(\mathbf{0}) - \mathbf{J}_R(\mathbf{0})) \leq 0$ (if $\lambda(\mathbf{J}_H(\mathbf{0}) - \mathbf{J}_S(\mathbf{0})) \leq 0$), and $\mathbf{x}^* \gg \mathbf{0}$ ($\mathbf{y}^* \gg \mathbf{0}$) otherwise.

We first state the result when the virus-free equilibrium is globally attractive. We prove this by presenting simple arguments which require only Theorem 4.3.4 for SIS model along with the monotonicity properties derived in the previous section, eliminating the need of a Lyapunov based approach.

Theorem 4.4.2 (Convergence to virus-free equilibria)**.** *If* $\lambda(\mathbf{J}_G(\mathbf{0}) - \mathbf{J}_R(\mathbf{0})) \leq 0$ *and* $\lambda(\mathbf{J}_H(\mathbf{0}) - \mathbf{J}_S(\mathbf{0})) \leq 0$*, trajectories of* (4.8) *starting from any point in* D *converge to* $(\mathbf{0},\mathbf{0})$.

We next characterize the conditions when the system globally converges to equilibria when only one of the viruses survives over the network. Let $\mathbf{S}_\mathbf{x} \triangleq \text{diag}(\mathbf{1}-\mathbf{x})$ and $\mathbf{S}_\mathbf{y} \triangleq \text{diag}(\mathbf{1}-\mathbf{y})$ for any $\mathbf{x},\mathbf{y} \in \mathbb{R}^N$. Also denote by $B_x \triangleq \{(\mathbf{x},\mathbf{y}) \in D \mid \mathbf{x} > \mathbf{0}\}$ the set of all points $(\mathbf{x},\mathbf{y}) \in D$ for which $x_i > 0$ for some $i \in \mathbb{N}$, and let $B_y \triangleq \{(\mathbf{x},\mathbf{y}) \in D \mid \mathbf{y} > \mathbf{0}\}$ be a similar set for the y_i entries.

Theorem 4.4.3 (Convergence to single-virus equilibria)**.** *When* $\lambda\big(\mathbf{S}_{\mathbf{y}^*}\mathbf{J}_G(\mathbf{0}) - \mathbf{J}_R(\mathbf{0})\big) > 0$ *and* $\lambda(\mathbf{S}_{\mathbf{x}^*}\mathbf{J}_H(\mathbf{0}) - \mathbf{J}_S(\mathbf{0})) \leq 0$, $(\mathbf{x}^*,\mathbf{0})$ *is globally attractive in* B_x,[6] *that is, every trajectory of system* (4.8) *starting from points in* B_x *converges to* $(\mathbf{x}^*,\mathbf{0})$.

Similarly, when $\lambda\big(\mathbf{S}_{\mathbf{y}^*}\mathbf{J}_G(\mathbf{0}) - \mathbf{J}_R(\mathbf{0})\big) \leq 0$ *and* $\lambda(\mathbf{S}_{\mathbf{x}^*}\mathbf{J}_H(\mathbf{0}) - \mathbf{J}_S(\mathbf{0})) > 0$, $(\mathbf{0},\mathbf{y}^*)$ *is globally attractive in* B_y.

[6] We consider B_x as the global domain of attraction instead of D because $\mathbf{x} = 0$ for all points in the set $D \setminus B_x$. Starting from such points the system is no longer a bi-virus epidemic, but a single-virus SIS system for Virus 2.

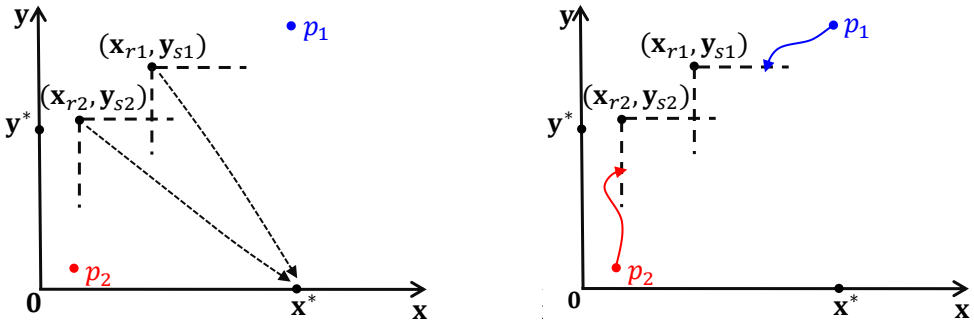

(a) For every point p_k, there is a point $(\mathbf{x}_{rk}, \mathbf{y}_{sk})$ starting from which, trajectories converge monotonically $(\leq_K)$ to $(\mathbf{x}^*, 0)$.

(b) Trajectories starting from p_k eventually bounded by $(\mathbf{x}_{rk}, \mathbf{y}_{sk})$; monotonicity of the system gives convergence to $(\mathbf{x}^*, 0)$.

Figure 4.2 Illustration of the convergence to $(\mathbf{x}^*, 0)$

Sketch of the proof (convergence to $(\mathbf{x}^*, \mathbf{0})$*).* The idea behind the proof is illustrated in Figure 4.2. For every $(\mathbf{x}, \mathbf{y}) \in B_x$ (for example p_1 and p_2 in Figure 4.2), we construct a point $(\mathbf{x}_r, \mathbf{y}_s)$ which eventually bounds the trajectory starting from $(\mathbf{x}, \mathbf{y})$; that is, we have $(\mathbf{x}_r, \mathbf{y}_s) \ll_K \phi_{t_1}(\mathbf{x}, \mathbf{y}) \leq_K (\mathbf{x}^*, \mathbf{0})$[7] for some $t_1 \geq 0$. From the monotonicity shown in Proposition 4.4.1, we have $\phi_t(\mathbf{x}_r, \mathbf{y}_s) \ll_K \phi_{t+t_1}(\mathbf{x}, \mathbf{y}) \leq_K (\mathbf{x}^*, \mathbf{0})$ for all time $t \geq 0$. We prove that the trajectory starting from $(\mathbf{x}_r, \mathbf{y}_s)$ converges to $(\mathbf{x}^*, 0)$ monotonically, with respect to the southeast cone-ordering (Figure 4.2(a)). Using this, we show the convergence of trajectories starting from $(\mathbf{x}, \mathbf{y})$ via a sandwich argument (Figure 4.2(b)). See Appendix C.6 for detailed proof. □

Finally, we give the necessary and sufficient conditions that guarantee the co-existence of the two viruses in the long run. Let E denote the set of all fixed points of the system in (4.8).

Theorem 4.4.4 (Convergence to coexistence equilibria)**.** *Suppose that* $\lambda\left(\mathbf{S}_{\mathbf{y}^*}\mathbf{J}_G(\mathbf{0}) - \mathbf{J}_R(\mathbf{0})\right) > 0$ *and* $\lambda(\mathbf{S}_{\mathbf{x}^*}\mathbf{J}_H(\mathbf{0}) - \mathbf{J}_S(\mathbf{0})) > 0$*, then there exist fixed points of system* (4.8) $(\hat{\mathbf{x}}, \hat{\mathbf{y}}) \gg (\mathbf{0}, \mathbf{0})$ *and* $(\bar{\mathbf{x}}, \bar{\mathbf{y}}) \gg (\mathbf{0}, \mathbf{0})$ *such that*

$$(\mathbf{0}, \mathbf{y}^*) \ll_K (\hat{\mathbf{x}}, \hat{\mathbf{y}}) \leq_K (\bar{\mathbf{x}}, \bar{\mathbf{y}}) \ll_K (\mathbf{x}^*, \mathbf{0}),$$

with the possibility that $(\hat{\mathbf{x}}, \hat{\mathbf{y}}) = (\bar{\mathbf{x}}, \bar{\mathbf{y}})$*. All trajectories of system* (4.8) *starting from* $B_x \cap B_y$ *converge to the set of coexistence fixed points* $S \triangleq \left\{(\mathbf{x}_e, \mathbf{y}_e) \in E \mid (\hat{\mathbf{x}}, \hat{\mathbf{y}}) \leq_K (\mathbf{x}_e, \mathbf{y}_e) \leq_K (\bar{\mathbf{x}}, \bar{\mathbf{y}})\right\}$.

[7] $\phi_t(\mathbf{x}, \mathbf{y})$ denotes the solution of (4.4) at $t \geq 0$, with initial point $(\mathbf{x}, \mathbf{y})$.

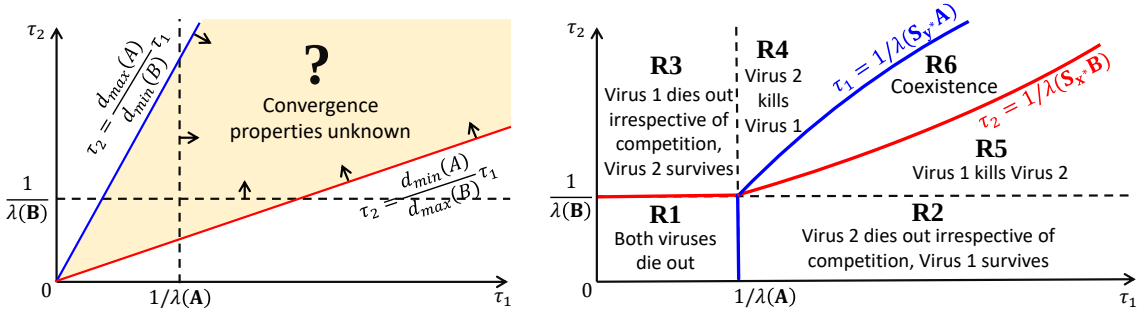

(a) Limitations of the literature.

(b) Complete characterization of the convergence trichotomy.

Figure 4.3 Characterization of the parameter space

The proof of Theorem 4.4.4 follows similar arguments to that of the previous theorem, and is the first convergence result for coexistence fixed points in the competing SIS literature. Note that while we have convergence to 'a' coexistence equilibrium, it may or may not be unique in the state space. The global convergence is therefore to the set of possible coexistence equilibria, and not necessarily a singular point. Thus, via Theorems 4.4.2, 4.4.3 and 4.4.4 we cover all possible convergence scenarios of the bi-virus SIS system (4.8), and successfully establish the complete theoretical characterization for the trichotomy of possible outcomes.

4.5 Linear Infection and Recovery rates - Discussion and Comparison to Literature

In this section, we provide corollaries of Theorems 4.4.2, 4.4.3 and 4.4.4 which characterize convergence to the trichotomy of possible outcomes for the special case of linear infection and recovery rates. These results, along with Figure 4.3, are reproduced here as they originally were in our previous work [41] which focused only on characterizing the convergence properties in the case of linear infection and recovery rates. We do this for the sake of completeness, and also with the intention to better explain our contribution, using visual aids in the form of Figure 4.3, helping us compare our work with existing literature more effectively.

Consider the linear bi-virus system (4.4). By setting $G(\mathbf{x}) = \beta_1 \mathbf{A}\mathbf{x}$, $R(\mathbf{x}) = \delta_1 \mathbf{x}$ and $H(\mathbf{y}) =$

$\beta_2\mathbf{By}$, $S(\mathbf{y})=\delta_2\mathbf{y}$, we get

$$\mathbf{J}_G(\mathbf{0})=\beta_1\mathbf{A},\ \ \mathbf{J}_R(\mathbf{0})=\delta_1\mathbf{I},$$

and

$$\mathbf{J}_H(\mathbf{0})=\beta_2\mathbf{B},\ \ \mathbf{J}_S(\mathbf{0})=\delta_2\mathbf{I}.$$

Defining $\tau_1 \triangleq \beta_1/\delta_1$, $\tau_2=\triangle\beta_2/\delta_2$, and plugging in the above expressions for the Jacobians in Theorems 4.4.2 and 4.4.3, we have the following Corollaries.

Corollary 4.5.1. *If* $\tau_1\lambda(\mathbf{A})\leq 1$ *and* $\tau_2\lambda(\mathbf{B})\leq 1$, *trajectories of* (4.4) *starting from any point in* D *converge to* $(\mathbf{0},\mathbf{0})$.

Corollary 4.5.2. *When* $\tau_1\lambda(\mathbf{S}_{\mathbf{y}^*}\mathbf{A})>1$ *and* $\tau_2\lambda(\mathbf{S}_{\mathbf{x}^*}\mathbf{B})\leq 1$, $(\mathbf{x}^*,\mathbf{0})$ *is globally attractive in* B_x;[8] *that is, every trajectory of system* (4.4) *starting from points in* B_x *converges to* $(\mathbf{x}^*,\mathbf{0})$.

Similarly, when $\tau_1\lambda(\mathbf{S}_{\mathbf{y}^*}\mathbf{A})\leq 1$ *and* $\tau_2\lambda(\mathbf{S}_{\mathbf{x}^*}\mathbf{B})>1$, $(\mathbf{0},\mathbf{y}^*)$ *is globally attractive in* B_y.

From Corollary 4.5.2, we can deduce that the threshold values for τ_1 and τ_2 below which each of the viruses will die out are given by the equations $\tau_1=1/\lambda(\mathbf{S}_{\mathbf{y}^*}\mathbf{A})$ and $\tau_2=1/\lambda(\mathbf{S}_{\mathbf{x}^*}\mathbf{B})$, respectively. Figure 4.3(b) plots these threshold values for Virus 1 (in blue) and Virus 2 (in red) for varying values of τ_1 and τ_2, and partitions the entire parameter space into regions R1 – R6 as shown. When $\tau_1>1/\lambda(\mathbf{A})$ and $\tau_2>1/\lambda(\mathbf{B})$, for which values of τ_1,τ_2 do not lie in regions R1, R2 or R3, the blue curve lies above the red curve as in Figure 4.3(b). This was originally shown in [108] by deducing that the ratio of slopes of the red and blue curves at point $(\tau_1,\tau_2)=(1/\lambda(\mathbf{A}),1/\lambda(\mathbf{B}))$ is less than one. This means there exist combinations of τ_1,τ_2 for which τ_1 lies to the right of the blue curve ($\tau_1\lambda(\mathbf{S}_{\mathbf{y}^*}\mathbf{A})>1$), and τ_2 lies above the red curve ($\tau_2\lambda(\mathbf{S}_{\mathbf{x}^*}\mathbf{B})>1$).[9] This corresponds to region R6 in Figure 4.3(b), and our final corollary (derived from Theorem 4.4.4) shows that for values of τ_1,τ_2 which lie in R6, we observe convergence to coexistence equilibria.

Corollary 4.5.3 (Convergence to coexistence equilibria)**.** *If* $\tau_1\lambda(\mathbf{S}_{\mathbf{y}^*}\mathbf{A})>1$ *and* $\tau_2\lambda(\mathbf{S}_{\mathbf{x}^*}\mathbf{B})>1$, *there exist fixed points of system* (4.4) $(\hat{\mathbf{x}},\hat{\mathbf{y}})\gg(\mathbf{0},\mathbf{0})$ *and* $(\bar{\mathbf{x}},\bar{\mathbf{y}})\gg(\mathbf{0},\mathbf{0})$ *such that*

$$(\mathbf{0},\mathbf{y}^*)\ll_K(\hat{\mathbf{x}},\hat{\mathbf{y}})\leq_K(\bar{\mathbf{x}},\bar{\mathbf{y}})\ll_K(\mathbf{x}^*,\mathbf{0}),$$

[8] We consider B_x as the global domain of attraction instead of D because $\mathbf{x}=0$ for all points in the set $D\setminus B_x$. Starting from such points the system is no longer a bi-virus epidemic, but a single-virus SIS system for Virus 2.

[9] Note that $\tau_1\lambda(\mathbf{S}_{\mathbf{y}^*}\mathbf{A})\leq 1$ and $\tau_2\lambda(\mathbf{S}_{\mathbf{x}^*}\mathbf{B})\leq 1$ is only possible in region R1, since it is the only region where τ_1 can lie to the left of the blue curve, and τ_2 can lie below the red curve. This effectively reduces the expressions to $\tau_1\lambda(\mathbf{A})\leq 1$ and $\tau_2\lambda(\mathbf{B})\leq 1$, the conditions for convergence to the virus-free equilibrium as in Corollary 4.5.1.

with the possibility that $(\hat{\mathbf{x}}, \hat{\mathbf{y}}) = (\bar{\mathbf{x}}, \bar{\mathbf{y}})$. *All trajectories of system* (4.4) *starting from* $B_x \cap B_y$ *converge to the set of coexistence fixed points* $S \triangleq \left\{(\mathbf{x}_e, \mathbf{y}_e) \in E \mid (\hat{\mathbf{x}}, \hat{\mathbf{y}}) \leq_K (\mathbf{x}_e, \mathbf{y}_e) \leq_K (\bar{\mathbf{x}}, \bar{\mathbf{y}})\right\}$.

Comparison to existing literature

Now that we have established all our results, we briefly compare our work with results from [138, 109], which also talk about global convergence to single-virus equilibria. To this end, we illustrate the limitations of the existing conditions for global convergence in [138, 109] in Figure 4.3(a); and use Figure 4.3(b), where we provide complete characterization of the parameter space, to draw comparisons with our results.

When translated to the setting of linear infection and recovery rates, the result from [109] says that when $\tau_1 d_{min}(\mathbf{A}) > \tau_2 d_{max}(\mathbf{B})$, the Virus 2 is sure to die out (Virus 1 could persist or die out), and similarly when $\tau_1 d_{max}(\mathbf{A}) < \tau_2 d_{min}(\mathbf{B})$, the Virus 1 is sure to die out. We illustrate these conditions in Figure 4.3(a), where Virus 1 (Virus 2) is sure to die out if parameters (τ_1, τ_2) lie above (below) the blue (red) line. Therefore, the entire yellow-shaded region in Figure 4.3(a), between the blue and red lines, is left uncharacterized in [109]. When $\mathbf{A}$ and $\mathbf{B}$ are regular graphs with the same degree ($d_{min} = d_{max} = d$), the blue and red lines coincide, making coexistence infeasible. This is also mentioned in [108] where they show that for regular graphs with same degree, the system behaves as if the two graphs were the same - rendering coexistence impossible (which is also in line with results in [104]). In contrast, the maximum degree of graphs can also be much larger than the minimum degree (e.g., power law graphs), causing the yellow-shaded space to become very large, possibly spanning almost the entire parameter space.

The main result in [138], when similarly translated to our setting as above, says that when $\tau_1 \lambda(\mathbf{A}) > 1$ and $\tau_2 \lambda(\mathbf{B}) \leq 1$, Virus 1 survives and Virus 2 dies out. Similarly, when $\tau_2 \lambda(\mathbf{B}) > 1$ and $\tau_1 \lambda(\mathbf{A}) \leq 1$, Virus 2 survives and Virus 1 dies out. These correspond to regions R2 and R3 in Figure 4.3(b). However, their results do not cover the convergence properties for τ_1, τ_2 which lie in regions R4 – R6. Our Theorems 4.4.3 and 4.4.4, through their corresponding corollaries, do account for these values of τ_1, τ_2, and show convergence to $(\mathbf{0}, \mathbf{y}^*)$, $(\mathbf{x}^*, \mathbf{0})$ or to a coexistence fixed point whenever they lie in regions R4, R5, or R6, respectively.

In summary, without our Theorems 4.4.3 and 4.4.4, results from literature fail to characterize a sizeable portion of the parameter space as shown in Figure 4.3(a) by the '**?**' region (part of the shaded region surrounded by the arrows). The parameters leading to coexistence are entirely contained in this region as well - explaining the dearth of convergence

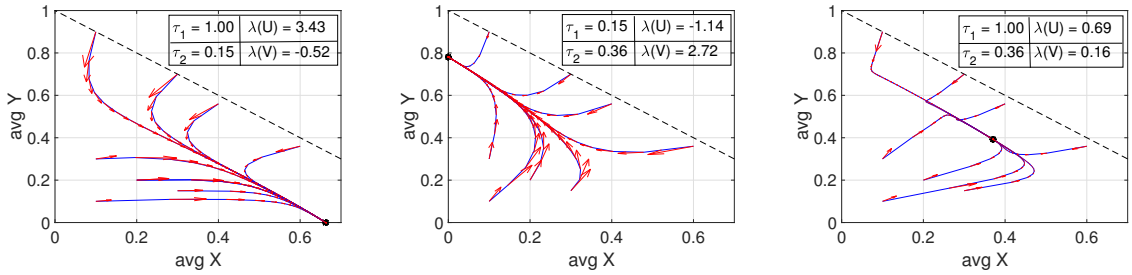

(a) $\lambda(U)>0$, $\lambda(V)<0$; Virus 1 survives

(b) $\lambda(U)<0$, $\lambda(V)>0$; Virus 2 survives

(c) $\lambda(U)>0$, $\lambda(V)>0$; Both coexist

Figure 4.4 Phase plots for a system with linear infection and recovery rates (CASE 1) on the AS-733 graph.

results for such equilibria in the existing literature.

4.6 Numerical Results

In this section, we present simulation results to support our theoretical findings for the bi-virus SIS model for combinations of non-linear as well as linear infection and recovery rates. To this end, we consider an undirected, connected graph (103 nodes, 239 edges), called Autonomous System (AS-733), from the SNAP repository [79]. For both the linear and non-linear bi-virus model, we generate an additional graph, overlaid on the same set of nodes, by modifying the original graph (AS-733-A with $\lambda(\mathbf{A})$=12.16), removing and adding edges while ensuring connectivity between the nodes. The new additional graph, AS-733-B, has 741 edges with $\lambda(\mathbf{B})$=15.53. Note that since our theoretical results hold for any general graphs, we only use this set as example graphs to numerically demonstrate the convergence properties. Similar numerical results can indeed be obtained for any other networks (such as social networks).

We test the convergence dynamics of the bi-virus model over a range of combinations of linear and non-linear infection and recovery rates. To this end, we consider three different bi-virus models, and Table 4.1 summarizes the three cases with the corresponding infection and recovery rate functions as shown. Note that for non-linear infection and recovery rates, we consider the logarithmic and polynomial functions briefly mentioned in Section 4.2, to ensure that our three cases satisfy assumptions (A1)–(A5).

For each of the three cases, we construct combinations of parameters (τ_1 or τ_2 for linear

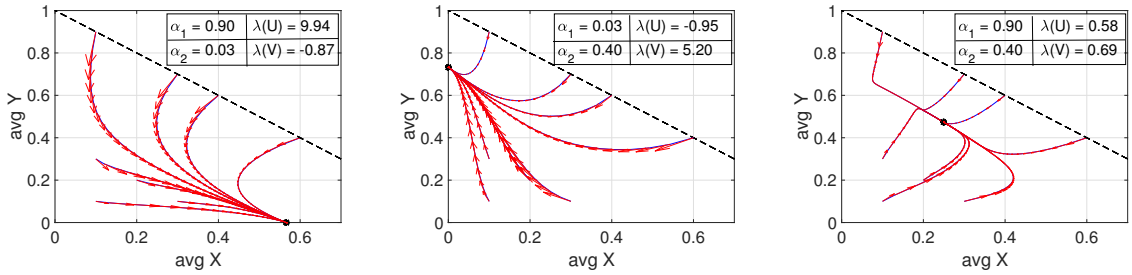

(a) $\lambda(U)>0$, $\lambda(V)<0$; Virus 1 survives

(b) $\lambda(U)<0$, $\lambda(V)>0$; Virus 2 survives

(c) $\lambda(U)>0$, $\lambda(V)>0$; Both coexist

Figure 4.5 Phase plots for a system with non-linear infection and linear recovery rates (CASE 2) on the AS-733 graph.

rates, and α_1 or α_2 for non-linear rates), to develop three convergence scenarios, that satisfy the assumptions of Theorems 4.4.3 and 4.4.4. These three scenarios correspond to global convergence of the bi-virus system to fixed points where (a) Virus 1 is the surviving epidemic (which spreads on graph AS-733-A), (b) Virus 2 is the surviving epidemic (which spreads on graph AS-733-B), (c) both viruses coexist, (where Virus 1 spreads on graph AS-733-A and Virus 2 on AS-733-B). Parameters corresponding to these three scenarios are provided in the table inset in Figures 4.4–4.6(a)–(c) corresponding to the three cases.

To visualize our system in two dimensions, we use $avgX \triangleq (1/N)\sum_{i\in\mathcal{N}} x_i$ on the x-axis, and $avgY \triangleq (1/N)\sum_{i\in\mathcal{N}} y_i$ on the y-axis. We plot trajectories of the bi-virus system starting from different initial points in the state space D to observe their convergence, with red arrows representing the trajectories' direction of movement at various time intervals. Here, the state space D is the region that lies below the dotted-line (for example, in Figure 4.4), ensuring $x_i + y_i \leq 1$ for all $i \in \mathcal{N}$, for every initial point. To ensure that the convergences observed in our phase plots match the conditions laid out in Theorems 4.4.3 and 4.4.4, we track the eigenvalues $\lambda(\mathbf{U}) \triangleq \lambda(\mathbf{S}_{\mathbf{y}^*}\mathbf{J}_G(0) - \mathbf{J}_R(0))$ and $\lambda(\mathbf{V}) \triangleq \lambda(\mathbf{S}_{\mathbf{x}^*}\mathbf{J}_H(0) - \mathbf{J}_S(0))$. $\lambda(\mathbf{U})$ ($\lambda(\mathbf{V})$) being positive or negative corresponds to Virus 1 (Virus 2) surviving or dying out, respectively.

Table 4.1 Summary of infection and recovery rate functions chosen

	$g_i(\mathbf{x})$	$h_i(\mathbf{y})$	$r_i(\mathbf{x})$	$s_i(\mathbf{y})$
CASE 1	$\sum_j a_{ij}x_j$	$\sum_j b_{ij}y_j$	$\delta_1 x_i$	$\delta_2 y_i$
CASE 2	$\sum_j a_{ij}\ln(1+\alpha_1 x_j)$	$\sum_j b_{ij}\ln(1+\alpha_2 y_j)$	$\delta_1 x_i$	$\delta_2 y_i$
CASE 3	$\sum_j a_{ij}\ln(1+\alpha_1 x_j)$	$\sum_j b_{ij}\ln(1+\alpha_2 y_j)$	$(1+x_i)^2-1$	$(1+y_i)^2-1$

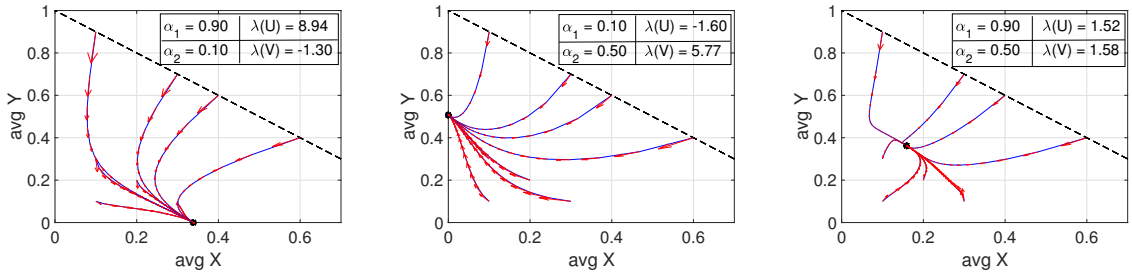

(a) $\lambda(U) > 0$, $\lambda(V) < 0$; Virus 1 survives

(b) $\lambda(U) < 0$, $\lambda(V) > 0$; Virus 2 survives

(c) $\lambda(U) > 0$, $\lambda(V) > 0$; Both coexist

Figure 4.6 Phase plots for a system with non-linear infection and recovery rates (CASE 3) on the AS-733 graph.

In Figures 4.4–4.6(a)–(c), we show numerical results for the three cases, respectively. Figures 4.4–4.6(a) and 4.4–4.6(b) show convergence to the two different single-virus equilibria, where the parameters therein satisfy the two set of conditions as in Theorem 4.4.3. Figures 4.4–4.6(c) show convergence to the coexistence equilibria, which also satisfies the coexistence conditions as outlined in Theorem 4.4.4. We observe a unique coexistence equilibrium when the viruses are competing over graphs AS-733-A and AS-733-B, for which the eigenvalues $\lambda(\mathbf{A})$ and $\lambda(\mathbf{B})$ are significantly different. Interestingly, we also observe multiple coexistence equilibria as shown in Figure 4.7. We obtain this result by creating another additional graph by modifying the original graph AS-733-A such that the eigenvalue of this

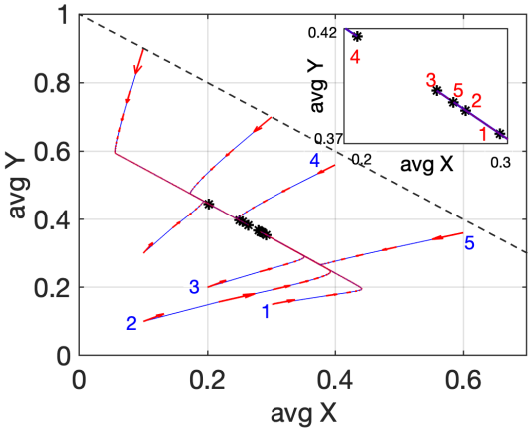

Figure 4.7 Coexistence condition with Multiple equilibrium points

new graph is as close to the original one where this new graph AS-733-C has 259 edges with $\lambda(\mathbf{C})$=12.26. The 'upper left' and 'lower right' coexistence fixed points characterize the set S of all such equilibria, as in Theorem 4.4.4. This can be seen more closely in the inset in Figure 4.7, where the number beside each fixed point (in red) corresponds to the different initial starting points (in blue) of the trajectories. Thus, convergence to set S occurs globally over the state space, but exactly which coexistence fixed point the system converges to is dependent on the initial point. We are thus able to observe all possible convergence scenarios from Section 4.4.2, including multiple coexistence equilibria.

4.7 Conclusion

By utilizing the techniques from Monotone Dynamical Systems (MDS), in this chapter, we show that a generic bi-virus epidemic model with nonlinear infection and recovery rates is monotone with respect to a specially constructed partial ordering. This monotonicity allows us to give necessary and sufficient conditions on the non-linear infection and recovery rates, and thus completely characterize the entire parameter space of the bi-virus system, a contrast to the usual Lyapunov based approach. We bridge the gap between linear stability properties and global convergence results (or lack thereof) for the bi-virus model with nonlinear rates (including the special case with linear rates) in the literature, and succeed in providing a complete characterization of the trichotomy of possible outcomes for such competing epidemics - a well known open problem. Our results demonstrate how powerful these alternative proving techniques can be, compared to classical Lyapunov approaches; and we note that it may be worth exploring such monotonicity properties in other dynamics on graphs as well, where competition is a general theme.

Chapter 5

Bi-SIS Epidemics on Graphs - Quantitative Analysis of Coexistence Equilibria

The chapter is organized as follows. In Section 5.1, we give succinct overview on bi-SIS model with a summary of existing convergence results. Section 5.2 contains our main results of the chapter, with the proofs deferred to the Appendices. We then provide brief numerical results in Section 5.3, followed by the conclusion.

5.1 Bi-SIS Epidemic Model - A Primer

5.1.1 Basic Notations

We use lower case, bold-faced letters to denote column vectors $\mathbf{v} \in \mathbb{R}^N$, and upper case, bold-faced letters to denote square matrices $\mathbf{M} \in \mathbb{R}^{N\times N}$. We denote by $\lambda(\mathbf{M})$ the spectral radius of a non-negative matrix $\mathbf{M}$. We use diag($\mathbf{v}$) to denote the $N \times N$ diagonal matrix with entries of vector $\mathbf{v} \in \mathbb{R}^N$ on the main diagonal, and $\mathbf{1}/\mathbf{0}$ for all one/zero vectors with appropriate dimensions. We write $[\mathbf{x}]_i$ or normal letter x_i with index i to represent the i-th entry of vector $\mathbf{x}$. For vectors, $\mathbf{x} \leq \mathbf{y}$ means $x_i \leq y_i$ for all i; $\mathbf{x} < \mathbf{y}$ if $\mathbf{x} \leq \mathbf{y}$ and $\mathbf{x} \neq \mathbf{y}$; $\mathbf{x} \ll \mathbf{y}$ if $x_i < y_i$ for all i. Let $\mathcal{G}(\mathcal{N}, \mathcal{E})$ denote a general, undirected and connected graph with its adjacency matrix $\mathbf{A} = [a_{ij}]$, where $a_{ij} = \mathbb{1}_{(i,j)\in\mathcal{E}}$ for any $i, j \in \mathcal{N}$.

5.1.2 The Bi-SIS Model

We consider the spread of Virus 1 and 2 on overlaid graphs $\mathcal{G}_1(\mathcal{N},\mathcal{E}_1)$ and $\mathcal{G}_2(\mathcal{N},\mathcal{E}_2)$ respectively, sharing the same set of nodes $\mathcal{N}$, but different edge sets $\mathcal{E}_1$ and $\mathcal{E}_2$ through which the respective epidemics propagate.[1] At any given time, a node $i\in\mathcal{N}$ is either *susceptible*, or is *infected by either Virus 1 or Virus 2*. If infected by Virus 1, the node infects one of its susceptible neighbors with rate $\beta_1>0$, where neighbors are determined with respect to the edge set $\mathcal{E}_1$ of the graph $\mathcal{G}_1(\mathcal{N},\mathcal{E}_1)$. Virus 2 is transmitted similarly with rate $\beta_2>0$ through the edge set $\mathcal{E}_2$. Also, infected nodes recover with rates $\delta_1,\delta_2>0$ depending on whether they are infected by Virus 1 or 2 respectively. We call $\tau_1\triangleq\beta_1/\delta_1$ and $\tau_2\triangleq\beta_2/\delta_2$ as the effective infection rates of two corresponding viruses. The system dynamics are described by the following set of ordinary differential equations (ODEs):

$$\begin{aligned}\dot{x}_i(t)&=\beta_1(1-x_i(t)-y_i(t))\sum_{j\in\mathcal{N}}a_{ij}x_j(t)-\delta_1x_i(t),\\ \dot{y}_i(t)&=\beta_2(1-x_i(t)-y_i(t))\sum_{j\in\mathcal{N}}b_{ij}y_j(t)-\delta_2y_i(t)\end{aligned}\tag{5.1}$$

for all $i\in\mathcal{N}$, where $x_i(t),y_i(t)\in[0,1]$ are the probabilities that node $i\in\mathcal{N}$ is infected by Virus 1 or 2 respectively at any time $t\geq 0$. Note that $x_i(t)+y_i(t)\in[0,1]$ at all time. In a matrix-vector form, (5.1) can be written as

$$\begin{aligned}\dot{\mathbf{x}}&=\beta_1\mathrm{diag}(\mathbf{1}-\mathbf{x}-\mathbf{y})\mathbf{A}\mathbf{x}-\delta_1\mathbf{x},\\ \dot{\mathbf{y}}&=\beta_2\mathrm{diag}(\mathbf{1}-\mathbf{x}-\mathbf{y})\mathbf{B}\mathbf{y}-\delta_2\mathbf{y},\end{aligned}\tag{5.2}$$

where $\mathbf{A}=[a_{ij}]$ and $\mathbf{B}=[b_{ij}]$ are the adjacency matrices of the overlaid graphs $\mathcal{G}_1(\mathcal{N},\mathcal{E}_1)$ and $\mathcal{G}_2(\mathcal{N},\mathcal{E}_2)$, respectively. We denote by $E\subset[0,1]^{2N}$ the set of all possible equilibria of system (5.2), which trivially contains $(\mathbf{0},\mathbf{0})$.

The *single-SIS* dynamics for Virus 1 can be obtained by setting $\mathbf{y}=0$ in (5.2), and is given by

$$\dot{\mathbf{x}}=\beta_1\mathrm{diag}(\mathbf{1}-\mathbf{x})\mathbf{A}\mathbf{x}-\delta_1\mathbf{x}.\tag{5.3}$$

When $\tau_1>\tau_1^*=1/\lambda(\mathbf{A})$, this system converges to a positive equilibrium $\mathbf{x}^*\gg\mathbf{0}$, otherwise the system converges to $\mathbf{0}$ [74]. Similarly, single-SIS model for Virus 2 can be obtained

[1] Using overlaid graphs with different edge sets $\mathcal{E}_1$ and $\mathcal{E}_2$ model the different media through which epidemics, opinions, malware and other such phenomena propagate.

by substituting $(\beta_2, \delta_2, \mathbf{B})$ for $(\beta_1, \delta_1, \mathbf{A})$ in (5.3), with its positive equilibrium $\mathbf{y}^* \gg \mathbf{0}$ when $\tau_2 > \tau_2^* = 1/\lambda(\mathbf{B})$.

A preliminary result for bi-SIS epidemics [138] is that any virus which fails to satisfy its respective single-SIS survival threshold will die out in the long run; that is, Virus 1 (Virus 2) will die out irrespective of the presence of its competing virus if $\tau_1 \leq 1/\lambda(\mathbf{A})$ ($\tau_2 \leq 1/\lambda(\mathbf{B})$). If, at any given time $s \geq 0$, a trajectory of (5.2) enters the sets $[0,1]^N \times \{\mathbf{0}\}$ (Virus 2 dies out) or $\{\mathbf{0}\} \times [0,1]^N$ (Virus 1 dies out), it remains in that set for all times $t > s$, and the bi-SIS model effectively reduces to a single-SIS model corresponding to the surviving virus, whose long run behaviour is governed by the single-virus convergence criterion as outlined earlier.

The non-trivial case arises when both $\tau_1 > 1/\lambda(\mathbf{A})$ and $\tau_2 > 1/\lambda(\mathbf{B})$, for which the techniques used to derive the single-SIS convergence criterion no longer apply. Specifically, both positive equilibria of the related single-virus systems $\mathbf{x}^*, \mathbf{y}^* \gg \mathbf{0}$ may exist, and it is only under this scenario when the system can possibly converge to one of (finitely) many *coexistence equilibria* of the kind $(\hat{\mathbf{x}}, \hat{\mathbf{y}}) \gg (\mathbf{0}, \mathbf{0})$. The complete convergence criterion derived in [41] does include the case when $\tau_1 > 1/\lambda(\mathbf{A})$ and $\tau_2 > 1/\lambda(\mathbf{B})$, and gives the following additional conditions on τ_1, τ_2 and the respective outcomes:

(C1) If $\tau_1 \lambda(\text{diag}(\mathbf{1} - \mathbf{y}^*)\mathbf{A}) > 1$ and $\tau_2 \lambda(\text{diag}(\mathbf{1} - \mathbf{x}^*)\mathbf{B}) \leq 1$, the bi-SIS system (5.2) converges to $(\mathbf{x}^*, \mathbf{0})$;

(C2) If $\tau_1 \lambda(\text{diag}(\mathbf{1} - \mathbf{y}^*)\mathbf{A}) \leq 1$ and $\tau_2 \lambda(\text{diag}(\mathbf{1} - \mathbf{x}^*)\mathbf{B}) > 1$, the bi-SIS system (5.2) converges to $(\mathbf{0}, \mathbf{y}^*)$;

(C3) If $\tau_1 \lambda(\text{diag}(\mathbf{1} - \mathbf{y}^*)\mathbf{A}) > 1$ and $\tau_2 \lambda(\text{diag}(\mathbf{1} - \mathbf{x}^*)\mathbf{B}) > 1$, the bi-SIS system (5.2) converges to one CE fixed point $(\hat{\mathbf{x}}, \hat{\mathbf{y}}) \gg (\mathbf{0}, \mathbf{0})$ in the equilibria set E;

Since our focus is quantitative characterization of CE fixed points, in the rest of this chapter, we will assume that τ_1, τ_2 always satisfy $\tau_1 > 1/\lambda(\mathbf{A})$ and $\tau_2 > 1/\lambda(\mathbf{B})$ and condition (C3), unless mentioned otherwise.

5.2 Quantitative analysis of the Bi-SIS model

Before presenting our results for the bi-SIS case, we give a bound on the positive equilibria for single-virus SIS models.

Proposition 5.2.1. *Consider the single-virus SIS system* (5.3)*, and let* $\tau_1 > 1/\lambda(\mathbf{A})$ *with* $\mathbf{x}^* \gg \mathbf{0}$ *being the corresponding positive, globally attractive equilibrium. Then, we have*

$$\frac{\mathbf{1}^T\mathbf{x}^*}{N} \leq 1 - \frac{1}{\tau_1\lambda(\mathbf{A})} \leq x^*_{\max} \triangleq \max_{i\in\mathcal{N}} x^*_i. \tag{5.4}$$

This upper bound on the average infection probability $\mathbf{1}^T\mathbf{x}^*/N$ in (5.4) has also been alluded to in [129] as emerging out of the convexity of $\mathbf{x}^*$ in $1/\tau_1$ [90]. Here, we present a formal statement for the bound in the form of Proposition 5.2.1, providing a more direct proof using the FKG and Jensen's inequalities in Appendix D, without the need of first showing convexity via lengthy computations. Our approach also allows us to provide the lower bound on the largest entry of $\mathbf{x}^*$, the second inequality in (5.4).

For regular graphs (with degree d for every node), both the inequalities in (5.4) become equality since we know from Lemma 7 [130] that $\mathbf{x}^*_i = 1-1/\tau_1 d$ for each $i \in \mathcal{N}$, and $\lambda(\mathbf{A}) = d$. When τ_1 is only slightly larger than the threshold $1/\lambda(\mathbf{A})$, intuitively speaking, the virus should not infect a large portion of the network, since it is barely strong enough to survive. The first inequality in (5.4) confirms this intuition since $\mathbf{1}^T\mathbf{x}^*/N$ is still close to zero for such τ_1, implying that the virus barely survives in the long run. If τ_1 is very large, or $1/\tau_1\lambda(\mathbf{A}) \to 0$, the upper bound of $\mathbf{1}^T\mathbf{x}^*/N$ in (5.4) gets closer to 1 and doesn't tell much information about $\mathbf{x}^*$. From (5.4), however, the node with largest infection probability has $x^*_{\max} \to 1$, showing that the virus has at least infected the 'weakest' node in the network that is susceptible to infection.

We now provide quantitative results for the bi-SIS CE fixed points. A CE fixed point $(\hat{\mathbf{x}}, \hat{\mathbf{y}}) \gg (\mathbf{0}, \mathbf{0})$ of system (5.2) satisfies the following equations for each $i \in \mathcal{N}$:

$$\sum_{j\in\mathcal{N}} a_{ij}\hat{x}_j = \frac{\hat{x}_i}{\tau_1(1-\hat{x}_i-\hat{y}_i)}, \ \sum_{j\in\mathcal{N}} b_{ij}\hat{y}_j = \frac{\hat{y}_i}{\tau_2(1-\hat{x}_i-\hat{y}_i)}. \tag{5.5}$$

Analyzing these equations by first trying to show the convexity of CE in the system parameters, as done in [90] for the single-virus SIS model, would be infeasible. This is because the second-order derivatives of the bi-SIS model quickly become intractable due to the highly coupled nature of the ODE system and its fixed point equations, as seen in (5.2) and (5.5) respectively. Instead, our approach is to first leverage the underlying monotonicity properties of the bi-SIS system. Apart from the bi-virus ODE system (5.2) being MDS [41], i.e., the trajectories of (5.2) preserving the ordering of the initial points, we show in the

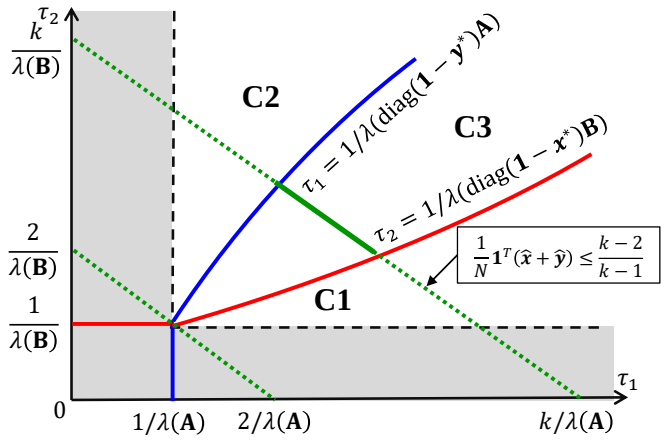

Figure 5.1 The unshaded region is divided by blue curve and red curve (boundary conditions of τ_1, τ_2) into three parts, corresponding to (C1)-(C3) in Section 5.1.2. The discussion on the equilibrium in the shaded region is deferred to previous Chapter 4. Green solid-line is the set of system parameters (τ_1, τ_2) inside C3 such that they exhibit the same upper bound $(\mathbf{1}^T\hat{\mathbf{x}}+\mathbf{1}^T\hat{\mathbf{y}})/N \le (k-2)/(k-1)$ for $k>2$.

following lemma that the CE (which is the limiting state of the system) also exhibits strong monotonicity with respect to the effective infection rates τ_1 and τ_2.

Lemma 5.2.2. *Let $(\hat{\mathbf{x}}, \hat{\mathbf{y}}) \gg (\mathbf{0}, \mathbf{0})$ be a CE of the bi-SIS ODE (5.2). For all $i \in \mathcal{N}$, entries $\hat{x}_i$ of $\hat{\mathbf{x}}$ increase in τ_1 (decrease in τ_2), while entries $\hat{y}_i$ of $\hat{\mathbf{y}}$ decrease in τ_1 (increase in τ_2). That is,*

$$\frac{\partial \hat{x}_i}{\partial \tau_1} > 0, \ \frac{\partial \hat{y}_i}{\partial \tau_1} < 0, \ \text{and} \ \ \frac{\partial \hat{x}_i}{\partial \tau_2} < 0, \ \frac{\partial \hat{y}_i}{\partial \tau_2} > 0.$$

From Lemma 5.2.2, we can see that changes in $\hat{\mathbf{x}}$ and $\hat{\mathbf{y}}$, caused by perturbation to any of the system parameters, are always in the opposite direction. Moreover, changes in both $\hat{\mathbf{x}}_i$ and $\hat{\mathbf{y}}_i$ with respect to τ_1 and τ_2 are strict. This form of strong monotonicity helps us establish the following result, which better captures the coupled relationship of $\hat{\mathbf{x}}$ and $\hat{\mathbf{y}}$ with the system parameters in (5.5).

Theorem 5.2.3. *The term $\hat{y}_i/(1-\hat{x}_i)$ strictly decreases (increases) in τ_1 (τ_2) for all $i \in \mathcal{N}$. Similarly, the term $\hat{x}_i/(1-\hat{y}_i)$ strictly increases (decreases) in τ_1 (τ_2) for all $i \in \mathcal{N}$.* □

Lemma 1 implies that $1/(1-\hat{x}_i)$ increases in τ_1 due to $\hat{x}_i$ increasing in τ_1, while $\hat{y}_i$ decreases in τ_1. However, their product $\hat{y}_i/(1-\hat{x}_i)$ may not possess any apparent monotonicity in τ_1, depending on the amount of increase and decrease observed by $\hat{x}_i$ and $\hat{y}_i$. Theorem

5.2.3 asserts that this term indeed decreases monotonically in τ_1, implying that the decrease in $1-\hat{x}_i$ is not large enough to offset that of $\hat{y}_i$ for all values of τ_1 in (C3). Thus, Theorem 5.2.3 is much sharper in capturing the coupled change in entries of $\hat{\mathbf{x}}$ and $\hat{\mathbf{y}}$ as the system parameters τ_1 and τ_2 are varied, and we are able to do this by combining Lemma 1 with careful analysis of the first order derivatives of the CE fixed point equations (5.5). We have the following corollary as a consequence of Theorem 5.2.3.

Corollary 5.2.4. *For each $i \in \mathcal{N}$, we have the inequalities*

$$\hat{x}_i < x_i^*(1-\hat{y}_i), \quad \hat{y}_i < y_i^*(1-\hat{x}_i). \qquad \square \tag{5.6}$$

To understand the implication of Corollary 5.2.4, we consider briefly consider the example of competing products (modelled as viruses). Where a new product (Product 1) enters a market, more often than not, there is another existing dominant product (Product 2) enjoying its own market share $\hat{\mathbf{y}} = \mathbf{y}^*$. Through mechanisms such as marketing techniques, the Product 1 increases its own influence τ_1, and eventually gains a foothold into the market $\hat{\mathbf{x}} \gg \mathbf{0}$. From Lemma 1, we can only guess that the market share $\hat{\mathbf{y}}$ would fall below its initial dominating value $\mathbf{y}^*$, but there is not much one can say in terms of quantifying the reduction in $\hat{\mathbf{y}}$. From Corollary 5.2.4, we now know that the at each node $i \in \mathcal{N}$, the influence of Product 1 $\hat{y}_i$ will fall by a factor of at least $(1-\hat{x}_i)$ compared to its original value of y_i^*. This is particularly useful when the competing viruses have access to the information about each others' local market share at each node. When this in formation is not available, we have the following proposition which decouples the complicated relationship between CE fixed points.

Proposition 5.2.5. *Let $(\hat{\mathbf{x}}, \hat{\mathbf{y}})$ be a CE fixed point of the bi-SIS system* (5.2)*. Then, the average number of infected nodes in the network $(\mathbf{1}^T\hat{\mathbf{x}} + \mathbf{1}^T\hat{\mathbf{y}})/N$ is upper bounded as*

$$\frac{1}{N}(\mathbf{1}^T\hat{\mathbf{x}} + \mathbf{1}^T\hat{\mathbf{y}}) < 1 - \frac{1}{\tau_1\lambda(\mathbf{A}) + \tau_2\lambda(\mathbf{B}) - 1}. \tag{5.7}$$

Suppose that $\tau_1\lambda(\mathbf{A})$ and $\tau_2\lambda(\mathbf{B})$ are only slightly larger than 1, implying (in light of condition (C3)) that quantities $\tau_1\lambda(\text{diag}(\mathbf{1}-\mathbf{y}^*)\mathbf{A})$ and $\tau_2\lambda(\text{diag}(\mathbf{1}-\mathbf{x}^*)\mathbf{B})$ are also only slightly larger than 1, and just barely satisfy the coexistence condition (C3) by a small margin. In this case, the average number of infected nodes $(\mathbf{1}^T\hat{\mathbf{x}} + \mathbf{1}^T\hat{\mathbf{y}})/N$ must also be small (albeit strictly positive), as would be expected. Note however that the upper bound in (5.7) holds for much

larger values of τ_1, τ_2 as long as they satisfy the CE condition (C3). For instance in Figure 5.1, the green dash-line represents the set of all possible τ_1, τ_2 in the CE condition satisfying $\tau_1\lambda(\mathbf{A}) + \tau_2\lambda(\mathbf{B}) = k$ such that the upper bound remains the same for all the parameters in this (level) set. We also note that the upper bound in (5.7) holds for all possible (finitely many) CE fixed points. In addition, our bound on the CE decouples the cross-dependency of competing viruses on overlaid graphs, into *each* of single-SIS on its own graph. This will shed some light on how to fine-tune the system parameters τ_1, τ_2 or how tho modify the graph adjacency matrices $\mathbf{A}, \mathbf{B}$ for some real-world applications, e.g, strategy design in the medical area in order to control the infection probability of either of two viruses with limited medical resources.

5.3 Numerical Results

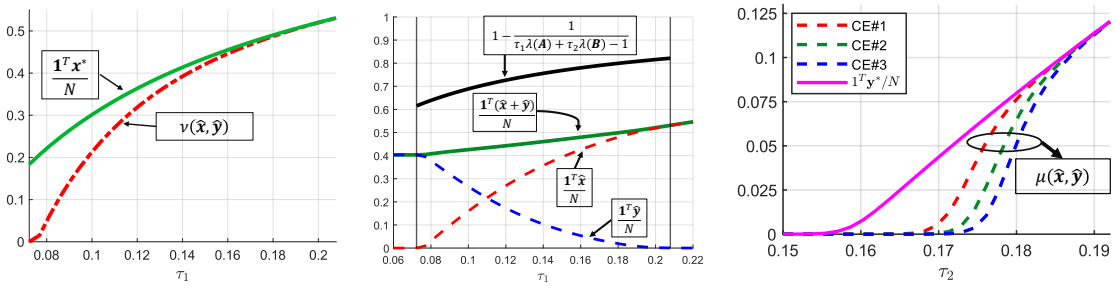

(a) Using AS-733-A and AS-733-B as overlaid graphs for Corollary 5.2.4.

(b) Using AS-733-A and AS-733-B as overlaid graphs for Proposition 5.2.5.

(c) Using AS-733-B and AS-733-C as overlaid graphs for Corollary 5.2.4 with three CE fixed points.

Figure 5.2 Numerical results on the AS-733 graph.

In this section, we present numerical results to assess the tightness of the upper bounds in Corollary 5.2.4 and Proposition 5.2.5. To this end, we consider an undirected, connected

Table 5.1 System Parameters

$\tau_1 : 0.06 \sim 0.22,\ \tau_2 = 0.3173$	$\lambda(\mathbf{A}) = 22.13,\ \lambda(\mathbf{B}) = 6.3$
$\tau_1 = 0.17,\ \tau_2 : 0.15 \sim 0.92$	$\lambda(\mathbf{C}) = 6.59,\ \lambda(\mathbf{B}) = 6.3$

graph AS-733 from the SNAP repository [79] and generate three graphs with the same 103 nodes but with different edge sets, by modifying the edges of AS-733 while preserving the connectivity. The new graphs AS-733-A, AS-733-B and AS-733-C have 616, 267, and 297 edges, respectively. Table 5.1 summarizes the range of system parameters, chosen in a way to ensure that $\tau_1 > 1/\lambda(\mathbf{A})$ and $\tau_2 > 1/\lambda(\mathbf{B})$, i.e., the infection rates never lie in the gray region in Figure 5.1. We numerically solve the ODE system (5.2) for the chosen parameters until convergence is observed.

To capture how the upper bounds behave with change in system parameters, we fix τ_2 and vary τ_1 in Figure 5.2a, 5.2b. Denote by $\mu(\hat{\mathbf{x}},\hat{\mathbf{y}}) \triangleq (1/N)\sum_i \hat{y}_i/(1-\hat{x}_i)$, and $\nu(\hat{\mathbf{x}},\hat{\mathbf{y}}) \triangleq (1/N)\sum_i \hat{x}_i/(1-\hat{y}_i)$. In Figure 5.2a, the range of τ_1 and $\tau_2$values are under the CE condition. We can see that $\nu(\hat{\mathbf{x}},\hat{\mathbf{y}})$ is increasing in τ_1, as is expected from Theorem 5.2.3. In addition, $\nu(\hat{\mathbf{x}},\hat{\mathbf{y}})$ gets closer to the average infection probability of Virus 1 in the single-SIS case as τ_1 increases because Virus 1 becomes more dominant over Virus 2 and the bi-SIS ODE system (5.2) behaves similar to the single-virus system. For Figure 5.2b, as τ_1 increases over the range of values from the first row in Table 5.1, the system parameters transit from regions (C1) to (C3) to (C2) of Figure 5.1; Virus 1 dies out for $\tau_1 \in [0.06, 0.072]$ while Virus 2 survives, both viruses survive for $\tau_1 \in (0.072, 0.208)$, and Virus 2 dies out while Virus 1 survives for $\tau_1 \in [0.208, 0.22]$. The upper bound (in black line) also captures the trend for the average probability of being infected by either virus and has good estimation as τ_1 increases.

Next, we fix τ_1 and vary τ_2, which is given in the second row in Table 5.1, in order to see how τ_2, instead of τ_1, can affect $\mu(\hat{\mathbf{x}},\hat{\mathbf{y}})$ in Corollary 5.2.4. Unlike to Figure 5.2a and 5.2b that only contain single CE, we use AS-733-B and AS-733-C as overlaid graphs to show the existence of multiple CE fixed points in Figure 5.2c, which all satisfy (5.6) in Corollary 5.2.4. The curves in Figure 5.2c also share the similar trend in Figure 5.2a that the upper bound becomes tight for large τ_2.

5.4 Conclusion

In this chapter we have provided, for the first time, quantitative results on the coexistence equilibria of bi-SIS epidemic models for general graphs. A future direction can include similar analysis for graphs with special topologies such as star, and line graphs, as well as cases such as ER random graphs, for which one could potentially obtain tighter results than those in Section 5.2 which were presented for general graphs.

Chapter 6

Concluding Remarks

In this dissertation, we first studied how interaction based dynamics can be used for the design of randomized algorithms on general graphs.

- In Chapter 2, we developed a framework of multiple interacting random walkers, where interactions were with the density distribution of the walkers over the network. This enabled us to prove convergence of a suitably scaled version of the density distribution, to the *second* eigenvector of any time-reversible Markov chain. Thus, by leveraging *non-linearities* induced by the interaction mechanism (typical, non-iteration based Markov chains can be thought of as linear operators), we are able to design a random walk based algorithm which converges to a higher-order eigenvector - a first in literature.

- In Chapter 3, we consider random walks which interact with their own past history, often termed as *self-interacting*. We show that using self-interacting, specifically self-*repelling* mechanisms, which are purely random walk in nature without the need of employing jumps to distant nodes as is common for many adaptive MCMC procedures, we are able to design a random walk procedure that, in the sense of Loewner ordering of co-variance matrices, performs better in estimating a given target distribution.

Through our research, it is evident that introducing interaction based mechanisms to randomized algorithms can allow one to better control their convergence, and increase their utility for algorithm design. The design of non-linear Markov kernels for practical algorithms is a fairly young field of research, and we believe that the results in Chapters 2 and 3 are still simply scratching on the surface.

We then turn our attention to existing interacting dynamics on networks which often have a stochastic interpretation - epidemic models. Specifically, we examine the bi-SIS model on general, multi-layer graphs.

- In Chapter 4, we provide the complete convergence criterion for bi-SIS models which allow for the infection and recovery rates to be non-linear, thereby solving an open problem. We utilize techniques from the theory of *monotone dynamical systems*, showing that the bi-SIS system is monotone with respect to a specifically constructed partial ordering.

- Building up on the monotonicity properties deduced in Chapter 5, we provide the first quantitative results on the behaviour of equilibria of the system, specifically co-existence equilibria where the two epidemics coexist over the network.

Studying epidemic models as monotone dynamical systems is a departure from typical Lyapunov function based methods which are commonly used to prove convergence results for epidemic models. Thus, our results present a case where analysis of the system's fundamental monotonicity properties enables us to provide a more complete set of results than what can be shown using typical Lyapunov functions, which difficult to construct in general.

BIBLIOGRAPHY

[1] David Aldous and James Allen Fill. Reversible markov chains and random walks on graphs, 2002. Unfinished monograph, recompiled 2014, available at `http://www.stat.berkeley.edu/~aldous/RWG/book.html`.

[2] David Aldous, Barry Flannery, and José Luis Palacios. Two applications of urn processes the fringe analysis of search trees and the simulation of quasi-stationary distributions of markov chains. *Probability in the Engineering and Informational Sciences*, 2(3):293–307, 1988.

[3] Daniel J. Amit, G. Parisi, and L. Peliti. Asymptotic behavior of the "true" self-avoiding walk. *Phys. Rev. B*, 27:1635–1645, Feb 1983.

[4] R. Andersen, F. Chung, and K. Lang. Local graph partitioning using pagerank vectors. In *2006 47th Annual IEEE Symposium on Foundations of Computer Science*, FOCS'06, pages 475–486, 2006.

[5] Christophe Andrieu, Ajay Jasra, Arnaud Doucet, and Pierre Del Moral. Non-linear markov chain monte carlo. *Esaim: Proceedings*, 19:79–84, 01 2007.

[6] Christophe Andrieu, Ajay Jasra, Arnaud Doucet, and Pierre Del Moral. On nonlinear Markov chain Monte Carlo. *Bernoulli*, 17(3):987 – 1014, 2011.

[7] Christophe Andrieu, Éric Moulines, and Pierre Priouret. Stability of stochastic approximation under verifiable conditions. *SIAM Journal on control and optimization*, 44(1):283–312, 2005.

[8] Krzysztof R Apt and Evangelos Markakis. Diffusion in social networks with competing products. In *International Symposium on Algorithmic Game Theory*, 2011.

[9] B. Aspvall and J. Gilbert. Graph coloring using eigenvalue decomposition. *SIAM Journal on Algebraic Discrete Methods*, 5(4):526–538, 1984.

[10] John Ball. Semiflows, Lyapunov functions and approach to equilibrium. University lecture, 2016.

[11] S. Banerjee, A. Chatterjee, and S. Shakkottai. Epidemic thresholds with external agents. In *IEEE INFOCOM*, Toronto, ON, 2014.

[12] S Bansal, BT Grenfell, and LA Meyers. When individual behaviour mattersl homogeneous and network models in epidemiology. *Journal Royal Society, Interface*, 4(16):879–891, 2007.

[13] N. D. Barlow. Non-linear transmission and simple models for bovine tuberculosis. *Journal of Animal Ecology*, 69(4):703–713, 2000.

[14] S. T. Barnard, A. Pothen, and H. D. Simon. A spectral algorithm for envelope reduction of sparse matrices. In *Proceedings of the 1993 ACM/IEEE Conference on Supercomputing*, SC'93, pages 493–502, 1993.

[15] Stephen T. Barnard and Horst D. Simon. A fast multilevel implementation of recursive spectral bisection for partitioning unstructured problems. *Concurrency - Practice and Experience*, 6:101–117, 1993.

[16] Michel Benaïm. Vertex-reinforced random walks and a conjecture of pemantle. *Annals of Probability*, 25(1):361–392, 01 1997.

[17] Michel Benaïm. *Dynamics of stochastic approximation algorithms*, pages 1–68. Springer Berlin Heidelberg, 1999.

[18] Michel Benaim. On gradient like properties of population games, learning models and self reinforced processes. In *Dynamics, Games and Science*, pages 117–152, Cham, 2015. Springer International Publishing.

[19] Michel Benaïm and Bertrand Cloez. A stochastic approximation approach to quasi-stationary distributions on finite spaces. *Electronic Communications in Probability*, 20:1–14, 2015.

[20] Michel Benaïm and Pierre Tarres. Dynamics of vertex-reinforced random walks. *The Annals of Probability*, 39(6):2178–2223, 2011.

[21] Michel Benaimï, Olivier Raimond, and Bruno Schapira. Strongly vertex-reinforced-random-walk on the complete graph. *arXiv preprint arXiv:1208.6375*, 2012.

[22] Michel Benaïm and Jörgen W. Weibull. Deterministic approximation of stochastic evolution in games. *Econometrica*, 71(3):873–903, 2003.

[23] Abraham Berman and Robert J. Plemmons. *Nonnegative Matrices in the Mathematical Sciences*. SIAM, 1994.

[24] Alexander Bertrand and Marc Moonen. Distributed computation of the fiedler vector with application to topology inference in ad hoc networks. *Signal Processing*, 93(5):1106–1117, 2013.

[25] J. Blanchet, P. Glynn, and S. Zheng. Theoretical analysis of a Stochastic Approximation approach for computing Quasi-Stationary distributions. *ArXiv e-prints*, January 2014.

[26] P. Brémaud. *Markov chains: Gibbs fields, Monte Carlo simulation, and queues*. Springer-Verlag, 1999.

[27] Pierre Brémaud. Markov chains gibbs fields, monte carlo simulation, and queues. 2020.

[28] Anthony Brockwell, Pierre Del Moral, and Arnaud Doucet. Sequentially interacting markov chain monte carlo methods. *The Annals of Statistics*, pages 3387–3411, 2010.

[29] John C. Urschel, Xiaozhe Hu, Jinchao Xu, and Ludmil T. Zikatanov. A cascadic multigrid algorithm for computing the fiedler vector of graph laplacians. *Journal of Computational Mathematics*, 33:209–226, 2015.

[30] Claudio Castellano and Romualdo Pastor-Satorras. Thresholds for Epidemic Spreading in Networks. *Phys. Rev. Lett.*, 105:218701, Nov 2010.

[31] Jun Chen. Two particles' repelling random walks on the complete graph. *Electronic Journal of Probability*, 19(none):1 – 17, 2014.

[32] F. R. K. Chung. *Spectral Graph Theory*. American Mathematical Society, 1997.

[33] Richard Combes and Mikael Touati. Computationally efficient estimation of the spectral gap of a markov chain. *Proc. ACM Meas. Anal. Comput. Syst.*, 3(1):7:1–7:21, 2019.

[34] K.Ch. Das. The laplacian spectrum of a graph. *Computers & Mathematics with Applications*, 48(5):715–724, 2004.

[35] Pierre Del Moral and L. Miclo. Self-interacting markov chains. *Stochastic Analysis and Applications - STOCHASTIC ANAL APPL*, 24:615–660, 07 2006.

[36] Pierre Del Moral and Laurent Miclo. On convergence of chains with occupational self-interactions. *Proceedings of the Royal Society of London. Series A: Mathematical, Physical and Engineering Sciences*, 460(2041):325–346, 2004.

[37] Bernard Delyon. Stochastic approximation with decreasing gain: Convergence and asymptotic theory. Technical report, Université de Rennes, 2000.

[38] Inderjit S. Dhillon, Yuqiang Guan, and Brian Kulis. Kernel k-means: Spectral clustering and normalized cuts. In *Proceedings of the Tenth ACM SIGKDD International Conference on Knowledge Discovery and Data Mining*, KDD '04, pages 551–556, 2004.

[39] C. H. Q. Ding, Xiaofeng He, Hongyuan Zha, Ming Gu, and H. D. Simon. A min-max cut algorithm for graph partitioning and data clustering. In *Proceedings 2001 IEEE International Conference on Data Mining*, ICDM'01, pages 107–114, 2001.

[40] Chris Ding, Xiaofeng He, and Horst D. Simon. On the equivalence of nonnegative matrix factorization and spectral clustering. In *SIAM International Conference on Data Mining*, ICDM'05, 2005.

[41] V. Doshi, S. Mallick, and D. Y. Eun. Competing Epidemics on Graphs - Global Convergence and Coexistence. In *IEEE INFOCOM*, 2021.

[42] Vishwaraj Doshi and Do Young Eun. Fiedler Vector Approximation via Interacting RandomWalks. *ACM SIGMETRICS Performance Evaluation Review*, 48(1):101–102, 2020.

[43] Moez Draief and Laurent Massouli. *Epidemics and Rumours in Complex Networks*. Cambridge University Press, New York, NY, USA, 1st edition, 2010.

[44] Rafael Van Driessche and Dirk Roose. A Graph Contraction Algorithm for the Fast Calculation of the Fiedler Vector of a Graph. In *Proceedings of the seventh SIAM conference on Parallel Processing for Scientific Computing*, PPSC'95, 1995.

[45] Miroslav Fiedler. Algebraic connectivity of graphs. *Czechoslovak Mathematical Journal*, 23(98):298–305, 1973.

[46] Miroslav Fiedler. A property of eigenvectors of nonnegative symmetric matrices and its application to graph theory. *Czechoslovak Mathematical Journal*, 25(100)(4):619–633, 1975.

[47] Gersende Fort. Central limit theorems for stochastic approximation with controlled markov chain dynamics. *ESAIM: Probability and Statistics*, 19:60–80, 2015.

[48] Ayalvadi Ganesh, Laurent Massoulie, and Don Towsley. The effect of network topology on the spread of epidemics. In *IEEE INFOCOM*, Miami, FL, 2005.

[49] Michele Garetto, Weibo Gong, and Don Towsley. Modeling malware spreading dynamics. In *IEEE INFOCOM*, San Francisco, CA, 2003.

[50] Alison Gray, David Greenhalgh, Liangjian Hu, Xuerong Mao, and Jiafeng Pan. A stochastic differential equation sis epidemic model. *SIAM Journal on Applied Mathematics*, 71(3):876–902, 2011.

[51] Dongchao Guo, Stojan Trajanovski, Ruud van de Bovenkamp, Huijuan Wang, and Piet Van Mieghem. Epidemic threshold and topological structure of susceptible-infectious-susceptible epidemics in adaptive networks. *Physical Review E*, 88(4):042802, 2013.

[52] L. Hagen and A. B. Kahng. New spectral methods for ratio cut partitioning and clustering. *IEEE Transactions on Computer-Aided Design of Integrated Circuits and Systems*, 11(9):1074–1085, 1992.

[53] Insu. Han, Dmitry. Malioutov, Haim. Avron, and Jinwoo. Shin. Approximating spectral sums of large-scale matrices using stochastic chebyshev approximations. *SIAM Journal on Scientific Computing*, 39(4):A1558–A1585, 2017.

[54] G. George Yin Harold J. Kushner. *Stochastic Approximation Algorithms and Applications*. Springer, 1997.

[55] W. K. Hastings. Monte carlo sampling methods using markov chains and their applications. *Biometrika*, 57(1):97–109, 1970.

[56] Herbert W Hethcote. The mathematics of infectious diseases. *SIAM Review*, 42(4):599–653, 2000.

[57] Morris W. Hirsch. Systems of differential equations which are competitive or cooperative: I. limit sets. *SIAM Journal on Mathematical Analysis*, 13(2):167–179, 1982.

[58] Morris W. Hirsch. Systems of differential equations that are competitive or cooperative : II. convergence almost everywhere. *SIAM Journal on Mathematical Analysis*, 16(3):423–439, 1985.

[59] Morris W. Hirsch. Systems of differential equations which are competitive or cooperative: III. competing species. *Nonlinearity*, 1(1):51–71, 1988.

[60] Morris W Hirsch. Systems of differential equations that are competitive or cooperative. v. convergence in 3-dimensional systems. *Journal of Differential Equations*, 80(1):94 – 106, 1989.

[61] Morris W. Hirsch. System of differential equations that are competitive or cooperative. iv: Structural stability in three-dimensional systems. *SIAM Journal on Mathematical Analysis*, 21(5):1225–1234, 1990.

[62] Morris W. Hirsch and Stephen Smale. *Differential equations, dynamical systems, and linear algebra*. Acad. Press, San Diego, CA, USA, 1974.

[63] Morris W. Hirsch and Hal L. Smith. Generic quasi-convergence for strongly order preserving semiflows: A new approach. *Journal of Dynamics and Differential Equations*, 16:433–439, 2004.

[64] Michael E. Hochberg. Non-linear transmission rates and the dynamics of infectious disease. *Journal of Theoretical Biology*, 153(3):301–321, 1991.

[65] Roger A. Horn and Charles R. Johnson. *Matrix Analysis*. Cambridge University Press, New York, NY, USA, 2nd edition, 2012.

[66] Soodeh Hosseini and Mohammad Abdollahi Azgomi. A model for malware propagation in scale-free networks based on rumor spreading process. *Computer Networks*, 108:97–107, 2016.

[67] Daniel Hsu, Aryeh Kontorovich, and Csaba Szepesvári. Mixing time estimation in reversible markov chains from a single sample path. In *Proceedings of the 28th International Conference on Neural Information Processing Systems - Volume 1*, NIPS'15, page 1459–1467, 2015.

[68] Hao Hu, Karima Nigmatulina, and Philip Eckhoff. The scaling of contact rates with population density for the infectious disease models. *Mathematical Biosciences*, 244(2):125–134, 2013.

[69] Vassili N Kolokoltsov. *Nonlinear Markov processes and kinetic equations*, volume 182. Cambridge University Press, 2010.

[70] Yehuda. Koren, Liran. Carmel, and David. Harel. Drawing huge graphs by algebraic multigrid optimization. *Multiscale Modeling & Simulation*, 1(4):645–673, 2003.

[71] SC Kou, Qing Zhou, and Wing Hung Wong. Equi-energy sampler with applications in statistical inference and statistical mechanics. *The annals of Statistics*, 34(4):1581–1619, 2006.

[72] Ulrich Krause and Peter Ranft. A limit set trichotomy for monotone nonlinear dynamical systems. *Nonlinear Analysis: Theory, Methods & Applications*, 19(4):375 – 392, 1992.

[73] Sibsankar Kundu, Dan C. Sorensen, and George N. Phillips, Jr. Automatic domain decomposition of proteins by a gaussian network model. *Proteins: Structure, Function, and Bioinformatics*, 57(4):725–733, 2004.

[74] Ana Lajmanovich and James A. Yorke. A deterministic model for gonorrhea in a nonhomogeneous population. *Mathematical Biosciences*, 28(3):221 – 236, 1976.

[75] Line C Le Goff and Olivier Raimond. Vertex reinforced non-backtracking random walks: an example of path formation. *Electronic Journal of Probability*, 23:1–38, 2018.

[76] Chul-Ho Lee, Min Kang, and Do Young Eun. Non-markovian monte carlo on directed graphs. In *Proceedings of the ACM SIGMETRICS/IFIP Performance 2019*, SIGMETRICS'19, 2019.

[77] Chul-Ho Lee, Xin Xu, and Do Young Eun. Beyond Random Walk and Metropolis-Hastings Samplers: Why You Should Not Backtrack for Unbiased Graph Sampling. In *Proceedings of the ACM SIGMETRICS/PERFORMANCE Joint International Conference on Measurement and Modeling of Computer Systems*, SIGMETRICS'12, pages 319–330, 2012.

[78] B. Lemmens and R. Nussbaum. *Nonlinear Perron-Frobenius Theory*. Cambridge University Press, 2012.

[79] Jure Leskovec and Andrej Krevl. SNAP Datasets: Stanford large network dataset collection. `http://snap.stanford.edu/data`, June 2014.

[80] David A. Levin, Yuval Peres, and Elizabeth L. Wilmer. *Markov chains and mixing times*. American Mathematical Society, 2006.

[81] Cong Li, Ruud van de Bovenkamp, and Piet Van Mieghem. Susceptible-infected-susceptible model: A comparison of n-intertwined and heterogeneous mean-field approximations. *Physical Review E*, 86(2):026116, 2012.

[82] Xue Lin, Qiang Jiao, and Long Wang. Opinion propagation over signed networks: Models and convergence analysis. *IEEE Transactions on Automatic Control*, 64(8):3431–3438, 2018.

[83] Ji Liu, Philip E Paré, Angelia Nedich, Choon Yik Tang, Carolyn L Beck, and Tamer Basar. Analysis and control of a continuous-time bi-virus model. *IEEE Transactions on Automatic Control*, 2019.

[84] Jun S. Liu. *Monte Carlo Strategies in Scientific Computing*. Springer-Verlag, 2004.

[85] WM Liu, HW Hetchote, and SA Levin. Dynamical behavior of epidemiological models with nonlinear incidence rates. *Journal of Mathematical Biology*, 25(4):359–380, 1987.

[86] D. Lusseau, K. Schneider, O. J. Boisseau, P. Haase, E. Slooten, and S. M. Dawson. The bottlenose dolphin community of Doubtful Sound features a large proportion of long-lasting associations. *Behavioral Ecology and Sociobiology*, 54:396–405, 2003.

[87] Thomas m. Liggett. *Interacting Particle Systems*. Springer-Verlag Berlin Heidelberg, 2005.

[88] Carl D. Meyer. *Matrix Analysis and Applied Linear Algebra*. SIAM, 2000.

[89] Carl D Meyer. *Matrix analysis and applied linear algebra*, volume 71. SIAM, 2000.

[90] Piet Mieghem and Jasmina Omic. In-homogeneous Virus Spread in Networks. *arXiv:1306.2588*, 06 2013.

[91] R. K. Miller and A. N. Michel. *Ordinary Differential Equations*. Academic Press, New York, NY, USA, 1982.

[92] Pierre Del Moral and Arnaud Doucet. Interacting Markov chain Monte Carlo methods for solving nonlinear measure-valued equations. *The Annals of Applied Probability*, 20(2):593 – 639, 2010.

[93] Berenice Anne Neumann. Nonlinear markov chains with finite state space: Invariant distributions and long-term behaviour. *arXiv preprint arXiv:2007.02555*, 2020.

[94] A.Y. Ng, Michael Jordan, and Y Weiss. On spectral clustering: Analysis and an algorithm. *Adv. Neural Inf. Process. Syst.*, 2, 11 2001.

[95] J Omic and P Van Mieghem. Epidemic spreading in networks—variance of the number of infected nodes. *Delft University of Technology, Report*, 2009.

[96] Pekka Orponen and Satu Elisa Schaeffer. Local clustering of large graphs by approximate fiedler vectors. In *Proceedings of the 4th International Conference on Experimental and Efficient Algorithms*, WEA'05, pages 524–533, 2005.

[97] Robin Pemantle. Vertex-reinforced random walk. *Probability Theory and Related Fields*, 92(1):117–136, 1992.

[98] Robin Pemantle. A survey of random processes with reinforcement. *Probability surveys*, 4:1–79, 2007.

[99] Robin Pemantle and Stanislav Volkov. Vertex-reinforced random walk on Z has finite range. *The Annals of Probability*, 27(3):1368–1388, 1999.

[100] Lawrence Perko. *Differential Equations and Dynamical Systems (Third ed.)*. New York: Springer, 2001.

[101] P. H. Peskun. Optimum monte-carlo sampling using markov chains. *Biometrika*, 60(3):607–612, 1973.

[102] Alex Pothen, Horst D. Simon, and Kan-Pu Liou. Partitioning sparse matrices with eigenvectors of graphs. *SIAM J. Matrix Anal. Appl.*, 11(3):430–452, 1990.

[103] Alex. Pothen, Horst D. Simon, and Kang-Pu. Liou. Partitioning sparse matrices with eigenvectors of graphs. *SIAM Journal on Matrix Analysis and Applications*, 11(3):430–452, 1990.

[104] B Aditya Prakash, Alex Beutel, Roni Rosenfeld, and Christos Faloutsos. Winner takes all: competing viruses or ideas on fair-play networks. In *ACM World Wide Web*, 2012.

[105] Rafael A Rosales, Fernando PA Prado, and Benito Pires. Vertex reinforced random walks with exponential interaction on complete graphs. *Stochastic Processes and their Applications*, 148:353–379, 2022.

[106] S.M. Ross. *Stochastic processes*. Wiley, 1996.

[107] Sebastian F Ruf, Keith Paarporn, Philip E Pare, and Magnus Egerstedt. Dynamics of opinion-dependent product spread. In *IEEE Conference on Decision and Control*, Melbourne, Australia, 2017.

[108] Faryad Darabi Sahneh and Caterina Scoglio. Competitive epidemic spreading over arbitrary multilayer networks. *Physical Review E*, 89(6):062817, 2014.

[109] A. Santos, J. M. F. Moura, and J. M. F. Xavier. Bi-virus sis epidemics over networks: Qualitative analysis. *IEEE Transactions on Network Science and Engineering*, 2(1):17–29, 2015.

[110] Amandine Schreck, Gersende Fort, and Eric Moulines. Adaptive equi-energy sampler: Convergence and illustration. *ACM Trans. Model. Comput. Simul.*, 23(1), 2013.

[111] S. J. Shepherd, C. B. Beggs, and S. Jones. Amino acid partitioning using a fiedler vector model. *European Biophysics Journal*, 37(1):105–109, 2007.

[112] Jianbo Shi and J. Malik. Normalized cuts and image segmentation. *IEEE Transactions on Pattern Analysis and Machine Intelligence*, 22(8):888–905, 2000.

[113] H.D. Simon. Partitioning of unstructured problems for parallel processing. *Computing Systems in Engineering*, 2(2):135–148, 1991.

[114] Brian Slininger. Fiedlers theory of spectral graph partitioning, 2013.

[115] Jean-Jacques E. Slotine and Weiping Li. *Applied Nonlinear Control*. Prentice-Hall, 1991.

[116] Hal L. Smith. Systems of ordinary differential equations which generate an order preserving flow. a survey of results. *SIAM Review*, 30(1):87–113, 1988.

[117] Hal L. Smith. Is my system of odes cooperative?, 2012.

[118] Hal L Smith. *Monotone dynamical systems: an introduction to the theory of competitive and cooperative systems*. American Mathematical Society, 2014.

[119] Hal L. Smith. Monotone dynamical systems: Reflections on new advances and applications. *Discrete and Continuous Dynamical Systems - A*, 37:485, 2017.

[120] Hal L. Smith and Horst R. Thieme. Quasi convergence and stability for strongly order-preserving semiflows. *SIAM Journal on Mathematical Analysis*, 21(3):673–692, 1990.

[121] Hal L. Smith and Horst R. Thieme. Convergence for strongly order-preserving semiflows. *SIAM Journal on Mathematical Analysis*, 22(4):1081–1101, 1991.

[122] Daniel A. Spielman and Nikhil. Srivastava. Graph sparsification by effective resistances. *SIAM Journal on Computing*, 40(6):1913–1926, 2011.

[123] Daniel A. Spielman and Shang-Hua. Teng. A local clustering algorithm for massive graphs and its application to nearly linear time graph partitioning. *SIAM Journal on Computing*, 42(1):1–26, 2013.

[124] Daniel A. Spielman and Shang-Hua. Teng. Nearly linear time algorithms for preconditioning and solving symmetric, diagonally dominant linear systems. *SIAM Journal on Matrix Analysis and Applications*, 35(3):835–885, 2014.

[125] Ashok Srinivasan and Michael Mascagni. Monte carlo techniques for estimating the fiedler vector in graph applications. In *Proceedings of the International Conference on Computational Science-Part II*, ICCS'02, pages 635–645, 2002.

[126] Pierre Tarrès. Vertex-reinforced random walk on Z eventually gets stuck on five points. *The Annals of Probability*, 32(3B):2650–2701, 2004.

[127] Balint Toth. The "True" Self-Avoiding Walk with Bond Repulsion on $\mathbb{Z}$: Limit Theorems. *The Annals of Probability*, 23(4):1523 – 1556, 1995.

[128] Daniel Trpevski, Wallace KS Tang, and Ljupco Kocarev. Model for rumor spreading over networks. *Physical Review E*, 81(5):056102, 2010.

[129] Piet Van Mieghem. The Viral Conductance of a Network. *Comput. Commun.*, 35(12):1494–1506, Jul 2012.

[130] Piet Van Mieghem, Jasmina Omic, and Robert Kooij. Virus spread in networks. *IEEE/ACM Transactions on Networking*, 17(1):1–14, 2009.

[131] Balint Veto and Balint Toth. Self-repelling random walk with directed edges on Z. *Electronic Journal of Probability*, 13(none):1909 – 1926, 2008.

[132] M. Vidyasagar. *Nonlinear Systems Analysis*. Prentice-Hall, Englewood Cliffs, NJ, USA, 1993.

[133] Stanislav Volkov. Vertex-reinforced random walk on arbitrary graphs. *The Annals of Probability*, 29(1):66–91, 2001.

[134] Stanislav Volkov. Phase transition in vertex-reinforced random walks on Z with non-linear reinforcement. *J. Theoret. Probab*, 19(3):691–700, 2006.

[135] Ulrike von Luxburg. A tutorial on spectral clustering. *Statistics and computing*, 17(4):395–416, 2007.

[136] Yi Wang, Zhen Jin, Zimo Yang, Zi-Ke Zhang, Tao Zhou, and Gui-Quan Sun. Global analysis of an sis model with an infective vector on complex networks. *Nonlinear Analysis: Real World Applications*, 13(2):543–557, 2012.

[137] Lu-Xing Yang, Xiaofan Yang, Jiming Liu, Qingyi Zhu, and Chenquan Gan. Epidemics of computer viruses: a complex-network approach. *Applied Mathematics and Computation*, 219(16):8705–8717, 2013.

[138] Lu-Xing Yang, Xiaofan Yang, and Yuan Yan Tang. A bi-virus competing spreading model with generic infection rates. *IEEE Transactions on Network Science and Engineering*, 5(1):2–13, 2017.

[139] Mengbin Ye, Brian Anderson, and Ji Liu. Convergence and equilibria analysis of a networked bivirus epidemic model. *arXiv:2111.07507*, 2021.

[140] J Yeh. *Real Analysis*. WORLD SCIENTIFIC, 2006.

[141] Yu and Shi. Multiclass spectral clustering. In *Proceedings Ninth IEEE International Conference on Computer Vision*, ICCV'03, pages 313–319, 2003.

[142] Laijun Zhao, Hongxin Cui, Xiaoyan Qiu, Xiaoli Wang, and Jiajia Wang. Sir rumor spreading model in the new media age. *Physica A: Statistical Mechanics and its Applications*, 392(4):995–1003, 2013.

APPENDICES

Appendix A

Appendix for Chapter 2

A.1 Appendix for Section 2.2

A.1.1 Proof of Proposition 2.2.1:

We only show that (2.7) implies (2.9), since the steps relating (2.8) and (2.10) are exactly the same in terms of algebra. By substituting (2.7) into (2.3), we obtain

$$F_x(\mathbf{x},\mathbf{y}) = \sum_{i\in\mathcal{N}} \sum_{j\in\mathcal{N}, j\neq i} (\mathbf{e}_i - \mathbf{e}_j) Q_{ji} x_j + \sum_{i\in\mathcal{N}} \sum_{j\in\mathcal{N}, j\neq i} (\mathbf{e}_i - \mathbf{e}_j)(\kappa x_j y_j) x_i = \mathbf{u} + \mathbf{w}, \tag{A.1}$$

where we use $\mathbf{u}\in\mathbb{R}^N$ and $\mathbf{w}\in\mathbb{R}^N$ to denote the two summation terms. Observe that the k^{th} entry of $\mathbf{u}$ can be written as

$$u_k = \sum_{j\neq k}(1-0)Q_{jk}x_j + \Big[\sum_{i\neq k}(0-1)Q_{ki}\Big]x_k = \sum_{j\neq k} Q_{jk}x_j + Q_{kk}x_k = \sum_{j\in\mathcal{N}} Q_{jk}x_j = [\mathbf{Q}^T\mathbf{x}]_k,$$

suggesting that $\mathbf{u} = [u_k]$ can be written as $\mathbf{u} = \mathbf{Q}^T\mathbf{x}$. Similarly, the k^{th} entry of $\mathbf{w}$ can be written as

$$\begin{aligned} w_k &= \Big[\sum_{j\neq k}(1-0)\kappa x_j y_j\Big]x_k + \sum_{i\neq k}(0-1)(\kappa x_k y_k)x_i \\ &= \Big[\sum_{j\neq k}(1-0)\kappa x_j y_j\Big]x_k + (\kappa x_k y_k)x_k + \sum_{i\neq k}(0-1)(\kappa x_k y_k)x_i - (\kappa x_k y_k)x_k \\ &= \Big[\sum_{j\in\mathcal{N}}\kappa x_j y_j\Big]x_k - \kappa x_k y_k \sum_{i\in\mathcal{N}} x_i = [\kappa\mathbf{x}^T\mathbf{y}]x_k - \kappa x_k y_k, \end{aligned}$$

suggesting that $\mathbf{w} = [w_k]$ can be written as $\mathbf{w} = [\kappa \mathbf{x}^T \mathbf{y}]\mathbf{x} - \kappa \mathbf{D}_\mathbf{y}\mathbf{x}$. Substituting the expressions for $\mathbf{u}$ and $\mathbf{w}$ in (A.1), we obtain (2.9), which completes the proof.

A.1.2 Proof of Proposition 2.2.2:

For this proof, we make a change of notation. Vectors $(\mathbf{x}, \mathbf{y}) \in \mathbb{R}^{2N}$ will now be written as $\begin{bmatrix} \mathbf{x} \\ \mathbf{y} \end{bmatrix}$. Similarly, we have

$$F(\mathbf{x}, \mathbf{y}) = \begin{bmatrix} F_x(\mathbf{x}, \mathbf{y}) \\ F_y(\mathbf{x}, \mathbf{y}) \end{bmatrix} = \begin{bmatrix} \mathbf{Q}^T - \kappa \mathbf{D}_\mathbf{y} & 0 \\ 0 & \mathbf{Q}^T - \kappa \mathbf{D}_\mathbf{x} \end{bmatrix} \begin{bmatrix} \mathbf{x} \\ \mathbf{y} \end{bmatrix} + [\kappa \mathbf{x}^T \mathbf{y}] \begin{bmatrix} \mathbf{x} \\ \mathbf{y} \end{bmatrix}.$$

Denote by $\|\cdot\|$ the 2−norm for any vector in $\mathbb{R}^{2N}$, and the induced matrix norm for any $2N \times 2N$ dimensional matrix. Using this notation for any $(\mathbf{x}, \mathbf{y}) \in S$ and $(\mathbf{u}, \mathbf{w}) \in S$, by the mean value theorem, there exists a point $(\mathbf{a}, \mathbf{b}) \in S$ on the line segment joining $(\mathbf{x}, \mathbf{y})$ and $(\mathbf{u}, \mathbf{w})$ such that

$$\|F(\mathbf{x}, \mathbf{y}) - F(\mathbf{u}, \mathbf{w})\| = \|\mathbf{J}_F(\mathbf{a}, \mathbf{b})\| \left\| \begin{bmatrix} \mathbf{x} \\ \mathbf{y} \end{bmatrix} - \begin{bmatrix} \mathbf{u} \\ \mathbf{w} \end{bmatrix} \right\|, \tag{A.2}$$

where $\mathbf{J}_F(\mathbf{a}, \mathbf{b}))$ is the Jacobian matrix of F evaluated at $(\mathbf{a}, \mathbf{b})$, given by

$$\mathbf{J}_F(\mathbf{a}, \mathbf{b}) = \begin{bmatrix} \mathbf{Q} & 0 \\ 0 & \mathbf{Q} \end{bmatrix} + \kappa \begin{bmatrix} \mathbf{a}\mathbf{b}^T + \mathbf{D}_\mathbf{a}\mathbf{D}_\mathbf{b} - \mathbf{D}_\mathbf{b} & \mathbf{a}\mathbf{a}^T - \mathbf{D}_\mathbf{a} \\ \mathbf{b}\mathbf{b}^T - \mathbf{D}_\mathbf{b} & \mathbf{b}\mathbf{a}^T + \mathbf{D}_\mathbf{b}\mathbf{D}_\mathbf{a} - \mathbf{D}_\mathbf{a} \end{bmatrix}.$$

All elements of the Jacobian matrix are bounded uniformly over the line segment joining $(\mathbf{x}, \mathbf{y})$ and $(\mathbf{u}, \mathbf{w})$, which in turn means that $\|\mathbf{J}_F(\mathbf{a}, \mathbf{b})\|$ is bounded too. Therefore, $F : S \to \mathbb{R}^{2N}$ is Lipschitz continuous which is necessary and sufficient for the existence and uniqueness of solutions to (2.11) [62, 91].

A.1.3 Proof of Theorem 2.2.4

Proof. (Theorem 2.2.4) Before the main part of the proof, we borrow some results from literature which will be used later.

Proposition A.1.1. *(Proposition 5.2 in [43]) Let Y be a Poisson process with unit rate (i.e. $Y(t) \sim$*

Poisson(t) *for all* $t \geq 0$*). Then for any* $\epsilon > 0$ *and* $T > 0$*,*

$$\mathbf{P}\Big(\sup_{0 \leq t \leq T} |Y(t) - t| \geq \epsilon \Big) \leq 2\epsilon \exp\big(-T \cdot h(\epsilon/T) \big)$$

where $h(x) = (1+x)\log(1+x) - x$*.*

We also state Gronwall's inequality.

Lemma A.1.2. *(Gronwall's inequality) Let* f *be a bounded, real valued function on* $[0, T]$ *satisfying* $f(t) \leq a + b \int_0^t u(s) ds$ *for all* $t \in [0, T]$*, where* a *and* b *are non-zero, real valued constants. Then,* $f(t) \leq a \exp(b\, t)$ *for all* $t \in [0, T]$*.*

Observe that since $Q_{ji} = -L_{ji} = A_{ji}$ is no bigger than 1 for all $j \neq i$ and $x_i, y_i \in (0,1)$ for all $i \in \mathcal{N}$,we can bound the terms in (2.3) and (2.4), and obtain[1]

$$\bar{Q}^n_{x:j\to i}(\mathbf{x}, \mathbf{y}) \leq n(1+\kappa) \quad \text{and} \quad \bar{Q}^n_{y:j\to i}(\mathbf{x}, \mathbf{y}) \leq n(1+\kappa). \tag{A.3}$$

We now proceed with the main body of our proof.

For a unit rate Poisson process $Y(t)$, its centered version is given by $\hat{Y}(t) \triangleq Y(t) - t$ for all $t \geq 0$. Let Y^x_{ji} and Y^y_{ji} for all $i, j \in \mathcal{N},\ j \neq i$ be independent Poisson processes of unit rate. Let $\hat{Y}^x_{ji}$ and $\hat{Y}^y_{ji}$ be their centered versions, i.e. $\hat{Y}^x_{ji}(t) = Y^x_{ji}(t) - t$ and $\hat{Y}^y_{ji}(t) = Y^y_{ji}(t) - t$ for any $t \geq 0$.

The continuous time Markov chain $\{\mathbf{x}^n(t), \mathbf{y}^n(t)\}_{t \geq 0}$ can be constructed for any $t \geq 0$ as

$$\begin{aligned}\big(\mathbf{x}^n(t), \mathbf{y}^n(t)\big) = \big(\mathbf{x}^n(0), \mathbf{y}^n(0)\big) &+ \sum_{i \in \mathcal{N}} \sum_{j \neq i} \Big(\frac{\mathbf{e}_i - \mathbf{e}_j}{n}, 0 \Big) Y^x_{ji}\Big(\int_0^t \bar{Q}^n_{x:j\to i}\big(\mathbf{x}^n(s), \mathbf{y}^n(s)\big) ds \Big) \\ &+ \sum_{i \in \mathcal{N}} \sum_{j \neq i} \Big(0, \frac{\mathbf{e}_i - \mathbf{e}_j}{n} \Big) Y^y_{ji}\Big(\int_0^t \bar{Q}^n_{y:j\to i}\big(\mathbf{x}^n(s), \mathbf{y}^n(s)\big) ds \Big).\end{aligned} \tag{A.4}$$

Indeed, for any $i, j \in \mathcal{N},\ j \neq i$, $\Big(\frac{\mathbf{e}_i - \mathbf{e}_j}{n}, 0\Big)$ and $\Big(0, \frac{\mathbf{e}_i - \mathbf{e}_j}{n}\Big)$ are the admissible jumps. From (2.3) and (2.4), at any instant $s \in [0, t]$, these jumps take place with rate $\bar{Q}^n_{x:j\to i}\big(\mathbf{x}^n(s), \mathbf{y}^n(s)\big)$ and $\bar{Q}^n_{y:j\to i}\big(\mathbf{x}^n(s), \mathbf{y}^n(s)\big)$. The Poisson processes that counts the number of such jumps up till time $t \in [0, \infty)$ are therefore non-homogeneous Poisson processes, which are given by $Y^x_{ji}\Big(\int_0^t \bar{Q}^n_{x:j\to i}\big(\mathbf{x}^n(s), \mathbf{y}^n(s)\big)\Big)$ and $Y^y_{ji}\Big(\int_0^t \bar{Q}^n_{y:j\to i}\big(\mathbf{x}^n(s), \mathbf{y}^n(s)\big)\Big)$.

[1] for $\mathbf{Q} \neq -\mathbf{L}$, the entries are still bounded by some positive constant given by $C = \max_{i,j \in \mathcal{N}} Q_{ji}$. In this case, we use C instead of 1 to bound Q_{ji}. The rest of the steps remain the same.

(A.4) can be rewritten in terms of F, $\hat{Y}^x_{ji}$ and $\hat{Y}^y_{ji}$ (the centered verions of Y^x_{ji} and Y^y_{ji}) as

$$\begin{aligned}\big(\mathbf{x}^n(t),\mathbf{y}^n(t)\big)=\big(\mathbf{x}^n(0),\mathbf{y}^n(0)\big)&+\sum_{i\in\mathcal{N}}\sum_{j\neq i}\Big(\frac{\mathbf{e}_i-\mathbf{e}_j}{n},0\Big)\hat{Y}^x_{ji}\Big(\int_0^t \bar{Q}^n_{x:j\to i}\big(\mathbf{x}^n(s),\mathbf{y}^n(s)\big)\Big)ds\\&+\sum_{i\in\mathcal{N}}\sum_{j\neq i}\Big(0,\frac{\mathbf{e}_i-\mathbf{e}_j}{n}\Big)\hat{Y}^y_{ji}\Big(\int_0^t \bar{Q}^n_{y:j\to i}\big(\mathbf{x}^n(s),\mathbf{y}^n(s)\big)\Big)ds+\int_0^t F\big(\mathbf{x}(s),\mathbf{y}(s)\big)ds.\end{aligned}\tag{A.5}$$

Subtracting (2.6) from (A.5) and taking norm yields

$$\begin{aligned}\Big\|\big(\mathbf{x}^n(t),\mathbf{y}^n(t)\big)-\big(\mathbf{x}(t),\mathbf{y}(t)\big)\Big\|\le&\Big\|\big(\mathbf{x}^n(0),\mathbf{y}^n(0)\big)-\big(\mathbf{x}(0),\mathbf{y}(0)\big)\Big\|\\&+\int_0^t\Big\|F\big(\mathbf{x}^n(s),\mathbf{y}^n(s)\big)-F\big(\mathbf{x}(s),\mathbf{y}(s)\big)\Big\|ds\\&+\sum_{i\in\mathcal{N}}\sum_{j\neq i}\Big\|\Big(\frac{\mathbf{e}_i-\mathbf{e}_j}{n},0\Big)\Big\|\Big|\hat{Y}^x_{ji}\Big(\int_0^t \bar{Q}^n_{x:j\to i}\big(\mathbf{x}^n(s),\mathbf{y}^n(s)\big)\Big)ds\Big|\\&+\sum_{i\in\mathcal{N}}\sum_{j\neq i}\Big\|\Big(0,\frac{\mathbf{e}_i-\mathbf{e}_j}{n}\Big)\Big\|\Big|\hat{Y}^y_{ji}\Big(\int_0^t \bar{Q}^n_{y:j\to i}\big(\mathbf{x}^n(s),\mathbf{y}^n(s)\big)\Big)ds\Big|\end{aligned}\tag{A.6}$$

where the inequality comes from repeated applications of triangle inequality. Note that $\Big\|\Big(0,\frac{\mathbf{e}_i-\mathbf{e}_j}{n}\Big)\Big\|=\Big\|\Big(\frac{\mathbf{e}_i-\mathbf{e}_j}{n},0\Big)\Big\|=\sqrt{2}/n$. Thus, we can rewrite the above inequality as

$$\begin{aligned}\Big\|\big(\mathbf{x}^n(t),\mathbf{y}^n(t)\big)-\big(\mathbf{x}(t),\mathbf{y}(t)\big)\Big\|\le&\Big\|\big(\mathbf{x}^n(0),\mathbf{y}^n(0)\big)-\big(\mathbf{x}(0),\mathbf{y}(0)\big)\Big\|\\&+\int_0^t\Big\|F\big(\mathbf{x}^n(s),\mathbf{y}^n(s)\big)-F\big(\mathbf{x}(s),\mathbf{y}(s)\big)\Big\|ds\\&+\sum_{i\in\mathcal{N}}\sum_{j\neq i}\frac{\sqrt{2}}{n}\Big|\hat{Y}^x_{ji}\Big(\int_0^t \bar{Q}^n_{x:j\to i}\big(\mathbf{x}^n(s),\mathbf{y}^n(s)\big)\Big)ds\Big|\\&+\sum_{i\in\mathcal{N}}\sum_{j\neq i}\frac{\sqrt{2}}{n}\Big|\hat{Y}^y_{ji}\Big(\int_0^t \bar{Q}^n_{y:j\to i}\big(\mathbf{x}^n(s),\mathbf{y}^n(s)\big)\Big)ds\Big|.\end{aligned}$$

(A1) says $\|\big(\mathbf{x}(0),\mathbf{y}(0)\big)-\big(\mathbf{x}^n(0),\mathbf{y}^n(0)\big)\|=0$ for all $n\in\mathbb{N}$. From (A1), Proposition 2.2.2, and using

the bounds from (A.3), we obtain

$$\begin{aligned}\left\|\left(\mathbf{x}^n(t),\mathbf{y}^n(t)\right)-\left(\mathbf{x}(t),\mathbf{y}(t)\right)\right\| \le \int_0^t M\left\|\left(\mathbf{x}^n(t),\mathbf{y}^n(t)\right)-\left(\mathbf{x}(t),\mathbf{y}(t)\right)\right\| ds \\ + \sum_{i\in\mathcal{N}}\sum_{j\neq i}\frac{\sqrt{2}}{n}\Big[\Big|\hat{Y}^x_{ji}\big(n(1+\kappa)t\big)\Big| + \Big|\hat{Y}^y_{ji}\big(n(1+\kappa)t\big)\Big|\Big].\end{aligned} \tag{A.7}$$

Define

$$\varepsilon^n_{ji}(t) \triangleq \sqrt{2}\Big[\Big|\hat{Y}^x_{ji}\big(n(1+\kappa)t\big)\Big| + \Big|\hat{Y}^y_{ji}\big(n(1+\kappa)t\big)\Big|\Big] \tag{A.8}$$

for any $i, j \in \mathcal{N},\ j \neq i$. This quantity is what we would like to control. Observe that

$$\begin{aligned}\mathbf{P}\Big(\sup_{0\le t\le T}\sum_{i\in\mathcal{N}}\sum_{j\neq i}\frac{1}{n}\varepsilon^n_{ji}(t)\ge\epsilon\Big) &\le \sum_{i\in\mathcal{N}}\sum_{j\neq i}\mathbf{P}\Big(\sup_{0\le t\le T}\varepsilon^n_{ji}(t)\ge\frac{n\epsilon}{N(N-1)}\Big)\\ &\le \sum_{x,y}\sum_{i\in\mathcal{N}}\sum_{j\neq i}\mathbf{P}\Big(\sup_{0\le t\le T}|\hat{Y}(n(1+\kappa)t)|\ge\frac{n\epsilon}{\sqrt{2}N(N-1)}\Big)\\ &= 2N(N-1)\mathbf{P}\Big(\sup_{0\le s\le n(1+\kappa)T}|\hat{Y}(s)|\ge\frac{n\epsilon}{\sqrt{2}N(N-1)}\Big)\\ &\le 4N(N-1)\exp\left(-n(1+\kappa)T\cdot h\Big(\frac{\epsilon}{\sqrt{2}N(N-1)(1+\kappa)T}\Big)\right).\end{aligned} \tag{A.9}$$

The first inequality comes from the fact that $\mathbf{P}\big(\sum_{i=1}^k X_i\ge\epsilon\big)\le\sum_{i=1}^k\mathbf{P}\big(X_i\ge\epsilon/n\big)$.. Applying the same to $\varepsilon^n_{ji}(t)$ in (A.8), which contains two terms (one corresponding to x and the other to y), gives us the second inequality. The centered Poisson processes $\hat{Y}$ are written in an un-indexed manner to emphasize their independence, which gives us the (third) equality. Finally, last inequality is a result of applying Proposition A.1.1.

Applying Lemma A.1.2 (Gronwall's inequality) to (A.7), we get

$$\begin{aligned}\mathbf{P}\Big(\sup_{0\le t\le T}\left\|\left(\mathbf{x}^n(t),\mathbf{y}^n(t)\right)-\left(\mathbf{x}(t),\mathbf{y}(t)\right)\right\|\ge\epsilon e^{MT}\Big)\\ \le \mathbf{P}\Big(\sup_{0\le t\le T}\Big(\sum_{i\in\mathcal{N}}\sum_{j\neq i}\frac{1}{n}\varepsilon^n_{ji}(t)\Big)e^{MT}\ge\epsilon e^{MT}\Big)\\ = \mathbf{P}\Big(\sup_{0\le t\le T}\sum_{i\in\mathcal{N}}\sum_{j\neq i}\frac{1}{n}\varepsilon^n_{ji}(t)\ge\epsilon\Big)\\ \le 2N(N-1)\exp\left(-n(1+\kappa)T\cdot h\Big(\frac{\epsilon}{2\sqrt{2}N(N-1)(1+\kappa)T}\Big)\right).\end{aligned}$$

This can also be written as

$$\begin{aligned}&\mathbf{P}\Big(\sup_{0\le t\le T}\big\|\big(\mathbf{x}^n(t),\mathbf{y}^n(t)\big)-\big(\mathbf{x}(t),\mathbf{y}(t)\big)\big\|\ge\epsilon\Big)\\&\quad\le 4N(N-1)\exp\left(-n(1+\kappa)T\cdot h\Big(\frac{\epsilon e^{-MT}}{\sqrt{2}N(N-1)(1+\kappa)T}\Big)\right)\end{aligned}$$

which is (2.15). Now observe that the above bound is finite and decreasing exponentially as n increases. Therefore,

$$\sum_{n=1}^{\infty}\mathbf{P}\Big(\sup_{0\le t\le T}\big\|\big(\mathbf{x}^n(t),\mathbf{y}^n(t)\big)-\big(\mathbf{x}(t),\mathbf{y}(t)\big)\big\|\ge\epsilon\Big)<\infty$$

and the almost sure convergence in (2.14) follows from the *Borel Cantelli Lemma*. This completes the proof of Theorem 2.2.4. □

A.2 Lyapunov theory and LaSalle invariance principle

In this section, we collect some definitions and results from the Lyapunov theory for non-linear systems. By the term *Flow* (or *Semi-flow*) with respect to some deterministic system, denoted by a function $\Phi:\mathbb{R}\times X\to X$, we mean that $\Phi(x_0,t)$ gives the solution to that deterministic system at time t and starting at x_0 at time 0 (note that $t\ge 0$ always in case of semi-flows, while $t\in(-\infty,+\infty)$ for flows).

Often in literature, the term 'Lyapunov function' $V:X\to\mathbb{R}$ is defined as a non-negative function, with $V(0)=0$ and $d(V)/dt<0$ for any $x\in X, x\neq 0$. This is useful for analyzing systems with only one fixed point that can be easily translated to the origin $0\in X$ without loss of generality. However, our ODE system (2.18) consists of multiple fixed points. The results we state below are accordingly adjusted to cover such general cases.

Definition A.2.1. *(Section 3 in [10]) Consider a flow $\Phi:\mathbb{R}\times X\to X$ contained within some set X. A point in $z\in X$ is a fixed point of the flow Φ if $\Phi(t,z)=z$ for all time $t\ge 0$. A function $V:X\to\mathbb{R}$ is called a 'Lyapunov function' if*

(i) V is continuous over X,

(ii) $V(\phi(t,x))\le V(x)$ for all $x\in X$ and $t\ge 0$ (negative semi-definiteness),

(iii) If $V(\psi(t)) = c$, where c is some constant, for some periodic oribit $\psi(t)$ for all $t \in R$, then $\psi(t)$ is actually some fixed point x of the flow ϕ.

Such Lyapunov functions can be used to prove convergence of a flow induced by a system of ODEs using the following famous theorem.

Theorem A.2.2 (LaSalle's invariance principle)**.** *(Theorem 3.1 in [10], Chapter 5 in [132], Chapter 3 in [115]). Let $V : X \to \mathbb{R}$ be a 'Lyapunov function' for some set X and flow Φ. Let $\gamma^+(x)$ denote the forward (in time) orbit of the flow $\Phi(\cdot, x)$, i.e. starting at x. If $\gamma^+(x)$ is relatively compact, and all fixed points of Φ are isolated, then for all $x \in X$, $\Phi(t, x) \to z$ for some fixed point z.*

To help characterize fixed points of the system, we give the definitons of Lyapunov stability, and then state a theorem that helps characterize the stable and unstable fixed points in terms of the Lyapunov function $V : X \to \mathbb{R}$.

Definition A.2.3. *(Stable, unstable and asymptotically stable fixed points).*

(i) A fixed point $z \in X$ of a flow Φ is 'stable' if for all $\epsilon > 0$, there exists a $\delta > 0$ such that for any $x \in X$, $\|x - z\| < \delta \implies \|\Phi(t, x) - z\| < \epsilon$ for all $t \geq 0$.

(ii) A fixed point $z \in X$ of a flow Φ is 'unstable' if it is not stable.

(iii) A fixed point $z \in X$ of a flow Φ is 'asymptotically stable' if it is stable and there exists a $\delta > 0$ such that $x \in X$, $\|x - z\| < \delta \implies \|\Phi(t, x) - z\| \to 0$ as $t \to \infty$.

Theorem A.2.4. *(Theorems 4.1 and 4.2 in [10], Chapter 5 in [132], Chapter 4 in [115]). Let $z \in X$ be an isolated fixed point of flow Φ, and let $V : X \to \mathbb{R}$ be a Lyapunov function. Let $\gamma^+(x)$ be relatively compact for any $x \in X$ with $\gamma^+(x)$ bounded. Then,*

(i) z is 'asymptotically stable' if there exists a $\delta > 0$ such that $V(x) > V(z)$ for any $x \in X$ where $\|x - z\| < \delta$, implying that z is a local minimizer of V.

(ii) z is 'unstable' if it is not a local minimizer of V, i.e. for any $\epsilon > 0$, there exists an $x \in X$ such that $\|x - z\| < \epsilon$ and $V(x) < V(z)$.

Appendix B

Appendix for Chapter 3

B.1 Appendix for Section 3.3

Proof of Proposition 3.3.2. To show that $\boldsymbol{\pi}(\mathbf{x})$ in (3.6) is indeed a stationary distribution, it is enough to check that $(\boldsymbol{\pi}(\mathbf{x}), \mathbf{K}[\mathbf{x}])$ satisfies the balance equation, that is $\pi_i(\mathbf{x})K[\mathbf{x}]_{ij} = \pi_j(\mathbf{x})K[\mathbf{x}]_{ji}$ for all $i, j \in \mathcal{N}$ and $\mathbf{x} \in \text{Int}(\Sigma)$. Indeed, for $\boldsymbol{\pi}(\mathbf{x})$ and $\mathbf{K}[\mathbf{x}]$ given by (3.6) and (3.4) respectively, we have

$$\begin{aligned}
\pi_i(\mathbf{x})K[\mathbf{x}]_{ij} &= \frac{\left(\frac{x_i}{d_i}\right)^{-\alpha} \sum_{k\in\mathcal{N}} a_{ik}\left(\frac{x_k}{d_k}\right)^{-\alpha}}{\sum_{m\in\mathcal{N}}\sum_{n\in\mathcal{N}} a_{mn}\left(\frac{x_m}{d_m}\right)^{-\alpha}\left(\frac{x_n}{d_n}\right)^{-\alpha}} \frac{a_{ij}\left(\frac{x_j}{d_j}\right)^{-\alpha}}{\sum_k a_{ik}\left(\frac{x_k}{d_k}\right)^{-\alpha}} \\
&= \frac{\left(\frac{x_j}{d_j}\right)^{-\alpha} \sum_{k\in\mathcal{N}} a_{jk}\left(\frac{x_k}{d_k}\right)^{-\alpha}}{\sum_{m\in\mathcal{N}}\sum_{n\in\mathcal{N}} a_{mn}\left(\frac{x_m}{d_m}\right)^{-\alpha}\left(\frac{x_n}{d_n}\right)^{-\alpha}} \frac{a_{ji}\left(\frac{x_i}{d_i}\right)^{-\alpha}}{\sum_k a_{jk}\left(\frac{x_k}{d_k}\right)^{-\alpha}} \\
&= \pi_j(\mathbf{x})K[\mathbf{x}]_{ji},
\end{aligned}$$

for all $i, j \in \mathcal{N}$, where the third equality follows by using $a_{ij} = a_{ji}$ and rearranging the terms. Moreover, since the underlying graph is connected, $\mathbf{A}$ is an irreducible matrix, and so is $\mathbf{K}[\mathbf{x}]$ since it shares the same sign structure as $\mathbf{A}$ for all $\mathbf{x} \in \text{Int}(\Sigma)$. The uniqueness of $\boldsymbol{\pi}(\mathbf{x})$ then follows from the Perron Frobenius theorem for non-negative, irreducible matrices. □

B.2 Appendix for Section 3.4

First, we introduce Hilbert's projection metric on the *cone* $\mathbb{R}^N_+$.

Definition B.2.1. *For any* $\mathbf{x} \gg \mathbf{0}$ *and* $\mathbf{y} \gg \mathbf{0}$*, let*

$$M(\mathbf{x};\mathbf{y}) \triangleq \inf\{\beta > 0 \; ; \; \mathbf{x} \leq \beta \mathbf{y}\} = \max_i \frac{x_i}{y_i},$$

and

$$m(\mathbf{x};\mathbf{y}) \triangleq \sup\{\alpha > 0 \; ; \; \mathbf{x} \geq \alpha \mathbf{y}\} = \min_i \frac{x_i}{y_i}.$$

Then, the Hilbert's projective metric $d_H(\mathbf{x},\mathbf{y})$ *is given by*

$$d_H(\mathbf{x},\mathbf{y}) \triangleq \begin{cases} \log\left(\frac{M(\mathbf{x};\mathbf{y})}{m(\mathbf{x};\mathbf{y})}\right) = \max_{i,j} \log\left(\frac{x_i y_j}{y_i x_j}\right), & \text{if } \mathbf{x},\mathbf{y} \gg \mathbf{0} \\ 0, & \text{if } \mathbf{x} = \mathbf{0}, \mathbf{y} = \mathbf{0} \\ \infty, & \text{otherwise.} \end{cases} \tag{B.1}$$

Proof of Lemma 3.4.1. Let $\mathbf{h}(\mathbf{x}) \triangleq [h_i(\mathbf{x})]_{i \in \mathcal{N}}$, where

$$h_i(\mathbf{x}) \triangleq \sum_j a_{ij} \left(\frac{x_i}{d_i}\right)^{-\alpha} \left(\frac{x_j}{d_j}\right)^{-\alpha}. \tag{B.2}$$

Then, $\pi_i(\mathbf{x}) = h_i(\mathbf{x})/\mathbf{1}^T\mathbf{h}(\mathbf{x})$ for all $i \in \mathcal{N}$. For vectors in $\mathbb{R}^N$, let $(\geq, >, \gg)$ be the cone ordering induced by the positive orthant $\mathbb{R}^N_+$. Then, observe that we have the following properties for $\mathbf{h}(\cdot)$:

- $\mathbf{h}(\mathbf{x}) \geq \mathbf{h}(\mathbf{y})$ for any $\mathbf{x} \leq \mathbf{y}$, where $\mathbf{x},\mathbf{y} \gg \mathbf{0}$, (order reversing)
- $\mathbf{h}(\lambda \mathbf{x}) = \lambda^{-2\alpha}\mathbf{h}(\mathbf{x})$ for any $\mathbf{x} \gg \mathbf{0}$, and $\alpha \in [0, 1/2)$. (-2α-homogeniety)

Now, let $c_1 \triangleq m(\mathbf{x};\mathbf{y})$ and let $c_2 \triangleq M(\mathbf{x};\mathbf{y})$. By definition, we have

$$c_1 \mathbf{y} \leq \mathbf{x} \leq c_2 \mathbf{y},$$

and due to the order reversing nature of $\mathbf{h}(\cdot)$, we have

$$\mathbf{h}(c_1\mathbf{y}) \geq \mathbf{h}(\mathbf{x}) \geq \mathbf{h}(c_2\mathbf{y}).$$

From the -2α-homogeniety of $\mathbf{h}(\cdot)$, we have

$$c_1^{-2\alpha}\mathbf{h}(\mathbf{y}) \geq \mathbf{h}(\mathbf{x}) \geq c_2^{-2\alpha}\mathbf{h}(\mathbf{y}).$$

Since $\pi(\mathbf{x}) = \mathbf{h}(\mathbf{x})/\mathbf{1}^T\mathbf{h}(\mathbf{x})$, and from the upper bound $c_1^{-2\alpha}\mathbf{h}(\mathbf{y}) \geq \mathbf{h}(\mathbf{x})$ in the previous equation, we have

$$c_1^{-2\alpha}\frac{\mathbf{1}^T\mathbf{h}(\mathbf{y})}{\mathbf{1}^T\mathbf{h}(\mathbf{x})}\pi(\mathbf{y}) = c_1^{-2\alpha}\frac{\mathbf{h}(\mathbf{y})}{\mathbf{1}^T\mathbf{h}(\mathbf{x})} \geq \frac{\mathbf{h}(\mathbf{x})}{\mathbf{1}^T\mathbf{h}(\mathbf{x})} = \pi(\mathbf{x}).$$

Performing the same steps using the lower bound $\mathbf{h}(\mathbf{x}) \geq c_2^{-2\alpha}\mathbf{h}(\mathbf{y})$ and combining with the above equation, we can obtain

$$c_1^{-2\alpha}\frac{\mathbf{1}^T\mathbf{h}(\mathbf{y})}{\mathbf{1}^T\mathbf{h}(\mathbf{x})}\pi(\mathbf{y}) \geq \pi(\mathbf{x}) \geq c_2^{-2\alpha}\frac{\mathbf{1}^T\mathbf{h}(\mathbf{y})}{\mathbf{1}^T\mathbf{h}(\mathbf{x})}\pi(\mathbf{y}) \tag{B.3}$$

We now have

$$M(\pi(\mathbf{x});\pi(\mathbf{y})) = \max_i \frac{\pi_i(\mathbf{x})}{\pi_i(\mathbf{y})} \leq c_1^{-2\alpha}\frac{\mathbf{1}^T\mathbf{h}(\mathbf{y})}{\mathbf{1}^T\mathbf{h}(\mathbf{x})},$$

and

$$m(\pi(\mathbf{x});\pi(\mathbf{y})) = \min_i \frac{\pi_i(\mathbf{x})}{\pi_i(\mathbf{y})} \geq c_2^{-2\alpha}\frac{\mathbf{1}^T\mathbf{h}(\mathbf{y})}{\mathbf{1}^T\mathbf{h}(\mathbf{x})}$$

where the inequality comes from the upper bound in (B.3). Thus, we have

$$\begin{aligned} d_H(\pi(\mathbf{x}),\pi(\mathbf{y})) &= \log\left(\frac{M(\pi(\mathbf{x});\pi(\mathbf{y}))}{m(\pi(\mathbf{x});\pi(\mathbf{y}))}\right) \leq \log\left(\frac{c_1^{-2\alpha}}{c_2^{-2\alpha}}\right) \\ &= \log\left(\frac{c_2^{|-2\alpha|}}{c_1^{|-2\alpha|}}\right) = |-2\alpha|\log\left(\frac{M(\mathbf{x};\mathbf{y})}{m(\mathbf{x};\mathbf{y})}\right) = |-2\alpha| d_H(\mathbf{x},\mathbf{y}), \end{aligned}$$

where the third equality is because $-2\alpha < 0$, and the fourth equality comes from the def. of c_1, c_2. $\pi(\mathbf{x})$ is a strict contraction for $\alpha \in (0, 1/2)$. The uniqueness follows from Banach contraction principle.

□

Proof of Lemma 3.4.2. We use the notation $\left[\frac{\mathbf{x}}{\mathbf{d}}\right]^{-\alpha}$ to denote a vector with the i'th entry being $\left[\frac{x_i}{d_i}\right]^{-\alpha}$, for any $\alpha \in \mathbb{R}$. For any vector $\mathbf{v} \in \mathbb{R}^N$, we will occasionally use the notation $[\mathbf{v}]_i$ to denote its i'th entry. Taking partial derivative of the Lyapunov function with respect to x_i, we have

$$\frac{\partial V(\mathbf{x})}{\partial x_i} = \frac{-2\alpha}{d_i}\left[\frac{x_i}{d_i}\right]^{-\alpha-1}\left[\mathbf{A}\left[\frac{\mathbf{x}}{\mathbf{d}}\right]^{-\alpha}\right]_i \tag{B.4}$$

Taking derivative of $V(\mathbf{x})$ along trajectories of the ODE system (3.8), we get

$$\begin{aligned}
\frac{d}{dt}V(\mathbf{x}) &= \sum_i \frac{\partial V(\mathbf{x})}{\partial x_i}\frac{dx_i}{dt} = -2\alpha \sum_{i\in\mathcal{N}} \left(\frac{1}{d_i}\left[\frac{x_i}{d_i}\right]^{-\alpha-1}\left[\mathbf{A}\left[\frac{\mathbf{x}}{\mathbf{d}}\right]^{-\alpha}\right]_i\right)\cdot(\pi_i(\mathbf{x})-x_i) \\
&= -2\alpha \sum_{i\in\mathcal{N}} \left(\frac{1}{d_i}\left[\frac{x_i}{d_i}\right]^{-\alpha-1}\left[\mathbf{A}\left[\frac{\mathbf{x}}{\mathbf{d}}\right]^{-\alpha}\right]_i\right)\cdot\left(\frac{1}{V(\mathbf{x})}\left[\frac{x_i}{d_i}\right]^{-\alpha}\left[\mathbf{A}\left[\frac{\mathbf{x}}{\mathbf{d}}\right]^{-\alpha}\right]_i - x_i\right) \\
&= \frac{-2\alpha}{V(\mathbf{x})} \sum_{i\in\mathcal{N}} \left(\frac{1}{d_i}\left[\frac{x_i}{d_i}\right]^{-\alpha-1}\left[\mathbf{A}\left[\frac{\mathbf{x}}{\mathbf{d}}\right]^{-\alpha}\right]_i\right)\cdot\left(\left[\frac{x_i}{d_i}\right]^{-\alpha}\left[\mathbf{A}\left[\frac{\mathbf{x}}{\mathbf{d}}\right]^{-\alpha}\right]_i - V(\mathbf{x})x_i\right) \\
&= \frac{-2\alpha}{V(\mathbf{x})} \sum_{i\in\mathcal{N}} B_i(\mathbf{x}) + C_i(\mathbf{x}),
\end{aligned} \tag{B.5}$$

where

$$B_i(\mathbf{x}) = \left(\frac{1}{d_i}\left[\frac{x_i}{d_i}\right]^{-\alpha-1}\left[\mathbf{A}\left[\frac{\mathbf{x}}{\mathbf{d}}\right]^{-\alpha}\right]_i\right)\cdot\left(\left[\frac{x_i}{d_i}\right]^{-\alpha}\left[\mathbf{A}\left[\frac{\mathbf{x}}{\mathbf{d}}\right]^{-\alpha}\right]_i\right),$$

and

$$C_i(\mathbf{x}) = \left(\frac{1}{d_i}\left[\frac{x_i}{d_i}\right]^{-\alpha-1}\left[\mathbf{A}\left[\frac{\mathbf{x}}{\mathbf{d}}\right]^{-\alpha}\right]_i\right)\cdot(V(\mathbf{x})x_i).$$

Define a random variable $Z(\mathbf{x})$ which takes values $Z_i(\mathbf{x}) = \frac{1}{d_i}\left[\frac{x_i}{d_i}\right]^{-\alpha-1}\left[\mathbf{A}\left[\frac{\mathbf{x}}{\mathbf{d}}\right]^{-\alpha}\right]_i$ with probability x_i. Then, we can see that

$$B_i(\mathbf{x}) = \left(\frac{1}{d_i}\left[\frac{x_i}{d_i}\right]^{-\alpha-1}\left[\mathbf{A}\left[\frac{\mathbf{x}}{\mathbf{d}}\right]^{-\alpha}\right]_i\right)\cdot\left(\frac{1}{d_i}\left[\frac{x_i}{d_i}\right]^{-\alpha-1}\left[\mathbf{A}\left[\frac{\mathbf{x}}{\mathbf{d}}\right]^{-\alpha}\right]_i\right)\cdot x_i = Z_i(\mathbf{x})^2 x_i,$$

and as a result,

$$\sum_{i\in\mathcal{N}} B_i(\mathbf{x}) = \sum_{i\in\mathcal{N}} Z_i(\mathbf{x})^2 x_i = \mathbb{E}[Z(\mathbf{x})^2]. \tag{B.6}$$

We can similarly write $\sum_{i\in\mathcal{N}} C_i(\mathbf{x})$ as

$$\begin{aligned}
\sum_{i\in\mathcal{N}} C_i(\mathbf{x}) &= -V(\mathbf{x}) \sum_{i\in\mathcal{N}} \frac{1}{d_i}\left[\frac{x_i}{d_i}\right]^{-\alpha-1}\left[\mathbf{A}\left[\frac{\mathbf{x}}{\mathbf{d}}\right]^{-\alpha}\right]_i \cdot x_i \\
&= -\left(\sum_{k\in\mathcal{N}} \frac{1}{d_k}\left[\frac{x_k}{d_k}\right]^{-\alpha-1}\left[\mathbf{A}\left[\frac{\mathbf{x}}{\mathbf{d}}\right]^{-\alpha}\right]_k \cdot x_k\right)\left(\sum_{i\in\mathcal{N}} \frac{1}{d_i}\left[\frac{x_i}{d_i}\right]^{-\alpha-1}\left[\mathbf{A}\left[\frac{\mathbf{x}}{\mathbf{d}}\right]^{-\alpha}\right]_i \cdot x_i\right) \\
&= -\left(\sum_{k\in\mathcal{N}} Z_k(\mathbf{x})x_k\right)\left(\sum_{i\in\mathcal{N}} Z_i(\mathbf{x})x_i\right) = \mathbb{E}[Z(\mathbf{x})]^2.
\end{aligned} \tag{B.7}$$

Substituting (B.6) and (B.7) in (B.5) gives us

$$\frac{d}{dt}V(\mathbf{x}) = \frac{-2\alpha}{V(\mathbf{x})}\sum_{i\in\mathcal{N}} B_i(\mathbf{x}) + C_i(\mathbf{x}) = \frac{-2\alpha}{V(\mathbf{x})}\left(\mathbb{E}[Z(\mathbf{x})^2] - \mathbb{E}[Z(\mathbf{x})]^2\right) = \frac{-2\alpha}{V(\mathbf{x})}\mathrm{Var}[Z(\mathbf{x})] \leq 0. \tag{B.8}$$

To show that the equality is only achieved at the fixed point, all we need to show is that $\mathrm{Var}[Z(\mathbf{x})] = 0 \iff \mathbf{x} = \boldsymbol{\pi}(\mathbf{x})$. The Variance term is zero if and only if $Z_i = Z_j$ for all $i, j \in \mathcal{N}$, that is

$$\begin{aligned} &\frac{1}{d_i}\left[\frac{x_i}{d_i}\right]^{-\alpha-1}\left[\mathbf{A}\left[\frac{\mathbf{x}}{\mathbf{d}}\right]^{-\alpha}\right]_i = \frac{1}{d_i}\left[\frac{x_j}{d_j}\right]^{-\alpha-1}\left[\mathbf{A}\left[\frac{\mathbf{x}}{\mathbf{d}}\right]^{-\alpha}\right]_j \qquad (B.9)\\ \iff &\frac{\pi_i(\mathbf{x})}{x_i} = \frac{\pi_j(\mathbf{x})}{x_j} \end{aligned}$$

for all $i, j \in \mathcal{N}$, where (B.9) comes by rewriting the form for Z_i as $w(\mathbf{x})\pi_i(\mathbf{x})/x_i$. Equation (B.9) is true if and only if $\pi_i(\mathbf{x}) = x_i$ for all $i \in \mathcal{N}$, which completes the proof. □

Proof of Theorem 3.4.3. Observe that trajectories $\{\mathbf{x}(t)\}_{t\geq 0}$ starting from any $\mathbf{x}(0) \in \mathrm{Int}(\Sigma)$ are relatively compact and bounded, since the flow of the ODE system (3.8) leaves the probability simplex positively invariant. Then, the global stability of $\mathbf{d} \in \mathrm{Int}(\Sigma)$ follows by application of Lemma 3.4.1, Lemma 3.4.2, and Theorem A.2.2 (LaSalle's Invariance principle). □

Proof of Proposition 3.4.4. Let $h_i(\mathbf{x})$ as in (B.2), for all $\mathbf{x} \in \mathrm{Int}(\Sigma)$, and let $g(\mathbf{x}) \triangleq \sum_{k\in\mathcal{N}} h_k(\mathbf{x})$. Then, for $f_i(\mathbf{x})$ as in (3.9), we have

$$f_i(\mathbf{x}) = \frac{h_i(\mathbf{x})}{g(\mathbf{x})}, \tag{B.10}$$

for all $i \in \mathcal{N}$ and $\mathbf{x} \in \mathrm{Int}(\Sigma)$, and its partial derivatives follow

$$\frac{\partial f_i(\mathbf{x})}{\partial \mathbf{x}_j} = \frac{g(\mathbf{x})\frac{\partial h_i(\mathbf{x})}{\partial x_j} - h_i(\mathbf{x})\frac{\partial g(\mathbf{x})}{\partial x_j}}{g(\mathbf{x})^2}. \tag{B.11}$$

To deduce $\frac{\partial f_i(\mathbf{x})}{\partial \mathbf{x}_j}\Big|_{\mathbf{x}=\mathbf{d}}$, we evaluate each quantity the above equation evaluated at $\mathbf{x} = \mathbf{d}$, and

then substitute them back in the above expression. We have

$$
\begin{aligned}
&h_i(\mathbf{d}) = \deg(i), && \forall\ i \in \mathcal{N},\\
&g(\mathbf{d}) = \sum_{i\in\mathcal{N}} \deg(i) \triangleq \hat{D},\\
&\left.\frac{\partial h_i(\mathbf{x})}{\partial \mathbf{x}_i}\right|_{\mathbf{x}=\mathbf{d}} = -\frac{\alpha}{x_i}\sum_{j\in\mathcal{N}} a_{ij}\left(\frac{x_i}{d_i}\right)^{-\alpha}\left(\frac{x_j}{d_j}\right)^{-\alpha} - \frac{\alpha}{x_i}a_{ii}\left(\frac{x_i}{d_i}\right)^{-2\alpha}\Bigg|_{\mathbf{x}=\mathbf{d}} = -\alpha\hat{D} - \alpha\frac{a_{ii}}{d_i}, && \forall\ i \in \mathcal{N},\\
&\left.\frac{\partial h_i(\mathbf{x})}{\partial \mathbf{x}_j}\right|_{\mathbf{x}=\mathbf{d}} = -\frac{\alpha}{x_j}a_{ij}\left(\frac{x_i}{d_i}\right)^{-\alpha}\left(\frac{x_j}{d_j}\right)^{-\alpha}\Bigg|_{\mathbf{x}=\mathbf{d}} = -\alpha\frac{a_{ij}}{d_j}, && \forall\ i \neq j \in \mathcal{N},\\
&\left.\frac{\partial g(\mathbf{x})}{\partial \mathbf{x}_i}\right|_{\mathbf{x}=\mathbf{d}} = -\frac{2\alpha}{x_i}\sum_{j\in\mathcal{N}} a_{ij}\left(\frac{x_i}{d_i}\right)^{-\alpha}\left(\frac{x_j}{d_j}\right)^{-\alpha}\Bigg|_{\mathbf{x}=\mathbf{d}} = -2\alpha\hat{D}, && \forall\ i \in \mathcal{N}.
\end{aligned}
$$

Substituting the above expressions in (B.11) and simplifying it yields

$$
\begin{aligned}
\left.\frac{\partial f_i(\mathbf{x})}{\partial \mathbf{x}_i}\right|_{\mathbf{x}=\mathbf{d}} &= 2\alpha d_i - \alpha\frac{a_{ii}}{\deg(i)} - \alpha - 1, && \forall\ i \in \mathcal{N},\\
\left.\frac{\partial f_i(\mathbf{x})}{\partial \mathbf{x}_j}\right|_{\mathbf{x}=\mathbf{d}} &= 2\alpha d_i - \alpha\frac{a_{ij}}{\deg(j)} - \alpha, && \forall\ i \neq j \in \mathcal{N},
\end{aligned}
$$

and by rewriting the above in matrix form, we get

$$
\mathbf{J}(\alpha) = 2\alpha\mathbf{d}\mathbf{1}^T - \alpha\mathbf{A}\mathbf{D}^{-1} - (\alpha+1)\mathbf{I} \tag{B.12}
$$

which is the same as (3.11).

We now prove the eigenvalue result in (3.12). Recall that $\mathbf{A}\mathbf{D}^{-1} = \mathbf{K}^{\mathrm{srw}T}$ since $\mathbf{A}$ is a symmetric matrix. For each μ_i for $i \in \{1,\cdots,N\}$, we have

$$
\mathbf{J}(\alpha)^T\mathbf{u}_i = 2\alpha\mathbf{d}\mathbf{1}^T\mathbf{u}_i - \alpha\mathbf{K}^{\mathrm{srw}T}\mathbf{u}_i - (\alpha+1)\mathbf{u}_i.
$$

When $i = N$, that is $\mathbf{u}_i = \mathbf{u}_N = \mathbf{d}$, then we have $\mathbf{d}\mathbf{1}^T\mathbf{u}_N = \mathbf{u}_N\mathbf{1}^T\mathbf{d} = \mathbf{d} = \mathbf{u}_N$, and $\mathbf{K}^{\mathrm{srw}T}\mathbf{u}_N = \mathbf{u}_N$, and so the above equation becomes

$$
\mathbf{J}(\alpha)^T\mathbf{u}_N = (2\alpha - \alpha - \alpha - 1)\mathbf{u}_N = (-1)\mathbf{u}_N.
$$

When $i \neq N$, we have $\mathbf{d}\mathbf{1}^T\mathbf{u}_i = \mathbf{d}\mathbf{v}_N^T\mathbf{u}_i = 0$, and $\mathbf{K}^{\text{srw}T}\mathbf{u}_i = \lambda_i\mathbf{u}_i$, and we similarly have

$$\mathbf{J}(\alpha)^T\mathbf{u}_N = (0-\alpha\lambda_i-\alpha-1)\mathbf{u}_N = (\alpha(-1-\lambda_i)-1)\mathbf{u}_N.$$

Similar steps follow when we start from $\mathbf{v}_i^T\mathbf{J}(\alpha)^T$ instead, and $\mu_N = -1$, $\mu_i = (\alpha(-1-\lambda_i)-1)$ for all $i \in \{1,\cdots,N-1\}$ are the eigenvalues of $\mathbf{J}(\alpha)$ with $\mathbf{u}_i$ and $\mathbf{v}_i$ being the corresponding left and right eigenvectors. Since $(-\lambda_i - 1) < 0$ for all $i \in \{1,\cdots,N-1\}$, μ_i's follow the same ordering as λ_i's and this completes the proof. □

B.3 Appendix for Section 3.5

Proof of 3.5.2. The proof is divided into two parts, the first one for showing almost sure convergence, and the second part for proving the CLT result.

Almost sure convergence: The term $\frac{1}{n+2}$ in (3.5) is the *step-size* of the SA sequence, sometimes denoted by γ_n for all $n \geq 0$. We prove our first order result for step size sequence $\{\gamma_n\}_{n\geq 0}$ satisfying

B1 $\sum_{k\geq 0}\gamma_k = \infty$, and $\sum_{k\geq 0}\gamma^{2-\epsilon} < \infty$ for some $\epsilon \in (0,1)$.

The above assumption is only slightly stricter than the typical one where $\epsilon = 0$, such as A4 in [47] and (D) in [37] , and we show that ϵ need only be very small. Therefore in practice, B1 is nearly indistinguishable from A4 in [47] and (D) in [37]. For our choice of step-size $\gamma_n = 1/n+1$, there exists $\epsilon > 0$ small enough such that (γ_n, ϵ) satisfy B1.

We first introduce a sequence $\{\varepsilon_n\}$ where $\varepsilon_n = 2\gamma_n^\delta$ for some $\delta \in (0,1)$ (and thus $2\gamma_n < \varepsilon_n$). The condition for acceptance of $\mathbf{x}_{n+\frac{1}{2}}$ can then be rewritten as requiring $\|\mathbf{x}_{n+\frac{1}{2}} - \mathbf{x}_n\| < \epsilon_{\varsigma_n}$ along with $\mathbf{x}_{n+\frac{1}{2}} \in \mathscr{K}_{\kappa_n}$, where the former is trivially satisfied since $\|\mathbf{x}_{n+\frac{1}{2}} - \mathbf{x}_n\| \leq \gamma_{\varsigma_n}\|\delta_{X_{n+1}-\mathbf{x}_n}\| \leq 2\gamma_{\varsigma_n} < \varepsilon_{\varsigma_n}$. With this modification, update rule (3.5) is then a special case of the general SA algorithm described in Section 3.2 in [7]. The rest of the proof will then be checking that the assumptions required for applying Theorem 5.5 in [7] are satisfied.

Assumption (A1) in [7] is satisfied with $V(\mathbf{x})$ in (3.10) as the choice of Lyapunov function. A1(i)–(iv) in [7] all follow from Lemma 3.4.2, coupled with the fact that $\mathbf{x}^* = \mathbf{d} \in \text{Int}(\Sigma)$ is the unique fixed point; the set of equilibria $\mathscr{L} = \{\mathbf{d}\}$ is a singleton and therefore a closed set with non-empty interior, and the constants M_0 and M_1 can be any real numbers such that $V(\mathbf{d}) < M_0 < M_1 < \infty$.

Assumption (A2) in [7] is naturally satisfied by the construction of our SA algorithm, since $K[\mathbf{x}]$ is irreducible for any $\mathbf{x} \in \text{Int}(\Sigma)$.

We now check the set of assumptions (DRI) in [7]. The condition (DRI1) is satisfied by any ergodic Markov chain [cite], and therefore also by $K[\mathbf{x}]$ for any $\mathbf{x} \in \mathscr{K} \subset \text{Int}(\Sigma)$ with $V(i) = 1$ for all $i \in \mathscr{N}$, where $\mathscr{K}$ is any compact subset of $\text{Int}(\Sigma)$. Condition (DRI2) when translated to our setting requires checking for any compact $\mathscr{K}, \mathscr{K}' \subset \text{Int}(\Sigma)$ that

$$\sup_{\mathbf{x} \in \mathscr{K}} \|\boldsymbol{\delta}_i - \mathbf{x}\| \leq C_1, \text{ and } \sup_{(\mathbf{x},\mathbf{y}) \in \mathscr{K} \times \mathscr{K}'} \|\mathbf{y} - \mathbf{x}\|^{-\beta} \|\mathbf{y} - \mathbf{x}\| \leq C_1$$

for some $C \in \mathbb{R}$ and $\beta \in [0,1]$. This clearly holds true with $C_1 = 2$ and $\beta = 1$. The condition (DRI3) when translated to our setting requires showing for any $(\mathbf{x},\mathbf{y}) \in \mathscr{K} \times \mathscr{K}'$ that there exists $C_2 \in \mathbb{R}$ such that

$$\|\mathbf{K}[\mathbf{x}]\mathbf{u} - \mathbf{K}[\mathbf{y}]\mathbf{u}\| \leq C_2 \|\mathbf{u}\| \|\mathbf{x} - \mathbf{y}\|^{\beta}, \quad \forall \mathbf{u} \in \mathbb{R}^N, \|\mathbf{u}\| < \infty.$$

This is again clearly holds with $\beta = 1$ and for some $C_2 < \infty$, since $\mathbf{K}[\cdot]$ is not just continuous but also Lipschitz in any compact subset of $\text{Int}(\Sigma)$. Thus, update rule (3.5) satisfies (DRI) which implies (A3) in [7].

In order to satisfy (A4) in [7], we need to show that the sequences $\{\gamma_n\}_{n \geq 0}$ and $\{\varepsilon_n\}_{n \geq 0}$ are non-increasing, positive, and satisfy $\sum_{k \geq 0} \gamma_k = \infty$, $\lim_{k \to \infty} \varepsilon_k = 0$, and

$$\sum_{k \geq 0} \left\{ \gamma_k^2 + \gamma_k \epsilon^a + (\epsilon_k^{-1} \gamma_k)^p \right\} < \infty.$$

Here, we can set $0 < a < \beta = 1$ and $p \geq 2$ (these can be deduced from the drift conditions (DRI), as discussed in Section 6 of [7]). By setting $\varepsilon_n = 2\gamma_n^{\delta}$ for some small $\delta \in (0,1)$, the condition boils down to choosing $\alpha \in (0,1)$ such that

$$\sum_{k \geq 0} \gamma_k^{a\delta + 1} < \infty.^{1}$$

By setting $\epsilon = 1 - a\delta > 0$ in assumption B1, we can see that (A4) in [7] is satisfied. Note that $a\delta$ can be chosen to be very close to 1, which implies that in practice, B1 is no stricter than the square suitability assumption typically found in SA literature.

[1] This implies summability of γ_k^2 term, while that of the $(\varepsilon_k^{-1}\gamma_k)^p$ is ensured by setting $p \geq 2$ to a large enough value.

We can now apply Theorem 5.5 in [7] to obtain the almost sure convergence.

Central Limit Theorem: From Theorem 5.4 in [7], the number of truncations are always finitely many. Therefore, there exists some $n_1 > 0$ such that the sequence $\{\mathbf{x}_n\}_{n \geq n_1}$ satisfies the original update rule (3.8). Then, it suffices to show that assumptions (C), (D) and (MS) in [37] are satisfied and apply Theorem 25 therein to prove our CLT result.

Our choice of step size, $\gamma_n = \frac{1}{n+2}$ satisfies $\sum_{n \in \mathbb{N}_0} \gamma_n = \infty$ and $\sum_{n \in \mathbb{N}_0} \gamma_n^2 < \infty$. Besides,

$$\gamma_n - \gamma_{n+1} = \frac{1}{n+2} - \frac{1}{n+3} = \frac{(n+3)-(n+2)}{(n+2)(n+3)} \leq \frac{1}{(n+2)^2}.$$

Then, we have $\sum_{n \in \mathbb{N}_0} |\gamma_n - \gamma_{n+1}| \leq \sum_{n \in \mathbb{N}_0} 1/(n+2)^2 < \infty$, and (D) in [37] is satisfied.

Since our mean field $F(\mathbf{x})$ is differentiable everywhere in $\text{Int}(\Sigma)$ and therefore continuous, it is Lipschitz for all compact subsets $\mathscr{K} \subset \text{Int}(\Sigma)$, and thus also Lipschitz over some neighborhood of $\mathbf{d} \in \text{Int}(\Sigma)$. Moreover linear stability of $\mathbf{d}$ follows from the global stability of shown in Theorem 3.4.3, and all eigenvalues of $\mathbf{J}_F(\mathbf{d})$ have negative real parts. This ensures that (C) in [37] is satisfied.

Now, since $\mathbf{K}[\mathbf{x}]$ is irreducible for all $\mathbf{x} \in \text{Int}(\Sigma)$, the semigroup $\{e^{t(\mathbf{K}[\mathbf{x}]-\mathbf{I})}\}_{t \geq 0}$ of the related CTMC kernel $\mathbf{K}[\mathbf{x}]-\mathbf{I}$ converges exponentially towards $\mathbf{1}\boldsymbol{\pi}(\mathbf{x})^T$ (geometric ergodicity). Thus, for all $\mathbf{x} \in \text{Int}(\Sigma)$, or equivalently for all $\mathbf{x} \in \mathscr{K}$ for any compact $\mathscr{K} \subset \text{Int}(\Sigma)$, the matrix

$$\mathbf{Q}[\mathbf{x}] = \int_0^\infty \left(e^{t(\mathbf{K}[\mathbf{x}]-\mathbf{I})} - \mathbf{1}\boldsymbol{\pi}(\mathbf{x})^T \right) dt$$

is well defined. Moreover, it solves the Poisson equation, that is

$$\begin{aligned}(\mathbf{I}-\mathbf{K}[\mathbf{x}])\mathbf{Q}[\mathbf{x}] &= \int_0^\infty \left((\mathbf{I}-\mathbf{K}[\mathbf{x}])e^{-t(\mathbf{I}-\mathbf{K}[\mathbf{x}])} - (\mathbf{I}-\mathbf{K}[\mathbf{x}])\mathbf{1}\boldsymbol{\pi}(\mathbf{x})^T \right) dt \\ &= \int_0^\infty (\mathbf{I}-\mathbf{K}[\mathbf{x}])e^{-t(\mathbf{I}-\mathbf{K}[\mathbf{x}])} dt = \mathbf{I} - \mathbf{1}\boldsymbol{\pi}(\mathbf{x})^T = \mathbf{I} - e^{t(\mathbf{K}[\mathbf{x}]-\mathbf{I})}\Big|_0^\infty = \mathbf{I} - \mathbf{1}\boldsymbol{\pi}(\mathbf{x})^T\end{aligned}$$

where the last inequality is because $-e^{t(\mathbf{K}[\mathbf{x}]-\mathbf{I})}$ the semi-group operator of an ergodic CTMC. The solution of the Poisson equation $\mathbf{Q}[\mathbf{x}]$, as well as the state dependent update (matrix) $\mathbf{I}-\mathbf{1}\boldsymbol{\pi}(\mathbf{x})^T$, have bounded entries for all $\mathbf{x} \in \mathscr{K} \subset \text{Int}(\Sigma)$, which implies that

$$\sup_{\mathbf{x} \in \mathscr{K}, i \in \mathscr{N}} \|\mathbf{Q}[\upsilon x]^T \mathbf{e}_i\|_2 + \|(\mathbf{I}-\mathbf{1}\boldsymbol{\pi}(\mathbf{x})^T)^T \mathbf{e}_i\|_2 = \|\mathbf{Q}[\upsilon x]_{\cdot,i}\|_2 + \|\boldsymbol{\delta}_i - \boldsymbol{\pi}(\mathbf{x})\|_2 < \infty.$$

Moreover, since $\mathbf{K}[\mathbf{x}]$ and $\mathbf{Q}[\mathbf{x}]$ are continuous, they are also Lipchitz in $\mathscr{K}$. Thus fore each $\mathscr{K}$, there exists a constant $C_{\mathscr{K}}$ such that for any $\mathbf{x},\mathbf{y}\in\mathscr{K}$,

$$\sup_{i\in\mathscr{N}} \| [\mathbf{K}[\mathbf{x}]\mathbf{Q}[\mathbf{x}]]_{\cdot,i} - [\mathbf{K}[\mathbf{y}]\mathbf{Q}[\mathbf{y}]]_{\cdot,i} \|_2 \le C_{\mathscr{K}} \|\mathbf{x}-\mathbf{y}\|_2.$$

With this, we satisfy (MS) in [37] and can apply Theorem 25 therein to obtain the CLT result.

To obtain the closed form of $\mathbf{U}$, we first provide Lemma 6.3.7 in [27]), but re-written for vector-valued functions instead.

Lemma B.3.1 (Lemma 6.3.7 in [27])**.** *Let $\{X_k\}_{k\ge 0}$ be an ergodic Markov chain (reversible) with finite state space $[n]$, transition probability matrix $\mathbf{P}$ and stationary distribution $\boldsymbol{\pi}$. For any function $\mathbf{f}:[n]\to\mathbb{R}^d$, we have*

$$U(\mathbf{f}) = 2\mathbf{F}^T \mathit{diag}(\boldsymbol{\pi})\mathbf{Z}\mathbf{F} - \mathbf{F}^T \mathit{diag}(\boldsymbol{\pi})\mathbf{F} - \mathbf{F}^T\boldsymbol{\pi}\boldsymbol{\pi}^T\mathbf{F}, \tag{B.13}$$

where $U(\mathbf{f})$ is the asymptotic covariance matrix for function $\mathbf{f}$, matrix $\mathbf{F}$ is given by $\mathbf{F}\triangleq[\mathbf{f}(1),\cdots,\mathbf{f}(n)]^T$, and $\mathbf{Z}\triangleq(\mathbf{I}-\mathbf{P}+\mathbf{1}\boldsymbol{\pi}^T)^{-1}$. Moreover, since $\mathbf{P}$ is reversible, we have (equation 6.34 in [27])

$$U(\mathbf{f}) = \sum_{k=1}^{n-1} \frac{1+\lambda_k}{1-\lambda_k}\mathbf{F}^T\mathbf{u}_k\mathbf{u}_k^T\mathbf{F}, \tag{B.14}$$

where $\mathbf{u}_k$ are the left eigenvectors of $\mathbf{P}$ with $\mathbf{u}_n=\boldsymbol{\pi}$.

For our update rule (3.8), we have $\mathbf{F}=\mathbf{I}-\mathbf{1}\mathbf{d}^T$.[2] The asymptotic covariance matrix $\mathbf{U}$ is the same for all $\alpha\ge 0$, since is given with respect to $\mathbf{F}$ and the transition kernel $\mathbf{P}=\mathbf{K}[\mathbf{d}]=\mathbf{K}^{\mathrm{srw}}=\mathbf{D}^{-1}\mathbf{A}$ (that is $\alpha=0$ case), which means that $\boldsymbol{\pi}=\mathbf{d}$. Thus, we can write down $\mathbf{U}$ as

$$\mathbf{U} = \sum_{k=1}^{N-1}\frac{1+\lambda_k}{1-\lambda_k}(\mathbf{I}-\mathbf{d}\mathbf{1})\mathbf{u}_k\mathbf{u}_k^T(\mathbf{I}-\mathbf{1}\mathbf{d}^T) = \sum_{k=1}^{N-1}\frac{1+\lambda_k}{1-\lambda_k}\mathbf{u}_k\mathbf{u}_k^T \tag{B.15}$$

where the last equality is because $\mathbf{u}_N=\mathbf{d}$ and $\mathbf{v}_N=\mathbf{1}$, and since $\mathbf{u}_i\mathbf{v}_j=0$ for all $i\ne j$. □

Proof of Proposition 3.5.3. Proposition 3.4.4 allows us to write down the spectral decomposition of $e^{t(\mathbf{J}(\alpha)+\mathbf{I}/2)}$ as

$$e^{t(\mathbf{J}(\alpha)+\mathbf{I}/2)} = \sum_{i\in\mathscr{N}} e^{t(\mu_i+1/2)}\mathbf{u}_i\mathbf{v}_i^T = e^{-1/2}\mathbf{u}_N\mathbf{v}_N^T + \sum_{i=1}^{N-1} e^{t(\alpha(-1-\lambda_i)-1/2)}\mathbf{u}_i\mathbf{v}_i^T. \tag{B.16}$$

[2] The map $\mathbf{f}$ can be thought as a function to be estimated by sampled at X_{n+1} and corresponding to the update rule evaluated at $\mathbf{x}_n=\mathbf{d}$, that is, $\mathbf{F}_{X_{n+1},\cdot}=\mathbf{f}(X_{n+1})=\boldsymbol{\delta}_{X_{n+1}}-\mathbf{d}$.

Substituting (B.15) and (B.16) in (3.16), we get

$$\begin{aligned}\mathbf{V}(\alpha) &= \left(e^{-1/2}\mathbf{u}_N\mathbf{v}_N^T + \sum_{i=1}^{N-1} e^{t(\alpha(-1-\lambda_i)-1/2)}\mathbf{u}_i\mathbf{v}_i^T \right)\left(\sum_{k=1}^{N-1} \frac{1+\lambda_k}{1-\lambda_k}\mathbf{u}_k\mathbf{u}_k^T \right)\left(e^{-1/2}\mathbf{u}_N\mathbf{v}_N^T + \sum_{i=1}^{N-1} e^{t(\alpha(-1-\lambda_i)-1/2)}\mathbf{u}_i\mathbf{v}_i^T \right) \\ &= \left(\sum_{i=1}^{N-1} e^{t(\alpha(-1-\lambda_i)-1/2)}\mathbf{u}_i\mathbf{v}_i^T \right)\left(\sum_{k=1}^{N-1} \frac{1+\lambda_k}{1-\lambda_k}\mathbf{u}_k\mathbf{u}_k^T \right)\left(\sum_{i=1}^{N-1} e^{t(\alpha(-1-\lambda_i)-1/2)}\mathbf{u}_i\mathbf{v}_i^T \right) \\ &= \sum_{i=1}^{N-1} e^{2t(\alpha(-1-\lambda_i)-1/2)}\frac{1+\lambda_i}{1-\lambda_i}\mathbf{u}_i\mathbf{u}_i^T\end{aligned}$$

where all the equalities follow from orthonormality of the left and right eigenvectors.

For any vector $\mathbf{x}\in\mathbb{R}^N$, we then have

$$\mathbf{x}^T\mathbf{V}(\alpha)\mathbf{x} = \sum_{i=1}^{N-1} e^{2t(\alpha(-1-\lambda_i)-1/2)}\frac{1+\lambda_i}{1-\lambda_i}\mathbf{x}^T\mathbf{u}_i\mathbf{u}_i^T\mathbf{x} < \sum_{i=1}^{N-1} e^{2t(-1/2)}\frac{1+\lambda_i}{1-\lambda_i}\mathbf{x}^T\mathbf{u}_i\mathbf{u}_i^T\mathbf{x} = \mathbf{x}^T\mathbf{V}(0)\mathbf{x},$$

where the inequality is because $\lambda_i\in(-1,1)$, and as a result, $\alpha(-\lambda_i-1)<0$ for all $i\in\{1,\cdots,N-1\}$. In fact, the ordering is monotone in $\alpha>0$. This completes the proof. □

Appendix C

Appendix for Chapter 4

C.1 Basic Definitions and Results from Matrix Theory

We first provide some well known results surrounding irreducible square matrices.

Definition C.1.1. *[89] A square matrix* $\mathbf{A}$ *is* ***reducible*** *if there exists a permutation matrix* $\mathbf{P}$ *such that* $\mathbf{P}^T\mathbf{A}\mathbf{P}$ *is a block diagonal matrix. If no such permutation matrix exists, we say that* $\mathbf{A}$ *is* ***irreducible****.*

One way to check if a matrix is irreducible is by observing the underlying directed graph, where there is an edge between two nodes only if $a_{ij} \neq 0$. The matrix A is irreducible if and only if this underlying directed graph is strongly connected.

Definition C.1.2. *[23] A* ***M-matrix*** *is a matrix with non-positive off-diagonal elements with eigenvalues whose real parts are non-negative.*

We use the following well known result for non-negative, irreducible matrices heavily throughout the chapter.

Theorem C.1.3. *(Perron-Frobenius)[89] Let* $\mathbf{A}$ *be a non-negative, irreducible matrix. Then,* $\lambda(\mathbf{A})$ *is a strictly positive real number, and the corresponding eigenvector* $\mathbf{v}$ *where* $\mathbf{A}\mathbf{v} = \lambda(\mathbf{A})\mathbf{v}$ *is also strictly positive. We call* $\lambda(\mathbf{A}) > 0$ *and* $\mathbf{v} \gg \mathbf{0}$ *the* ***PF eigenvalue*** *and* ***PF eigenvector*** *of the matrix respectively.*

The following result is on irreducible M-matrices.

Lemma C.1.4. *[23] Given an irreducible and non-singular M-matrix* $\mathbf{M}$*, its inverse* $\mathbf{M}^{-1}$ *has strictly positive entries.*

C.2 Definitions and results from ODE literature

We use the following definitions and results from the ODE literature throughout the chapter.

Definition C.2.1. *The 'flow' of a dynamical system in a metric space X is a map $\phi : X\times\mathbb{R}\to X$ such that for any $x_0\in X$ and all $s,t\in\mathbb{R}$, we have $\phi_0(x_0)=x_0$ and $\phi_s\left(\phi_t(x_0)\right)=\phi_{t+s}(x_0)$.*

Definition C.2.2. *A flow $\phi : X\times\mathbb{R}\to X$ is **positively invariant** in set $P\subset X$ if for every $x_0\in P$, $\phi_t(x_0)\in P$ for all $t>0$.*

Definition C.2.3. *Given a flow ϕ, an 'equilibrium' or a 'fixed point' of the system is a point $x^*\in X$ such that $\{x^*\}$ is a positively invariant set. For the ODE system $\dot{x}=F(x)$, we have $F(x^*)=0$ at the equilibrium.*

For an equilibrium point $x^*\in X$ we say that the trajectory starting at $x_0\in X$ *converges* to x^* if $\lim_{t\to\infty}\phi_t(x_0)=x^*$. The following result is true for stable fixed points of the ODE system from Definition C.2.1.

Proposition C.2.4. *[100] Let $\mathbf{J}F(x_0)$ be the Jacobian of the ODE system evaluated at a fixed point x_0 and assume it to be an irreducible matrix. Let $\lambda(\mathbf{J}F(x_0))<0$ and suppose the corresponding eigenvalue $\mathbf{v}$ is strictly positive ($\mathbf{v}\gg\mathbf{0}$). Then, there exists an $\epsilon>0$ such that $F(x_0+r\mathbf{v})\ll 0$ for all $r\in(0,\epsilon]$ and $F(x_0+r\mathbf{v})\gg 0$ for all $r\in(0,-\epsilon]$*[1].

C.3 DFR Processes as Non-Linear Recovery Rates

In this appendix, we form the connection between *failure rates* from reliability theory [106], and the infection duration at any node in SIS type epidemics. To this end, we start by formally defining the term *failure rate*.

Definition C.3.1. *[106] Let $T>0$ be any continuous random variable with distribution $F_T(s)=\mathbb{P}(T\le s)$, and density function $f_T(s)$ for all $s>0$, with $\bar{F}_T(s)=1-F_T(s)=\mathbb{P}(T>s)$. Then, the failure rate at any given time $s>0$ is defined as*

$$r_T(s)\triangleq\frac{f_T(s)}{\bar{F}_T(s)}. \tag{C.1}$$

[1] In other words eigenvector $\mathbf{v}$ is tangent to the stable manifold of the ODE system at the stable fixed points x_0.

We say T has a decreasing/increasing failure rate (DFR/IFR) if $r_T(s)$ is a decreasing/increasing function of $s > 0$.

When T is the lifetime of a system, the DFR case corresponds to the system aging *negatively*. This means that as time elapses, the residual time (time till the system fails) is more likely to increase rather than decrease. T could also have an interpretation in the context of node recovery. For the linear SIS epidemic model as in (4.1), consider an infected node $i \in \mathcal{N}$ and define $T \triangleq$ time taken for node i to recover (random), with $f_T(s)$ and $\bar{F}_T(s)$ as in Definition C.3.1. Loosely speaking, we can ignore the infection rate terms in (4.1) to take a closer look at the recovery process via the ODE

$$\dot{x}_i(s) = -\delta\, x_i(s), \tag{C.2}$$

with the initial condition $x_i(0) = 1$ (implying that node i is last infected at time $s = 0$). The ODE (C.2) has an exact solution for all $s > 0$, given by $x_i(s) = e^{-\delta s}$. This solution allows us to interpret x_i as the cumulative distribution function (CCDF) of an exponential random variable[2] with rate $\delta > 0$. Using this interpretation, we have $x_i(s) = P(T > s) = \bar{F}_T(s)$, and $-\dot{x}_i(s) = f_T(s)$. (C.2) can then be rewritten as

$$r_T(s) = \frac{-\dot{x}_i(s)}{x_i(s)} = \delta,$$

for any $s > 0$. T is thus exponentially distributed, and has a *constant failure rate* (it is both DFR and IFR).

We now consider the case where the random variable T is defined for the more general SIS epidemic model with non-linear recovery rate $q_i(x_i)$ for node i.[3] Ignoring the infection rate terms in (4.5) like before, we obtain

$$\dot{x}_i(s) = -q_i(x_i(s)), \tag{C.3}$$

retaining the previous interpretation of x_i as the CCDF of T. This can be further rearranged to obtain an expression for the failure rate as

$$r_T(s) = \frac{-\dot{x}_i(s)}{x_i(s)} = \frac{q_i(x_i(s))}{x_i(s)}$$

[2] When $T \sim \exp(\delta)$, we have $\bar{F}_T(s) = P(T > s) = e^{-\delta s}$.

[3] Note that this is the special case where q_i is only a function of x_i, not of x_j for neighbors j of node i.

for any $s > 0$. From Definition C.3.1 we know T is DFR if $r_T(s)$ is decreasing in $s > 0$. Supposing q_i is such that T is indeed DFR, $\log(r_T(s))$ is also decreases in s, and we get

$$\frac{d}{ds}\log(r_T(s)) = \frac{q_i'(x_i(s))\dot{x}_i(s)}{q(x_i(s))} - \frac{\dot{x}_i(s)}{x_i(s)} \leq 0,$$

where $q_i'(x_i(s))$ denotes the derivative with respect to x_i. Since $\dot{x}_i(s) = -q_i(x_i(s))$ from (C.3) and $q_i'(x(s)) \geq 0$ from (A3), rearranging the previous equation gives us following the condition for T to be DFR

$$x_i q_i'(x_i) - q_i(x_i) \geq 0. \tag{C.4}$$

In (C.4), the (s) notation has been suppressed for clarity. Since $q_i(0) = 0$, the convexity of q_i with respect to x_i implies (C.4).

Roughly speaking, the DFR case (which also includes linear recovery rates as in (4.1)) is a subclass of recovery rate functions $q_i(\mathbf{x})$ satisfying assumptions (A1)–(A5). Even though the above steps may not be exact, they provide intuition on how infections which fester and grow worse with time form part of our modelling assumptions in Section 4.2.

C.4 Results from MDS and Cooperative Systems

Definition C.4.1. *[57, 116, 119] A flow ϕ is said to be **monotone** if for all $\mathbf{x}, \mathbf{y} \in \mathbb{R}^n$ such that $\mathbf{x} \leq_K \mathbf{y}$ and any $t \geq 0$, we have $\phi_t(\mathbf{x}) \leq_K \phi_t(\mathbf{y})$.*

*If the flow represents the solution of an ODE system, we say that the ODE system is **co-operative**.*

Definition C.4.2. *Consider the system* (4.9) *and let $\mathbf{J}F(\mathbf{x}) \triangleq \left[d f_i(\mathbf{x})/d x_j\right]$ be the Jacobian of the right hand side evaluated at any point $\mathbf{x} \in \mathbb{R}^n$. We say that* (4.9) *is an **irreducible ODE** in set $D \in \mathbb{R}^n$ if for all $\mathbf{x} \in D$, $\mathbf{J}F(\mathbf{x})$ is an irreducible matrix.*

Definition C.4.3. *[116, 118, 119] The flow ϕ is said to be **strongly monotone** if it is monotone, and for all $\mathbf{x}, \mathbf{y} \in \mathbb{R}^n$ such that $\mathbf{x} <_K \mathbf{y}$, and time $t \geq 0$, we have $\phi_t(\mathbf{x}) \ll_k \phi_t(\mathbf{y})$.*

Theorem C.4.4. *[116, 118, 119] Let* (4.9) *be irreducible and co-operative in some set $D \subset \mathbb{R}^n$. Then the solution ϕ (restricted to $t \geq 0$) is strongly monotone.*

As part of the main result of monotone dynamical systems, trajectories of strongly monotone systems, starting from almost anywhere (in the measure theoretic sense) in the

state space, converge to the set of equilibrium points [58, 121, 63, 119]. However, often the systems are strongly monotone only in the interior of the state spaces instead of the entirety of the state space. In such cases, the following results are useful.

Proposition C.4.5. *(Proposition 3.2.1 in [118]) Consider the ODE system* (4.9) *which is cooperative in a compact set $D \subset \mathbb{R}^n$ with respect to some cone-ordering, and let $<_r$ stand for any of the order relations $\leq_K, <_K, \ll_K$. Then, $P_+ \triangleq \{\mathbf{x} \in D \mid \mathbf{0} <_r F(\mathbf{x})\}$ and $P_- \triangleq \{\mathbf{x} \in D \mid F(\mathbf{x}) <_r \mathbf{0}\}$ are positively invariant, and the trajectory $\{\phi_t(\mathbf{x})\}_{t \geq 0}$ for any point $\mathbf{x} \in P_+$ or $\mathbf{x} \in P_-$ converges to an equilibrium.*

Theorem C.4.6. *(Theorem 4.3.3 in [118]) Let* (4.9) *be cooperative (with respect to some cone-ordering $\leq_K$) in a compact set $D \subset \mathbb{R}^n$ and let $\mathbf{x}_0 \in D$ be an equilibrium point. Suppose that $s \triangleq \lambda(\mathbf{J}F(\mathbf{x}_0)) > 0$ (i.e. $\mathbf{x}_0$ is an unstable fixed point) and there is an eigenvector $\mathbf{v} \gg_K \mathbf{0}$ such that $\mathbf{J}F(\mathbf{x}_0)\mathbf{v} = s\mathbf{v}$. Then, there exists $\epsilon_0 \in (0, \epsilon]$ and another equilibrium point $\mathbf{x}_e$ such that for each $r \in (0, \epsilon_0]$, the solution $\phi_t(\mathbf{x}_r)$ has the following properties:*

(1) $\mathbf{x}_r \ll_K \phi_{t_1}(\mathbf{x}_r) \ll_K \phi_{t_2}(\mathbf{x}_r) \ll_K \mathbf{x}_e$, *for any* $0 < t_1 < t_2$.

(2) $d\phi_t(\mathbf{x}_r)/dt \gg_K \mathbf{0}$, *for any* $t > 0$.

(3) $\phi_t(\mathbf{x}_r) \to \mathbf{x}_e$, *as* $t \to \infty$.

C.5 Proofs of the results in Section 4.3

Proof of Proposition 4.3.3. To prove that system (4.6) is co-operative with respect to the positive orthant, we show that it satisfies Kamke's condition in (4.10). Differentiating the right hand side of (4.5) with respect to x_j, we get

$$\frac{\partial \bar{f}_i(\mathbf{x})}{\partial x_j} = (1 - x_i)\frac{\partial f_i(x)}{\partial x_j} = \frac{\partial q_i(\mathbf{x})}{\partial x_j}.$$

This corresponds to the $(i\,j)$'th off-diagonal entry of the Jacobian $\mathbf{J}_{\bar{F}}(\mathbf{x})$ evaluated at $\mathbf{x} \in [0,1]^N$. It is non-negative for any $i \neq j \in \mathcal{N}$ since $(1 - x_i) \geq 0$ and due to assumption (A3), and the ODE (4.6) is therefore co-operative in $[0,1]^N$ with respect to the regular cone ordering.

From assumption (A3), $\mathbf{J}_{\bar{F}}(\mathbf{x})_{ij}$ is also strictly positive for any $\mathbf{x} \in (0,1)^N$ whenever $a_{ij} > 0$. This means that $\mathbf{J}_{\bar{F}}(\mathbf{x})$, and as a consequence the ODE system, is irreducible for any $\mathbf{x} \in (0,1)^N$. □

To derive the convergence properties of the non-linear SIS model, we make use of a result form [72], rewritten below in a simpler form suitable for our setting.

Theorem C.5.1. *(Theorem 4 in [72]) Consider a generic ODE system* (4.9) *invariant to some subset* $S \subset \mathbb{R}^N_+$*, and let* $\mathbf{J}_{\bar{F}}$ *stand for its Jacobian matrix. Suppose that:*

(C1) $f_i(\mathbf{x}) \geq 0$ *for all* $\mathbf{x} \geq 0$ *with* $x_i = 0$*;*

(C2) for all $\mathbf{x} \gg \mathbf{0}$ *in* S*,* $\alpha \in (0,1)$*, it satisfies* $\mathbf{J}_{\bar{F}}(\mathbf{x})_{ij} \leq \mathbf{J}_{\bar{F}}(\alpha\mathbf{x})_{ij}$ *for all* $i, j \in \mathcal{N}$*, with strict inequality for at least one pair of* i, j*;*

(C3) for all $\mathbf{u} \ll \mathbf{w}$ *in* S*, it satisfies* $\mathbf{J}_{\bar{F}}(\mathbf{w}) \leq \mathbf{J}_{\bar{F}}(\mathbf{u})$*;*

(C4) it is co-operative in S *with respect to the regular ordering relation, and irreducible in Int*(S)*.*

Then, exactly one of the following outcomes occurs:

(i) $\phi_t(\mathbf{x})$ *is unbounded for all* $\mathbf{x} \in S \setminus \{\mathbf{0}\}$*;*

(ii) $\phi_t(\mathbf{x}) \to \mathbf{0}$ *as* $t \to \infty$*, for all* $\mathbf{x} \in S \setminus \{\mathbf{0}\}$*;*

(iii) There exists a unique, strictly positive fixed point $\mathbf{x}^* \gg \mathbf{0}$ *such that* $\phi_t(\mathbf{x}) \to \mathbf{x}^*$ *as* $t \to \infty$*, for all* $\mathbf{x} \in S \setminus \{\mathbf{0}\}$*.*

We now use the above to prove Theorem 4.3.4.

Proof of Theorem 4.3.4. We prove Theorem 4.3.4 by showing that it satisfies conditions (C1)-(C4) of Theorem C.5.1, and then performing stability analysis to evaluate conditions for each of the three possible outcomes therein.

From Proposition (4.3.3), we know that (4.6) already satisfies (C4). The right hand side of (4.5) satisfies (C1) because $q_i(x_i) = 0$ when $x_i = 0$, and because $(1 - x_i)$ and $f_i(\mathbf{x})$ are all non-negative for any $\mathbf{x} \in [0,1]^N$. To check whether (C2) and (C3) is satisfied, observe that from assumptions (A2)–(A5), we have

$$\mathbf{J}_F(\mathbf{u}) > \mathbf{J}_F(\mathbf{w}) \tag{C.5}$$

$$\mathbf{J}_Q(\mathbf{u}) < \mathbf{J}_Q(\mathbf{w}) \tag{C.6}$$

for all $\mathbf{u} < \mathbf{w}$.[4] Here, $\mathbf{J}_Q$ is a diagonal matrix since $\partial q_i / \partial x_j = 0$ for all $i \neq j \in \mathcal{N}$.

Denote by $\mathbf{J}_{\bar{F}}$ the Jacobian matrix of system (4.6). Note that for any point $\mathbf{x} \in [0,1]^N$, we have

$$\mathbf{J}_{\bar{F}}(\mathbf{x}) = \text{diag}(\mathbf{1} - \mathbf{x})\mathbf{J}_F(\mathbf{x}) - \text{diag}(F(\mathbf{x})) - \mathbf{J}_Q(\mathbf{x}) \tag{C.7}$$

Combining the above with (C.5) and (C.6), we have for any points $\mathbf{u} < \mathbf{w}$ that

$$\begin{aligned}
\mathbf{J}_{\bar{F}}(\mathbf{u}) &= \text{diag}(\mathbf{1} - \mathbf{u})\mathbf{J}_F(\mathbf{u}) - \text{diag}(F(\mathbf{u})) - \mathbf{J}_Q(\mathbf{u}) \\
&> \text{diag}(\mathbf{1} - \mathbf{w})\mathbf{J}_F(\mathbf{w}) - \text{diag}(F(\mathbf{u})) - \mathbf{J}_Q(\mathbf{w}) \\
&\geq \text{diag}(\mathbf{1} - \mathbf{w})\mathbf{J}_F(\mathbf{w}) - \text{diag}(F(\mathbf{w})) - \mathbf{J}_Q(\mathbf{w}) \\
&= \mathbf{J}_{\bar{F}}(\mathbf{w}),
\end{aligned}$$

where the first inequality is due to $(\mathbf{1} - \mathbf{u}) > (\mathbf{1} - \mathbf{w})$ and (C.5) and (C.6). The second inequality is from the non-negativity and monotonicity assumptions (A2) and (A3) implying $F(\mathbf{u}) \leq F(\mathbf{w})$. Since $\mathbf{J}_{\bar{F}}(\mathbf{u}) > \mathbf{J}_{\bar{F}}(\mathbf{w})$ for any $\mathbf{u} < \mathbf{w}$, this is enough to satisfy both conditions (C2) and (C3).

Since system (4.6) satisfies (C1)–(C4), Theorem C.5.1 applies. Since the system is invariant in $[0,1]^N$, which is a bounded subset of $\mathbb{R}^N$, outcome (i) of Theorem C.5.1 never occurs. From assumption (A1), the vector $\mathbf{0} = [0, \cdots, 0]^T$ (the virus-free equilibrium) is always a fixed point of the system. We now find conditions under which trajectories of (4.6) starting from anywhere in $[0,1]^N \setminus \{\mathbf{0}\}$ converge to either zero, or to a unique strictly positive fixed point (outcomes (ii) and (iii) in Theorem C.5.1 respectively), by check the stability properties of the system.

The virus-free fixed point zero is unstable [100] when $\lambda(\mathbf{J}_{\bar{F}}(\mathbf{0})) = \lambda(\mathbf{J}_F(\mathbf{0}) - \mathbf{J}_Q(\mathbf{0})) \leq 0$. Under this condition, outcome (ii) in Theorem C.5.1 is not possible, and there exists a unique, strictly positive fixed point $\mathbf{x}^* \gg \mathbf{0}$ which is globally asymptotically stable in $[0,1]^N \setminus \{\mathbf{0}\}$. Conversely when zero is a stable fixed point, that is when $\lambda(\mathbf{J}_{\bar{F}}(\mathbf{0})) = \lambda(\mathbf{J}_F(\mathbf{0}) - \mathbf{J}_Q(\mathbf{0})) > 0$, it is globally attractive. □

[4] Here, the ordering between matrices $\mathbf{M}^a < \mathbf{M}^b$ means $\mathbf{M}^a_{ij} \leq \mathbf{M}^b_{ij}$ with the inequality being strict for at least one pair of i, j.

C.6 Proofs of the Main Results

Throughout this Section, we use $\phi_t(\mathbf{x}_0, \mathbf{y}_0)$ to represent the solution of (4.8) at time $t \geq 0$, starting from $(\mathbf{x}_0, \mathbf{y}_0) \in D$. We will need the following results to prove the theorems from Section 4.4.2.

Proposition C.6.1. *Starting from any point $D \setminus \{(\mathbf{0},\mathbf{0})\}$, trajectories of* (4.8) *converge to the set*

$$Z \triangleq \left\{(\mathbf{u},\mathbf{w}) \in D \mid (\mathbf{0},\mathbf{y}^*) \leq_K (\mathbf{u},\mathbf{w}) \leq_K (\mathbf{x}^*,\mathbf{0})\right\}.$$

Proof. For any $(\mathbf{r},\mathbf{s}) \in D \setminus \{(\mathbf{0},\mathbf{0})\}$, there exists points $\mathbf{x},\mathbf{y} \in [0,1]^N$ such that $(\mathbf{0},\mathbf{y}) \leq_K (\mathbf{r},\mathbf{s}) \leq_K (\mathbf{x},\mathbf{0})$. Then, from Definition C.4.1 of a monotone system, we have $\phi_t(\mathbf{0},\mathbf{y}) \leq_K \phi_t(\mathbf{r},\mathbf{s}) \leq_K \phi_t(\mathbf{x},\mathbf{0})$ for any $t > 0$. Since $\phi_t(\mathbf{x},\mathbf{0}) \to (\mathbf{x}^*,\mathbf{0})$ and $\phi_t(\mathbf{0},\mathbf{y}) \to (\mathbf{0},\mathbf{y}^*)$, we get $(\mathbf{0},\mathbf{y}^*) \leq_K \lim_{t\to\infty} \phi_t(\mathbf{r},\mathbf{s}) \leq_K (\mathbf{x}^*,\mathbf{0})$. Thus the trajectory $\left\{\phi_t(\mathbf{r},\mathbf{s})\right\}_{t\geq 0}$ converges to Z, completing the proof. □

Since the set Z depends on $\mathbf{x}^*$ and $\mathbf{y}^*$, the fixed points of systems (4.13) and (4.14), and we can determine when these fixed points are positive or zero, Proposition C.6.1 helps us to quickly point out a subset of the state space to which trajectories starting from any point in $D \setminus \{(\mathbf{0},\mathbf{0})\}$ converge.

Proof of Theorem 4.4.2. When $\lambda(\mathbf{J}_G(\mathbf{0}) - \mathbf{J}_R(\mathbf{0})) \leq 0$ and $\lambda(\mathbf{J}_H(\mathbf{0}) - \mathbf{J}_S(\mathbf{0})) \leq 0$, we know from Theorem 4.3.4 that $\mathbf{x}^* = \mathbf{y}^* = 0$. Therefore, trajectories of (4.8) starting from any point in $D \setminus \{(\mathbf{0},\mathbf{0})\}$ converge to the set $Z \triangleq \{(\mathbf{u},\mathbf{w}) \in D \mid (\mathbf{0},\mathbf{0}) \leq_K (\mathbf{u},\mathbf{w}) \leq_K (\mathbf{0},\mathbf{0})\} = \{(\mathbf{0},\mathbf{0})\}$. Hence, the virus-free equilibrium is globally asymptotically stable in D, which completes the proof. □

Proposition C.6.1 can also be applied to show that $(\mathbf{x}^*,\mathbf{0})$ where $\mathbf{x}^* \gg \mathbf{0}$ is globally attractive when $\lambda(\mathbf{J}_G(\mathbf{0}) - \mathbf{J}_R(\mathbf{0})) > 0$ and $\lambda(\mathbf{J}_H(\mathbf{0}) - \mathbf{J}_S(\mathbf{0})) \leq 0$. This is because from Theorem 4.3.4, we know that $\mathbf{x}^* \gg \mathbf{0}$ and $\mathbf{y}^* = \mathbf{0}$. We then have $Z \triangleq \{(\mathbf{u},\mathbf{w}) \in D \mid (\mathbf{0},\mathbf{0}) \leq_K (\mathbf{u},\mathbf{w}) \leq_K (\mathbf{x}^*,\mathbf{0})\}$, implying that the system (4.8) ultimately reduces to the single SIS system (4.13), which we know globally converges to $\mathbf{x}^*$. By a symmetric argument, we also have that $(\mathbf{0},\mathbf{y}^*)$ where $\mathbf{y}^* \gg \mathbf{0}$ is globally attractive when $\lambda(\mathbf{J}_G(\mathbf{0}) - \mathbf{J}_R(\mathbf{0})) \leq 0$ and $\lambda(\mathbf{J}_H(\mathbf{0}) - \mathbf{J}_S(\mathbf{0})) > 0$. Therefore these cases are easily analyzed by applying Proposition C.6.1 in conjunction with Theorem 4.3.4. In terms of the linear bi-virus model whose parameters are easier to visualize, values of τ_1 and τ_2 which satisfy these conditions, lie in regions R2 and R3 of Figure 4.3(b) and we henceforth exclude them from our analysis, considering only those values of τ_1 and τ_2 for which $\tau_1\lambda(\mathbf{A}) > 1$ and $\tau_2\lambda(\mathbf{B}) > 1$ always holds; equivalently considering only the cases where $\lambda(\mathbf{J}_G(\mathbf{0}) - \mathbf{J}_R(\mathbf{0})) > 0$

and $\lambda(\mathbf{J}_H(\mathbf{0})-\mathbf{J}_S(\mathbf{0}))>0$ always hold for nonlinear infection and recovery rates. Thus, $\mathbf{x}^*$ and $\mathbf{y}^*$ are henceforth implied to be strictly positive vectors.

Before formally proving Theorems 4.4.3 and 4.4.4, we provide some additional constructions and notations which will help simplify the proofs. As in the proof of Theorem 4.3.4, the Jacobians $\mathbf{J}F^x(\mathbf{x})$ and $\mathbf{J}F^y(\mathbf{y})$ of systems (4.13) and (4.14), respectively, are

$$\mathbf{J}F^x(\mathbf{x}) = \operatorname{diag}(\mathbf{1}-\mathbf{x})\mathbf{J}_G(\mathbf{x}) - \operatorname{diag}(G(\mathbf{x})) - \mathbf{J}_R(\mathbf{x}),$$
$$\mathbf{J}F^y(\mathbf{y}) = \operatorname{diag}(\mathbf{1}-\mathbf{y})\mathbf{J}_H(\mathbf{y}) - \operatorname{diag}(H(\mathbf{y})) - \mathbf{J}_S(\mathbf{y}),$$

for all $\mathbf{x},\mathbf{y}\in[0,1]^N$. Now recall the Jacobian $\mathbf{J}_{\bar{G}\bar{H}}(\mathbf{x},\mathbf{y})$ of the bi-virus ODE (4.8) from (4.12). When evaluated at $(\mathbf{x}^*,\mathbf{0})$ and at $(\mathbf{0},\mathbf{y}^*)$, we get

$$\mathbf{J}_{\bar{G}\bar{H}}(\mathbf{x}^*,\mathbf{0}) = \begin{bmatrix} \mathbf{J}F^x(\mathbf{x}^*) & \mathbf{K} \\ \mathbf{0} & \mathbf{J}_y \end{bmatrix} \tag{C.8}$$

where $\mathbf{K}=-\operatorname{diag}(G(v\,x^*))$, $\mathbf{J}_y=\operatorname{diag}(\mathbf{1}-\mathbf{x}^*)\mathbf{J}_H(\mathbf{0})-\mathbf{J}_S(\mathbf{0})$, and

$$\mathbf{J}_{\bar{G}\bar{H}}(\mathbf{0},\mathbf{y}^*) = \begin{bmatrix} \mathbf{J}_x & \mathbf{0} \\ \mathbf{L} & \mathbf{J}F^y(\mathbf{y}^*) \end{bmatrix} \tag{C.9}$$

where $\mathbf{L}=-\operatorname{diag}(H(\mathbf{y}^*))$, $\mathbf{J}_x=\operatorname{diag}(\mathbf{1}-\mathbf{y}^*)\mathbf{J}_G(\mathbf{0})-\mathbf{J}_R(\mathbf{0})$. This leads us to the following proposition, where the ordering $\leq_K$ ($<_K, \ll_K$) stands for the south east cone-ordering.

Proposition C.6.2. *When* $\lambda\big(\mathbf{S}_{\mathbf{y}^*}\mathbf{J}_G(\mathbf{0})-\mathbf{J}_R(\mathbf{0})\big)>0$, *we have* $\lambda(\mathbf{J}_{\bar{G}\bar{H}}(0,\mathbf{y}^*))=\lambda(\mathbf{J}_x)>0$, *and the corresponding eigenvector* $(\mathbf{u},\mathbf{v})\in\mathbb{R}^{2N}$ *of* $\mathbf{J}_{\bar{G}\bar{H}}(0,\mathbf{y}^*)$ *satisfies* $(\mathbf{u},\mathbf{v})\gg_K(\mathbf{0},\mathbf{0})$.

Proof. First, recall that $\mathbf{y}^*\gg\mathbf{0}$ is the asymptotically stable fixed point of (4.14). This implies that the real parts of all eigenvalues of the Jacobian $\mathbf{J}F^y(\mathbf{y}^*)$ of (4.14) evaluated at $\mathbf{y}^*$ are negative. Since $\mathbf{J}F^y(\mathbf{y}^*)$ is an irreducible matrix as discussed in Section 4.4.1, with non-negative off-diagonal elements, its PF eigenvalue (obtained by perturbing with a large multiple of the identity matrix) is real and negative, that is $\lambda(\mathbf{J}F^y(\mathbf{y}^*))<0$.

From the assumption, we have $\lambda\big(\mathbf{S}_{\mathbf{y}^*}\mathbf{J}_G(\mathbf{0})-\mathbf{J}_R(\mathbf{0})\big)=\lambda(\mathbf{J}_x)>0$. Since $\mathbf{J}_{\bar{G}\bar{H}}(\mathbf{0},\mathbf{y}^*)$ is a block triangle matrix, we have $\lambda(\mathbf{J}_{\bar{G}\bar{H}}(\mathbf{0},\mathbf{y}^*))=\max\big\{\lambda(J_x),\lambda(\mathbf{J}F^y(\mathbf{y}^*))\big\}$, and since $\lambda(\mathbf{J}F^y(\mathbf{y}^*))<0$, we obtain $\lambda(\mathbf{J}_{\bar{G}\bar{H}}(\mathbf{0},\mathbf{y}^*))=\lambda(\mathbf{J}_x)>0$. Then, the corresponding eigenvector $(\mathbf{u},\mathbf{v})$ satisfies

$$\mathbf{J}_x\mathbf{u}=\lambda(\mathbf{J}_x)\mathbf{u} \quad \text{and} \quad \mathbf{L}\mathbf{u}+\mathbf{J}F^y(\mathbf{y}^*)\mathbf{v}=\lambda(\mathbf{J}_x)\mathbf{v}.$$

From the first equation, we can tell that $\mathbf{u}$ is the eigenvector of $\mathbf{J}_x$ corresponding to its PF eigenvalue, and thus satisfies $\mathbf{u} \gg \mathbf{0}$. Now recall that $\mathbf{J}F^y(\mathbf{y}^*)$ had eigenvalues with strictly negative real parts. $\lambda(\mathbf{J}_x)\mathbf{I} - \mathbf{J}F^y(\mathbf{y}^*)$ is then a matrix with eigenvalues having strictly positive real parts (since $\lambda(\mathbf{J}_x) > 0$). The matrix $\mathbf{M} \triangleq \lambda(\mathbf{J}_x)\mathbf{I} - \mathbf{J}F^y(\mathbf{y}^*)$ is then, by Definition C.1.2, an M-matrix. By construction, it is also irreducible and invertible and from Lemma C.1.4, we obtain that $\mathbf{M}^{-1}$ is a (strictly) positive matrix. The second equation in the above can then be rewritten as $\mathbf{v} = \mathbf{M}^{-1}\mathbf{L}\mathbf{u} \ll \mathbf{0}$, where the inequality is because $\mathbf{L} = -\text{diag}(H(\mathbf{y}^*))$ has strictly negative diagonal elements ($H(\mathbf{y}^*)$ being positive from assumptions (A2) and (A3)). Therefore, since $\mathbf{u} \gg \mathbf{0}$ and $\mathbf{v} \ll \mathbf{0}$, we have $(\mathbf{u}, \mathbf{v}) \gg_K \mathbf{0}$, completing the proof. □

The intention behind introducing Proposition C.6.2 was to satisfy the assumptions of Theorem C.4.6. In particular, when $\lambda\left(\mathbf{S}_{\mathbf{y}^*}\mathbf{J}_G(\mathbf{0}) - \mathbf{J}_R(\mathbf{0})\right) > 0$, $(0, \mathbf{y}^*)$ is an unstable fixed point; by Proposition C.6.2 and Theorem C.4.6, there exists an $\epsilon_1 > 0$ and another fixed point $(\mathbf{x}_e, \mathbf{y}_e)$ such that for any point $(\mathbf{x}_r, \mathbf{y}_r) \triangleq (\mathbf{0}, \mathbf{y}^*) + r(\mathbf{u}, \mathbf{v})$ where $r \in (0, \epsilon_1]$, we have

$$(0, \mathbf{y}^*) \ll (\mathbf{x}_r, \mathbf{y}_r) \ll_K \phi_t(\mathbf{x}_r, \mathbf{y}_r) \ll_K \phi_s(\mathbf{x}_r, \mathbf{y}_r) \leq_K (\mathbf{x}^*, \mathbf{0})$$

for all $s > t > 0$. Moreover, for all $(\mathbf{x}, \mathbf{y})$ such that $(\mathbf{0}, \mathbf{y}^*) \ll_K (\mathbf{x}, \mathbf{y}) \leq_K (\mathbf{x}_e, \mathbf{y}_e)$, there exists an $r \in (0, \epsilon]$ sufficiently small such that $(\mathbf{x}_r, \mathbf{y}_r) \leq_K (\mathbf{x}, \mathbf{y}) \leq_K (\mathbf{x}_e, \mathbf{y}_e)$. Since $\phi_t(\mathbf{x}_r, \mathbf{y}_r) \to (\mathbf{x}_e, \mathbf{y}_e)$, monotonicity implies $\phi_t(\mathbf{x}, \mathbf{y}) \to (\mathbf{x}_e, \mathbf{y}_e)$ as $t \to \infty$.

Now, we can either have $(\mathbf{x}_e, \mathbf{y}_e) = (\mathbf{x}^*, \mathbf{0})$, which occurs when $(\mathbf{x}^*, \mathbf{0})$ is the other stable fixed point of (4.8), or $(\mathbf{x}_e, \mathbf{y}_e) = (\hat{\mathbf{x}}, \hat{\mathbf{y}}) \gg \mathbf{0}$ which occurs when $(\mathbf{x}^*, \mathbf{0})$ is an unstable fixed point. Note that $(\mathbf{x}^*, \mathbf{0})$ is stable (unstable) if and only if $\lambda\left(\mathbf{S}_{\mathbf{y}^*}\mathbf{J}_G(\mathbf{0}) - \mathbf{J}_R(\mathbf{0})\right) \leq 0$ (> 0). We will talk about both these possibilities one by one and exploring these will eventually lead to Theorems 4.4.3 and 4.4.4. But before we do that, we first prove the following proposition about convergence to the fixed point $(\mathbf{x}_e, \mathbf{y}_e)$ (whichever of the two it may be).

Proposition C.6.3. *Trajectories of the system* (4.4) *starting from any point* $(\mathbf{x}, \mathbf{y})$ *such that* $(\mathbf{0}, \mathbf{y}^*) <_K (\mathbf{x}, \mathbf{y}) \leq_K (\mathbf{x}_e, \mathbf{y}_e)$ *converge to* $(\mathbf{x}_e, \mathbf{y}_e)$.

Proof. Recall that we already know that for all $(\mathbf{0}, \mathbf{y}^*) \ll_K (\mathbf{x}, \mathbf{y}) \leq (\mathbf{x}^*, \mathbf{y}^*)$, $\phi_t(\mathbf{x}, \mathbf{y}) \to (\mathbf{x}^*, \mathbf{0})$. We would however like to show this for all $(\mathbf{x}, \mathbf{y}) \in Z \setminus (\mathbf{0}, \mathbf{y}^*)$, that is even when $(\mathbf{x}, \mathbf{y})$ satisfies $(\mathbf{0}, \mathbf{y}^*) <_K (\mathbf{x}, \mathbf{y}) \leq (\mathbf{x}^*, \mathbf{0})$. To do this, we create a set of points which converge to $(\mathbf{x}^*, \mathbf{0})$, just like we created $(\mathbf{x}_r, \mathbf{y}_r)$ before, and then use a monotonicity argument to show convergence to $(\mathbf{0}, \mathbf{y}^*)$ of trajectories starting for all points $(\mathbf{x}, \mathbf{y})$ satisfying $(\mathbf{0}, \mathbf{y}^*) <_K (\mathbf{x}, \mathbf{y}) \leq (\mathbf{x}^*, \mathbf{0})$.

Recall that, $\mathbf{y}^*$ is an asymptotically stable fixed point of (4.14), and from the proof of Proposition C.6.2 we know that $\lambda(\mathbf{J}F^y(\mathbf{y}^*)) < 0$. Let $\mathbf{w} \gg \mathbf{0}$ be the corresponding PF eigenvector. Then by Proposition C.2.4, there exists an $\epsilon_2 > 0$ such that for all $s \in (0, \epsilon_2]$, $F^y(\mathbf{y}^* + s\mathbf{w}) \ll \mathbf{0}$. We can then define points $(\mathbf{x}_r, \mathbf{y}_s) \triangleq (r\mathbf{u}, \mathbf{y}^* + s\mathbf{w})$ for any $r \in (0, \epsilon_1]$ and $s \in (0, \epsilon_2]$, where $\mathbf{u} \gg \mathbf{0}$ is the eigenvector of $\mathbf{J}_x$ from Proposition C.6.2. We will first show that trajectories starting from these points converge to $(\mathbf{x}_e, \mathbf{y}_e)$. By rearranging the terms of (4.8), we can rewrite it as

$$\begin{aligned}
\dot{\mathbf{x}} &= \operatorname{diag}(\mathbf{1}-\mathbf{y}^*)G(\mathbf{x}) - R(\mathbf{x}) + \operatorname{diag}(\mathbf{y}^* - \mathbf{x} - \mathbf{y})G(\mathbf{x}) \\
&= \operatorname{diag}(\mathbf{1}-\mathbf{y}^*)\mathbf{J}_G(\mathbf{0})\mathbf{x} - \mathbf{J}_R(\mathbf{0})\mathbf{x} \\
&\quad + \operatorname{diag}(\mathbf{y}^* - \mathbf{x} - \mathbf{y})G(\mathbf{x}) + O\left(\|\mathbf{x}\|^2\right) \\
&= \mathbf{J}_x\mathbf{x} + O\left(\|\mathbf{x}\|\left[\|\mathbf{y}-\mathbf{y}^*\| + \|\mathbf{x}\|\right]\right), \\
\dot{\mathbf{y}} &= \operatorname{diag}(\mathbf{1}-\mathbf{y})H(\mathbf{y}) - S(\mathbf{y}) - \operatorname{diag}(\mathbf{x})H(\mathbf{y}) \\
&= F^y(\mathbf{y}) + O\left(\|\mathbf{y}\|\right),
\end{aligned}$$

for all $(\mathbf{x}, \mathbf{y}) \in D$,[5] where the first equality is from a Taylor series expansion of G and R around $\mathbf{0}$. For any point $(\mathbf{x}_r, \mathbf{y}_s) = (r\mathbf{u}, \mathbf{y}^* + s\mathbf{w})$, the above equations can be written as

$$\begin{aligned}
\dot{\mathbf{x}} &= r\lambda(\mathbf{J}_x)\mathbf{u} + rO\left(\|\mathbf{u}\|\left[s\|\mathbf{w}\| + r\|\mathbf{u}\|\right]\right) \\
&= r\left[\lambda(\mathbf{J}_x)\mathbf{u} + O(r+s)\right] \\
\dot{\mathbf{y}} &= F^y(\mathbf{y}^* + s\mathbf{w}) + O\left(\|s\mathbf{y}\|\right) \\
&= F^y(\mathbf{y}^* + s\mathbf{w}) + O\left(s\right).
\end{aligned}$$

For sufficiently small r and s, we have $\dot{\mathbf{x}} \gg \mathbf{0}$ (since $\lambda(\mathbf{J}_x) > 0$ and $\mathbf{u} \gg \mathbf{0}$) and $\dot{\mathbf{y}} \ll \mathbf{0}$ (since $F^y(\mathbf{y}^* + s\mathbf{w}) \ll \mathbf{0}$ for all $s \in (0, \epsilon_2]$). This satisfies the conditions for Proposition C.4.5, and trajectories starting from such points will be monotonically increasing (according to the south-east cone ordering), eventually converging to the fixed point $(\mathbf{x}_e, \mathbf{y}_e)$.

Now see that for any point $(\mathbf{x}, \mathbf{y})$ such that $(\mathbf{0}, \mathbf{y}^*) <_K (\mathbf{x}, \mathbf{y}) \leq_K (\mathbf{x}_e, \mathbf{y}_e)$, where $\mathbf{x} > \mathbf{0}$ and $\mathbf{y} \leq \mathbf{y}^*$, by the nature of the ODE system (4.4) all zero entries of the $\mathbf{x}$ term will eventually become positive (if it isn't already). Therefore, there exists a time $t_1 > 0$ such that $\mathbf{x}(t_1) \gg \mathbf{0}$, and there exist r, s small enough such that $(\mathbf{x}_r, \mathbf{y}_s) \ll_K \phi_{t_1}(\mathbf{x}, \mathbf{y}) \leq_K (\mathbf{x}_e, \mathbf{y}_e)$. Again by monotonicity, since $\phi_t(\mathbf{x}_r, \mathbf{y}_s) \to (\mathbf{x}_e, \mathbf{y}_e)$, we have $\phi_{t+t_1}(\mathbf{x}, \mathbf{y}) \to (\mathbf{x}_e, \mathbf{y}_e)$ as $t \to \infty$, completing the proof. □

[5] Here, $O(x)$ is used to represent terms which satisfy $O(x) \to 0$ as $x \to 0$.

We now consider the case where $(\mathbf{x}_e, \mathbf{y}_e) = (\mathbf{x}^*, \mathbf{0})$ and give the proof for Theorem 4.4.3. We prove it only for when $\tau_1 \lambda(\mathbf{S}_{\mathbf{y}^*}\mathbf{A}) > 1$ and $\tau_2 \lambda(\mathbf{S}_{\mathbf{x}^*}\mathbf{B}) \leq 1$, since the other case follows by a symmetric argument.

Proof of Theorem 4.4.3. When $\lambda(\mathbf{J}_H(\mathbf{0}) - \mathbf{J}_S(\mathbf{0})) \leq 0$, $(\mathbf{x}^*, \mathbf{0})$ is a stable fixed point of system (4.8), since all eigenvalues of $\mathbf{J}_{\bar{G}\bar{H}}(\mathbf{x}^*, \mathbf{0})$ have non-positive real parts, and we have $(\mathbf{x}_e, \mathbf{y}_e) = (\mathbf{x}^*, \mathbf{0})$. Proposition C.6.3 then implies that trajectories starting from all points in $Z \setminus \{(\mathbf{0}, \mathbf{y}^*)\}$ converge to $(\mathbf{x}^*, \mathbf{0})$. According to Proposition C.6.1, trajectories starting from all points $(\mathbf{x}, \mathbf{y}) \in B_x$ in the system eventually enter the set Z, thereby eventually converging to $(\mathbf{x}^*, \mathbf{0})$, giving us global convergence in B_x. □

Similarly, we use Propositon C.6.3 to prove Theorem 4.4.4.

Proof of Theorem 4.4.4. When $\lambda(\mathbf{J}_G(\mathbf{0}) - \mathbf{J}_R(\mathbf{0})) > 0$ and $\lambda(\mathbf{J}_H(\mathbf{0}) - \mathbf{J}_S(\mathbf{0})) > 0$, both $(\mathbf{0}, \mathbf{y}^*)$ and $(\mathbf{x}^*, \mathbf{0})$ are unstable fixed points, and $(\mathbf{x}_e, \mathbf{y}_e)$ takes the form of a positive fixed point $(\hat{\mathbf{x}}, \hat{\mathbf{y}}) \gg \mathbf{0}$ (it cannot be $(\mathbf{x}^*, \mathbf{0})$, which is unstable). Then from Proposition C.6.3, it attracts trajectories beginning from all points $(\mathbf{x}, \mathbf{y})$ satisfying $(\mathbf{0}, \mathbf{y}^*) <_K (\mathbf{x}, \mathbf{y}) \leq_K (\hat{\mathbf{x}}, \hat{\mathbf{y}})$.

Similarly, we have a symmetric result beginning from $\tau_2 \lambda(\mathbf{S}_{\mathbf{x}^*}\mathbf{B}) > 1$ (symmetric to Proposition C.6.2 which assumes $\tau_1 \lambda(\mathbf{S}_{\mathbf{y}^*}\mathbf{A}) > 1$ instead), and we can say that there exists another fixed point $(\bar{\mathbf{x}}, \bar{\mathbf{y}}) \gg \mathbf{0}$ which attracts all points $(\mathbf{x}, \mathbf{y})$ satisfying $(\bar{\mathbf{x}}, \bar{\mathbf{y}}) \leq_K (\mathbf{x}, \mathbf{y}) <_K (\mathbf{x}^*, \mathbf{0})$. By construction, we then have $(\hat{\mathbf{x}}, \hat{\mathbf{y}}) \leq_K (\bar{\mathbf{x}}, \bar{\mathbf{y}})$, with the possibility of being equal.

To prove global convergence to the set $S = \{(\mathbf{x}_e, \mathbf{y}_e) \in E \mid (\hat{\mathbf{x}}, \hat{\mathbf{x}}) \leq_K (\mathbf{x}_e, \mathbf{y}_e) \leq_K (\bar{\mathbf{x}}, \bar{\mathbf{y}})\}$, observe first that as part of the proof of Proposition C.6.3 we showed that for trajectories starting from any point $(\mathbf{x}, \mathbf{y})$ in the state space, there exists $r > 0$ and $s > 0$ small enough, and $t_1 > 0$ such that $(\mathbf{x}_r, \mathbf{y}_s) \ll_K \phi_{t_1}(\mathbf{x}, \mathbf{y}) \leq_K (\hat{\mathbf{x}}, \hat{\mathbf{y}})$ where $(\mathbf{x}_r, \mathbf{y}_s)$ is a point very close to $(\mathbf{x}^*, \mathbf{0})$. By a parallel argument, we can find a similar point $(\mathbf{x}_p, \mathbf{y}_q)$ very close to $(\mathbf{0}, \mathbf{y}^*)$ and a time t_2 such that $(\bar{\mathbf{x}}, \bar{\mathbf{y}}) \leq_K \phi_{t_2}(\mathbf{x}, \mathbf{y}) \ll_K (\mathbf{x}_p, \mathbf{y}_q)$. Then, we have $(\mathbf{x}_r, \mathbf{y}_s) \ll_K \phi_{\max\{t_1, t_2\}}(\mathbf{x}, \mathbf{y}) \ll_K (\mathbf{x}_p, \mathbf{y}_q)$. Since $\phi_t(\mathbf{x}_r, \mathbf{y}_s) \to (\hat{\mathbf{x}}, \hat{\mathbf{x}}) \in S$, and $\phi_t(\mathbf{x}_p, \mathbf{y}_q) \to (\bar{\mathbf{x}}, \bar{\mathbf{x}}) \in S$, we can once again, due to monotonicity of the system and by invoking a sandwich argument, say that $\phi_{t+\max\{t_1, t_2\}}(\mathbf{x}, \mathbf{y})$ converges to an equilibrium point in S as $t \to \infty$. This completes the proof. □

Appendix D

Appendix for Chapter 5

Proof of Proposition 5.2.1. By considering the i-th entry in (5.3) and setting $dx_i/dt = 0$, we obtain the fixed point equation

$$\sum_{j\in\mathcal{N}} a_{ij}x_j^* = \frac{1}{\tau}\frac{x_i^*}{1-x_i^*}. \tag{D.1}$$

From the min-max theorem, we write $\lambda(\mathbf{A})$ in the Rayleigh quotient form such that

$$\lambda(\mathbf{A}) = \max_{\mathbf{y}\neq\mathbf{0}} \frac{\mathbf{y}^T\mathbf{A}\mathbf{y}}{\mathbf{y}^T\mathbf{y}} \geq \frac{(\mathbf{x}^*)^T\mathbf{A}\mathbf{x}^*}{(\mathbf{x}^*)^T\mathbf{x}^*} = \frac{\sum_{i\in\mathcal{N}} x_i^* \sum_{j\in\mathcal{N}} a_{ij}x_j^*}{\sum_{i\in\mathcal{N}}(x_i^*)^2}. \tag{D.2}$$

where the inequality comes from picking $\mathbf{y} = \mathbf{x}^*$ and the second equality is by rewriting the matrix multiplication in the summation notation. Define a random variable Y which takes values x_i^* with probability $1/N$ for all $i \in \mathcal{N}$, and $\mathbb{E}[Y] = \mathbf{1}^T\mathbf{x}^*/N$. Then, replacing $\sum_{j\in\mathcal{N}} a_{ij}x_j^*$ in (D.2) with (D.1) gives

$$\lambda(\mathbf{A}) \geq \frac{\frac{1}{N}\sum_{i\in\mathcal{N}}(x_i^*)^2/(1-x_i^*)}{\tau\frac{1}{N}\sum_{i\in\mathcal{N}}(x_i^*)^2} = \frac{\mathbb{E}[Y^2/(1-Y)]}{\tau\mathbb{E}[Y^2]}. \tag{D.3}$$

Since Y^2 and $1/(1-Y)$ are both increasing functions in $Y \in (0,1)$, FKG inequality gives $\mathbb{E}[Y^2/(1-Y)] \geq \mathbb{E}[Y^2]\mathbb{E}[1/(1-Y)]$. Then, from (D.3) we have

$$\tau\lambda(\mathbf{A}) \geq \frac{\mathbb{E}[Y^2]\mathbb{E}[1/(1-Y)]}{\mathbb{E}[Y^2]} = \mathbb{E}\left[\frac{1}{1-Y}\right] \geq \frac{1}{1-\mathbb{E}[Y]}, \tag{D.4}$$

where the second inequality comes from Jensen's inequality. Rearranging (D.4) gives (5.4).

We denote $\mathbb{R}_+$ the set of all positive real numbers. Then, with the Collatz-Wielandt formula [**?**], we rewrite $\lambda(\mathbf{A})$ as

$$\lambda(\mathbf{A}) = \min_{\mathbf{y}\in\mathbb{R}_+^N} \max_{i\in\mathcal{N}} \frac{[\mathbf{A}\mathbf{y}]_i}{y_i} \leq \max_{i\in\mathcal{N}} \frac{[\mathbf{A}\mathbf{x}^*]_i}{x_i^*} = \frac{1}{\tau(1-x_{\max})}, \tag{D.5}$$

where the inequality is from choosing $\mathbf{y} = \mathbf{x}^*$. The second equality in (D.5) comes from (D.1). Then, rearranging (D.5) gives $x_{\max} \geq 1 - 1/\tau\lambda(\mathbf{A})$. □

Proof of Lemma 5.2.2. We only present the proof for the behaviour of $\hat{\mathbf{x}}$ and $\hat{\mathbf{y}}$ in τ_1, since the case involving τ_2 follows by symmetry. Consider the bi-SIS model

$$\begin{aligned} \dot{\mathbf{x}} &= (\beta_1 + \epsilon)\mathrm{diag}(\mathbf{1}-\mathbf{x}-\mathbf{y})\mathbf{A}\mathbf{x} - \delta_1\mathbf{x} \\ \dot{\mathbf{y}} &= \beta_2\mathrm{diag}(\mathbf{1}-\mathbf{x}-\mathbf{y})\mathbf{B}\mathbf{y} - \delta_2\mathbf{y}, \end{aligned} \tag{D.6}$$

where we use ϵ as the parameter to vary τ_1. It is enough to show that entries $\hat{x}_i$ of $\hat{\mathbf{x}}$ ($\hat{y}_i$ of $\hat{\mathbf{y}}$) increase (decrease) in ϵ.[1].

We now consider trajectories of system (D.6) starting from $(\hat{\mathbf{x}}, \hat{\mathbf{y}})$. Note that by definition $(\hat{\mathbf{x}}, \hat{\mathbf{y}}) \gg (\mathbf{0}, \mathbf{0})$ is a fixed point of the system when $\epsilon = 0$, and in this case we have $\dot{\mathbf{x}} = 0$ and $\dot{\mathbf{y}} = 0$. However for any $\epsilon > 0$, we have $\dot{\mathbf{x}} \gg \mathbf{0}$ and $\dot{\mathbf{y}} = \mathbf{0}$. Let $\phi_t(\mathbf{x}, \mathbf{y}) \in [0,1]^2 N$ denote the flow of the system at time $t > 0$, with initial point $(\mathbf{x}, \mathbf{y}) \in D$, with $\phi_t^x(\mathbf{x}, \mathbf{y}) \in [0,1]^N$ corresponding to the the infection probabilities for Virus 1, and $\phi_t^y(\mathbf{x}, \mathbf{y}) \in [0,1]^N$ corresponding to those of Virus 2. Then for any $\epsilon > 0$ sufficiently small $s > 0$ we have $\phi_s^x(\hat{\mathbf{x}}, \hat{\mathbf{y}}) > \phi_0^x(\hat{\mathbf{x}}, \hat{\mathbf{y}}) = \hat{\mathbf{x}}$, and $\phi_s^y(\hat{\mathbf{x}}, \hat{\mathbf{y}}) = \phi_0^y(\hat{\mathbf{x}}, \hat{\mathbf{y}}) = \hat{\mathbf{y}}$.

As a consequence of Proposition 3.1 in [41], the bi-SIS system is considered to be *strongly monotone* in Int(D).[2] The result is that $\phi_{t+s}^x(\hat{\mathbf{x}}, \hat{\mathbf{y}}) \gg \mathbf{x}$, and $\phi_{t+s}^y(\hat{\mathbf{x}}, \hat{\mathbf{y}}) \ll \mathbf{y}$ for all $t > 0$. For any $\epsilon > 0$, let $(\hat{\mathbf{x}}_\epsilon, \hat{\mathbf{y}}_\epsilon) \triangleq \lim_{t\to\infty} \phi_t(\hat{\mathbf{x}}, \hat{\mathbf{y}})$ denote the convergent point of trajectory starting from $(\hat{\mathbf{x}}, \hat{\mathbf{y}})$. Since we consider only small enough $\epsilon > 0$ that still satisfying the coexistence conditions (C3), the point $(\hat{\mathbf{x}}_\epsilon, \hat{\mathbf{y}}_\epsilon) \gg (\mathbf{0}, \mathbf{0})$ is now the CE fixed point corresponding to the choice of $\epsilon > 0$, and satisfies $\hat{\mathbf{x}}_\epsilon \gg \hat{\mathbf{x}}$ and $\hat{\mathbf{y}}_\epsilon \ll \hat{\mathbf{y}}$. By similar arguments, the reverse holds true when $\epsilon < 0$, while still satisfying conditions (C3), that is the trajectories starting from $(\hat{\mathbf{x}}, \hat{\mathbf{y}})$ converge to another CE fixed point such that $\hat{\mathbf{x}}_\epsilon \ll \hat{\mathbf{x}}$ and $\hat{\mathbf{y}}_\epsilon \gg \hat{\mathbf{y}}$.

Therefore, for all system parameters τ_1, τ_2 satisfying coexistence conditions (C3), and

[1] Instead of $\beta_1 + \epsilon$, we could also vary τ_1 by replacing δ_1 with $\delta - \epsilon$. The steps of the proof remain similar, with both methods leading to the same conclusion.

[2] A short educational primer on MDS is included in [41].

lying within the corresponding region in Figure 5.1, the entries of $\hat{\mathbf{x}}$ increase (entries of $\hat{\mathbf{y}}$ decrease) in τ_1 for any CE. This completes the proof. □ □

Proof of Theorem 5.2.3. Let $f_i \triangleq \hat{y}_i/(1-\hat{x}_i)$ and $g_i \triangleq \hat{x}_i/(1-\hat{y}_i)$ for notation simplicity. We only prove that f_i is decreasing (increasing) in τ_1 (τ_2), since the similar result for g_i follows by a symmetric argument.

We use the notation by $\left[\partial \hat{y}_i/\partial \hat{x}_j\right]_{\tau_1} \triangleq \frac{\partial \hat{y}_i/\partial \tau_1}{\partial \hat{x}_j/\partial \tau_1}$ to denote the change in $\hat{y}_i$ with respect to change $\hat{x}_i$ due to increase or decrease in τ_1. Similarly, we use the notation $\left[\partial \hat{x}_i/\partial \hat{y}_j\right]_{\tau_2}$ to denote the change in $\hat{x}_i$ with respect to change in $\hat{y}_i$ due increase or decrease in τ_2. We first prove the following inequalities:

$$\left[\frac{\partial \hat{y}_i}{\partial \hat{x}_i}\right]_{\tau_1} < -\frac{\hat{y}_i}{1-\hat{x}_i}, \quad \left[\frac{\partial \hat{y}_i}{\partial \hat{x}_i}\right]_{\tau_2} < -\frac{\hat{y}_i}{1-\hat{x}_i} \tag{D.7}$$

Taking partial derivative of the logarithm of $\sum_j b_{ij}\hat{y}_j$ in the fixed point equation (5.5) with respect to τ_2, we obtain

$$\frac{1}{\sum\limits_{j\in\mathcal{N}} b_{ij}\hat{y}_j}\sum_{j\in\mathcal{N}} b_{ij}\frac{\partial \hat{y}_j}{\partial \tau_2} = \frac{\partial \hat{y}_i}{\partial \tau_2}\left(\frac{1}{\hat{y}_i} + \frac{1+\left[\frac{\partial \hat{x}_i}{\partial \hat{y}_i}\right]_{\tau_2}}{1-\hat{x}_i-\hat{y}_i} - \frac{\partial \tau_2}{\tau_2 \partial \hat{y}_i}\right). \tag{D.8}$$

The left-hand side of (D.8) is positive since $b_{ij} \geq 0$, $\hat{x}_j \in (0,1)$, and $\partial \hat{y}_j/\partial \tau_2 > 0$ in Lemma 5.2.2 for all $i, j \in \mathcal{N}$. Then, we have

$$0 < \frac{1}{\hat{y}_i} + \frac{1+\left[\frac{\partial \hat{x}_i}{\partial \hat{y}_i}\right]_{\tau_2}}{1-\hat{y}_i-\hat{x}_i} - \frac{1}{\tau_2 \partial \hat{y}_i/\partial \tau_2} < \frac{1}{\hat{y}_i} + \frac{1+\left[\frac{\partial \hat{x}_i}{\partial \hat{y}_i}\right]_{\tau_2}}{1-\hat{x}_i-\hat{y}_i}, \tag{D.9}$$

where the first inequality is from the positivity of the terms in (D.8), and the second equality comes be removing the third summand, which we can do since $\partial \hat{y}_i/\partial \tau_2 > 0$ from Lemma 5.2.2. Then, rearranging (D.9) with respect to $\left[\partial \hat{y}_i/\partial \hat{x}_i\right]_{\tau_2}$ gives us $\left[\partial \hat{y}_i/\partial \hat{x}_i\right]_{\tau_2} < -\hat{y}_i/(1-\hat{x}_i)$. Performing the same steps by differentiating by the logarithm of the fixed point equation by τ_1 instead of τ_2 gives us $\left[\partial \hat{y}_i/\partial \hat{x}_i\right]_{\tau_1} < -\hat{y}_i/(1-\hat{x}_i)$, proving (D.7). Now, in order to show f_i is strictly decreasing in $\tau_1 > \tau_1^*$, it is enough to show $\partial f_i/\partial \tau_1 < 0$. Taking partial derivative of f_i with respect to τ_1 gives

$$\frac{\partial f_i}{\partial \tau_1} = \frac{(1-\hat{x}_i)\frac{\partial \hat{y}_i}{\partial \tau_1} + \hat{y}_i\frac{\partial \hat{x}_i}{\partial \tau_1}}{(1-\hat{x}_i)^2} = \frac{\partial \hat{x}_i}{\partial \tau_1}\cdot\frac{(1-\hat{x}_i)\left[\frac{\partial \hat{y}_i}{\partial \hat{x}_i}\right]_{\tau_1} + \hat{y}_i}{(1-\hat{x}_i)^2}. \tag{D.10}$$

The first inequality of (D.7) gives $(1-\hat{x}_i)\left[\partial \hat{y}_i/\partial \hat{x}_i\right]_{\tau_1}+\hat{y}_i<0$. Together with $\partial \hat{x}_i/\partial \tau_1>0$ from Lemma 5.2.2, we can see from (D.10) that $\partial f_i/\partial \tau_1<0$ for all $i\in\mathcal{N}$. Similarly, we have

$$\frac{\partial f_i}{\partial \tau_2}=\frac{\partial \hat{x}_i}{\partial \tau_2}\cdot\frac{(1-\hat{x}_i)\left[\frac{\partial \hat{y}_i}{\partial \hat{x}_i}\right]_{\tau_2}+\hat{y}_i}{(1-\hat{x}_i)^2}>0 \tag{D.11}$$

because $\partial \hat{x}_i/\partial \tau_2<0$ from Lemma 5.2.2, showing that f_i is strictly increasing in τ_2 for all $i\in\mathcal{N}$. □

Proof of Corollary 5.2.4. We follow the notations $f_i \triangleq \hat{y}_i/(1-\hat{x}_i)$ and $g_i \triangleq \hat{x}_i/(1-\hat{y}_i)$ and assume the coexistence condition $\tau_1>1/\lambda(\mathrm{diag}(\mathbf{1}-\mathbf{y}^*)\mathbf{A})$ and $\tau_2>1/\lambda(\mathrm{diag}(\mathbf{1}-\mathbf{x}^*)\mathbf{B})$.

If $\tau_1\le 1/\lambda(\mathrm{diag}(\mathbf{1}-\mathbf{y}^*)\mathbf{A})$, then virus 1 will die out, i.e., $\hat{x}_i=0$, $\hat{y}_i=y_i^*$ and $f_i=y_i^*$ for all $i\in\mathcal{N}$. Since f_i is decreasing in $\tau_1>1/\lambda(\mathrm{diag}(\mathbf{1}-\mathbf{y}^*)\mathbf{A})$, we have $f_i<y_i^*$.

Similarly, if $\tau_2\le 1/\lambda(\mathrm{diag}(\mathbf{1}-\mathbf{x}^*)\mathbf{B})$, Virus 2 will die out, i.e., $\hat{y}_i=0$, $\hat{x}_i=x_i^*$ and $g_i=x_i^*$ for all $i\in\mathcal{N}$. Since g_i is decreasing in $\tau_2>1/\lambda(\mathrm{diag}(\mathbf{1}-\mathbf{x}^*)\mathbf{B})$, we have $g_i<x_i^*$. □

Proof of Proposition 5.2.5. We first quantify the upper bound of $\hat{y}_i+\hat{x}_i$, $\forall i\in\mathcal{N}$. Rearranging (5.6) gives

$$\hat{y}_i<\min\left\{y_i^*(1-\hat{x}_i),1-\hat{x}_i/x_i^*\right\}. \tag{D.12}$$

Then, adding $\hat{x}_i$ on both sides in (D.12) gives

$$\hat{y}_i+\hat{x}_i<\min\left\{y_i^*(1-\hat{x}_i)+\hat{x}_i,1-\hat{x}_i/x_i^*+\hat{x}_i\right\}. \tag{D.13}$$

Note that $\hat{y}_i\in[0,y_i^*]$, $\hat{x}_i\in[0,x_i^*]$ and $y_i^*,x_i^*\le 1$, ensuring that the right-hand side term in (D.13) is concave in $\hat{x}_i\in[0,x_i^*]$. Then, the maximum of the upper bound in (D.13) is obtained by solving $y_i^*(1-\hat{x}_i)+\hat{x}_i=1-\hat{x}_i/x_i^*+\hat{x}_i$ in terms of $\hat{x}_i$, which gives us $\hat{x}_i=(x_i^*-y_i^*x_i^*)/(1-y_i^*x_i^*)$. Putting this expression back to (D.13) leads to $\hat{y}_i+\hat{x}_i<(x_i^*+y_i^*-2x_i^*y_i^*)/(1-x_i^*y_i^*)$, or equivalently,

$$1-\hat{y}_i-\hat{x}_i>\frac{(1-x_i^*)(1-y_i^*)}{1-x_i^*y_i^*}=\frac{1}{\frac{1}{1-x_i^*}+\frac{1}{1-y_i^*}-1}. \tag{D.14}$$

Note that $\mathbf{x}^*,\mathbf{y}^*$ are unrelated to each other because they are the fixed points in the single-virus SIS case where the other virus dies out. We define two independent random variables X,Y that take values x_i^*,y_i^* with probability $1/N$ for all $i\in\mathcal{N}$. From (D.4), we have

$$\tau_1\lambda(\mathbf{A})\ge\mathbb{E}[1/(1-X)],\quad \tau_2\lambda(\mathbf{B})\ge\mathbb{E}[1/(1-Y)]. \tag{D.15}$$

We also define a random variable Z that takes values $1/(1-x_i^*)+1/(1-y_i^*)$ with probability $1/N$ for all $i \in \mathcal{N}$, and $\mathbb{E}[Z] = \mathbb{E}[1/(1-X)] + \mathbb{E}[1/(1-Y)]$. From (D.15), we have

$$\mathbb{E}[Z] \geq \tau_1 \lambda(\mathbf{A}) + \tau_2 \lambda(\mathbf{B}). \tag{D.16}$$

Then, summing (D.14) over all $i \in \mathcal{N}$ and dividing by N gives

$$\frac{1}{N}\sum_{i\in\mathcal{N}}(1-\hat{y}_i-\hat{x}_i) > \frac{1}{N}\sum_{i\in\mathcal{N}}\frac{1}{\frac{1}{1-x_i^*}+\frac{1}{1-y_i^*}-1} = \mathbb{E}\left[\frac{1}{Z-1}\right]. \tag{D.17}$$

Using Jensen's inequality in (D.17) leads to

$$\frac{1}{N}\sum_{i\in\mathcal{N}}(1-\hat{y}_i-\hat{x}_i) > \frac{1}{\mathbb{E}[Z]-1} \geq \frac{1}{\tau_1\lambda(\mathbf{A})+\tau_2\lambda(\mathbf{B})-1}, \tag{D.18}$$

where the last inequality comes from (D.16). Rearranging (D.18) completes the proof. □